Characterization of the cellular network of ubiquitin conjugating and ligating enzymes

Ewa Katarzyna Blaszczak

ANNÉE 2015

THÈSE / UNIVERSITÉ DE RENNES 1
sous le sceau de l'Université Européenne de Bretagne

pour le grade de

DOCTEUR DE L'UNIVERSITÉ DE RENNES 1

Mention : BIOLOGIE

École doctorale Vie-Agro-Santé

présentée par

Ewa Katarzyna Blaszczak

Préparée à l'unité de recherche UMR 6290, IGDR
Institut de Génétique et Développement de Rennes
Université Rennes 1

Characterization of the cellular network of ubiquitin conjugating and ligating enzymes

Thèse soutenue à Rennes le 26.06.2015
devant le jury composé de :

Aude ECHALIER-GLAZER
Maître de conférence
University of Leicester / *rapporteur*

Lionel PINTARD
Directeur de recherche (DR2)
Institut Jacques Monod / *rapporteur*

Reynald GILLET
Professeur (PU2)
Université de Rennes 1, UMR 6290 / *examinateur*

Thimo KURZ
Chercheur étranger (équivalent DR)
University of Dundee / *examinateur*

Marc TRAMIER
Ingénieur de recherche (IRHC)
Université de Rennes 1, UMR 6290 / *examinateur*

Gwenaël RABUT
Chargé de recherche (CR1)
Université de Rennes 1, UMR 6290 / *directeur de thèse*

For three men of my life who made it all possible: my Husband, my Father and my Grandfather, although his journey finished right when my PhD journey had started. Also, for my little Sebastian, whose journey has started when my PhD is about to finish.

ACKNOWLEDGEMENTS

This work would not have been possible without an enormous help of many people.

First and foremost, I would like to thank my supervisor Gwénaël Rabut for his help, support and encouragement. He was always extremely generous with his time not only devoted to teaching me, both theory and practical work at the bench, but also to discussing and providing useful comments and feedback. I was extremely lucky to have an outstanding mentor like him, who apart from supervising was also advising, and more importantly listening and understanding.

I also thank Claude Prigent for his support, including a strong support in the organization of the Young Life Scientists' Symposium. My special thanks are extended to all the members of Cell Cycle team. It was indeed a privilege to work with all of you. In particular, I owe a special debt to Gaëlle Le Dez, who was involved in various steps of my PhD project and whose work greatly contributed to the results obtained. I thank Jacek Kubiak and Erwan Watrin for valuable discussions.

There are also two people for who may not be enough words to express my gratitude. First, I thank my best friend Blanca Gomez-Escoda, who was always there with me during the happiest moments and who was also helping me in the most difficult periods. This is when you know who your true friends are. Second, I am particularly grateful to Stéphane Dréano for doing lots of sequencing for this project but what is more helping me with everyday life situations and teaching me French. Merci car c'est grâce à toi que je peux parler français aujourd'hui.

Szczególne podziękowania składam Rodzicom oraz Mężowi za wsparcie, jakie od nich otrzymałam. Tomkowi również za troskę, opiekę, cierpliwość i wyrozumiałość. Dziękuję za to, że jesteś. Sebastiankowi, iż pomimo dręczących go kolek pozwolił mi na dokończenie tego manuskryptu.

Last but not least, I thank *Ministère de l'Enseignement supérieur et de la Recherche* for funding of the three years of my PhD and giving me an opportunity to work on this interesting and perspective project, and *La Ligue Contre Le Cancer* for additional six months prolongation. I also thank all our international collaborators for their great contribution to the work on the functional part of this project.

TABLE OF CONTENTS

ABSTRACT

Protein ubiquitylation is a post-translational modification that plays a crucial role in regulating many cellular functions, including cell growth and proliferation. Defects in this control mechanism cause cancer and other diseases. The ubiquitylation process involves a cascade of enzymatic reactions catalyzed by a family of structurally-related enzymes, namely ubiquitin activating enzymes (E1s), ubiquitin conjugating enzymes (E2s) and ubiquitin ligases (E3s). Interactions between E2s and E3s are in the centre of ubiquitylation cascade and it is a combination of particular E2/E3 pairs that determine what types of ubiquitin chains are made, thus determining the regulatory functions of the ubiquitin pathway. To date, only a small fraction of all possible E2/E3 pairs have been investigated, mainly using biochemical and *in vitro* approaches that may not accurately reflect the conditions that occur in living cells. We aimed to develop a method capable of detecting specific E2/E3 interactions under physiological conditions. Using budding yeast as a model organism, we found that the Bimolecular Fluorescence Complementation (BiFC) enables sensitive detection of the well described Ubc4/Ufd4 pair under endogenous conditions. The assay is specific since the interaction signal is lost in yeasts expressing Ubc4 mutants truncated in its E3 interaction domain. We then used this system to further analyze the physiological network of E2 and E3 enzymes in living yeast. We performed a microscopy screen to assay all interactions between eleven E2s and 57 E3s/putative E3s. Our results show that approximately 20% of all E2/E3 combinations give a detectable BiFC signal. Few E3s interacted only with a single E2, whereas most E3s produced a BiFC signal with multiple E2s. Ubc13, Ubc1 and Ubc4 were found to be the most frequently interacting E2s. Our results match many examples from current literature but we also detected 95 new E2/E3 interactions. In particular we identified an interaction between the proteins Asi1 and Asi3 and E2s Ubc6 and Ubc7. Asi1 and Asi3 are known to form a complex (the Asi1/3 complex) at the inner nuclear membrane and are involved in the regulation of the response to extracellular amino acids. The Asi1/3 complex was suspected to function as a ubiquitin ligase, since the Asi1 and Asi3 proteins contain a RING domain, but its function as an E3 has previously not been demonstrated. We therefore further characterized it functionally.

RÉSUMÉ

L'ubiquitylation des protéines est une modification post-traductionnelle qui correspond à l'ajout d'une protéine d'ubiquitine sur d'autres protéines de la cellule et joue un rôle capital dans la régulation de nombreuses fonctions cellulaires, en particulier la croissance et la prolifération cellulaire. Des dysfonctionnements de ce mécanisme sont à l'origine de cancers et d'autres maladies. Le processus d'ubiquitylation met en jeu une cascade des réactions enzymatiques catalysées par 3 familles d'enzymes : des enzymes d'activation de l'ubiquitine (E1s), des enzymes de conjugaison de l'ubiquitine (E2s) et des ubiquitine ligases (E3s). L'interaction entre une E2, qui porte l'ubiquitine activée et une E3, qui recrute la protéine à modifier, permet le transfert de l'ubiquitine sur sa cible. Les hétérodimères E2/E3 sont donc au cœur de la réaction d'ubiquitylation et dictent la manière précise dont les substrats sont modifiés. A ce jour, un nombre limité de couples E2/E3 ont été décrits, en particulier grâce à des approches biochimiques. L'objectif de ce doctorat était d'étudier les interactions E2/E3 dans des cellules vivantes afin de conserver les conditions physiologiques du fonctionnement de ces enzymes. Ce travail s'est déroulé en 4 étapes qui ont consisté à :

- identifier et optimiser une méthode capable de détecter les interactions E2/E3 dans une cellule vivante en utilisant la levure de boulanger (*Saccharomyces cerevisiae*) comme organisme modèle
- construire une collection de souches de levure permettant de tester les interactions entre E2s et E3s
- réaliser un crible systématique afin d'identifier de nouvelles paires E2/E3
- caractériser fonctionnellement une des paires E2/E3 nouvellement identifiées.

L'étude des interactions protéine-protéine dans des cellules vivantes est relativement difficile, en particulier lorsqu'il s'agit de détecter des interactions faibles et transitoires comme les interactions entre E2s et E3s. Nous avons testé deux techniques différentes et avons choisi la complémentation bimoléculaire de fluorescence, (BiFC, Bimolecular Fluorescence Complementation). Le principe de cette technique repose sur la fusion des partenaires d'interaction avec deux fragments complémentaires (N- et C-terminaux) d'une protéine fluorescente (ici Venus). L'interaction entre les protéines d'intérêt va positionner les deux fragments de la protéine Venus (VN et VC) à proximité l'un de

l'autre, ce qui leur permet de reformer la structure native de Venus qui peut ensuite être détectée par microscopie à fluorescence. Pour tester cette technique, nous avons construit une souche de la levure exprimant les enzymes Ubc4 et Ufd4 fusionnées respectivement avec VN et VC et sous contrôle de leur promoteur endogène. Ubc4 est une E2 et Ufd4 une E3 qui sont relativement abondantes et bien connues pour fonctionner ensemble dans l'ubiquitylation de protéines fusionnées à l'ubiquitine. Nous avons observé que des levures exprimant à la fois Ubc4-VN et Ufd4-VC étaient 10 à 15 fois plus fluorescentes que des levures exprimant Ubc4-VN portant des mutations empêchant son interaction avec Ufd4-VC. Ces résultats démontrent que la technique de BiFC permet de révéler de manière spécifique des interactions entre une E2 et une E3 dans les cellules vivantes.

Afin de procéder à une analyse systématique de paires potentielles E2/E3, nous avons construit 11 souches de levures exprimant chacune une E2 fusionnée à VC sous contrôle de son promoteur endogène. En parallèle, nous avons obtenu une collection de souches de levures où la majorité des gènes avaient été fusionnés à VN. A partir de cette collection nous avons pu obtenir 56 souches exprimant des E3s fusionnées à leur extrémité C-terminale avec VN. Cependant certaines E3s ont leur domaine d'interaction avec les E2s dans leur région N-terminale. Pour maximiser nos chances de détecter des interactions avec certaines de ces E3s, nous avons construit de nouvelles souches exprimant des E3s fusionnées avec VC à leur extrémité N-terminale. Nous avons également construit des souches de levures exprimant des E3s qui n'étaient pas présentes dans la collection initiale. Au total nous avons ainsi obtenus 63 souches exprimant des E3s fusionnées avec VC. Ces souches ont été systématiquement croisées avec les souches exprimant des E2s, ce qui nous a permis d'obtenir 704 souches dont 627 expriment une combinaison unique d'E2-VN et E3-VC. Toutes ces souches expriment également la sous-unité Rpn7 du protéasome fusionnée avec une protéine fluorescente tdimer2 qui nous a permis de segmenter les images obtenues par microscopie et de quantifier la fluorescence de Venus dans le noyau et dans le cytoplasme des cellules. Ces souches ont été soumises à l'imagerie BiFC dans deux expériences indépendantes, ce qui nous a permis, après analyse des images, d'identifier 128 interactions E2/E3 dont 33 avaient déjà été décrites dans la littérature. La grande majorité des E3s pour lesquelles nous avons pu détecter des interactions avec des E2s sont visiblement capables d'interagir avec plusieurs E2s et seules quelques E3s

semblent interagir avec une seule E2. Parmi les E2s, Ubc13, Ubc1 et Ubc4 sont celles qui interagissent avec le plus d'E3s.

Parmi les 95 interactions E2/E3 nouvellement identifiées, nous nous sommes particulièrement intéressés aux interactions entre les E3s Asi1 et Asi3 et les E2s Ubc6 et Ubc7. Asi1 et Asi3 sont deux protéines transmembranaires formant un complexe protéique localisé dans la membrane interne du noyau et qui étaient connues pour inhiber Stp1 et Stp2, deux facteurs de transcriptions régulant l'expression de perméases permettant le transport des acides aminés dans les levures. Asi1 et Asi3 contiennent un domaine RING caractéristique d'ubiquitine ligases, mais il n'avait pas été montré qu'elles fonctionnaient effectivement comme des ubiquitine ligases. En utilisant des expériences in vitro, nous avons pu démontrer que les domaines RING de Asi1 et Asi3 interagissent directement avec Ubc6 et Ubc7 et que le complexe Asi1/Asi3 est nécessaire pour l'ubiquitylation nucléaire de Stp2.

En conclusion ce travail a permis d'établir une carte des interactions E2/E3 chez la levure et servira de base pour des études ultérieures qui permettront de mieux comprendre le fonctionnement du réseau E2/E3 dans les cellules.

LIST OF ABBREVIATIONS

APC/C	Anaphase-promoting complex/cyclosome	kDa	kiloDalton
ATP	Adenosine-5'-triphosphate	N-terminal	Amino-terminal
BiFC	Bimolecular Fluorescence Complementation	O/N	Overnight
BiLC	Bimolecular Luminescence Complementation	PAGE	Polyacrylamide gel electrophoresis
bp(s)	base pair(s)	PCAs	Protein-fragment complementation assays
BRET	Bioluminescence resonance energy transfer	PCR	Polymerase chain reaction
C-terminal	Carboxy-terminal	PPIs	Protein-protein interactions
CUE	Coupling of ubiquitin conjugation to ER degradation	RT	Room temperature
DNA	Deoxyribonucleic acid	SDS	Sodium dodecyl sulphate
DUB	Deubiquitylating enzyme	TAP	Tandem affinity purification
DTT	Dithiothreitol	TCA	Trichloroacetic acid
E1	Ubiquitin activating enzyme	TCEP	Tris(2-carboxyethyl)phosphine
E2	Ubiquitin conjugating enzyme	Ub	Ubiquitin
E3	Ubiquitin ligating enzyme (ligase)	UBA	Ubiquitin-associated domain
E4	Ubiquitin chain elongation factor	UBC	Ubiquitin conjugating
ER	Endoplasmic reticulum	UBDs	Ubiquitin binding domains
ERAD	ER-associated protein degradation	Ubls	Ubiquitin-like proteins
FCCS	Fluorescence cross-correlation spectroscopy	USP	Ubiquitin-specific proteases
FRET	Förster resonance energy transfer	UCH	Ubiquitin C-terminal hydrolase
GAT	GGA and TOM (target of myb)	UFD	Ubiquitin fusion degradation pathway
GFP	Green fluorescent protein	UPS	Ubiquitin proteasome system
HECT	Homologous to the E6-AP carboxyl terminus	Y2H	Yeast two-hybrid
JAMM	JAB1/MPN/Mov34 metalloenzyme	YFP	Yellow fluorescent protein

1 INTRODUCTION

1.1 The ubiquitin system

1.1.1 Historical perspective

Prior to the discovery of ubiquitin, Hershko and Tomkins observed that the degradation of the enzyme tyrosine aminotransferase (TAT) in hepatoma culture cells was blocked by potassium fluoride, an inhibitor of cellular ATP production (Hershko and Tomkins, 1971). This had already given the first indication that ATP may be required for the ubiquitin proteolytic system. Ubiquitin itself was discovered by Gideon Goldstein in 1974 and was put forward as a thymopoietic hormone (Goldstein, 1974). In the following year a complete amino acid sequence of ubiquitin was published and it was suggested that this protein is universal in living cells (Goldstein et al., 1975; Schlesinger et al., 1975). Still at that time, lysosome was assumed to be the organelle that degrades intracellular proteins. However, Etlinger and Goldberg further confirmed in 1977 the existence of a non-lysosomal and ATP-dependent proteolytic system responsible for the degradation of misfolded proteins in reticulocytes. All these laid the basis for seminal work on the ubiquitin proteasome system, dating back to the years 1978-1983 when the components of the ubiquitin system, including ubiquitin activating (E1), ubiquitin conjugating (E2) and ligating (E3) enzymes, were identified in the laboratory of Avram Hershko. Using biochemical fractionation and enzymology, he, together with his student Aaron Ciechanover and collaborator Irwin Rose, discovered that certain proteins are covalently conjugated to ubiquitin (initially named by them as ATP-dependent proteolysis factor 1, APF-1 – subsequently shown by Wilkinson et al. (1980) to be indeed ubiquitin) – a process now termed ‘ubiquitylation’ and that ubiquitylated proteins are destroyed by an ATP-dependent protease in the extract of rabbit reticulocytes (Ciechanover et al., 1978; Hershko et al., 1980). They went on to examine the characterization of those enzymes and demonstrated ubiquitin involvement in the regulation of protein degradation. For this discovery they were awarded the Nobel Prize in Chemistry in 2004. Later on, the laboratory of Martin Rechsteiner purified and characterized the ATP-dependent protease, now known as the 26S proteasome complex, which mediates destruction of ubiquitin conjugates (Hough et al., 1986). This group of

researchers also proposed for the first time that the smaller 20S protease is part of the 26S proteasome (Hough et al., 1987). In the 1980s, another set of discoveries was made in the laboratory of Alexander Varshavsky concerning the biological functions of the ubiquitin-proteasome system, i.e. its role in the cell cycle, DNA repair pathway, transcriptional regulation and protein synthesis as well as stress responses (Ciechanover et al., 1984; Finley et al., 1984; Varshavsky, 2006). In the 1990s various ubiquitin conjugating (E2s) and ligating enzymes (E3s) were identified and non-proteolytic functions for ubiquitin were discovered, opening up a new era in the ubiquitin field. The aforementioned pioneering discoveries are presented in the timeline below (Figure 1).

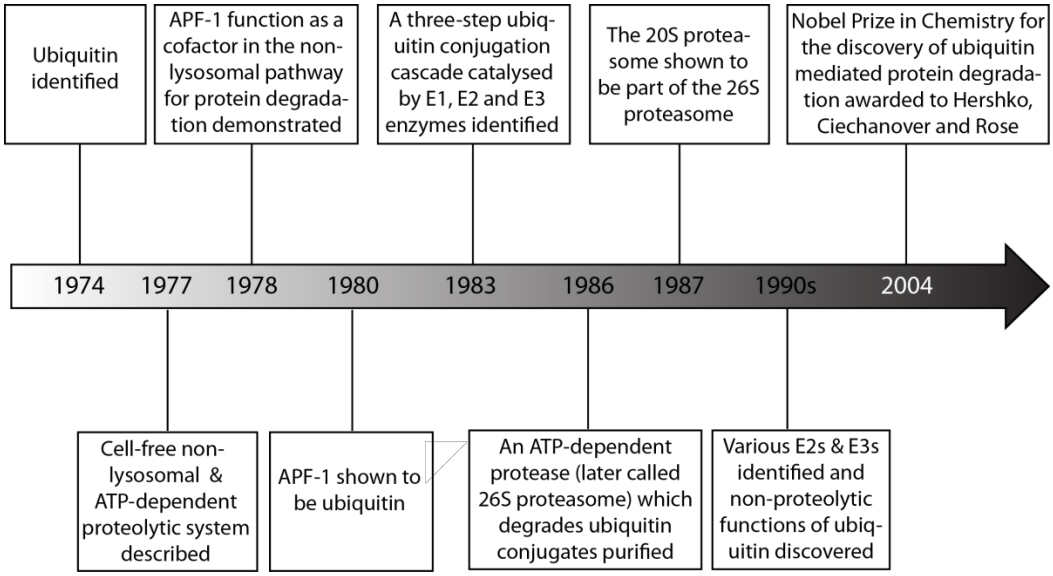

Figure 1. A timeline of some key discoveries in the ubiquitin field (adapted with permission from: Ciechanover, *Nature Reviews Molecular Cell Biology*, 2005).

1.1.2 Overview of the cellular functions of protein ubiquitylation

An important function of the ubiquitin-proteasome system is to serve as a quality control mechanism that selectively recognizes and targets misfolded or damaged proteins for degradation. This is a critical role as protein misfolding can have negative consequences for cells, including loss of function phenotypes, the production of toxic protein aggregates or non-functional protein products (Geiler-Samerotte et al., 2011). Several pathways can target misfolded proteins for proteasomal degradation in different cellular compartments. The most intensively studied pathway is probably endoplasmic reticulum-associated protein degradation (ERAD), which is highly conserved across

eukaryotes. ERAD consists of four steps, namely substrate selection, dislocation across the endoplasmic reticulum membrane, addition and subsequent removal of ubiquitin conjugates, and degradation by the 26S proteasome. Ubiquitin-dependent degradation at the ER in yeast has recently been reviewed by Zattas and Hochstrasser (2014), and in mammals by Olzmann et al. (2013). The link between ERAD machinery and human diseases is clearly established and has been reviewed by Guerriero and Brodsky (2012). In addition to ERAD, several ubiquitin ligases have been implicated in the quality control of cytoplasmic proteins, for example Ubr1 (Heck et al., 2010) or Hul5 (Fang et al., 2011). Gardner and colleagues also reported the existence of a protein quality control mechanism in the nucleus of *Saccharomyces cerevisiae* (henceforth *S. cerevisiae).* In this compartment, misfolded proteins are recognized and targeted to the proteasome by the San1 ubiquitin ligase, which functions together with the ubiquitin conjugating enzymes Cdc34 and Ubc1 (Gardner et al., 2005).

In addition to its role in quality control, proteasome-mediated degradation of ubiquitylated proteins acts as a regulatory mechanism in a myriad of cellular processes. The best example is probably the progression through cell cycle, where several Cullin-RING ubiquitin ligases (CRLs) play a dominant role in controlling the degradation of cell cycle proteins. The archetypes here are the anaphase promoting complex/cyclosome (APC/C) and the Skp1/Cullin/F-box protein (SCF complex) ubiquitin ligase. The APC/C is activated during late mitosis and the G1 phase of the cell cycle, eliminating proteins that block mitotic progression and that would have negative consequences for the cell upon accumulation in the G1 phase. The SCF complex ubiquitylates proteins marked by phosphorylation and drives cell cycle progression during G1 and S phases. Other important classes that have also been shown to play a prominent role in cell cycle regulation are CRL3 and CRL4 complexes. CRL3 complexes, with Aurora B as their best characterized substrate, have been linked to the control of mitosis via proteolytic and non-proteolytic mechanisms. CRL4 complexes, in addition to cell cycle regulation, are implicated in the DNA damage response and DNA replication (recently reviewed by Bassermann et al., 2014).

It is now known that ubiquitylation also acts as a signal targeting plasma membrane proteins for destruction in lysosomes or vacuoles (reviewed by Hicke, 2001). Moreover, ubiquitylation is involved in cellular processes such as cell differentiation, cell signaling, transcription (Zhou et al., 2008), DNA replication, DNA repair (Jentsch et al., 1987) and DNA damage response (Hochstrasser, 1996).

1.1.3 Examples of diseases associated with defective protein ubiquitylation

Aberrations in protein ubiquitylation have been associated with various diseases such as cancer, neurodegenerative or metabolic disorders, muscular atrophies and certain viral infections (reviewed by Petroski, 2008). For instance, mutations of RING-type ubiquitin ligases (E3s) or other alterations of their activity have been correlated with human cancers or inherited genomic instability disorders. Classic examples are the ubiquitin ligase BRCA1 and the FA complex. The former is mutated in familial breast and ovarian cancers (Welcsh and King, 2001), whereas mutations of the latter lead to defective monoubiquitylation of the substrate FANCD2, which results in Fanconi anaemia (Moldovan and D'Andrea, 2009). Mutations in the gene encoding the Parkin protein, a component of a multiprotein ubiquitin ligase complex, cause an autosomal recessive juvenile Parkinsonism (AR-JP) (Kitada et al., 1998). More examples on how the ubiquitin system is implicated in various diseases are presented in Table 1.

Table 1. Examples of an implication of ubiquitin system in disease pathways

Disease/ disorder	Defect/ impairment of the ubiquitin system	Key features
CANCERS:		
▪ Breast cancer	Mutation in BRCA1 ligase	Induction of proliferation
▪ Cervical cancer	Impairment of E6-AP ligase	Induction of proliferation
▪ Multiple myeloma	Increased proteasome activity	Suppression of apoptosis
▪ von Hippel-Lindau disease	Mutation in VHL ligase	Abnormal growth of tumours through the body
NEUROGENERATIVE DISORDERS:		
▪ Parkinson's disease	Mutation in Parkin ligase	Degenerative disorder of the central nervous system, primarily affects motor system
▪ Alzheimer's disease	Decreased proteasome activity	Dementia, β-amyloid plaques, neuronal loss
▪ Huntington's disease	Decreased proteasome activity	Neurodegenerative disorder affecting muscle coordination
OTHER DISEASES:		
▪ Fanconi anaemia	Mutation in the FA complex	Bonne marrow failure and aplastic anaemia
▪ Angelman syndrome	Mutation in the E6-AP ligase and aberrant accumulation of E6-AP substrates	Developmental disorder, causes intellectual disability and loss of speech
VIRAL INFECTIONS:		
▪ Human immunodeficiency virus (HIV)	Decreased expression and inhibition of proteasome	Impaired immune response
▪ Hepatitis B (HBV)	Proteasome inhibition	Severe liver infection
▪ Human T-cell lymphotropic virus (HTLV)	Proteasome activation	Neurological inflammation, leukaemia/lymphoma development

1.1.4 Ubiquitin

Ubiquitin (Ub) is a small 76-amino acids and 8.5 kDa globular, highly stable protein with an overall structure being 'extremely compact and tightly hydrogen-bonded'. Thanks to this compact globular structure, with an exposed C-terminal tail (COOH-terminus), Ub can form a covalent linkage with other proteins (Vijay-Kumar et al., 1987). Its surface is mainly polar, with a large hydrophobic area centered on the leucine 8 (Leu8), isoleucine 44 (Ile44), and valine 70 (Val70) residues (Beal et al., 1996) (Figure 2). Ubiquitin is present in all types of cells and tissues, with up to 10^8 copies per cell (Yewdell, 2001) and its cellular concentrations as high as ~85 µM (Kaiser et al., 2011). It is both a cytoplasmic and a nuclear protein (Lund et al., 1985).

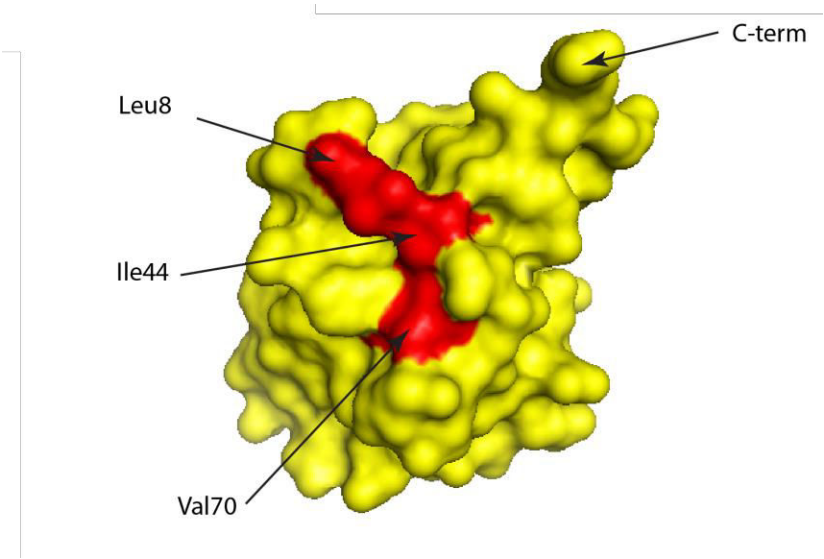

Figure 2. Ubiquitin structure (PDB ID: 1 UBQ) generated with PyMOL software (http://www.pymol.org/) with its hydrophobic patch (indicated in red) centered on the leucine 8 (Leu8), isoleucine 44 (Ile44), and valine 70 (Val70) and its C-terminal tail (C-term).

Ub demonstrates a high degree of conservation throughout the eukaryotic kingdom, with only three amino-acid changes from yeast to human (Weissman, 2001). Sequence alignment is shown in Figure 3. It appears to be absent in bacteria and *Archaea*. Yet, a ubiquitin-like conjugation system, termed pupylation with a ubiquitin-like protein – a 6.9 kDa Pup, was described in prokaryotic organisms (Pearce et al., 2008).

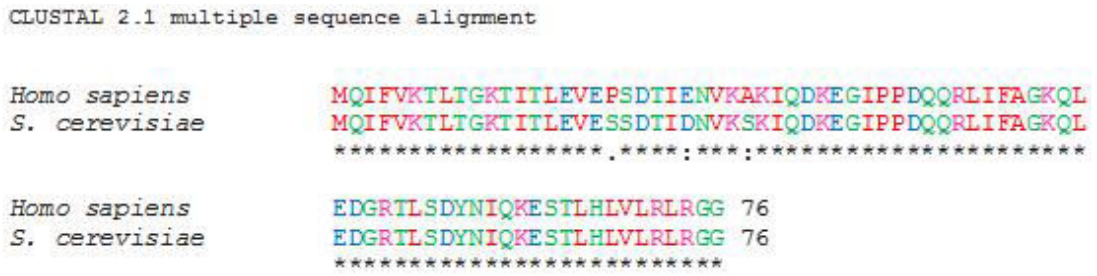

Figure 3. A protein sequence alignment of human and yeast ubiquitin produced by CLUSTALW2. Small, hydrophobic and aromatic amino acids are indicated in red, acidic amino acids in blue and basic amino acids in magenta. Green represents hydroxyl, amine, amide and basic residues. All identical amino acids in human and yeast are marked by asterisk. The differences in the sequence are marked with period (semi-conserved substitution) or colon (conserved substitutions). The sequences for the alignment were retrieved from PDB, accession number: AAA36789.1 and NP_013061.1 for human and yeast, respectively.

Nucleotide sequence analysis has shown that Ub is synthesized in the form of different precursors, which must subsequently be cleaved in order to release functional Ub units (Lund et al., 1985) (Figure 4). These precursors are a linear fusion protein consisting of four or more Ub copies (tandem Ub) and fusion proteins between Ub and ribosomal proteins (40S ribosomal protein L40 and 60S ribosomal protein S27) (Finley et al., 1989; Redman and Rechsteiner, 1989). The protein is encoded by four genes in mammals: *UBC, UBB, UBA52* and *UBA80*. The first two encode a tandem Ub (9 Ub units and 4 Ub units, respectively) and the last two encode fusions with ribosomal proteins (*UBA52* with L40 protein, whereas *UBA80* with S27) (Redman and Rechsteiner, 1989). In yeast there are also four Ub genes: *UBI1, UBI2, UBI3* and *UBI4* (Ozkaynak et al., 1987). *UBI1* and *UBI2* have non-homologous introns at the same positions and encode identical 52-residue tails. *UBI3* encodes a different 76-residue tail, whereas *UBI4* encodes a polyubiquitin precursor protein containing five Ub repeats (Ozkaynak et al., 1987). Interestingly, in yeast a single *UBI4* gene is not required under vegetative conditions. However, cells lacking *UBI4* are sensitive to high temperatures, starvation and other amino acid analogue-induced stresses (e.g. canavanine), and they are defective in sporulation (Finley et al., 1987).

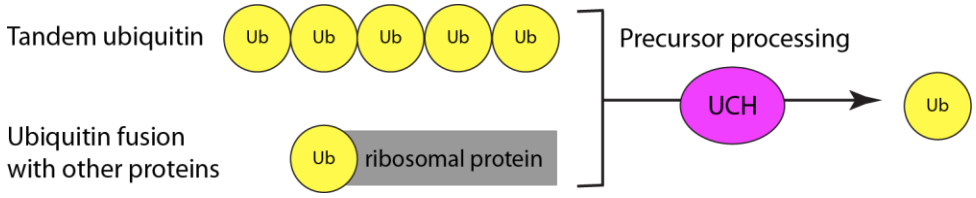

Figure 4. Ubiquitin is synthesized as a precursor. It is transcribed and translated as a linear fusion consisting of multiple copies of ubiquitin (tandem ubiquitin) or ubiquitin fused with other proteins (L40 or S27 ribosomal proteins). Generation of free ubiquitin is possible due to the action of deubiquitylating enzymes and more precisely ubiquitin C-terminal hydrolases (UCH).

1.1.5 Types of ubiquitylation and ubiquitin chain diversity

Ubiquitin, owing to its highly accessible C-terminal tail (COOH-terminus), is covalently attached via its glycine residue (Gly76) to the amino group (-NH_2) of lysine residues (Lys) in substrate proteins by the formation of an isopeptide bond. Types of ubiquitin modifications are immensely diverse (reviewed by Ikeda and Dikic, 2008; Kulathu and Komander, 2012) and form the so-called 'ubiquitin code' (Komander and Rape, 2012). The attachment to a substrate protein can be in either a monomeric or a polymeric form, monoubiquitylation or polyubiquitylation, respectively (Figure 5). Some substrates are modified with a single ubiquitin on several Lys residues. This is referred to as multiple monoubiquitylation, although the term multi-monoubiquitylation is also used (Hicke and Riezman, 1996; Haglund et al., 2003) (Figure 5).

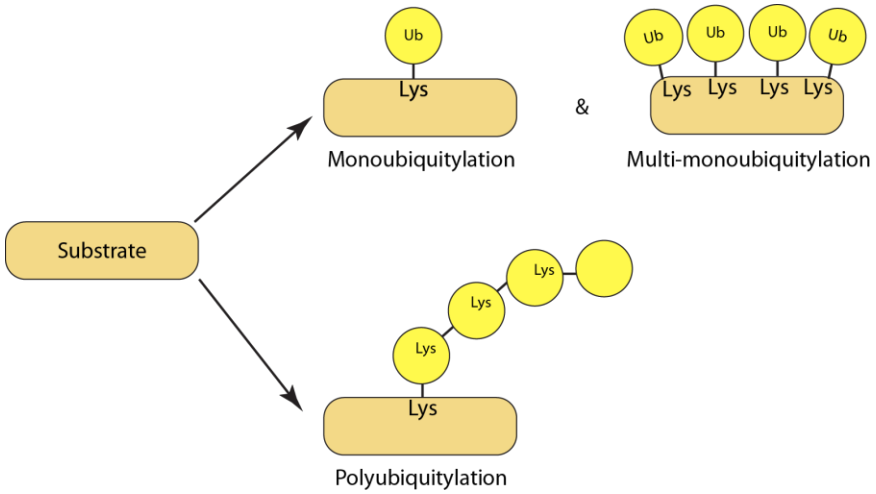

Figure 5. The different types of ubiquitylation. The attachment of a single ubiquitin to a substrate is known as monoubiquitylation, whereas multi-monoubiquitylation occurs when several single ubiquitin moieties are attached. The attachment of a series of ubiquitin molecules to a substrate protein known as polyubiquitylation.

1.1.5.1 Monoubiquitylation

The attachment of a single ubiquitin (monoubiquitin) to the substrate proteins is an important regulatory post-translational modification. It influences the activity of the substrates or their localization, and is therefore called a 'regulator of substrate-protein location and activity' (Hicke and Riezman, 1996). Monoubiquitylation is involved in various cellular functions, including endocytosis, histone regulation, and the budding of retroviruses from the plasma membrane (reviewed by Hicke, 2001). For example, an important role played by monoubiquitylation in histone function was first reported by Robzyk et al. (2000). Using budding yeast *S. cerevisiae*, they showed that yeast cells carrying the mutated histone H2B (predominantly ubiquitylated histone in yeast) lacking its ubiquitylation site, grow more slowly than wild-type cells and do not sporulate. They therefore concluded that monoubiquitylation of H2B is necessary for normal growth and meiosis (Robzyk et al., 2000). In addition, monoubiquitylation regulates the activity of the plasma membrane proteins by the endocytic pathway. Most of these proteins are then targeted for degradation in the lysosome (reviewed by Hicke, 2001). Haglund et al. (2003) noted that the epidermal growth factor (EGF) and platelet-derived growth factor receptors (PDGFRs) are monoubiquitylated at multiple sites following their ligand-induced activation, and that multi-monoubiquitylation is a main signal driving those receptor tyrosine kinases (RTKs) from the plasma membrane to the lysosome.

A principal model in the ubiquitin field is that contrary to polyubiquitylation, monoubiquitylation and multi-monoubiquitylation do not induce proteasomal degradation. This is due to the fact that an efficient proteasome binding and degradation requires at least four subunit-long ubiquitin chains (tetraubiquitin) (Thrower et al., 2000). However, several studies have shown that multi-monoubiquitylation and even monoubiquitylation can be sufficient to target some substrates for proteasomal degradation. For example, it has been demonstrated that it is multiple monoubiquitylation, rather than polyubiquitylation, which is responsible for processing the NF-κB transcription factor precursor p105 to its p50 active subunit by the proteasome. The proteasome recognizes the multiple monoubiquitylated p105 precursor. Interestingly and exceptionally in this case, the Ub system does not completely destroy its substrate. Nevertheless, this study suggests that not only a poly-Ub chain, but also a cluster of single ubiquitin, can control proteasomal processing (Kravtsova-Ivantsiv

et al., 2009). Other studies of the Pax3 protein, a key regulator of muscle differentiation, have also shown that it is monoubiquitylation which induces the proteasomal degradation (Boutet et al., 2010). Carvallo et al. (2010) reported that Syndecan4 (SDC4), a cell adhesion receptor required for cell migration, is monoubiquitylated in its cytoplasmic domain in the Wnt signaling pathway receptor Dishevelled (Dsh)-dependent manner and it is then degraded by the proteasome. Here however, the induction of the proteasomal degradation by monoubiquitylation has not been fully demonstrated.

1.1.5.2 Polyubiquitylation

All seven lysine residues (Lys6, Lys11, Lys27, Lys29, Lys33, Lys48 and Lys63) in Ub as well as N-terminal methionine (Met1) (Figure 6) are involved in the assembly of polyubiquitin chains, yielding a wide variety of structures (Peng et al., 2003; Xu et al., 2009). Current data demonstrate that Lys63, Lys48 and Lys11-linked polyubiquitin chains appear most frequent in budding yeast as well as in mammals. The level of Lys11-linked chains (29%) is equal of that of Lys48 chains (29%) and exceeding that of Lys63-linked chains (16%) (Figure 6). This indicates that the formation of polyubiquitin chains is a highly evolutionarily conserved mechanism (Peng et al., 2003; Xu et al., 2009).

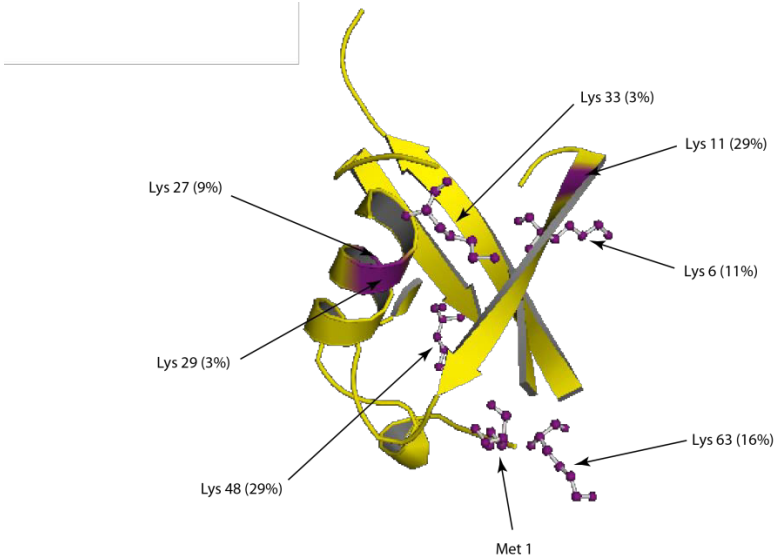

Figure 6. Ubiquitin structure (PDB ID: 1UBQ) with its seven lysine residues (Lys) and N-terminal methionine (Met1) generated with PyMOL software (http://www.pymol.org/).

Depending on the linkage, polymeric chains adapt alternative topologies. Chains linked via N-terminus or via one of the seven lysine residues of ubiquitin are homogenous, for example Met1-, Lys11-, Lys48-, or Lys63-linked chains. If different lysine residues are linked at subsequent positions in the chain, then it has a mixed topology (mixed-linkage chains). Moreover, one ubiquitin moiety linked with two or more ubiquitin molecules generates branched chains, whose function is still unknown (Komander and Rape, 2012) (Figure 7).

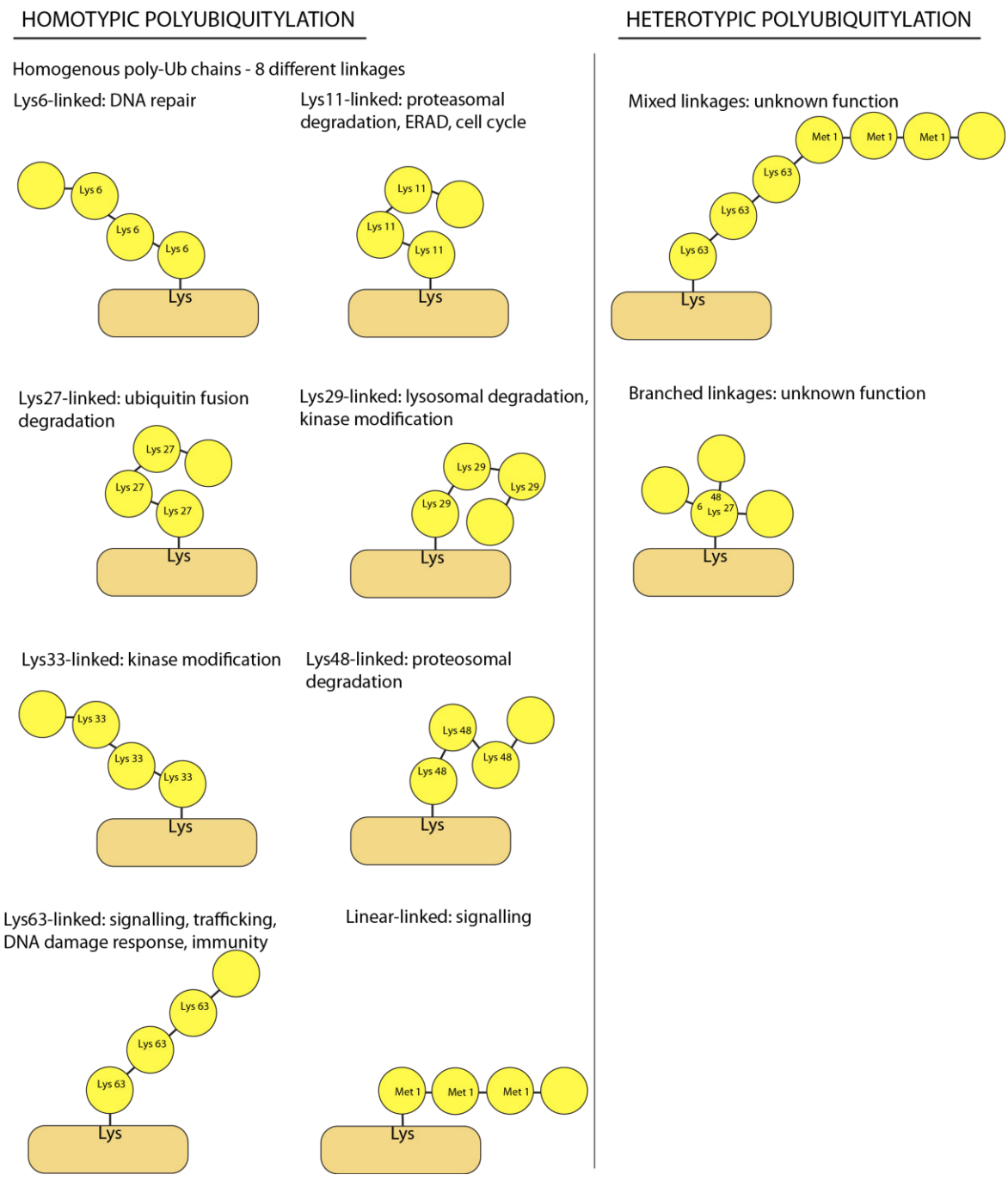

Figure 7. The different topologies of polyubiquitin chains with their main cellular functions.

Furthermore, different linkages result in specific chain conformations. Chains can either be 'compact', where neighboring molecules interact with one another, for example in the canonical Lys48-linked chains or Lys6 and Lys11, or adapt 'open' conformations, where there are no interactions between ubiquitin moieties. For instance, linear Lys63 and Met1-linked chains usually adapt an 'open' conformation. It is important to note, however, that the chain conformations observed in Ub-interacting protein complexes are frequently different from those observed in isolation. This suggests either a considerable dynamic flexibility of the chains or vast chain remodeling consequent to binding (Yu Ye et al., 2012). The study conducted by Peng et al. (2003) provided first evidence of a great diversity of polyubiquitin chains *in vivo*. Using a multidimensional liquid chromatography coupled with tandem mass spectrometry (LC/LC-MS/MS), they showed that all seven Lys residues can be used to assemble poly-Ub chains *in vivo* in *S. cerevisiae* (Peng et al., 2003). The physiological relevance of all poly-Ub chains combinations remains to be revealed. Another issue that remains to be resolved is the following: where and how are the ubiquitin chains assembled? The majority of experimental evidence suggests that chains are assembled on the substrate sequentially (i.e. initial substrate-attached ubiquitin is added what is followed by a stepwise addition of other single Ub moieties). Nonetheless, there is also evidence for chains being preassembled on E2s or E3s and then transferred as a whole to the substrates (Wang and Pickart, 2005; Li et al., 2007; Ravid and Hochstrasser, 2007).

Conjugation of polyubiquitin chains to proteins is crucial in regulating functions of many of these proteins (Figure 7). The formation of poly-Ub chains has mainly been implicated in targeting to 26S proteasome and giving a so-called, 'kiss of death' to proteins. A classic example are Lys48-linked chains, which are associated with proteasomal degradation (reviewed by Finley, 2009). On the contrary, Lys63-linked chains have been implicated in a variety of non-proteolytic functions (reviewed by Haglund and Dikic, 2005). Matsumoto et al. (2010) demonstrated that Lys11-chains are involved in the cell cycle and are abundant in mitotic cells during the degradation of the substrates of E3 ligase APC complex. This suggests that the chain assembly can provide cell-specific ubiquitome pattern (Matsumoto et al., 2010). Lys11-linked chains were also shown to play a role in the endoplasmic reticulum-associated degradation (ERAD) pathway (Xu et al., 2009). In addition, polyubiquitylation has been involved in inflammatory, anti-apoptotic and immune signaling processes (Tokunaga et al., 2009).

1.1.6 Mechanism of ubiquitylation

The attachment of ubiquitin to a substrate is catalyzed via a cascade of enzymatic reactions involving E1, E2 and E3s. The first step, the so-called initial activation, consists in the activation of the C-terminal glycine (Gly76) of ubiquitin by a ubiquitin activating enzyme (E1) in an ATP-dependent manner. In the intermediate step the activated ubiquitin is transferred from an E1 to the cysteine (Cys) residue within an active site of a ubiquitin conjugating enzyme (E2). Next, the E2 interacts with a ubiquitin ligase (E3), which recognizes both the E2 and a substrate, subsequently enabling the ubiquitin to become covalently attached to a substrate protein (Figure 8). During these final step reactions, the carboxyl group (-COOH) of the C-terminus of Ub and the amino group ($-NH_2$) of a lysine (Lys) residue within the substrate are linked by an isopeptide bond. The particular class of E3s, involved in ubiquitylation and more precisely in the elongation of Ub chains via the ligation of Ub to pre-existing poly-Ub chains, was also described and is referred to very often as E4 enzymes (Koegl et al., 1999; Pickart and Eddins, 2004). The mechanism of ubiquitylation is reversible through the action of so-called deubiquitylating enzymes (DUBs).

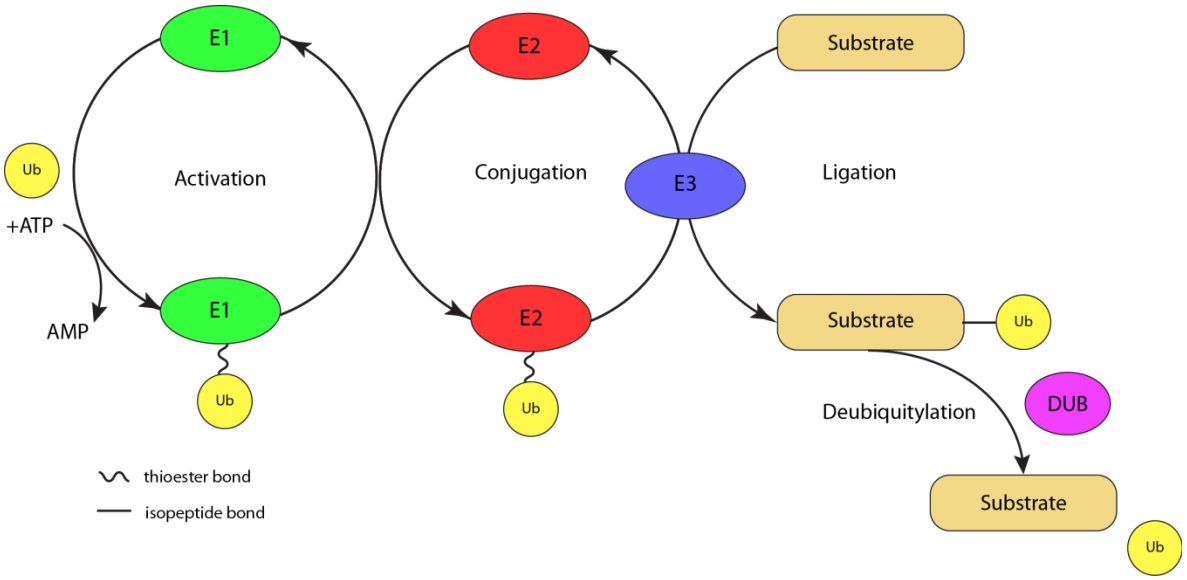

Figure 8. The schematic representation of the ubiquitylation process. Ubiquitin is activated by a Ub activating enzyme (E1) in an ATP-dependent manner, and then transferred into a ubiquitin conjugating enzyme (E2). E2 interacts with a ubiquitin ligase (E3), which enables Ub to be covalently attached to the substrate protein. The process is reversible through the action of deubiquitylating enzymes (DUB).

Apart from a typical attachment to Lys, it has been shown that Ub can also be attached to the substrates through serine (Ser), threonine (Thr) and cysteine (Cys) residues via the formation of oxyester or thioester bonds, respectively. For instance, in

yeast a conserved Cys residue is important for Pex4 (Ubc10) protein-dependent ubiquitylation of the peroxisomal import receptor Pex5 (Williams et al., 2007). Viral E3 ubiquitin ligases MIR1 and MIR2, which mediate ubiquitylation of major histocompatibility complex class I (MHC I), also target a Cys residue in the MHC I molecules (Cadwell and Coscoy, 2005; Cadwell and Coscoy, 2008). Another viral E3 ligase mK3 was shown to mediate Ub by its attachment to the Ser and Thr residues, except in the case of the conventional Lys linkage (Wang et al., 2007; Herr et al., 2009). In addition to conjugation to the amino acid side chains, Ub can also be attached to the amino group ($-NH_2$) at the N-terminal of certain substrate proteins (Breitschopf et al., 1998; Ciechanover and Ben-Saadon, 2004). Examples here are the latent membrane proteins LMP1 and LMP2A of the Epstein-Barr virus (EBV) that are ubiquitylated on their N-terminus rather than on the canonical Lys residues (Aviel et al., 2000; Ikeda et al., 2002). Interestingly, Scaglione et al. (2013) recently reported Ube2w as the first identified E2 that transfers ubiquitin to the N-terminal of substrates.

1.1.7 Ubiquitin activating enzymes (E1s)

The ubiquitin activating enzyme (E1) catalyzes the first step in the ubiquitylation cascade. Two members of the E1 enzymes exist in human and only one in yeast. In human this is Ube1, called Uba1 in yeast, and Uba6 (also called UBE1L2 in human) (Pelzer et al., 2007). Both enzymes, Uba1 and Uba6, share only 40% sequence identity (Jin et al., 2007). Uba1 is highly conserved in human, plants and yeast, whereas Uba6 is present only in vertebrates. Uba1 activates Ub and other ubiquitin-like proteins (Ulbs), whereas Uba6 can only activate Ub and the ubiquitin-like protein called FAT10 (Pelzer and Groettrup, 2010). Ub activation rates *in vitro* between these two enzymes are comparable. In the cell however, Uba6 is around 10-fold less abundant than Uba1 (Jin et al., 2007). Uba6 enzyme has been found to function in conjugation with an E2 enzyme Use1, while Uba1 functions with the other E2s (Aichem et al., 2010; Lee et al., 2011).

To date, the ubiquitin activating enzyme Uba1 (Ube1) has the best characterized mechanism of action (Figure 9). It has two active sites and can activate the carboxy-terminal glycine of ubiquitin via a two-step intramolecular ATP-dependent reaction. In the first step, E1 catalyzes the activation of Ub to a high energy adenylate intermediate with inorganic pyrophosphate (PPi) from ATP. The intermediate is then converted to

form AMP and a covalent E1~Ub thioester. Subsequently, a second Ub molecule is activated and bound to another site of the same E1. This forms a ternary complex, where a fully loaded E1 carries two Ub moieties, one as adenylate and the other as thioester. The double-Ub-bond E1 associates with an E2, and upon transthiolation reaction the Ub is transferred from the catalytic cysteine of E1 onto the catalytic cysteine of E2. Next, the Ub noncovalently attached as adenylate can be transferred to the downstream enzymes (Haas and Rose, 1982; Dye and Schulman, 2007).

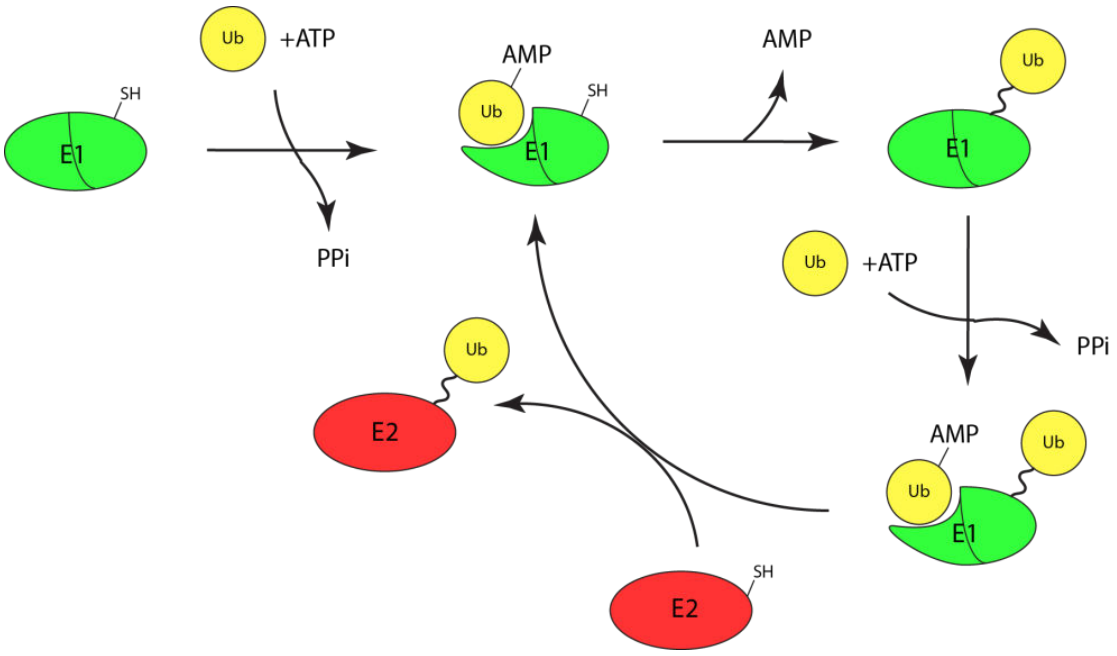

Figure 9. The mechanism of action of the ubiquitin conjugating enzyme (E1). SH refers to the free form of the catalytic cysteine, S~Ub represents the thioester bond between the catalytic cysteine and the C-terminal of ubiquitin, and PPi refers to inorganic pyrophosphate.

1.1.8 Ubiquitin conjugating enzymes (E2s)

Central in the hierarchical network of ubiquitylation enzymes is the family of ubiquitin-conjugating enzymes (E2s) that, together with the ubiquitin ligases (E3s), form a ubiquitin code writing machinery. These enzymes have the ability to interact with E1 activating enzyme and then form a highly-energetic conjugate with ubiquitin or ubiquitin-like proteins (Ubls). They influence the type of lysine used for substrate labeling, and therefore the fate of the substrate itself. The family is characterized by a highly conserved ~150-200 amino acid residue catalytic domain called ubiquitin binding domain (UBC), with conserved cysteine residue shared by all catalytically active E2s (VanDemark and Hill, 2002; Burroughs et al., 2008). Structurally, the UBC domain consists of N-terminal α-helix followed by a four stranded anti-parallel β-sheet. Some E2s have N-terminal or C-terminal extensions to their catalytic core and/or insertions into it. The E2 enzyme family can therefore be divided up according to the existence of these additional extensions (Table 2). The E2s that consist only of the catalytic UBC domain are in class I. Those in classes II and III have N- or C-terminal extensions, respectively, while class IV contains E2s with extensions on both terminals (van Wijk and Timmers, 2010). These sequence extensions result in functional differences between E2s that mainly involve their subcellular localization, stabilization of the E1/E2 interaction and E2/E3 interaction activity modulation. For example, the C-terminal extension of yeast Cdc34 E2 (residues 171-295) is a binding domain for Cdc4 and Cdc53 proteins – components of the SCF (Cdc4) ubiquitin ligase complex (Mathias et al., 1998). The yeast Ubc6 protein involved in the endoplasmic reticulum-associated degradation (ERAD), in addition to the catalytic core, has its transmembrane domain located at the C-terminus that contains hydrophobic amino acids. This 95 amino acid residues extension determines Ubc6 subcellular location at the cytosolic side of the endoplasmic reticulum membrane (Yang et al., 1997; Lenk et al., 2002). Lenk and colleagues (2002) identified and functionally characterized two distinct families of Ubc6 orthologues in mammals, Ubc6 and Ubc6e (Figure 10). Both families share significant sequence similarities with yeast Ubc6 enzyme and have analogous structural organization with their UBC domains (55.5% sequence identity between yeast and human) and tail-anchored protein motifs, consisting of hydrophobic amino acids (Lenk et al., 2002).

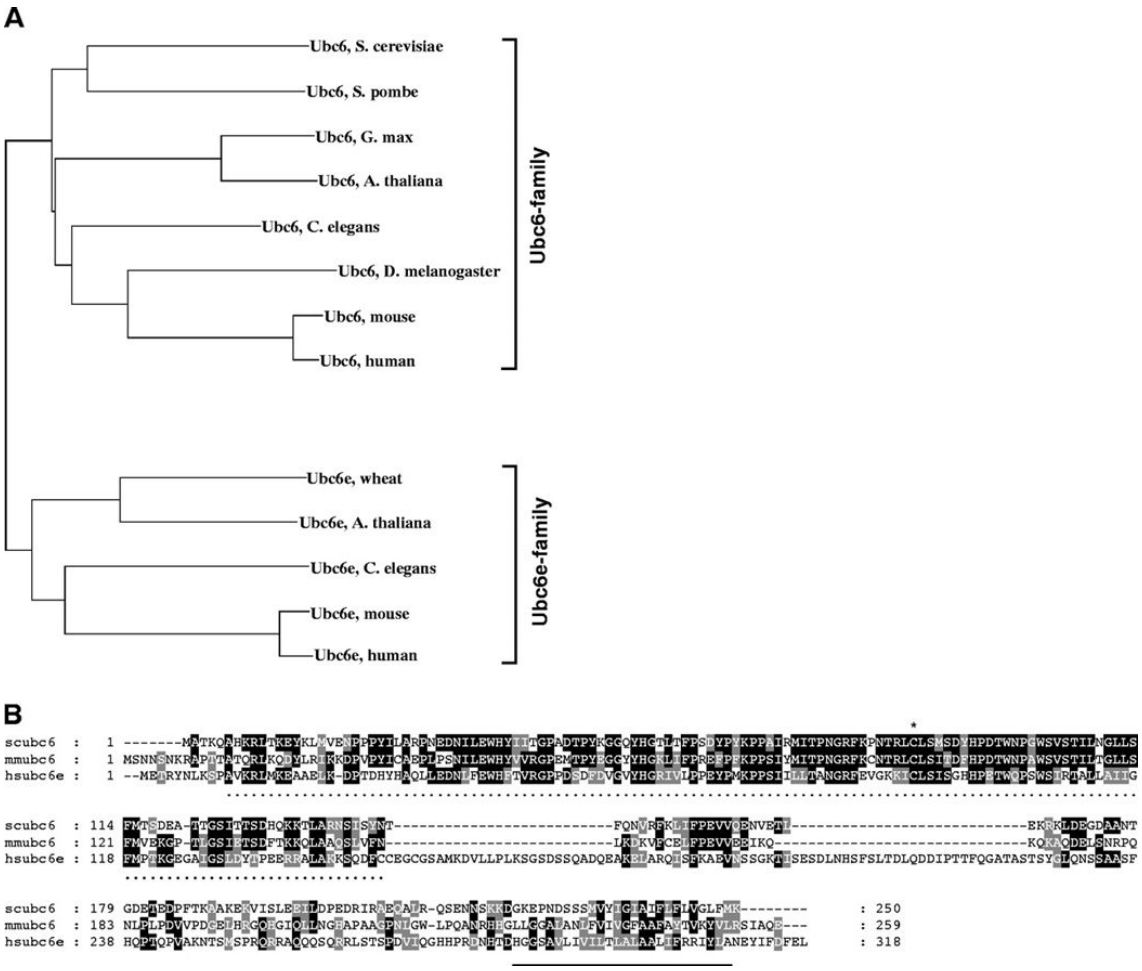

Figure 10. Phylogenetic analysis demonstrating two families of Ubc6 enzymes and protein sequence alignment of yeast mouse and human Ubc6. A) Two classes of Ubc6-related proteins, Ubc6 and Ubc6e. Ubc6e is not found in yeast and *D. melanogaster.* B) Comparison of the amino acid sequences of *S. cerevisiae* Ubc6, mouse Ubc6 and human Ubc6e. The CLUSTAL alignment shows the well-conserved N-terminal UBC domain (marked by a dotted line) and the less conserved C-terminal tail region containing the transmembrane segment in both Ubc6 families. Asterisk indicates the conserved active site cysteine. The region of the membrane spanning domains is underlined (adapted with permission from: Lenk et al., *Journal of Cell Science*, 2002).

All eukaryotes possess several E2s ranging from 8 in organisms such as *Giardia lamblia* to over 50 in multicellular plants and animals (Burroughs et al., 2008). There are eleven E2s that form thiolesters with Ub identified in *S. cerevisiae* (Pickart and Eddins, 2004) (Table 2). Sequence alignments and phylogenetic analysis of eleven yeast E2s are presented in Figure 11. No enzymes that possess the UBC-folds are present in bacteria (Iyer et al., 2008). The number variability amongst E2s within different organisms is mainly the result of gene duplication. For instance, the highly similar enzymes Ubc4 and Ubc5 in yeast *S. cerevisiae* that are involved in the degradation of abnormal or excess proteins are found to be UbcH5A-D (UBE2B1-4), UbcH6, UbcH8

and UbcH9 (UBE2E1-3) in higher eukaryotes (Seufert and Jentsch, 1990). Some E2s seem to be specific to higher eukaryotes. For example, UBE2U has only been identified in mammals, and the enormous 528 kDa E2 BIRC6 (BRUCE) has been found in *Drosophila*, mice and humans, whereas it is absent in *C. elegans* and yeast (Bartke et al., 2004; Lotz et al., 2004). Several of yeast E2s have a high expression level, however, the expression vary amongst different family members (personal observation).

Table 2. Ubiquitin conjugating enzymes in yeast (Data retrieved from: *Saccharomyces* Genome Database)

Standard gene name	Systematic name	Class	Size (aa)	Molecular weight (~kDa)	Subcellular localization (with GFP)	Main functions
Ubc1	YDR177W	Core	215	24	Cytoplasm Nucleus	Selective degradation of short-lived and abnormal proteins, ERAD, vesicle biogenesis
Ubc2 (Rad6)	YGL058W	C-term extension	172	20	Cytoplasm Nucleus	DNA repair, ERAD, ubiquitin-mediated N-end rule protein degradation
Ubc3 (Cdc34)	YDR054C	N- and C-term extensions	295	34	Cytoplasm Nucleus	Cell cycle control
Ubc4	YBR082C	Core	148	16	Cytoplasm Nucleus	Selective degradation of abnormal or excess proteins, involved in DNA replication, component of cellular stress response
Ubc5	YDR059C	Core	148	16	Cytoplasm Nucleus	Selective degradation of short-lived, abnormal or excess proteins, central component of cellular stress response
Ubc6	YER100W	C-term extension	250	28	ER	ERAD
Ubc7 (Qri8)	YMR022W	Core	165	19	ER	ERAD, proposed to be involved in chromatin assembly
Ubc8 (Gid3)	YEL012W	Core	218	25	Cytoplasm Nucleus	Gluconeogenesis regulation
Ubc10 (Pex4)	YGR133W	Core	183	21	Peroxisome	Peroxisomal matrix protein import and peroxisome biogenesis
Ubc11	YOR339C	C-term extension	156	18	Not visualized	Cell cycle regulation
Ubc13	YDR092W	Core	153	17	Cytoplasm	Involvement in the DNA post-replication repair pathway

A

```
UBC4    ----------MSSSKRIAKELSDLE--RDPPT---------SCSAGPVG-DDLYH 33
UBC5    ----------MSSSKRIAKELSDLG--RDPPA---------SCSAGPVG-DDLYH 33
UBC1    ----------MSRAKRIMKEIQAVK--DDPAA---------HITLEFVSESDIHH 34
UBC13   ----------MASLPKRIIKETEKLV--SDPVP---------GITAEPHD-DNLRY 34
UBC8    ----------MSSSKRRIETDVMKLL--MS-----------DHQVDLIN-DSMQE 31
CDC34   ---------MSSRKSTASSLLLRQYRELTDPKKAIP---------SFHIELEDDSNIFT 41
UBC7    ---------MS---KTAQKRLLKELQQLI--KDSPP---------GIVAGPKSENNIFI 36
RAD6    ---------MS---TPARRRLMRDFKRMK--EDAPP---------GVSASPLPDN-VMV 35
UBC11   --------MAVEEGGCVTKRLQNELLQLLS--STTE---------SISAFPVDDNDLTY 40
UBC6    ----------MATKQAHKRLTKEYKLMVE--NPPP---------YILARPNE-DNILE 36
PEX4    MPNFWILENRRSYTSDTCMSRIVKEYKVILKTLASDDPIANPYRGIIESLNPIDETDLSK 60
                             :  :   :                          :

UBC4    WQASIMGP-ADSPYAGGVFFLSIHFPTDYPFKPPKISFTT--KIYHPNIN-ANGNICLDI 89
UBC5    WQASIMGP-SDSPYAGGVFFLSIHFPTDYPFKPPKVNFTT--KIYHPNIN-SSGNICLDI 89
UBC1    LKGTFLGP-PGTPYEGGKFVVDIEVPMEYPFKPPKMQFDT--KVYHPNISSVTGAICLDI 91
UBC13   FQVTIEGP-EQSPYEDGIFELELYLPDDYPMEAPKVRFLT--KIYHPNID-RLGRICLDV 90
UBC8    FHVKFLGP-KDTPYENGVWRLHVELPDNYPYKSPSIGFVN--KIFHPNIDIASGSICLDV 88
CDC34   WNIGVMVLNEDSIYHGGFFKAQMRFPEDFPFSPPQFRFTP--AIYHPNVY-RDGRLCISI 98
UBC7    WDCLIQGP-PDTPYADGVFNAKLEFPKDYPLSPPKLTFTP--SILHPNIY-PNGEVCISI 92
RAD6    WNAMIIGP-ADTPYEDGTFRLLLEFDEEYPNKPPHVKFLS--EMFHPNVY-ANGEICLDI 91
UBC11   WVGYITGP-KDTPYSGLKFKVSLKFPQNYPFHPPMIKFLS--PMWHPNVD-KSGNICLDI 96
UBC6    WHYIITGP-ADTPYKGGQYHGTLTFPSDYPYKPPAIRMITPNGRFKPN-----TRLCLSM 90
PEX4    WEAIISGP-SDTPYENHQFRILIEVPSSYPMNPPKISFMQN-NILHCNVKSATGEICLNI 118
            .      : * .  :   : .  .:*  .* . :       : *       :*:.:

UBC4    LKD-------------QWSPALTLS-KVLLSICSLLTDANPDD---PLVPEIAHIYKT-D 131
UBC5    LKD-------------QWSPALTLS-KVLLSICSLLTDANPDD---PLVPEIAQIYKT-D 131
UBC1    LKN-------------AWSPVITLK-SALISLQALLQSPEPND---PQDAEVAQHYLR-D 133
UBC13   LKT-------------NWSPALQIR-TVLLSIQALLASPNPND---PLANDVAEDWIK-N 132
UBC8    INS-------------TWSPLYDLINIVEWMIPGLLKEPNGSD---PLNNEAATLQLR-D 131
CDC34   LHQSGD-PMTDEPDAETWSPVQTVE-SVLISIVSLLEDPNINS---PANVDAAVDYRK-N 152
UBC7    LHSPGDDPNMYELAEERWSPVQSVE-KILLSVMSMLSEPNIES---GANIDACILWRD-N 147
RAD6    LQN-------------RWTPTYDVA-SILTSIQSLFNDPNPAS---PANVEAATLFKD-H 133
UBC11   LKE-------------KWSAVYNVE-TILLSLQSLLGEPNNRS---PLNAVAAELWDA-D 138
UBC6    SDYHP----------DTWNPGWSVS-TILNGLLSFMTSDEATTGSITTSDHQKKTLAR-N 138
PEX4    LKP------------EEWTPVWDLL-HCVHAVWRLLREPVCDS---PLDVDIGNIIRCGD 162
         .              *..   :       :  :: .                    .

UBC4    RPKYEATAREWTKKYAV------------------------------------------ 148
UBC5    KAKYEATAKEWTKKYAV------------------------------------------ 148
UBC1    RESFNKTAALWTRLYASETSNGQKGNV--------EESDLYGIDHDLIDEFESQGFEKDK 185
UBC13   EQGAKAKAREWTKLYAKKKPE------------------------------------- 153
UBC8    KKLYEEKIKEYIDKYATKEKYQQMFGGDNDSDDSDSGGDLQEEDSDSDEDMDGTGVSSGD 191
CDC34   PEQYKQRVKMEVERSKQDIPKGFIMPTSESAYISQSKLDEPESNKDMADNFWYDSDLDDD 212
UBC7    RPEFERQVKLSILKS-----LGF------------------------------------ 165
RAD6    KSQYVKRVKETVEKS-----------------------------------WEDDMDDM 156
UBC11   MEEYRKKVLACYEEIDDY------------------------------------------ 156
UBC6    SISYNTFQNVRFKLIFPEVVQENVETLEKRKLDEGDAANTGDETEDPFTKAAKEKVISLE 198
PEX4    MSAYQGIVKYFLAERERINNH-------------------------------------- 183


UBC4    ------------------------------------------------------------
UBC5    ------------------------------------------------------------
UBC1    IVEVLRR--------------------------LGVKSLDPNDNNTANRIIEELLK--- 215
UBC13   ------------------------------------------------------------
UBC8    DSVDELS--------------------------EDLSDIDVSDDDDYDEVANQ------ 218
CDC34   ENGSVILQDDDYDDGNNHIPFEDDDVYNYNDNDDDDERIEFEDDDDDDDDSIDNDSVMDR 272
UBC7    ------------------------------------------------------------
RAD6    D-------------------------------DDDD------DDDDDDDDEAD------- 172
UBC11   ------------------------------------------------------------
UBC6    EILDPEDR---------------------IRAEQALRQSENNSKKDGKEPNDSSSMVYI 236
PEX4    ------------------------------------------------------------


UBC4    ----------------------
UBC5    ----------------------
UBC1    ----------------------
UBC13   ----------------------
UBC8    ----------------------
CDC34   KQPHKAEDESEDVEDVERVSKKI 295
UBC7    ----------------------
RAD6    ----------------------
UBC11   ----------------------
UBC6    GIAIFLFLVGLFMK--------- 250
PEX4    ----------------------
```

B

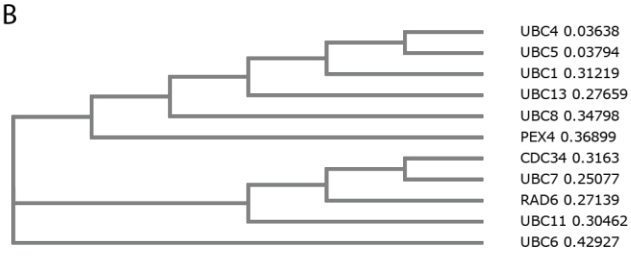

Figure 11. Sequence alignments and phylogenetic analysis of eleven yeast E2s. A) Protein sequence alignments performed with CLUSTALW2. Small, hydrophobic and aromatic amino acids are indicated in red, acidic amino acids in blue and basic amino acids in magenta. Green represents hydroxyl, amine, amide and basic residues. Asterisks and dots indicate identical and conserved amino acids, respectively. The differences in the sequence are marked with period (semi-conserved substitution) or colon (conserved substitutions). The sequences for the alignment were retrieved from *Saccharomyces* Genome Database. B) Phylogenetic tree of yeast E2s generated with CLUSTALW2. A cladogram showing branching patterns.

Polyubiquitin chain synthesis is associated with the function of specific E2s, and it is the combination of E2/E3 pairs that determines the Ub chains' linkages (Kirkpatrick et al., 2006; Kim et al., 2007; Jin et al., 2008; Xu et al., 2009). A well-known example of a single E2 that synthesizes primarily Lys48-linked poly-Ub chains is yeast Cdc34 (Ubc3) (Petroski and Deshaies, 2005). Petroski and Deshaies (2005) demonstrated that mutations of an acidic loop region of Cdc34 affect the linkage specificity and the processivity of Lys48 ubiquitin chain synthesis. Yeast Ubc6 mainly synthesizes Lys11-linked chains, and these linkages function in the endoplasmic reticulum-associated degradation (ERAD) pathway (Xu et al., 2009). Similarly to its yeast homolog, human Ubc6 (called also UBE2J2) was shown to functionally interact with a number of E3, and to be invlved in the regularion of its own proteosomal degradation (Lam et al., 2014). Interestingly, two E2 enzymes can act on a single target protein to synthesize the chain, with one enzyme as an initiator of chain formation and the other extending it. Examples to illustrate this mechanism are provided by yeast Ubc4 and Ubc1, which drive polyubiquitin chain assembly on the anaphase promoting complex/cyclosome (APC/C) targets (Rodrigo-Brenni and Morgan, 2007). Similarly, several E2s working with a heterodimeric human E3 ligase BRCA1-BARD1, including UBE2W and UBE2E2, are responsible for Ub chain initiation, while the heterodimer UBE2N–UBE2V1 and UBE2K function specifically in chain elongation (Christensen et al., 2007). In human, BRCA1, which in complex with BARD1 possesses ubiquitin-ligase activity, has the ability to catalyze Lys6-linked Ub chains (Wu-Baer et al., 2003).

1.1.9 Ubiquitin ligases (E3s)

The final step of ubiquitylation cascade is the transfer of Ub onto the substrate proteins mediated by ubiquitin ligases (E3s). To mediate this transfer, E3s interact with ubiquitin-loaded E2 enzymes and are able to recognize and bind particular substrates. Two major mechanistically distinct families of E3s have been identified, RING finger E3s that transfer ubiquitin directly from E2 to the substrate protein, and HECT domain E3s that facilitate ubiquitin transfer to the substrate via the formation of a covalent ubiquitin-E3 thioester intermediate (Scheffner et al., 1995). Moreover, another important family of mechanistically distinct Ub ligases is known as the RBR (RING-Between-RING-RING) or TRIAD (two RING fingers and a DRIL, i.e. double RING finger-linked). This family uses a combination of the RING and HECT ligases mechanisms to mediate the Ub transfer onto the substrate (Wenzel et al., 2011). The mechanism of Ub transfer by different E3 families is presented later in Figure 12.

The human genome encodes more than 600 E3s and substrate recognition subunits of E3 complexes, making the number of putative E3 genes even greater than the number of genes encoded for protein kinases. Approximately 95% of all putative E3s were found to be RING finger-dependent (Li et al., 2008). The numbers of putative ubiquitin ligases in both human and yeast are presented in Table 3, and the putative ubiquitin ligases in yeast along with their main functions are presented in Table 4.

Table 3. Numbers of ubiquitin ligases encoded by *H. sapiens* and *S. cerevisiae* genomes based on the presence of 'catalytic' domains

Catalytic subunit of E3s	Human	Yeast
RING		
▪ RING	~300	~50
▪ U-box	9	2
HECT	28	5
RBR	13	2

Table 4. The main known or putative ubiquitin ligases and components of E3 complexes in yeast (Data retrieved from: *Saccharomyces* Genome Database)*

Standard gene name	Systematic name	Size (aa)	Molecular weight (~kDa)	Subcellular localization (with GFP)	Main functions and/or unique features
E3s with a RING catalytic subunit:					
Air1	YIL079C	360	42	Cytoplasm Nucleus	Putative E3, nuclear RNA processing and degradation
Air2	YDL175C	344	39	Nucleus	Putative E3, nuclear RNA processing and degradation
Asi1	YMR119W	624	71	Nuclear periphery	Subunit of Asi Ub ligase complex that targets misfolded proteins and regulators of sterol biosynthesis for degradation; SPS-sensor signaling of amino acids
Asi3	YNL008C	676	78	Nuclear periphery	Subunit of Asi Ub ligase complex that targets misfolded proteins and regulators of sterol biosynthesis for degradation; SPS-sensor signaling of amino acids
Asr1	YPR093C	288	33	Not visualized	Modification and regulation of RNA Pol II, alcohol stress response
Bre1	YDL074C	700	81	Nucleus	Monoubiquitylation of histone H2B on Lys123
Cwc24	YLR323C	259	30	Nucleus	Involvement in splicing
Dma1	YHR115C	416	46	Ambiguous	Septin dynamics control, spindle positioning
Dma2	YNL116W	522	58	Cytoplasm	Septin dynamics control, spindle positioning
Doa10 (Ssm4)	YIL030C	1319	151	ER	ERAD
Etp1	YHL010C	585	67	Not visualized	Required for growth in ethanol
Fap1	YNL023C	965	109	Not visualized	Response to rapamycin
Far1	YJL157C	830	95	Nucleus	Cyclin dependent kinase inhibitor and nuclear anchor
Gid9 (Fyv10)	YIL097W	516	60	Nucleus	Subunit of GID complex, involved in ubiquitin ligation as a dimer with Rmd5
Hel2	YDR266C	639	73	Cytoplasm	Ubiquitylation and degradation of excess histones
Hrd1	YOL013C	551	64	ER	ERAD
Hrt1	YOL133W	121	14	Not visualized	Subunit of multiple ubiquitin ligase complexes, involvement in cell cycle
Irc20	YLR247C	1556	180	Nucleus	Putative E3, synthesis-dependent strand annealing-mediated homologous recombination, ensures precise end-joining, has helicase domain
Mag2	YLR427W	670	76	Cytoplasm	Unknown function, predicted to be involved in repair of alkylated DNA
Mot2 (Not4)	YER068W	587	65	Cytoplasm	Subunit of Ccr4-Not complex, involved in ubiquitylation of nascent polypeptide-associated complex (NAC) subunits and histone demethylase Jhd2p, transcription regulation
Mtc5	YDR128W	1148	131	Vacuolar membrane	Subunit of the SEA (Seh1-associated) complex, has N-terminal WD-40 repeats and a C-terminal RING motif
Nam7 (Upf1)	YMR080C	971	109	Cytoplasm	Nonsense mediated mRNA decay, required for efficient translation termination at nonsense codons
Pep3	YLR148W	918	107	Endosome	Vacuolar biogenesis
Pep5	YMR231W	1029	117	Endosome	Protein trafficking and vacuole biogenesis, involved in ubiquitylation and degradation of excess histones
Pex2	YJL210W	271	31	Peroxisome	Peroxisomal matrix protein import
Pex10	YDR265W	337	39	Peroxisome	Peroxisomal matrix protein import, Ubc4-dependent Pex5 ubiquitylation
Pex12	YMR026C	339	46	Peroxisome	Peroxisome biogenesis and peroxisomal matrix protein import
Pib1	YDR313C	286	33	Endosome	Phosphatidylinositol(3)-phosphate binding
Psh1	YOL054W	406	47	Nucleus	Polyubiquitylation and degradation of centromere-binding protein Cse4
Rad5	YLR032W	1169	134	Cytoplasm Nucleus	Postreplication repair, DNA damage tolerance, PCNA polyubiquitylation
Rad16	YBR114W	790	91	Cytoplasm Nucleus	Nucleotide excision repair
Rad18	YCR066W	487	55	Not visualized	Postreplication repair, PCNA monoubiquitylation
Rkr1 (Lnt1)	YMR247C	1562	180	Not visualized	Ubiquitin-mediated degradation of proteins translated from nonstop mRNAs
Rmd5 (Gid2)	YDR255C	421	49	Not visualized	Gluconeogenesis, polyubiquitylation and degradation of the gluconeogenic enzyme fructose-1,6-bisphosphatase
Rtc1 (Sea2)	YOL138C	1341	149	Vacuole	Subunit of the SEA (Seh1-associated) complex that associates dynamically with the vacuole
San1	YDR143C	610	66	Not visualized	Proteasome-dependent degradation of aberrant nuclear proteins
Ssl1	YLR005W	461	52	Nucleus	Subunit of the core form of RNA polymerase transcription factor TFIIH, transcription and nucleotide excision repair
Slx5 (Hex3)	YDL013W	619	71	Not visualized	Subunit of the Slx5-Slx8 SUMO-targeted ubiquitin ligase complex, genotoxic stress response

Slx8	YER116C	274	31	Cytoplasm Nucleus	Subunit of the Slx5-Slx8 SUMO-targeted ubiquitin ligase complex, genotoxic stress response
Snt2	YGL131C	1403	163	Cytoplasm Nucleus	Degradation of excess histones, role in regulating genes encoding amine transporters
Ste5	YDR103W	917	103	Cytoplasm Nucleus	Pheromone-responsive MAPK scaffold protein
Tfb3	YDR460W	321	38	Nucleus	Transcription initiation, nucleotide excision repair, Cul and Rtt101 needylation
Tul1	YKL034W	758	88	Not visualized	Membrane proteins sorting
Ubr1	YGR184C	1950	225	Not visualized	Ubiquitylation of substrates in the N-end rule pathway as heterodimer with Rad6, ERAD, targeting misfolded cytosolic proteins for degradation
Ubr2	YLR024C	1872	217	Cytoplasm	Ubiquitylation of Rpn4 protein
Uls1 (Ris1)	YOR191W	1619	184	Nucleus	SUMO-Targeted Ubiquitin Ligase (STUbL) with a translocase activity, antagonizing silencing during mating-type switching
Vps8	YAL002W	1274	145	Endosome	Putative E3, membrane-binding component of the CORVET complex, endosomal vesicle tethering and fusion in the endosome to vacuole protein targeting pathway
Yvh1	YIR026C	364	41	Cytoplasm	Putative E3, protein phosphatase, involved in vegetative growth at low temperatures, sporulation and glycogen accumulation
-	YBR062C	180	21	Not visualized	Putative E3, unknown function, may play a role in activation of the filamentous growth pathway
E3s with U-box catalytic subunit:					
Prp19	YLL036C	503	57	Nucleus	Splicing
Ufd2	YDL190C	961	110	Cytoplasm Nucleus	Ubiquitin chain assembly factor (E4), degradation of ubiquitin fusion proteins
E3s with HECT catalytic subunit:					
Hul4	YJR036C	892	103	Not visualized	Unknown function
Hul5	YGL141W	910	106	Nucleus	Multiubiquitin chain assembly factor (E4), polyUb chains elongation, retrograde transport of misfolded proteins during ERAD
Rsp5 (Mdp1)	YER125W	809	92	Cytoplasm, Nucleus	NEDD4 family E3, regulates many cellular processes including mutivesicular body (MVB) sorting, heat shock response, transcription, endocytosis, ribosome stability, degradation of excess histones
Tom1	YDR457W	3268	374	Nucleus Nucleolus	mRNA export from the nucleus, degradation of excess histones
Ufd4	YKL010C	1483	168	Cytoplasm Nucleus	Degradation of ubiquitin fusion proteins
E3s with RBR catalytic subunit:					
Hel1	YKR017C	551	64	Not visualized	Ubiquitylation and degradation of excess histones
Itt1	YML068W	464	54	Not visualized	Modulation of translation termination efficiency
Other components of E3 complexes:					
Apc11	YDL008W	165	19	Vacuolar membrane	APC/C core component (RING-finger subunit), cell cycle, degradation of anaphase inhibitors
Cdc53	YDL132W	815	94	Cytoplasm Nucleus	Cullin, structural protein of Skp, Cullin, F-box (SCF) containing complexes involved in cell cycle
Cul3 (CulB)	YGR003W	744	86	Cytoplasm Nucleus	In a complex with Elc1p ubiquitylates RNA polymerase II to trigger its proteolysis
Rtt101 (Cul8)	YJL047C	842	99	Cytoplasm Nucleus	Anaphase progression, DNA repair, rRNA decay

*Note that some of these proteins are only putative ubiquitin ligases, as the biochemical evidence of ligase activity has not yet been reported. Not all putative E3s may be presented in this table.

1.1.9.1 RING-type E3s

The Really Interesting New Gene (RING)-type E3s, also known as RING finger/RING motif/RING domain and RING finger-like ubiquitin ligases (E3s), such as U-box proteins or plant homeodomain/leukemia-associated protein (PHD/LAP), comprise the large majority of known E3s. The RING fold family includes proteins that either bind zinc (RING-H2, RING-HC, RING-v, RING-D, RING-G, RING-S/T, RING-C2, PHD) or do not (U-box proteins). RING-domains have different subfamilies according to their structural contexts. Structurally, they could be classified as the following: RING-H2, with histidines at positions 4 and 5; RING-HC, with histidine at position 4; RING-C domains that contain only zinc-chelating cysteines (Deshaies and Joazeiro, 2009). They can form homodimers (Zheng et al., 2000), for example, cIAP, BIRC7 and Prp19, or heterodimers, including BRCA1-BARD1 (Brzovic et al., 2001), and Mdm2-MdmX. Moreover, some exist as multi-subunit assemblies, as in the Cullin RING ligases subfamily. These have recently been reviewed by Metzger et al. (2013).

With respect to the mechanism of action (Figure 12 A), RING-type or U-box ligases do not form the covalent intermediate with ubiquitin, but rather simultaneously bind both substrate and E2~Ub conjugate. They can discharge thioesterfied ubiquitin to its active-site cysteine onto the lysine residue of the substrate protein by acting as molecular scaffolds and positioning both an E2 and a substrate in a ‘catalytic favorable orientation’ on their domain (Petroski and Deshaies, 2005). Catalytic active site residues for RING E3s have not been identified (Deshaies and Joazeiro, 2009). The RING or RING-like domain of these E3s is responsible for binding to the E2 and stimulates Ub transfer (Lorick et al., 1999).

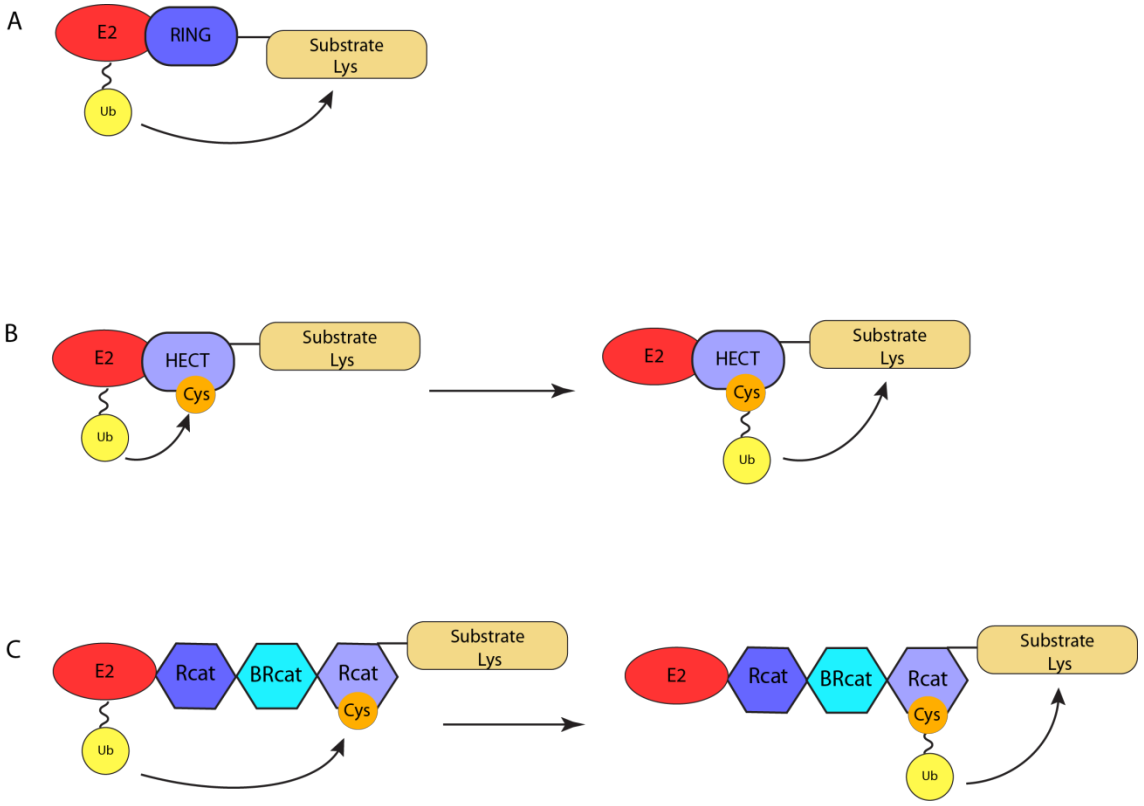

Figure 12. The mechanism of Ub transfer by different E3 families. A) RING E3 binds to the Ub conjugating enzyme (E2), from which Ub is transferred directly onto a substrate protein. B) HECT E3 binds to E2, from which Ub is first transferred to the catalytic cysteine of the ligase and is the transferred onto the substrate protein. C) RBR ligases use the combined mechanism of both RING and HECT ligases. E2~Ub conjugate is bound to the so-called Rcat domain (required-for-catalysis) of RBR ligase. Next, Ub is transferred from E2 to the Rcat domain with a catalytic cysteine, from which it is then transferred to the substrate protein.

The first suggestion that RING fingers are implicated in the process of ubiquitylation was made in 1998 by Bachmair, who observed that the plant N-end rule E3 shared the RING finger motif with other proteins involved in ubiquitylation, including the yeast N-end rule E3s Ubr1, Hrd1 and Rad18, as well as Apc11, an essential component of anaphase-promoting complex (APC) (cited by Joazeiro and Weissman, 2000). It is now known that different RING-types E3s can generate different Ub chain linkages depending on the E2 with which they are interacting. For instance, BRCA1-BARD1 RING E3 can attach mono-Ub as well as generate poly-Ub Lys63- or Lys48 linked chains, depending on the E2 they are interacting with. Thus, the human E2s UbcH6, Ube2e2, UbcM2 and Ube2w direct monoubiquitylation of BRCA 1, whereas Ubc13-Mms2 and Ube2k enable the synthesis of Lys63- or Lys48-linked ubiquitin chains (Christensen et al., 2007). Another example is the anaphase promoting complex or cyclosome (APC/C), which upon interaction with Ubc4 monoubiquitylates

multiple lysines on its targets, while upon interaction with Ubc1 generates Lys48-linked poly-Ub chains (Rodrigo-Brenni and Morgan, 2007). It has also been shown that RING E3s can act as regulators of Ub chain assembly and have the ability to prevent E2s from catalyzing the chain formation, as seen in the case of Rad18 and its E2 Rad6. Rad6 can synthesize either the canonical Lys48-linked chains or mixed chains. However, when interacting with Rad18 it promotes monoubiquitylation of PCNA, inhibiting the activity of Rad6 to Ub chains formation. This is caused by Rad18 competing with Ub for a noncovalent Ub binding site on Rad6 (Hibbert et al., 2011).

1.1.9.2 HECT E3s

HECT (Homologous to E6AP C-terminus) ligases were first reported in 1995 by Huibregtse et al., making them the first E3 family described. HECT E3s are of varying sizes ranging from 80 kDa to 500 kDa, and are characterized by the presence of the catalytic HECT domain at their C-terminal. This domain has approximately 350 amino acids in length and is composed of two lobes, an E2-binding N-terminal lobe and a C-terminal lobe that contains the active site cysteine (Huibregtse et al., 1995; Huang et al., 1999). Subsequently, the structures of the seven HECT domains, E6-AP, WWP1, Smurf2, NEDD4L, HUWE1, yeast Rsp5 and NEDD4, were solved by Huang et al. (1999), Verdecia et al. (2003), Ogunjimi et al. (2005), Kamadurai et al. (2009), Pandya et al. (2010), Kim et al. (2011) and Maspero et al. (2011), respectively. Furthermore, the C-terminal part of the HECT domain of UBR5 ubiquitin ligase has been published by Matta-Camacho et al. (2012). The crystal structure of the first identified member of the HECT family, E6-associated protein (E6-AP, also known as UBE3A) bound to the UbcH7 ubiquitin-conjugating enzyme revealed that the C-terminal lobe is a loosely packed architecture with its catalytic cysteine residues being 41Å apart (Huang et al., 1999). Another structural study of the NEDD4L HECT E3 in complex with the ubiquitin-conjugated E2 (UBCH5B~Ub, known as UBE2D2) showed that the Ub C-terminal tail is located between the catalytic centers of the E2 and the HECT domain C-terminal lobe, and that the distance between the catalytic cysteines of E2 and E3 is ~8Å (Kamadurai et al., 2009).

Contrary to RING E3s, HECT domain E3s directly catalyze ubiquitylation of proteins due to their defined enzymatic activity in two-step mechanism (Figure 12 B). The ubiquitin-charged E2 enzyme first transfers ubiquitin to the active site cysteine within the HECT domain in a transthiolation reaction, while preserving the high-energy ubiquitin thioester bond. Substrate ubiquitination then occurs through a subsequent nucleophilic attack of the HECT~Ub thioester bond by a lysine side chain of the target protein (Huibregtse et al., 1995; Scheffner et al., 1995).

The Ub-chain linkage specification mainly depends on the catalytic HECT domain. For example, yeast Rsp5 is involved in ubiquitylation of its substrates via Lys48- or Lys63-linked chains (Kee et at., 2005). Members of the Nedd4 family form predominantly Lys63- linked ubiquitin chains but can also assemble Lys48-linked chains, whereas E6-AP E3 has been shown to form Lys48-linked chains (Wang and Pickart, 2005; Kim et al., 2007). The substrate specificity is mainly determined by the N-terminal extensions. On this basis, HECT E3s were divided into the following three subfamilies: NEDD4/NEDD4-like E3s with double tryptophan residue (WW) domains, HERC (HECT and RCC1-like domains) with RLDs domains (RCC1-like domains), and others that contain neither WW nor RLDs domains (recently reviewed by Martin Scheffner and Kumar, 2014). WW domains, shared by many HECT E3s, are involved in protein-protein interactions, and play a role in targeting certain substrates for degradation (Hesselberth et al., 2006). Additionally, HECT E3s have a N-terminal C2 domain, responsible for plasma membrane translocation in response to increasing levels of intracellular Ca^{2+}. In yeast, Rsp5 is the only HECT E3 to have a C2-WW domain, and is capable of ubiquitylating different proteins in various cellular compartments (Rotin et al., 2000).

1.1.9.3 RBR E3s

The RBR family includes the parkin protein, whose dysfunction is associated with early-onset Parkinson's disease (Dawson and Dawson, 2010), HOIP (HOIL-1-interacting protein) and HOIL-1 (haem-oxidized IRP2 ubiquitin ligase 1) (Kirisako et al., 2006), which both belong to the multiprotein LUBAC (linear ubiquitin chain assembly complex), as well as other complex multidomain enzymes. This family is characterized by the presence of the RING-Between-RING domain, which was first identified in a *Drosophila* gene, ariadne-1 (ari-1), which is required for a proper differentiation of all cell types in an adult fly (Aguilera et al., 2000). This E3 family was named 'the RBR ubiquitin ligases' after the RBR domains that were also identified in several other proteins using sequence alignment methods. It was shown that the RING domains in the RBR region contain cysteine and histidine residues with the ability to bind metal ions. It was suggested that the N-terminal RING domain (RING 1) binds two zinc ions and folds into a classical ring finger, whereas the second C-terminal RING domain (RING 2) binds only one ion and forms a hydrophobic core different from that of the classical ring fingers (Capili et al., 2004). Additionally, the third domain with a central cysteine/histidine cluster is also likely to form a ring-finger type structure. This domain was named IBR (in between ring) (Morett and Bork, 1999) or DRIL (double ring finger linked) (van der Reijden et al., 1999). The RBR family was therefore given, a second name as TRIAD (two ring fingers and DRIL) (van der Reijden et al., 1999). Recently, however, Spratt et al. (2014) proposed renaming the RBR domains. The RING 1 and RING 2 domains as Rcat (required-for-catalysis) domain, while the IBR domain as BRcat (benign-catalytic) domain. This new nomenclature results from recent structural biology studies and biochemical findings. The RING 2 domain, which does not have a classical ring structure, has a single catalytic cysteine through which the Ub molecule is accepted from the E2. This domain is essential for RBR ligase activity. The IBR domain has the same fold as the Rcat domain, but lacks the catalytic cysteine residue and therefore ubiquitin ligase activity (recently reviewed by Spratt et al., 2014).

RBR ligases use the mechanism of both RING and HECT ligases to catalyze the ubiquitylation, a process termed as 'RING-HECT hybrid mechanism' (Wenzel, Lissounov, et al., 2011) (Figure 12 C). It was demonstrated that these ligases bind E2s through a RING domain but then transfer Ub via a thioester linked Ub in

a transthiolation reaction, requiring a catalytic cysteine in the RING 2 domain (Wenzel, Lissounov, et al., 2011), thereafter renamed the Rcat domain (Spratt et al., 2014). It was, however suggested that the recruitment of the E2 is not as straight-forward mechanism as in the case of the canonical RING E3s (Budhidarmo et al., 2012). The RBR ligases can recruit mono-Ub or be involved in the poly-Ub chain formation thanks to the presence of regions with different domains, such as UBA, NZF and ZnF (described in more detail in the chapter on *Ubiquitin binding proteins*). Interestingly, a multisubunit ubiquitin ligase complex, LUBAC, was shown to efficiently assemble linear (Met1) ubiquitin chains (Kirisako et al., 2006).

1.1.10 Deubiquitylating enzymes (DUBs)

Ubiquitylation is a reversible process, owing to the presence of deubiquitylating enzymes (DUBs) that remove Ub and Ub chains from proteins, thereby editing the ubiquitin code. All eukaryotic genomes harbor a set of deubiquitylating enzymes, with nearly 100 putative DUBs encoded in the human genome, 79 of which are predicted to be active (Clague et al., 2012). In yeast, Hutchins et al. (2013) predicted 24 DUBs encoding genes. DUBs belong to the family of proteases and can be divided into two main classes, cysteine proteases and metalloproteases, with the majority among the former. Cysteine proteases can be subdivided into four groups: ubiquitin C-terminal hydrolases (UCHs), ubiquitin specific proteases (USPs), ovarian tumor proteases (OTUs), and the Josephins. Metalloproteases comprise only the JAB1/MPN-domain associated metalloenzymes (JAMM) (Atanassov et al., 2011).

With regard to the catalytic mechanism, cysteine proteases 'perform a nucleophilic attack' on the carbonyl of a peptide bond via their cysteine (Figure 13). The target protein is cleaved and the cysteine protease subsequently forms a covalent intermediate with Ub. The reaction of this intermediate with a water molecule releases a free DUB and Ub. Contrary to cysteine proteases, metalloproteases generate a noncovalent intermediate with the substrate using a Zn^{2+} bound polarized water molecule. This intermediate is broken down by proton transfer from the molecule of water, thus releasing the enzyme (Nijman et al., 2005).

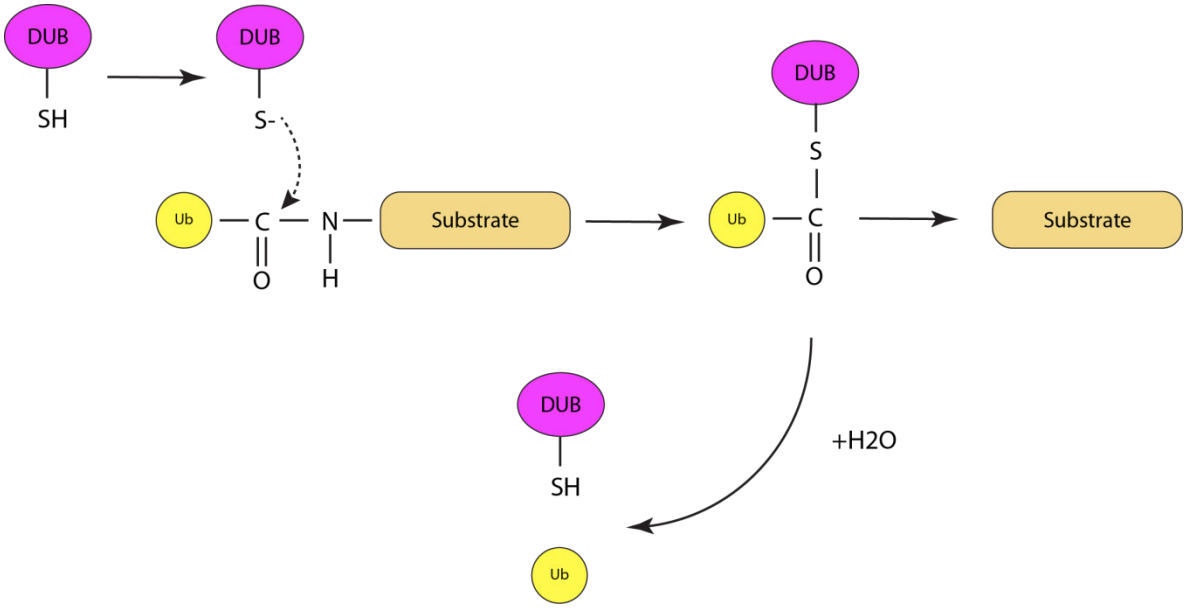

Figure 13. The mechanism of action of deubiquitylating enzymes, based on the example of the catalytic mechanism of cysteine proteases.

The main function of DUBs is the generation of free ubiquitin from ubiquitin precursors. The is performed by UCHs, which cleave Ub preferentially from peptides and small adducts, unlike USPs which cleave Ub from protein substrates (Kinner and Kölling, 2003). Moreover, by cleaving Ub-protein bonds, DUBs regulate ubiquitin pathways and are thereby involved in a broad range of cellular functions. They have been shown to play a role in membrane trafficking, protein quality control, and cell signaling by the establishment of protein-protein interactions. Moreover, they are implicated in the regulation of nuclear events such as DNA damage repair and transcription (reviewed by Clague et al., 2012). An example of a well characterized yeast DUB is Doa4 (Ubp4), significant for both proteasome-dependent degradation as well as Ub homeostasis (Amerik et al., 2000).

In order to control ubiquitin-dependent signaling, DUBs have to deal with Ub chains that have distinct linkages, show different topology, and vary in length (Komander and Rape, 2012). Therefore, they display specificity on several levels, which enables to distinguish isopeptides or linear peptides and different types of Ub linkage or chain structures, as well as to discriminate particular chain linkages. Due to the difficulties in Ub chain preparation (other than linear), we still lack in-depth knowledge on DUBs specificity. However, within the USP and OUT DUBs families, Lys48- and Lys63-linkage specific members are well described (Komander et al., 2009). For example, USP14 – the 26S proteasome associated DUB (the yeast homologue of

Ubp6) – shows specificity for Lys48-linked Ub chains (Hu et al., 2005), as does otubain 1 (OTUB1) (Wang et al., 2009). Interestingly, USP14 has so-called *exo*-activity and cleaves the chains from the distal end only, thus generating monoubiquitin (Hu et al., 2005; Komander et al., 2009). DUBs positioning on the ubiquitin chain can also be internal, which consequently releases longer chains from the substrates. Examples of DUBs that show *endo*-activity are those that regulate ubiquitin-mediated signaling, for instance CYDL (Komander et al., 2008) and A20 (Lin et al., 2008). Among the members of the OTU family, DUBA (also known as OTUD5) and Trabid are Lys63-linkage specific DUBs (Kayagaki et al., 2007; Tran et al., 2008). Lys11-linked ubiquitin chains are preferentially hydrolyzed by the deubiquitylating enzyme Cezanne, which also belongs to the OTU family (Bremm et al., 2010). The Josephin family belonging DUB, Ataxin3, edits Lys63 linkages in mixed-linkage chains (Winborn et al., 2008). Schaefer and Morgan (2011) reported that long Lys48-linked chains are resistant to many DUBs. They showed that the yeast Ubp15 deubiquitylating enzyme (and its human orthologue USP7) rapidly cleaves mono- and di-ubiquitin from the substrates, but that the removal of longer Lys48-linked chains is slow. On the contrary, the yeast Ubp12 easily cleaves the ends of long Lys48 chains on substrates, and like Ubp15 can also efficiently hydrolyze the short chains (Schaefer and Morgan, 2011).

1.1.11 Ubiquitin binding proteins

As described in previous chapters, ubiquitin not only has a proteolytic function but also acts as a cellular signal, controlling a myriad of biological processes. The specificity of ubiquitin signaling is determined by its interactions with ubiquitin binding proteins, so-called ubiquitin receptors that recognize and decode the ubiquitylated signals into different biochemical cascades in the cell (Ikeda et al., 2010; Husnjak and Dikic, 2012). In other words, ubiquitin binding proteins are the readers that interpret ‘the ubiquitin code’ and translate it in biological outcomes. Importantly, they have the abilty to read either Lys63- or Lys48-linked chains. This is thanks to various ubiquitin binding domains (UBDs). They noncovalently and weakly bind monoubiquitin and/or polyubiquitin chains (the most common binding affinities of monoubiquitin are with K_d > 100 μM) (Hurley et al., 2006). UBDs are usually small (20-150 amino acids) but structurally diverse, and can have various biological functions (Hicke et al., 2005).

Ubiquitin binding domains have been extensively reviewed by Dikic and colleagues (2009), and Husnjak and Dikic (2012). The main classes: UBA (ubiquitin associated), CUE (coupling of ubiquitin conjugation to endoplasmic reticulum degradation), UIM (ubiquitin interacting motif), GAT (GGA and TOM1), NZF (Np14 Zn-finger) – belonging to the largest class of ZnF (Zinc finger) domains, A20 – also belonging to the ZnF class, and UEV (Ubc E2 variant), which are briefly presented below.

UBA domain

The Ub-associated domain was described by Hofmann and Bucher in 1996, and it was the first UBD described. It is present among members of the E2 and E3 families and ubiquitin binding protein superfamily, or proteins that contain domains similar to Ub itself. The size of the UBA domain is ~55 residues, with about 45 residues (generally nonpolar) as the conserved core region (Hofmann and Bucher, 1996). The UBA domain has a preference for polyubiquitin chain binding, but also binds monoubiquitin. Pioneering work on the chain recognition of a number of UBA domains in the laboratory of Cecile Pickard showed that UBA domains recognize ubiquitin chains that are formed via different linkage types. Budding yeast Rad23 (human orthologue hHR23A) that contains an internal UBA1 domain and a C-terminal UBA2 domain preferentially binds Lys48 tetraubiquitin. The human ubiquitin-conjugating enzyme (E2-25K) is namely an example of Lys63 binding (Raasi et al., 2005). Binding to the Lys29-linked chains was also demonstrated (Rao and Sastry, 2002). Recently, Walinda et al. (2014) have shown that the UBA domain of human autophagy receptor NBR1 interacts with both monoubiquitin and polyubiquitin.

CUE domain

CUE domains are ~50 amino acids binding motifs, structurally related to UBA domains (both being three-helix bundles) despite their negligible sequence identity. They are found in proteins involved in the ubiquitylation pathways and trafficking. The CUE domain was first detected in the bioinformatics analysis of proteins in the endoplasmic reticulum-associated degradation (ERAD) pathway (Ponting, 2000). Subsequently, yeast studies have revealed the function of the CUE domain in the monoubiquitin binding (Davies et al., 2003; Donaldson et al., 2003; Shih et al., 2003). The CUE domain of yeast Vsp9 protein (the orthologue of mammalian Rabex-5), involved in the yeast endocytic pathway, is required for monoubiquitin binding. The CUE domain of

Vsp9 promotes monoubiquitylation by the HECT domain of Rsp5 ubiquitin ligase (Davies et al., 2003; Shih et al., 2003). CUE domains were named after the yeast Cue1 protein that plays a role in the ERAD pathway and recruits to the ER the ubiquitin conjugating enzyme Ubc7, which is necessary for the degradation of misfolded proteins (Biederer et al., 1997). Bagola et al. (2013) have shown that the CUE domain of Cue1 binds ubiquitin chains. It is important for an efficient formation of Lys48 polyubiquitin chains *in vitro* by the ERAD E3s and promotes the ubiquitylation of substrates (Bagola et al., 2013).

UIM domain

The UIM is a conserved motif, present mainly in proteins involved in ligand-activated receptor endocytosis and degradation that recognizes the S5a proteasome subunit (known as Rpn10 in yeast) and variety of other proteins involved in ubiquitylation. It is a short motif of around 20 amino acid residues, and can recognize both mono- and polyubiquitylated proteins (Hofmann and Falquet, 2001). It can recognize both Lys48- and Lys63-linked chains (Husnjak and Dikic, 2012).

GAT domain

GAT domains occur in GGA proteins (Golgi-localized, gamma-ear-containing, ADP-ribosylation-factor-binding proteins) as well as TOM1 and TOM1-like proteins (Suer et al., 2003). Puertollano and Bonifacino (2004) first discovered the GAT domain involvement in ubiquitin binding and suggested that GGA proteins may play further roles in sorting of ubiquitylated cargos. Structural studies using X-ray crystallography have shown that the GAT domain has a three-helix bundle structure, and that within its C-terminal there are several conserved hydrophobic residues (Collins et al., 2003). Bilodeau et al. (2004) have shown that the GAT domain can have two distinct Ub binding sites, suggesting that it could not only bind monoubiquitin but also promote the binding multi-monoubiquitylated and/or polyubiquitylated proteins (Hurley et al., 2006).

NZF domain

The NZF domains are compact zinc-binding modules of approximately 30 amino acid residues that have been found in many proteins involved in Ub-dependent processes. Ubiquitin binding by the NZF domain was discovered in studies of mammalian Npl4

protein (nuclear protein localization 4) (Meyer et al., 2002). Several NZF domains bind to both mono- and poly-Ub *in vitro.* For instance, the NZF domain of the HOIL-1L subunit of LUBAC (linear ubiquitin chain assembly complex) has been shown to bind linear polyubiquitin chains (Sato et al., 2011). However, certain NZF domains, for example Ran-binding protein 2, do not bind to ubiquitin. This is plausibly due to a lack of the hydrophobic residue responsible for ubiquitin recognition (Alam et al., 2004).

A20 ZnF domain

The A20 domain belongs to a class of zinc finger (ZnF) domains. It was first found to function as a ubiquitin ligase domain in the NF-κB (nuclear factor κB) signaling pathway. It is the C-terminal domain of the A20 protein, composed of seven zinc fingers, that catalyzes the formation of the Lys48 chain, thereby triggering the substrates for proteasomal degradation (Wertz et al., 2004). Interestingly, the A20 ZnF domain of the A20 protein can contact three ubiquitins through Ile-44 and Asp-58 residues as well as via another surface of Ub, the so-called TEK-box (Husnjak and Dikic, 2012). The A20 domain can also directly bind mono-Ub, as shown in the Rabex-5 protein (the mammalian orthologue of yeast Vps9), which has its A20 domain on the N-terminus (residues 1-76) (Mattera et al., 2006). The A20 ZnF domain of Rabex-5 binds ubiquitin with ~22 μM affinity within a polar region centered on the Asp-58 residue (Lee et al., 2006).

UEV domain

UEV domains are structurally similar to E2 enzymes, but lack the active site cysteine. This prevents them from catalyzing the Ub transfer as they cannot form a thioester bond with the C-terminus of Ub (Ponting et al., 1997; Pornillos et al., 2002). A well-known example of a UEV domain protein is the budding yeast Mms2 protein, which forms a complex with the E2 enzyme Ubc13 and facilitates the assembly of poly-Ub chains. *In vitro* Mms2 forms 1/1 complexes with a Ub dissociation constant of 98 +/- 15 μM, whereas the Ubc13-Mms2 heterodimer shows significantly stronger Ub-binding than Mms2 alone, with a dissociation constant of 28 +/- 6 μM (McKenna et al., 2003). The UEV domain binds monoubiquitin via the Ile-44 patch (Husnjak and Dikic, 2012).

1.2 The network of E2/E3 interactions

Different combinations of E2/E3 pairs catalyze either monoubiquitylation or the polyubiquitin chain formation (Kirkpatrick et al., 2006; Kim et al., 2007; Jin et al., 2008; Xu et al., 2009; Wickliffe et al., 2011). This 'combinatorial nature' of protein ubiquitylation networks appears in all eukaryotic systems (Markson et al., 2009). Several physiological E2/E3 pairs have been revealed to date and it is known that a given E2 may interact with several E3s and vice versa. However, the exact mechanism of E2/E3 pairs function as well as their selectivity and specificity are still not fully understood (Weissman, 2001). Major steps towards revealing the complex E2/E3 network have been made by two large-scale studies, both published in 2009, and based on the global screening of interactions between human E2s and RING domains of E3s (Markson et al., 2009; van Wijk et al., 2009).

Hence, van Wijk and colleagues (2009) performed a global yeast two-hybrid screen to investigate the specificity of the interactions between the catalytic domains (UBC-folds) of the 35 human E2s with the 250 RING-type E3s. The researchers uncovered 346 high-confidence E2/E3 interactions and found that multiple E2s can interact with multiple E3s, and conversely. The human UBE2U conjugating enzyme, which belongs to the UbcH5 family (members of this family are highly conserved and homologous to the yeast Ubc4 and Ubc5 enzymes), showed the highest number of interactions (52 interactions), followed by UBE2D2 (35), UBE2D3 and UBE2D4 (33), UBE2N (29) and UBE2D1 (28). Some of these interactions, including UBE2U with the ligase MDM2, were verified by independent GST-pull-down analysis (van Wijk et al., 2009). The second study by Markson et al., (2009) combined yeast two-hybrid screens, using full-length 39 human E2s, with homology modeling methods to show a map of E2/E3-RING interactions. They generated a set of 568 reproducible positive human E2/E3-RING interactions. 80 different E2/E3 pairs were tested to eliminate the false-positive interactions. To do so, they used either single- or double-point mutants with the mutated conserved amino acids involved in E2 binding. Approximately 92% of those interactions were abolished, indicating the specificity of the interactions. A large number of RING E3s were observed to interact with members of the UBE2D and UBE2E families of E2s (Markson et al., 2009).

The aforementioned studies have provided a genome-wide view of the E2/E3 interactions network in the human ubiquitin-proteasome system. Other studies by Christensen et al. (2007) looked at possible E2 interactors of the human RING ligase BRCA1/BARD1 and showed that it can interact with ten different E2s, including UbcH5a, UbcH5b, UbcH5c, UbcH6, UbcH7, Ube2e2, UbcM2, Ubc13, Ube2k, and Ube2w. Moreover, numbers of both large and small scale studies in human as well as yeast have expanded the E2/E3 network (data concerning interactions in yeast are presented in the chapter *Physiological E2/E3 pairs*, Table 5). So far, however, many E3s remain lone with no known interacting E2s and it is not possible to easily predict their functional E2 partners.

1.2.1 Canonical interaction between the E2 UBC domain and the E3 RING, HECT domains

Experimental structures have shown that interactions with E3s occur in the UBC domain of E2s (Huang et al., 1999; Zheng et al., 2000). Although the E2 core domain shows high sequence conservation, E3 enzymes interact physically and functionally only with particular E2 enzymes. Again, the key questions are how this selectivity is obtained and how it then determines the substrates specificity (Winkler et al., 2004). The first structural information on E2/E3 interaction specificity came from the crystal structures of the human HECT ligase E6-AP bound to the ubiquitin conjugating enzyme UbcH7 (Huang et al., 1999) and from the c-Cbl proto-oncogene, which belongs to a RING family E3s, also bound to UbcH7 (Zheng et al., 2000) (Figure 14). Both complexes had similar structures concerning hydrophobic residues located in the loop regions of UbcH7 and hydrophobic regions in the HECT or RING domains of E3s. The structural studies by comparison of E2/E3 interfaces showed that these E3s interacted with almost identical regions of the UbcH7 E2 (loops L1 and L2), despite the E3s belonging to two functionally and structurally distinct E3 families. The residues in the UbcH7 responsible for the most extensive contact are Phe-63, Pro-97, and Ala-98 (Huang et al., 1999; Zheng et al., 2000). In the majority of E2s, the residues involved in the specificity of the interactions are not located in a single point. They are, however, dispersed over the N-terminal helix flexible and divergent loop regions (L1 and L2) (van Wijk et al., 2012).

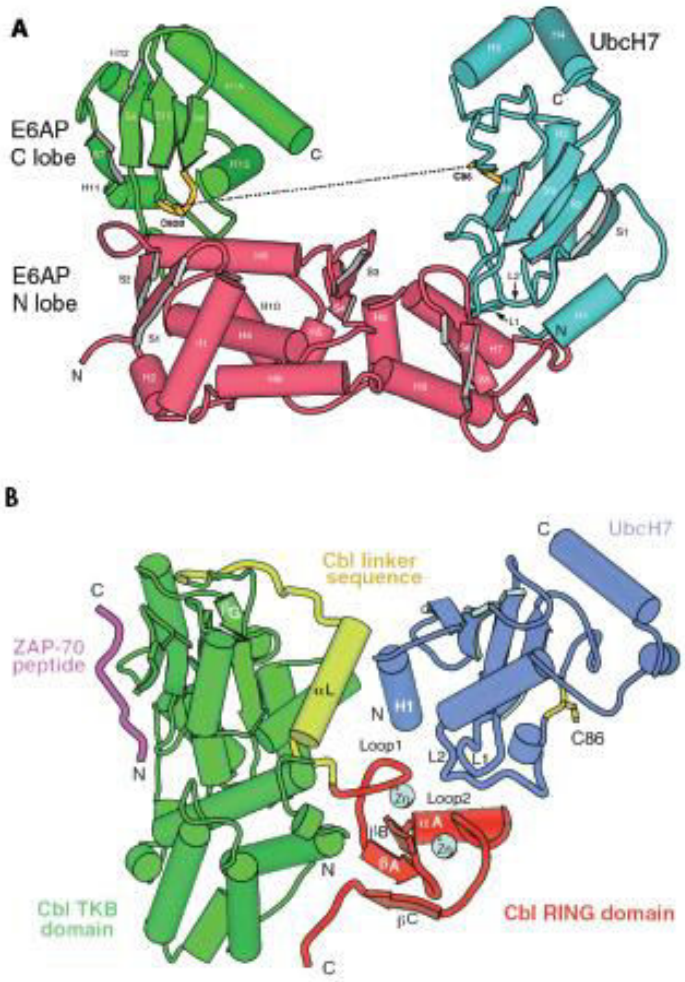

Figure 14. A schematic representation of the canonical E2/E3 complexes. A) The E6-AP HECT domain with UbcH7 conjugating enzyme, which forms a U-shaped structure. The E6-AP HECT domain N lobe (consisting of 12 α-helices and six β-strands), C lobe (six α-helices and four β-strands), and UbcH7 (four α-helices and four β-strands), colored in green, red, and cyan, respectively. The two active-site loops are colored yellow. The dotted line indicates the open line of sight between the active-site cysteines of E6-AP and UbcH7 (adapted with permission from: Huang et al., *Science*, 1999). B) The ternary complex of c-Cbl with UbcH7, and phosphorylated ZAP-70 peptide.The TKB domain is colored green, the RING domain red, and the linker region of c-Cbl yellow. UbcH7 is colored in cyan and its active-site cysteine in orange (adapted with permission from: Zheng et al., *Cell*, 2000).

More recent structure to function studies by Sheng et al. (2012), who performed E2 with HECT E3 analysis, determined the high-resolution three-dimensional structures of 15 human E2 core domains. They further demonstrated that HECT domains belonging to different subfamilies catalyze different types of Ub chain formation. In their autoubiquitylation assay, nine HECT domains were tested with 26 Ub-loaded E2 proteins and the interactions resulted in the synthesis of long Ub chains (Sheng et al., 2012). An example of structural view of the ubiquitin transfer cascade by HECT E3s presented schematically by Kamandurai and colleagues (2013) is shown in Figure 15.

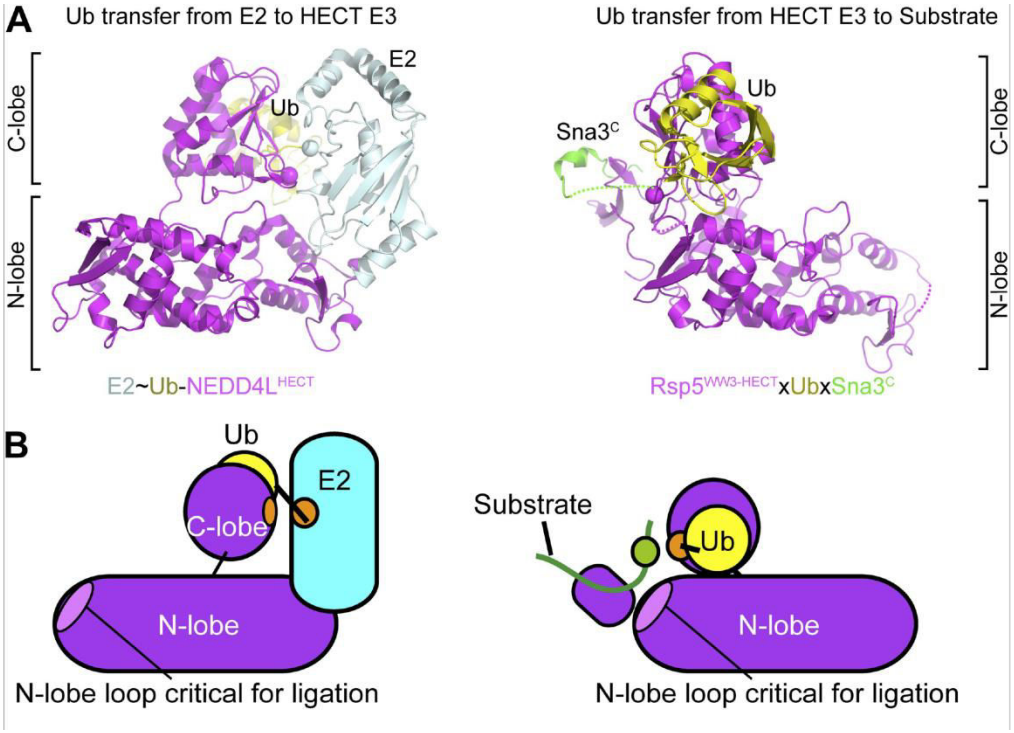

Figure 15. Ubiquitin transfer cascade by HECT E3s. A) Left: structure of E2 (pale cyan, with active site as sphere)~Ub (yellow) with E3 NEDD4L^{HECT} (violet, with active site as sphere) Right: structure of E3 Rsp5$^{WW3\text{-}HECT}$ (violet, with active site as sphere), Ub (yellow) and the substrate Sna3^{C} (green). B) Schematic views of E2-to-E3 Ub transfer and E3-to-substrate Ub ligation (adapted with permission from: Kamandurai, *Elife*, 2013).

1.2.2 'Backside' interactions

Although structural studies using recombinant proteins have demonstrated that all E2s interact with E3s by using a conserved interaction surface close to their active site, some E2s have in fact been shown to also contact proteins with the opposite surface (Figure 16). This so-called 'backside' was first identified by Brzovic et al. (2006) as a site for noncovalent ubiquitin binding of the human UbcH5c conjugating enzyme (UbcH5s are yeast homologues of Ubc4). Brzovic et al. (2006) found that Ub can recognize a surface on UbcH5c comprised of the β sheet, which is separate from the catalytic center. Upon this interaction, UbcH5c~Ub self-assemble into high molecular weight complexes, which is required for the BRCA1-directed polyubiquitin chain formation (Brzovic et al., 2006).

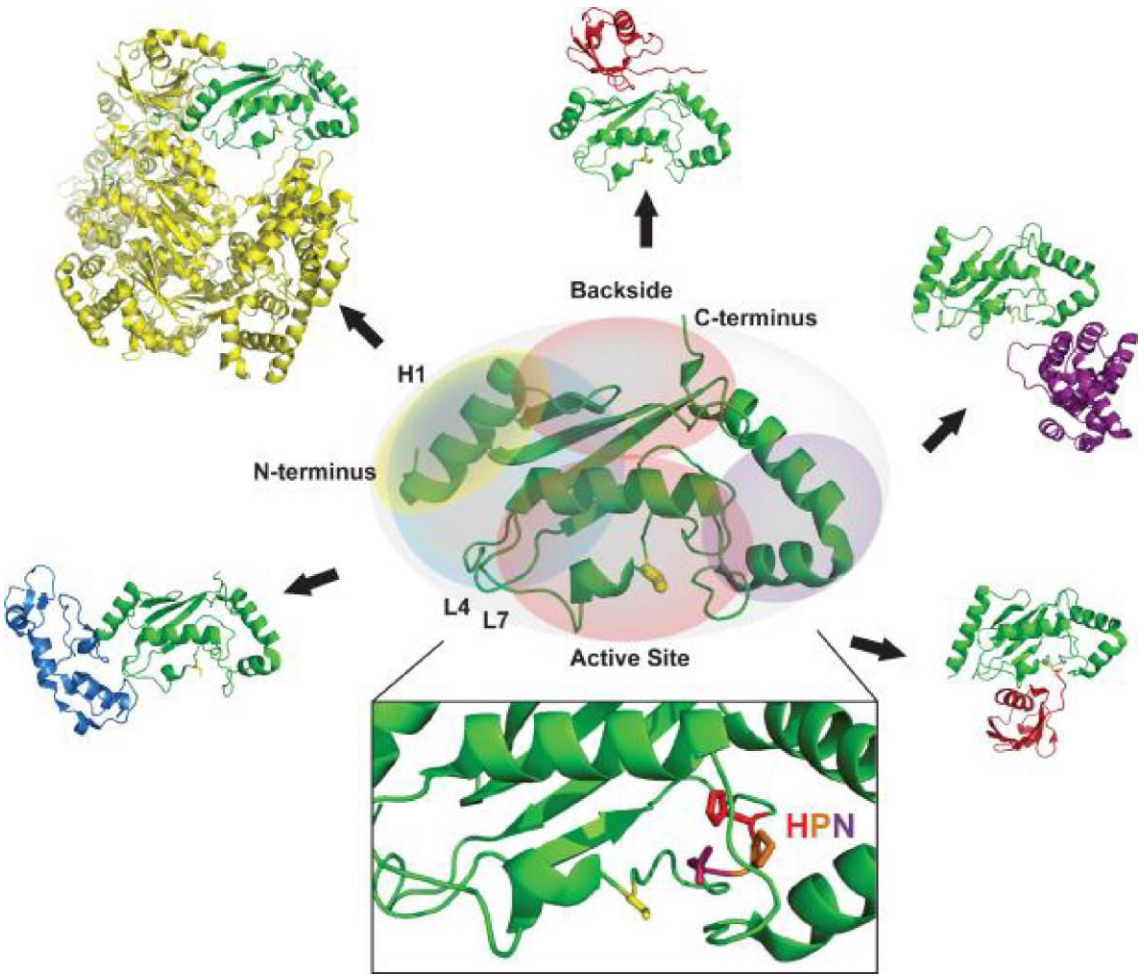

Figure 16. Structure of a UBC domain (here the E2, Ubc13 is shown as an example) and its interaction surfaces. In the center is the E2, Ubc13 in ribbon structure (PDB ID: 2GMI), with its interactors. The E2 in each interacting pair is shown as green. Clockwise from lower left corner: the E1/E3-binding surface as seen in complex of Ubc13 with the RING E3 Traf6 (blue) (PDB ID: 3HCT) and in Ubc12 in complex with the NEDD8-activating E1 (yellow) (PDB ID 2NVU); backside-binding surface as seen in the E2/Ub complex, UbcH5c/Ub (red) (PDB ID 2FUH); substrate-binding surface as seen in the SUMO E2 Ubc9 in complex with its substrate RANGAP1(purple) (PDB ID: 1Z5S); activated Ub/Ubl surface as seen in UbcH5b~Ub complex (PDB ID: 3A33). The active site Cys shown as yellow stick representation (adapted with permission from: Wenzel et al., *Biochemical Journal*, 2010).

A study conducted by Li et al. (2009) identified Ube2g2 as an E2 that may possibly use the 'backside' for mediating E3 interactions. It has been shown that Ube2g2 uses its 'backside' surface to interact with the endoplasmic reticulum-associated RING finger ubiquitin ligase, gp78 (also known as AMFR, the human tumor autocrine motility factor receptor), through its gp78 short region, known as the 'Ube2G2 binding region' (G2BR) (Li et al., 2009). In the same year, Das et al. (2009) also reported that the binding of the G2BR domain within gp78 occurs on a region of Ube2g2 that is distinct from the canonical E1 and RING finger E3 binding sites. The interaction results in ~50 fold increase in the affinity between the E2 and the gp78 RING finger, and considerably increases substrate ubiquitylation (Das et al., 2009).

More recently, Metzger et al. (2013) reported the crystal structure of the yeast Ubc7 conjugating enzyme, a homologue of Ube2g2, with a C-terminal Ubc7-binding region (U7BR) of the Cue1 protein (Cue1 recruits Ubc7 to the ER and is required for Ubc7 stability) (Figure 17). This structural data revealed that the U7BR has a domain that includes three α-helices that interact extensively with the 'backside' of Ubc7. Furthermore, the study of yeast ubiquitylation enzymes revealed that the E2 Rad6 uses its 'backside' to interact with RING E3s Rad18, Ubr1 and Bre1. Rad18 monoubiquitylates the target proliferating cell nuclear antigen (PCNA), and binds the E2 not only through its RING domain but also via a distinct α-helix which interacts with the 'backside' (Bailly et al., 1997; Notenboom et al., 2007). Worthy of note, the Rad6/Rad18 'backside' interaction has a low affinity and competes with a noncovalent Ub binding on Rad6, giving the Rad6 the ability to form free Ub chains in the absence of Rad18, and directing monoubiquitylation (Hibbert et al., 2011). Recently, Turco et al. (2014) demonstrated that the Bre1 RING ligase interacts with Rad6, both canonically via the RING domain as well as through its Rad6 binding domain (RBD) using a 'backside' of Rad6. This E2/E3 pair plays a role in the monoubiquitylation of the histone H2B during transcription. Although the 'backside' interaction is nonessential for histone monoubiquitylation, it has been shown that this binding strongly enhances Rad6 activation, thereby accelerating the overall reaction (Turco et al., 2014). The anaphase promoting complex (APC), was similarly found to recruit its E2 UBCH10 using both canonical interactions with the RING domain of APC11 and backside interactions with APC2 (Brown et al., 2015). Also, Ubr1 E3 was shown to interact with the Rad6 'backside'. This E2/E3 pair was, however, shown to be involved in the polyubiquitylation of N-end rule substrates (Xie and Varshavsky, 1999). The question remains as to, how the E2 'backside' surface is used for E3 interactions. It seems possible that 'backside' interactions serve to enhance and regulate the specificity of E2/E3 interactions.

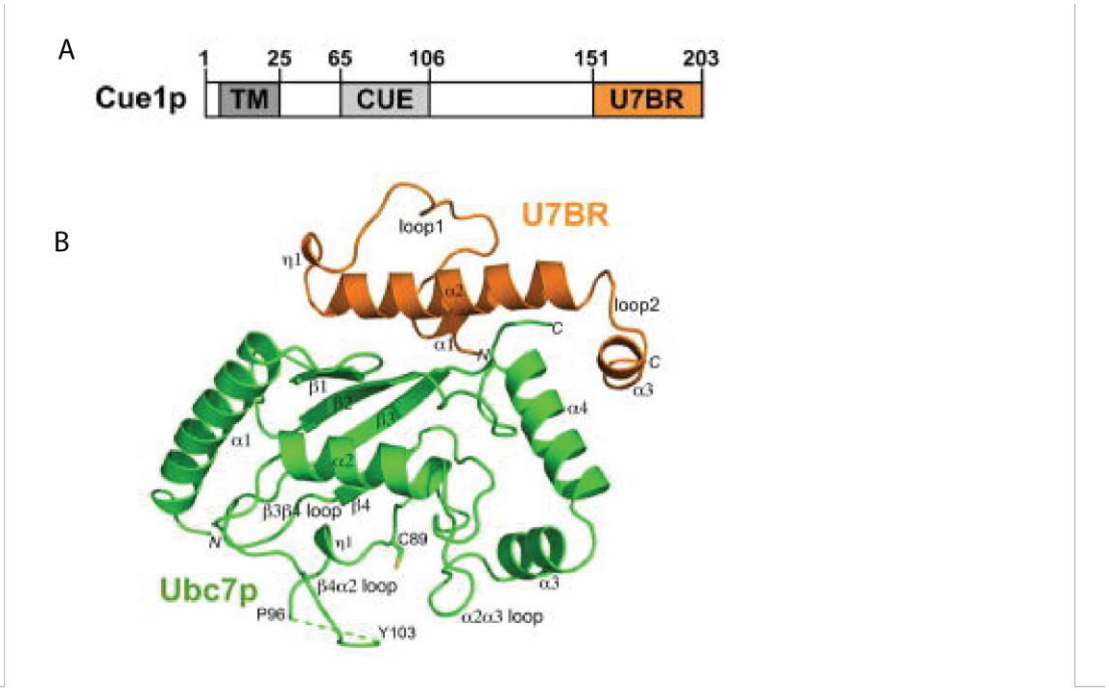

Figure 17. Crystal structure of the Ubc7:U7BR complex. A) Schematic representation of Cue1 protein showing its transmembrane (TM), ubiquitin-binding (CUE), and Ubc7-binding region (U7BR) domains. B) Ribbon diagram of the Ubc7p:U7BR structure. Helices, strands, and loops are illustrated as spirals, arrows, and tubes, respectively (adapted with permission from: Metzger et al., *Molecular Cell*, 2013).

1.2.3 Identification of E2/E3 interactions

The identification of functional E2/E3 pairs is hindered by two main factors. First, it is clear that the E2/E3 complexes have a modest affinity and are transient in nature (Wenzel et al., 2011). This makes the interactions difficult to study using conventional biochemical approaches, as the weak complexes very often do not survive, for example in case of pull down assays or co-immunoprecipitation (Christensen and Klevit, 2009). Although the binding affinities between E2/E3 enzymes can vary substantially, they are relatively low for most active E2/E3 complexes (often in the μM range). Recently, a difference in affinity of nearly 50-fold was reported in the binding of the E3 Rbx1 to Cdc34~Ub conjugate over free Cdc34 (Spratt et al., 2014). The second main factor that hinders the identification of E2/E3 pairs is that a significant number of E3s function as dimers (homo- or heterodimeric E3s are known) or as multicomponent protein complexes. In many cases, these E3s can only function within those contexts (Christensen and Klevit, 2009) and it is therefore not always easy to reconstitute these complexes *in vitro*.

1.2.4 Physiological network of E2/E3 interactions

David Komander and Michael Rape (2012) concluded in their excellent review on the ubiquitin code: 'Given the importance of E2s in determining specificity, it is surprising how little we know about physiological E2-E3 pairs'. Indeed, our current knowledge on E2/E3 pairs is mainly based on individual studies and E2/E3 interactions have rarely been investigated systematically (see Table 5 for a list of E2/E3 interactions reported in budding yeast). Hence, our knowledge on how E2s and E3s operate at a network level is still preliminary. How do E3s collaborate with multiple E2s to assemble specific ubiquitin signals on their substrate? Do E2s function redundantly or do they have distinct activities (e.g. to prime or elongate specific chains)? Do they serve to ubiquitylate identical or different substrates? Can they assemble heterologous ubiquitin chains with particular functions? These questions have been addressed only for few E3s (e.g. Christensen et al., 2007; Petroski et al., 2007; Rodrigo-Brenni and Morgan, 2007; Wu et al., 2010; Meyer and Rape, 2014) but remain completely unanswered for the vast majority of E3s.

Table 5. The known physical E2/E3 interactions in *S. cerevisiae* (Data retrieved from: BioGRID database of protein and genetic interactions)*

Ubiquitin ligase (E3)	Ubiquitin conjugating enzyme (E2)	Method/assay	Reference
Apc11	Ubc1	Reconstituted Complex	Kimata (2011)
Apc11	Ubc4	Reconstituted Complex	Enquist-Newman et al. (2008); Foster and Morgan (2012); Zhang et al. (2013)
Asr1	Ubc1	Two-hybrid	Yu (2008)
Asr1	Ubc5	Two-hybrid	Yu (2008)
Bre1	Rad6	Affinity Capture-Western Reconstituted Complex Biochemical Activity	Wood et al. (2003); Krogan et al. (2006) Kim and Roeder (2009)
Cdc53	Cdc34	Affinity Capture-Western	Patton et al. (1998); Skowyra et al. (1999)
Cul3	Cdc34	Reconstituted Complex	Michel et al. (2003)
Cul3	Ubc4	Affinity Capture-MS	Geyer et al. (2003)
Cul3	Ubc5	Reconstituted Complex	Harreman et al. (2009)
Dma1	Ubc4	Reconstituted Complex	Loring et al. (2008)
Dma1	Ubc13	Reconstituted Complex	Loring et al. (2008)
Dma2	Ubc4	Reconstituted Complex	Loring et al. (2008)
Dma2	Ubc5	Two-hybrid	Chahwan (2013)
Dma2	Ubc13	Two-hybrid Reconstituted Complex	Chahwan (2013) Loring et al. (2008)
Doa10	Ubc6	Affinity Capture-Western	Neuber et al. (2005)
Doa10	Ubc7	Affinity Capture-Western Reconstituted Complex	Neuber et al. (2005); Bagola et al. (2013); Kreft and Hochstrasser (2011) Bagola et al. (2013)
Doa10	Ubc13	Two-hybrid	Chahwan (2013)
Gid2	Ubc8	Biochemical activity	Santt et al. (2008)
Gid9	Ubc8	Biochemical activit	Santt et al. (2008)
Hel1	Ubc4	Affinity Capture-Western Reconstituted Complex	Singh et al. (2012)

Hel2	Ubc4	Affinity Capture-Western Reconstituted Complex	Singh et al. (2012)
Hrd1	Ubc1	Affinity Capture-Western Reconstituted Complex	Bays et al. (2001)
Hrd1	Ubc4	Reconstituted Complex	Bays et al. (2001)
Hrd1	Ubc7	Affinity Capture-Western	Deak and Wolf (2001)
Hul5	Ubc4	Affinity Capture-Western	Fang et al. (2011)
Hul5	Ubc5	Affinity Capture-Western	Fang et al. (2011)
Mot2	Ubc4	Affinity Capture-MS Two-hybrid Reconstituted Complex	Krogan et al. (2006) Winkler et al. (2004); Panasenko et al. (2006) Panasenko and Collart (2012)
Mot2	Ubc5	Two-hybrid	Albert et al. (2002); Winkler et al. (2004); Panasenko et al. (2006)
Nam7	Cdc34	Reconstituted Complex Affinity Capture-RNA	Takahashi et al. (2008) Johansson et al. (2007)
Nam7	Ubc11	Affinity Capture-RNA	Johansson et al. (2007)
Pep5	Ubc4	Affinity Capture-Western Reconstituted Complex	Singh et al. (2012)
Pex2	Ubc4	Affinity Capture-Western	Platta et al. (2009)
Pex2	Ubc10	Affinity Capture-Western	Platta et al. (2009)
Pex10	Ubc4	Biochemical Activity	El Magraoui et al. (2012)
Pex10	Ubc10	Protein Fragment-Complementation Assay (PCA)	Eckert and Johnsson (2003)
Pex12	Ubc10	Reconstituted Complex	Magraoui (2014)
Pib1	Ubc4	Reconstituted Complex	Shin et al. (2001)
Psh1	Ubc8	Affinity Capture-Western	Hewawasam et al. (2010)
Rad5	Ubc13	Affinity Capture-Western Two-hybrid Reconstituted Complex	Ulrich and Jentsch (2000) Ulrich and Jentsch (2000); Ulrich (2003); Ball et al. (2014) Carlile et al. (2009); Parker and Ulrich (2009)
Rad18	Rad6	Affinity Capture-Western Affinity Capture-MS Two-hybrid	Bailly et al. (1997); Ulrich and Jentsch (2000) Ho et al. (2002) Ulrich and Jentsch (2000); Uetz et al. (2000); Fu et al. (2008)
Rsp5	Ubc1	Reconstituted Complex	Kee et al. (2005); Alvaro et al. (2014)
Rsp5	Ubc4	Reconstituted Complex Co-Crystal Structure	Kim et al. (2011); Herrador et al. (2013); Lam and Emili (2013) Stoffregen et al. (2012)
Rsp5	Ubc5	Reconstituted Complex	Harreman et al. (2009); Zhu et al. (2011)
Rsp5	Ubc6	Protein-peptide	Hesselberth et al. (2006)
Rsp5	Ubc7	Affinity Capture-Western	Arnason et al. (2005)
Rsp5	Ubc8	Reconstituted Complex	Huibregtse et al. (1997)
Rtt101	Cdc34	Affinity Capture-MS Reconstituted Complex	Krogan et al. (2006); Collins et al. (2007); Michel et al. (2003); Zaidi et al. (2008); Han et al. (2013)
San1	Cdc34	Biochemical Activity	Gardner (2005), Wang and Prelich (2009)
Slx5	Cdc34	Pulldown assay	Uzunova (2007)
Slx5	Ubc4	Affinity Capture-Western Reconstituted Complex	Uzunova et al. (2007) Xie et al. (2010)
Slx8	Ubc4	Reconstituted Complex	Xie et al. (2010); Westerbeck et al. (2014)
Snt2	Ubc4	Affinity Capture-Western Reconstituted Complex	Singh et al. (2012)
Ssl1	Ubc4	Reconstituted Complex	Rabut et al. (2011)
Ste5	Ubc4	Two-hybrid	Garrenton (2009)
Tfb3	Ubc4	Reconstituted Complex	Rabut et al. (2011)
Tul1	Ubc4	Affinity Capture-Western Reconstituted Complex Two-hybrid	Reggiori and Pelham (2002)
Ubr1	Rad6	Affinity Capture-MS Affinity Capture-Western Reconstituted Complex Two-hybrid	Wood et al. (2003) Dohmen et al. (1991); Bailly et al. (1994); Du et al. (2002) Hwang et al. (2010) Madura et al. (1993); Xie and Varshavsky (1999)
Ubr2	Rad6	Affinity Capture-MS Affinity Capture-Western Reconstituted Complex Two-hybrid	Wood et al. (2003); Krogan et al. (2006) Wang et al. (2004); Ju et al. (2008) Ju et al. (2008) Yu et al. (2008)
Ufd2	Ubc4	Affinity Capture-Western	Tu et al. (2007)
Ufd4	Ubc4	Affinity Capture-MS Reconstituted Complex	Ho et al. (2002); Krogan et al. (2006) Koegl et al. (1999); Hwang et al. (2010)
Ufd4	Ubc7	Affinity Capture-Western	Ravid and Hochstrasser (2007)

*Note that some of the E2/E3 interactions may not be listed in this table.

1.3 Methods to detect protein-protein interactions

The study of protein-protein interactions (PPIs) is of particular interest in current research as it provides mechanistic insight into cellular processes. Approaches to PPIs detection can be divided into three groups: *in vitro* (detection performed outside the living organism), *in vivo* (detection performed in the living organism itself) and *in silico* methods (detection performed via a computer simulation that enable to predict the possible interactions). Several techniques exist that enable *in vitro* detection of PPIs, based for instance on Far-Western analysis, pull-down assays, tandem affinity purification tagging (TAP-tag), affinity chromatography, co-immunoprecipitation (Co-IP), chip arrays, surface plasmon resonance (SPR), mass spectrometry or X-ray crystallography, and NMR spectroscopy (Howell et al., 2006; Berggård et al., 2007). However, all these techniques remove proteins from their native physiological environment. The monitoring and visualization of PPIs in living cells and in organisms, as well as the characterization of the entire interaction networks, are necessary to understand precisely the molecular mechanisms that underlay biological processes.

A large set of data on PPIs in *S. cerevisiae* comes from the yeast two-hybrid analysis (Y2H) (Uetz et al., 2000; Ito et al., 2001), a very widely used approach in screening for PPIs in living yeast cells, designed by Fields and Song (1989). Y2H relies on monitoring the complex formation via transcriptional activation of reporter genes. Upon the interaction of two proteins, the DNA binding and activation domains of the transcription factor (‘bait’ and ‘prey’, respectively) are brought together, thereby producing a functional transcription activator. The detection is made possible by the expression of reporter genes that results in yeast viability or growth on selective media (Chien et al., 1991; Parrish et al., 2006). However, in the Y2H system proteins are usually overexpressed and thus present at concentrations far higher than under physiological conditions. This in turn often results in false positives (Bartel et al., 1993; Serebriiskii et al., 2000). It was also noted that the Y2H method is inappropriate for studying the interactions between proteins that cannot be transported to the nucleus, since for the reporter gene to be activated the interaction must occur in the nucleus (Sung et al., 2013). Another limitation of Y2H is that proteins overexpressed out of their physiological environment are prone to inappropriate folding. Advantages and

limitations of the Y2H method have been extensively reviewed by Semple and colleagues (2002).

Various methodologies exist for PPIs visualization in living cells, which minimalize perturbation of the natural cellular environment. The most prominent are Förster resonance energy transfer (FRET) (Förster, 1959), bioluminescence resonance energy transfer (BRET) (Xu et al., 1999; Pfleger et al., 2006; Pfleger, 2009) fluorescence cross-correlation spectroscopy (FCCS) (Bacia et al., 2006) and protein fragment complementation assays (PCAs), including the approach based on the use of fluorescent proteins such as the bimolecular fluorescence complementation (BiFC) (Hu et al., 2002), or luminescent reporter proteins for example luciferases (Paulmurugan et al., 2002; Stefan et al., 2007).

1.3.1 Methods to assay protein-protein interactions under near physiological conditions

1.3.1.1 Förster resonance energy transfer (FRET)

As stated in the preceding chapter, several methods exist for studying PPIs in living cells. One of the most popular and frequently applied methods is Förster resonance energy transfer, often referred to as fluorescence resonance energy transfer (FRET) analysis (Sorkin et al., 2000; Sekar and Periasamy, 2003). This method relies on the use of two fluorophores that are either genetically fused or chemically linked to two proteins of interest, and is based on the transfer of excitation energy between them (Förster, 1959). The energy is transferred from an excited state of one fluorophore, which is a donor, to the other fluorophore which is an acceptor. FRET allows for real-time detection of a complex formation and dissociation, and can detect PPIs occuring in different cellular compartments. However, it often requires the expression of proteins at high levels for energy transfer to be detectable. Moreover, it relies on the proper orientation and distance of the donor and the acceptor fluorophores. In practice, 10 nm (100 Å) is the maximum distance over which significant energy transfer can be detected between donor and acceptor fluorophores. Therefore, the detection of PPIs by FRET often requires extensive optimization and is restricted to relatively small proteins and complexes (Piehler, 2005; Piehler, 2014).

1.3.1.2 Bioluminescence resonance energy transfer (BRET)

Another method for studying protein-protein interactions in real-time *in vivo* is bioluminescence resonance energy transfer (BRET) (Pfleger et al., 2006b), first used to study the bacterial KaiB circadian clock protein dimerization (Xu et al., 1999b). BRET relies on the same principle as FRET, with the exception that the donor here is not a fluorophore but a bioluminescent molecule (typically *Renilla* luciferase). The transfer of energy from the donor enzyme to the acceptor fluorophore, such as GFP or YFP, occurs upon substrate oxidation. The main limitation of BRET is that *Renilla* luciferase generates a broad emission peak that considerably overlaps with the emission of the yellow fluorescent protein (YFP), contributing to the low signal-to-noise ratio when

YFP or its variants are used as an acceptor molecule (Xu et al., 1999b). BRET might be applicable to studying dynamic PPIs in a cell population, however the visualization of PPIs in the different subcellular compartments of a single living cell is more challenging due to the low intensity of luciferase light emission (Boute et al., 2002).

1.3.1.3 Fluorescence cross-correlation spectroscopy (FCCS)

In recent years, cross-correlation techniques that monitor correlated movement of interacting partners prior to protein complex formation have been widely developed, with fluorescence cross-correlation spectroscopy (FCCS) applied to the quantitative and selective monitoring of interactions in living cells (reviewed by Bacia et al., 2006 and recently by Ma et al., 2014). This technique is an extension of fluorescence correlation spectroscopy (FCS) that measures the fluctuations in the number of fluorescent molecules in a confocal volume. FCCS detects the fluctuations of two spectroscopically separated fluorescent labels (two dyes with well-separated emission wavelengths, for example green and red) (Schwille et al., 1997), and enables to quantify the formation of potential protein complexes. However, the absolute quantification is technically challenging, as it requires very precisely overlapping confocal volumes (Foo et al., 2012). A limiting factor for FCCS, as well as fluorescence correlation spectroscopy in general, is that the particles under study have to be sufficiently mobile in the detection volume. Moreover, FCCS is only applicable at relatively low fluorophores concentration (otherwise the fluctuations in fluorescence intensity are difficult to detect), and therefore cannot detect weak interactions that occur at higher concentrations (Bacia and Schwille, 2007). Some FCCS variants and improvement have been reported recently for studying PPIs in living cells (Padilla-Parra et al., 2011; Singh et al., 2013; Krieger et al., 2014; Sadaie et al., 2014).

1.3.2 Protein-fragment complementation assays (PCAs)

The first protein-fragment complementation assay (PCA) for *in vivo* protein interactions was demonstrated by Johnsson and Varshavsky (1994) using split-ubiquitin as a sensor. Here, the inactive N- and C-terminal fragments of ubiquitin with an

attached reporter protein (C-terminal attachment) were fused to proteins of interest and upon their interaction the Ub function was restored. Ub was then recognized by ubiquitin specific proteases (USPs) and the C-terminal attached reporter protein was cleaved, leading to the activation of gene expression (Johnsson and Varshavsky, 1994). The general principle was further applied in the laboratory of Stephen Michnick, starting with the enzyme murine dihydrofolate reductase (mDHFR) as a reporter. The group showed that the reporter enzyme folds into its native structure from its two inactive fragments, and its activity is reconstituted upon the interaction of two proteins of interest. The restored function was then detected by reconstituted enzyme activity. They demonstrated the principle on two PPIs *in vivo*, namely those of p21 ras GTPase with its target the ras-binding domain (RBD) of the Ser/Thr kinase raf, and the rapamycin-mediated interaction of the immunophillin FKBP with the *S. cerevisiae* target of rapamycin (TOR2) (Pelletier et al., 1998). Since then a number of enzymes, including β-lactamase (Galarneau et al., 2002; Wehrman et al., 2002), firefly (Luker et al., 2004), *Renilla* (Kim et al., 2004; Stefan et al., 2007) and *Gaussia* luciferases (Remy and Michnick, 2006), as well as fluorescent proteins such as green fluorescent protein (GFP) (Magliery et al., 2005), yellow fluorescent protein (YFP) (Nyfeler et al., 2005), Venus (Nakagawa et al., 2011; Ohashi et al., 2012) or mCherry (Fan et al., 2008), have been used in a broad range of PPIs analyses. The two most commonly applied types of PCAs for the detection of PPIs in living cells, based on bioluminescent and fluorescent protein-fragment complementation, are referred as bimolecular luminescence complementation (BiLC) and bimolecular fluorescence complementation (BiFC), respectively.

1.3.2.1 Bimolecular luminescence complementation (BiLC)

BiLC relies on the ability of split nonluminescent protein fragments to reconstitute functional luminescent proteins when these are brought into close contact by fused interacting partners (Figure 18). Among the BiLC are luciferase-based systems with various luciferases as aforementioned, and *Renilla* luciferase as the major reporter protein used to date in living cells and rodents. Luciferase complementation involves fusing the inactive N- and C-terminal luciferase fragments to two proteins of interests, which bring the fragments together upon their interaction and reconstitute an active enzyme. Luciferase then catalyses the oxidation of their cell membrane-permeable substrate coelenterazine, and the activity is detected by emitted bioluminescence in the form of blue light (400-500 nm). The bioluminescent signal is emitted only at the sites and times of interaction occurrence in cells (Kaihara et al., 2003). Luciferase-based assays can be applied to quantify regulation of protein-protein complexes in response to various signaling events, chemical probes or drugs (Luker and Luker, 2014).

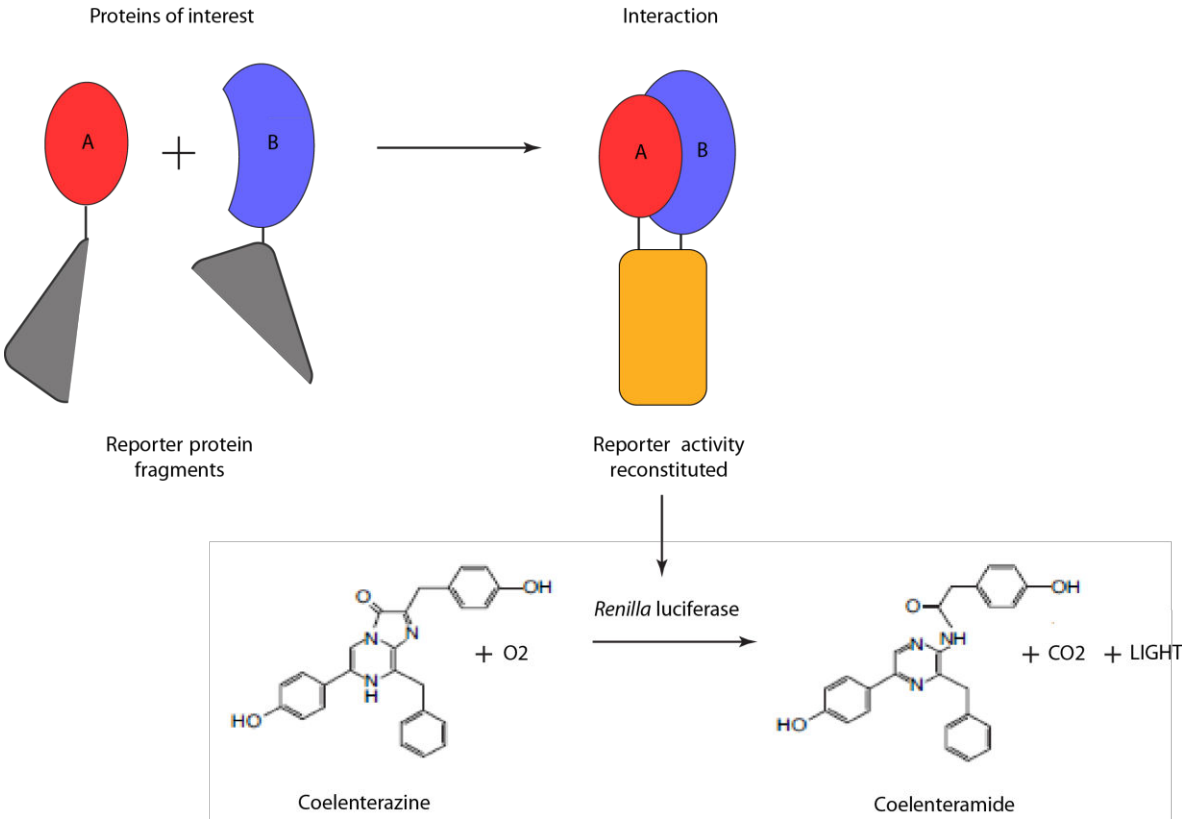

Figure 18. Principle of BiLC. A pair of interacting proteins A and B is fused to the inactive fragments of a luminescent reporter protein, e.g. *Renilla* luciferase. When proteins A and B interact the two reporter protein fragments are brought together and the reporter activity is reconstituted. This can be detected by the emission of light since *Renilla* luciferase catalyzes oxidation of its substrate coelenterazine to coelenteramide emitting photon of light.

1.3.2.2 Bimolecular fluorescence complementation (BiFC)

A widely used approach for visualizing interactions between proteins of interest is BiFC, which is also most valuable in determining subcellular localization of the complex. The BiFC assay is based on the fusion of two complementary amino- (N-) and carboxy-terminal (C-) fragments of a fluorescent reporter protein to the putative interacting proteins (Figure 19). The fluorescent reporter fragments can be fused to a putative interacting partner on either its N- or C-terminus. The fluorescent protein fragments alone remain inactive. Upon interaction, the fragments are brought into close proximity and fold into their native structure, and the activity of the reporter is reconstituted, giving fluorescent signal. The noncovalent association of the fluorescent protein fragments forms an irreversible BiFC complex (reviewed by Kerppola, 2008).

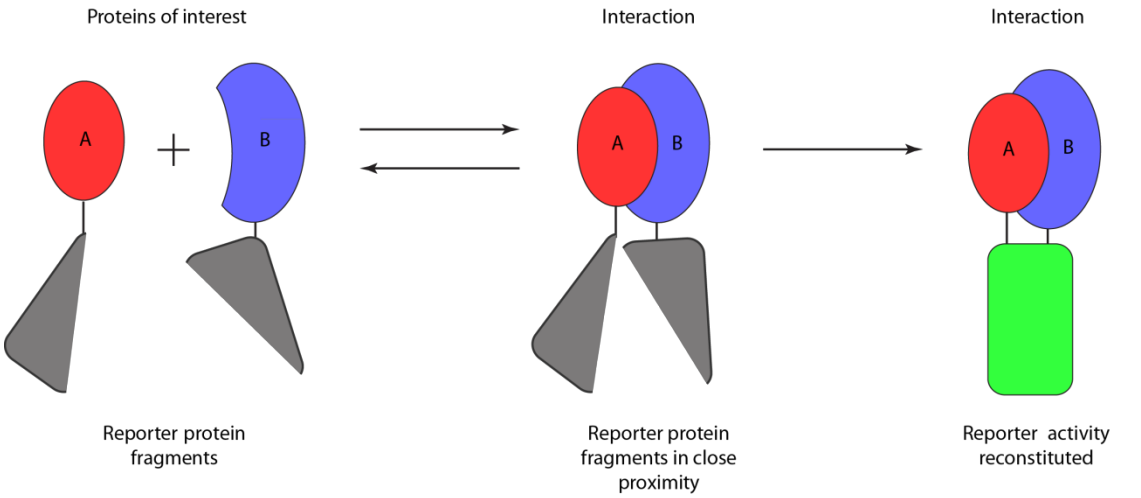

Figure 19. Principle of the BiFC assay. A pair of interacting proteins A and B is fused to the inactive N- and C-terminal fragments of a fluorescent reporter protein, respectively. When proteins A and B interact the two reporter protein fragments are brought together and the reporter activity is reconstituted, reproducing fluorescence emission under excitation.

1.3.2.2.1 Fluorescent protein fragments used in BiFC analysis

A considerable number of different fluorescent protein fragments have been used for BiFC analysis. The green fluorescent protein (GFP) from the jelly fish *Aequorea victoria* has emerged as a versatile tool in biology since its cloning and sequencing in 1992 (Prasher et al., 1992), and has been extensively used in various complementation

assays. The first split GFP assay to detect PPIs was described by Ghosh et al. in 2000. In their study they used antiparallel leucine zippers, which were attached via a linker sequence to two split (between residues 157 and 158) GFP N- and C-terminal fragments called NGFP and CGFP, containing 157 and 81 residues respectively. Leucine zippers were required to produce fluorescence, suggesting that the split fragments could not reassemble GFP on their own (Ghosh et al., 2000). A number of GFP variants have similarly been used in BiFC assays, including EGFP, EBFP, ECFP, yellow fluorescent protein (YFP) or its enhanced version (EYFP), Venus and Cerulean (Shyu et al., 2006; reviewed by Kodama and Hu, 2012). In addition, other proteins that show different spectral properties and stabilities have also been used, including mCherry (Fan et al., 2008), mRFP1 (Jach et al., 2006) or photoswitchable Dronpa (Lee et al., 2010).

Currently the most widely used fluorescent protein fragments are derived from EYFP and Venus. EYFP-based BiFC was first reported to visualize PPIs in living mammalian cells (Hu et al., 2002). However, these assays were sensitive to high temperatures. Venus (Figure 20), a YFP variant with an extra point mutation F46L, was shown to be less sensitive to the environment (Nagai et al., 2002). Moreover, Venus was identified by Nagai et al., (2002) as a bright fluorescent protein with fast and efficient maturation properties. It has been shown that Venus produces the brightest fluorescence intensity in BiFC assays, approximately ten times higher than that of EYFP-based BiFC (Shyu et al., 2006). Recently, several studies aiming to develop a Venus-based BiFC assay with low background fluorescence have been conducted (see for instance - Ohashi et al., 2012).

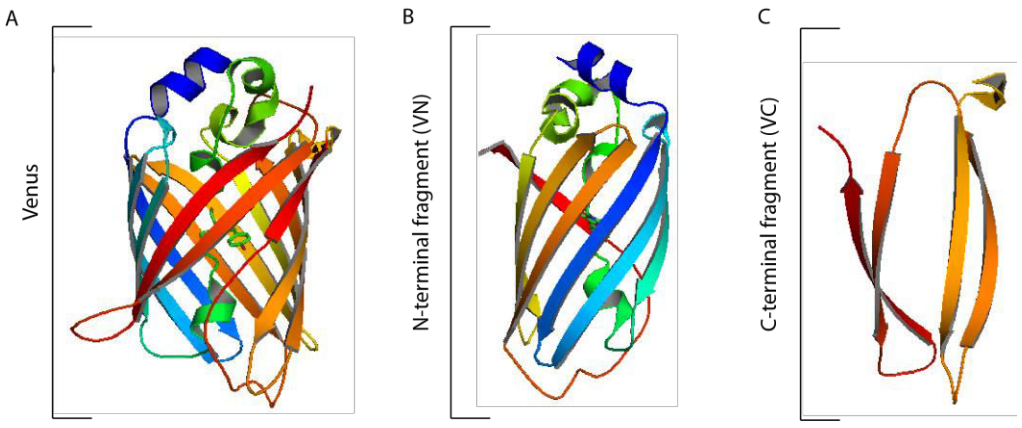

Figure 20. A) Structure of the Venus yellow fluorescent protein (PDB ID: 1MYW) with the α-helices and β-strands visualized in rainbow colors using PyMOL software (http://www.pymol.org/) B) N-terminal fragment of Venus (VN) C) C-terminal fragment of Venus (VC).

1.3.2.2.2 Use of BiFC to investigate protein-protein interactions in living cells

The BiFC approach has been extensively used to study PPIs in various cell types and organisms. PPIs have been visualized in bacteria, for example *E. coli* (Magliery et al., 2005; Pazos et al., 2013) or *Agrobacterium tumefaciens* (Cascales et al., 2005), in fungi – largely in *S. cerevisiae* (Blondel et al., 2005; Cole et al., 2007; Sung and Huh, 2007), nematode *C. elegans* (Hiatt, Shyu et al., 2008), plants (Bracha-Drori et al., 2004; Walter et al., 2004) and mammalian cells (Hu et al., 2002; Hynes et al., 2004). However, it is interesting to note that molecular oxygen is required in the chemistry of fluorophore formation, rendering the approach ineligible for use in anaerobic organisms (Kerppola, 2006). Several studies have revealed that BiFC enables simple and direct visualization of PPIs (Hu et al., 2002; Hu and Kerppola, 2003; Hudry et al., 2011). This can be performed directly in living cells, eliminating possible artifacts inherent in cell lysis or fixation. PPIs using BiFC can be detected without the addition of fluorogenic or chromogenic agents, thereby avoiding cells perturbation by those agents. Aside from determining whether two proteins can interact, BiFC provides information on the localization of protein complexes. Previous studies have reported visualization of BiFC complexes in various subnuclear structures (Hu et al., 2002), lysosomes (Fang and Kerppola, 2004), plasma membrane (Remy and Michnick, 2004), endoplasmic reticulum (ER) (Anderie et al., 2007) and lipid droplets (Granneman et al., 2007). BiFC has been also applied to examine cell cycle regulated PPIs. Examining the individual stages of the cell cycle remains however still a challenging subject for BiFC imaging (Blondel et al., 2005; Cole et al., 2007).

1.3.2.2.3 Advantages and limitations of BiFC

BiFC is an attractive method for investigating PPIs. Its main advantage is the capacity to detect transient and weak interactions. Indeed, the association of two fluorescent protein fragments is irreversible and stabilizes interactions between the binding partners (transient interactions can be trapped in a complex). Therefore not only weakly associating proteins but also interactions with short half-lives can be detected (Magliery et al., 2005). This irreversible complex formation is however a drawback as it might potentially influence the function or activity of the complex. It is now known that

BiFC assay can be used to detect interactions within minutes after the complexes being formed, but the limitation here is that it does not provide real-time measurement of the amount of formed complexes and does not provide information on complex dissociation (Kerppola, 2013). Another advantage however is that proteins those interactions are to be examined are not overexpressed but rather are expressed in their cellular context, ideally at similar levels as the endogenous proteins. This helps to avoid the false-positive results derived from a self-association of two fluorescent protein fragments, when expressed at sufficiently high concentrations (Cabantous et al., 2005) in the absence of the interaction. It is important therefore to test the fluorescence complementation using fusion proteins with the mutated interaction interface. The mutant proteins should be fused in the same manner to the wild-type proteins (Hu et al., 2002). Another benefit of this method is that the fluorescence of BiFC complex can be measured using a widely available fluorescence microscope or a flow cytometer without the need for any specialist equipment.

2 AIM OF THIS STUDY

Interactions between ubiquitin conjugating enzymes and ubiquitin ligases are in the center of ubiquitylation cascade. E2 enzymes constitute a passage between the first step of activation and the final covalent conjugation, and the combination of particular E2/E3 pairs determine what types of Ub chains are made, thus determining the regulatory functions of the Ub pathway. To date, only a small fraction of all possible E2/E3 pairs have been investigated, mainly using biochemical and *in vitro* approaches that often may not accurately reflect the conditions that occur in living cells.

The primary goal of my PhD project was therefore to establish a method suitable to systematically assay E2/E3 interactions under near physiological conditions and then screen for new E2/E3 pairs in living cells, using yeast *Saccharomyces cerevisiae* as a model organism. Looking at the E2/E3 interactions under near physiological conditions is of great importance to preserve features that influence biologically relevant interactions such as protein localization, concentration, posttranslational modifications and incorporation into interacting partners as well as E2~Ub conjugates, and other regulatory mechanisms.

This project was set with the following objectives:

1. Identification and optimization of a method to detect and quantify E2/E3 interactions in living yeast cells.
2. Construction of an array of yeast strains to systematically assay E2/E3 interactions.
3. Unbiased screening for new putative E2/E3 pairs in budding yeast.
4. Functional characterization of one candidate E2/E3 pair.

3 MATERIALS AND METHODS

3.1 Materials

All chemicals and reagents used in this study were of molecular biology and analytical grade. Plasmid DNA extraction kits as well as PCR products clean-up and gel extraction kits were purchased from Macherey-Nagel. Restriction enzymes and Gibson Assembly Master Mix used for molecular cloning were purchased from New England Biolabs. Other reagents, bacteria and yeast media, and all necessary equipment are listed below.

Reagents

- Bacto yeast extract (BD Biosciences, cat. no. 288620);
- Bacto peptone (BD Biosciences, cat. no. 211677);
- Difco dextrose (Glucose, BD Biosciences, cat. no. 215530). CRITICAL: Dextrose should be autoclaved separately from amino acids or protein containing reagents present in media components due to the Maillard's reaction that leads to the formation of brown pigments;
- Difco nutrient broth (BD Biosciences, cat. no. 234000);
- Difco yeast extract (BD Biosciences, cat. no. 210934);
- Difco yeast nitrogen base w/o amino acids and ammonium sulfate (BD Biosciences, cat. no. 233520);
- Zinc acetate (MW = 183.48 g mol^{-1}, Sigma-Aldrich, cat. no. 383317) (see REAGENT SETUP);
- Potassium acetate (MW = 98.14 g mol^{-1}, Sigma-Aldrich, cat. no. P1190);
- α-Glutamic acid (MW = 187.13 g mol^{-1}, Euromedex, cat. no. 2030);
- clonNAT (Nourseothricin-dihydrogen sulfate, MW = 1359.47 g mol^{-1}, Werner BioAgents, cat. no. 5.001.000) (see REAGENT SETUP);
- Hygromycin B (MW = 527.52 g mol^{-1}, TOKU-E, cat. no. H007) (see REAGENT SETUP);
- L-Canavanine sulfate salt (Canavanine, MW = 274.25 g mol^{-1}, Sigma-Aldrich, cat. no. C9758) (see REAGENT SETUP);

- S-(2-Aminoethyl)-L-cysteine hydrochloride (Thialysine, MW = 200.69 g mol^{-1}, Sigma-Aldrich, cat. no. A2636) (see REAGENT SETUP);
- Tetracycline hydrochloride (MW = 480.90 g mol^{-1}, Sigma-Aldrich, cat. no. T3383) (see REAGENT SETUP);
- Uracil (Ura, MW = 112.09 g mol^{-1} Sigma-Aldrich, cat. no. U1128);
- L-histidine (His, MW = 155.15 g mol^{-1} Sigma-Aldrich, cat. no. H8000);
- L-lysine (Lys, MW = 146.19 g mol^{-1} Sigma-Aldrich, cat. no. L5501);
- L-Leucine (Leu, MW = 131.17 g mol^{-1} Sigma-Aldrich, cat. no. L8000);
- L-methionine (Met, MW = 149.21 g mol^{-1} Sigma-Aldrich, cat. no. M9625);
- Amino acid stock solution (see REAGENT SETUP);
- Ammonium sulfate ($(NH_4)_2SO_4$, MW = 132.14 g mol^{-1}, Sigma-Aldrich, cat. no. A6387);
- Glutamic acid, monosodium salt (MW = 167.15 g mol^{-1}, Euromedex, cat. no. 2030);
- Potassium phosphate monobasic (KH_2PO_4, MW = 136.09 g mol^{-1}, Sigma-Aldrich, cat. no. P0662);
- Magnesium sulfate ($MgSO_4$, MW = 120.37 g mol^{-1}, Sigma-Aldrich, cat. no. 246972);
- Sodium chloride (NaCl, MW = 58.44 g mol^{-1}, Sigma-Aldrich, cat. no. S9888);
- Calcium chloride ($CaCl_2$, MW = 110.98 g mol^{-1}, Sigma-Aldrich, cat. no. 449709);
- Boric acid (H_3BO_3, MW = 61.83 g mol^{-1}, Merck Millipore, cat. no. 1007650500);
- Copper (II) sulfate pentahydrate ($CuSO_4.5H_20$, MW = 249.69 g mol^{-1}, Sigma-Aldrich, cat. no. 209198);
- Potassium iodide (KI, MW = 160.00 g mol^{-1}, Sigma-Aldrich, cat. no. P4286);
- Iron (III) chloride ($FeCl_3$, MW = 162.20 g mol^{-1}, Sigma-Aldrich, cat. no. F7134);
- Manganese (II) sulfate monohydrate ($MnSO_4.H_2O$, MW = 169.02 g mol^{-1}, Sigma-Aldrich, cat. no. 221287);
- Sodium molybdate (Na_2MoO_4, MW = 205.92 g mol^{-1}, Sigma-Aldrich, cat. no. 243655);

- Zinc sulfate monohydrate (ZnSO4. H_2O, MW = 179.47 g mol^{-1}, Sigma-Aldrich, cat. no. 96495);
- Biotin (Vitamin H, MW = 244.31 g mol^{-1}, Sigma-Aldrich, cat. no. B4501);
- Calcium pantothenate (MW = 244.31 g mol^{-1}, Sigma-Aldrich, cat. no. C8731);
- Myo-inositol (MW = 180.16 g mol^{-1}, Sigma-Aldrich, cat. no. 17508);
- Niacin (Vitamin B3, nicotinic acid, Sigma-Aldrich, cat. no. 72309);
- PABA (4-amniobenzoic acid, MW = 137.14 g mol^{-1}, Sigma-Aldrich, cat. no. A9878);
- Pyridoxine hydrochloride (MW = 205.64 g mol^{-1}, Sigma-Aldrich, cat. no. P9755);
- Thiamine hydrochloride (Vitamin B1, MW = 337.27 g mol^{-1}, cat. no. T4625);
- Low fluorescence yeast nitrogen base (yeast nitrogen base without riboflavin and folic acid), was prepared according to the protocol of Sheff and Thorn, 2004) (see REAGENT SETUP);
- YPD (Yeast extract/peptone/dextrose) medium (see REAGENT SETUP);
- GNA pre-sporulation medium (see REAGENT SETUP);
- Zinc acetate sporulation medium (ZnSPO) (see REAGENT SETUP);
- Diploid selection medium (Synthetic minimal medium based on glutamate (SED), here lacking leu and ura with an addition of clonNAT) (see REAGENT SETUP);
- Haploid selection medium (Synthetic minimal medium based on glutamate (SED), here lacking leu/lys/ura with an addition of clonNAT, hygromycin B, canavanine and thialysine for *MATα* haploid selection) (see REAGENT SETUP);
- Low fluorescence visualization medium (Yeast nitrogen base without riboflavin and folic acid) was prepared according to the protocol of Sheff and Thorn, (2004);
- Coelenterazine native (CTZ, Interchim, cat no. FP-BV0731);
- Coelenterazine h (CTZ h, Euromedex, cat. no. 21159-AAT);
- Coelenterazine hcp (CTZ hcp, Euromedex, cat. no 21154-AAT);
- Yeast extraction buffer (breaking buffer) (see REAGENT SETUP);
- TCA-sample buffer (see REAGENT SETUP).

Equipment

- Electronic 96-channel handheld pipette VIAFLO 96 (Integra Biosciences, cat. no. 6000);
- Refrigerated incubator shaker-incubator to grow yeast cultures at 20°C. Alternatively, cultures can be grown at 25°C or 30°C in a standard incubator;
- Inverted fluorescence microscope with 63x water immersion objective and 96-well plate adaptor. In our laboratory we were using Leica SP8 confocal microscope;
- Luminometer - after testing different luminometer, we were using Centro XS3 LB960 Microplate Luminometer (DLReady, Berthold Technologies) for the final measurements.

Consumables

- Pipet tips for VIAFLO electronic handheld pipettes (Griptips 125 µL, Integra Biosciences, cat. no. 4424);
- 96-well culture plates (ScreenMates, Matrix Technologies, cat. no. 4912). These plates were used to grow yeast culture, sporulate and select the haploids;
- Sealing films for yeast 96-well plate culture (Excel Scientific, cat. no. BS-25);
- 96-well glass imaging plates (Imaging plates CG (96-well), Zell-kontakt GMBH);
- 96-well white solid plates for bioluminescent assays (Fisher Scientific, cat. no. 3789).

Reagent setup

- Zinc acetate (5 mg/mL) - dissolved in dH_2O, filter sterilized;
- clonNAT (100 mg/mL) - dissolved in dH_2O, filter sterilized. This stock solution is stable for 4 weeks at 2-8°C. For longer storage the solution must be frozen at -20°C or deeper;
- Hygromycin B (300 mg/ mL) - dissolved in dH_2O, filter sterilized. This stock solution is stable for several months at 2-8°C. CRITICAL: Do not freeze hygromycin stock solutions;
- Canavanine (50 mg/mL) - dissolved in dH_2O, filter sterilized. This stock solution is stable for several weeks at 2-8°C. For longer storage needs freezing at -20°C;
- Thialysine (50 mg/mL) - dissolved in dH_2O, filter sterilized. This stock solution is stable for several weeks at 2-8°C. For longer storage needs freezing at -20°C;

- Tetracycline (10 mg/mL) - dissolved in dH_2O, filter sterilized. CRITICAL: Protect from light as it can affect the breakdown rate of this antibiotic;
- Coelenterazine and coelenterazine analogs solutions - dissolved in ethanol and prepared under indirect (dimmed) light. Aliquots should be prepared fresh, optimally one day prior use or on the day of use. For longer storage aliquots can be frozen at -20°C and need to be adjusted to RT prior using for at least 1h. CRITICAL: exposure of coelenterazine or its analogs to light and ambient oxygen must be avoided;
- Amino acid stock solution - 0.2 g L^{-1} uracil, 0.2 g L^{-1} L-histidine, 0.3 g L^{-1} L-lysine HCl, 0.6 g L^{-1} L-leucine, 0.2 g L^{-1} L-methionine. To select auxotrophic yeast strains appropriate amino acids were dropped out. Autoclaved using a short 15' cycle;
- YPD medium - 1% wt/vol Bacto yeast extract; 2% wt/vol Bacto peptone, 2% wt/vol dextrose in dH_2O, sterilized by autoclaving;
- GNA pre-sporulation medium - 3% wt/vol Difco nutrient broth, 1% wt/vol Difco yeast extract, 5% wt/vol dextrose in dH_2O, sterilized by autoclaving;
- ZnSPO medium - 1% vol/vol zinc acetate 2% wt/vol potassium acetate in dH_2O, add 10x complete amino acid stock sterilized by autoclaving;
- Diploid selection medium - 0.17% wt/vol Difco yeast nitrogen base w/o amino acids and ammonium sulfate, 0.1% wt/vol glutamic acid, 2% wt/vol dextrose. Yeast strains contain *NatMX6* resistance cassette that enable the cells to grow in the presence of the eukaryotic antibiotic clonNAT (nourseothricin) and a *URA3* auxotrophic marker for the selection in synthetic media lacking uracil. CRITICAL: Autoclaved and cooled to 50°C before adding antibiotics and the desired amino acids;
- Haploid selection medium - 0.17% wt/vol Difco yeast nitrogen base w/o amino acids and ammonium sulfate, 0.1% wt/vol glutamic acid, 2% wt/vol dextrose. As for diploid selection medium, yeast strains contain resistance cassettes with the *NatMX6* genes that enable the cells to grow in the presence of the eukaryotic antibiotic clonNAT and *URA3* marker for the selection in the media lacking uracil. Additionally, yeasts have a selection module conferring hygromycin resistance gene that in the presence of antibiotic hygromycin B enables to grow only *MATα* cells. Canavanine and thialysine needs to be added to this media.

CRITICAL: Autoclaved and cooled to 50°C before adding antibiotics, the desired amino acids as well as canavanine and thialysine. Note: For any synthetic media containing G418 or hygromycin monosodium glutamic acid is added as a nitrogen source instead of ammonium sulfate (Cheng et al. 2000);

- Low fluorescence yeast nitrogen base - This yeast nitrogen base is a component of a low fluorescence yeast visualization medium. For preparation use the following reagents at the appropriate concentrations: 5 g L^{-1} $(NH_4)_2SO_4$, 1 g L^{-1} KH_2PO_4, 0.5 g L^{-1} $MgSO_4$, 0.1 g L^{-1} NaCl, 0.1 g L^{-1} $CaCl_2$, 0.5 mg L^{-1} H_3BO_3, 0.04 mg L^{-1} $CuSO_4.5H_20$, 0.1 mg L^{-1}, 0.1 mg L^{-1} KI, 0.2 mg L^{-1} $FeCl_3$, 0.4 mg L^{-1} $MnSO_4.H_2O$, 0.2 mg L^{-1} Na_2MoO_4, 0.4 mg L^{-1} $ZnSO_4$, 2 µg L^{-1} biotin, 0.4 mg L^{-1} calcium pantothenate, 2 mg/l inositol, 0.4 mg L^{-1} niacin, 0.2 mg L^{-1} PABA, 0.4 mg L^{-1} pyroxidine HCl, 0.4 mg L^{-1} thiamine;
- Low fluorescence visualization medium - 2% wt/vol dextrose, low fluorescence yeast nitrogen base (as aforementioned). CRITICAL: Autoclaved and cooled to 50°C before adding the essential amino acids;
- Yeast extraction buffer (breaking buffer) – 2% Triton X-100, 1% SDS, 100mM NaCl, 100mM Tris-HCl (pH 8.0), 1 mM EDTA (pH 8.0);
- TCA-sample buffer - 2.2 ml 70% glycerol (final: 15%), 3 ml 1.5M Tris pH 8.8 (final: 450 mM), 0.5 ml 20% SDS (final: 1%), 40 µl 0.5M EDTA (final: 2 mM), 0.1 ml 0.5% bromophenol blue (or a ‘spatula tip’), 4.2 ml H_2O.

Antibodies

Table 6. Antibodies used in this study

Antibody	Type	Specificity	Company/ Reference	Dilution
Anti-GFP (9F6)	Mouse monoclonal	N-terminal part of GFP	Selleckchem	1:5000
Anti-GFP (clones 7.1 and 13.1)	Mixture of mouse monoclonal antibodies 7.1 and 13.1	C-terminal part of GFP	Roche	1:1000
Anti-GFP	Rabbit polyclonal	GFP	Clontech	1:1000
Anti-yRad6	Rabbit polyclonal	Rad6 from *S. cerevisiae*	Davies et al., 2010	1:5000
Anti-yUbc6	Rabbit polyclonal	Recombinant His-UBC6 (without the transmembrane domain) from *S. cerevisiae*	Walter et al., 2001	1:5000
Anti-yUbc13	Rabbit polyclonal	Recombinant His6-Ubc13 from *S. cerevisiae*	Ulrich, 2003	1:10000

Oligonucleotides

Table 7. Primers used in this study

Primer name	Description*	Sequence (5'→3')
oEB0001	Rad6-VN-F	tggacgatgatgatgatgatgacgacgacgacgacgaagcagacggtcgacggatccccgggtt
oEB0002	Rad6-R	tgattgaacaaaaaggtaatcgaattcataatatcggctcggcattcatcttcgacactggatggcggcgttag
oEB0003	Ubr1-VC-F	atgaggatgactctgatgataatgatgactctgatgagcgagagatttggggtcgacggatccccgggtt
oEB0004	Ubr1-R	tgtataagtttttatatacaaatatgtcaactataaaacatagtagagggttcgacactggatggcggcgttag
oEB0005	Ubc4-Rluc-F	acccaagtacgaagctacagccagagaatggacaaagaaatacgctgtatggcggtggcggatccggagg
oEB0006	Ubc4-R	aatcccatataaatcttgcttctctttttcagctgagtaaggacttctgtttcgacactggatggcggcgttag
oEB0007	Ufd4-Rluc-F	ctcgtctttgtcaagccattgaagagggtgcaggagcttttctactttccggcggtggcggatccggaggc
oEB0008	Ufd4-R	gaaataattttgaagtcatataaaacttaaatagaaaaagtaactaaaatttcgacactggatggcggcgttag
oEB0009	Rad6-LUC-F	tggacgatgatgatgatgatgacgacgacgacgacgaagcagacggcggtggcggatccggaggc
oEB0010	Ubr1-LUC-F	atgaggatgactctgatgataatgatgactctgatgagcgagagatttggggcggtggcggatccggaggc
oEB0011	Ubc4-VN-F	gacccaagtacgaagctacagccagagaatggacaaagaaatacgctgtaggtcgacggatccccgggtt
oEB0012	Ufd4-VC-F	ctcgtctttgtcaagccattgaagagggtgcaggagcttttctactttccggtcgacggatccccgggtt
oEB0013	Rad6-1F	acgacgacgacgaagcagac
oEB0014	Rad6-4R	acaaaagatacgggtatcgg
oEB0015	Ubr1-F	atgactctgatgagcgagag
oEB0016	Ubr1-R	ttgactatccgtgacaggac
oEB0017	Ubc4-F	gctacagccagagaatggac
oEB0018	Ubc4-R	aacgttgacgctccctcgac
oEB0019	Ufd4-F	ttgtcaagccattgaagagg
oEB0020	Ufd4-R	tttgttgtcgtaacttctcc
oEB0021	Ubc4 cloning-F	acggatccagctcaccttgaaaggccttggc
oEB0022	Ubc4 cloning-R	ccttaattaaagaaccaccagaaccacctacagcgtatttctttgtccattc
oEB0023	Rluc/Rluc8- F	atggatccttaattaatatgaccagcaaggtgtacgaccc
oEB0024	Rluc/Rluc8-R	atctcgagttaagcggccgcctgctcgttcttcagcactctctc
oEB0025	Gluc-F	atggatccttaattaatatgaagcccaccgagaacaacgaag
oEB0026	Gluc-R	atctcgagttaagcggccgcgtcaccaccggccccttgatctt
oEB0027	Ubc4(F63A)	ttcccaaccgactacccagccaagccaccaaagatctc
oEB0028	Ubc4(A97D)	ggatcaatggtctccagatctaactctatcgaagg
oEB0029	Ubc4-F	caaatggccgagcaacagg
oEB0030	Ubc4-R	cgcgcttgcgtgcatgtaac
oEB0031	ubc4(P62A,A63N)	ccatttcccaaccgactacgcaaacaagccaccaaagatctcc
oEB0032	ubc4(A63N)	ttcccaaccgactacccaaacaagccaccaaagatctc
oEB0033	ubc4(Δ)-F	aaaacatgggtggttctggtggttctttaattaac
oEB0034	ubc4(Δ)-R	gaaccacccatgtttttttggatgcttgtttatg
oEB0035	ubc4(Δ2-8)-F	aaaacatgaaagaactaagtgatctagaaagg
oEB0036	ubc4(Δ2-8)-R	agttctttcatgtttttttggatgcttgtttatg
oEB0037	ubc4(Δ2-20)-F	aaaacatgtcatgttcagccggtccagtcg
oEB0038	ubc4(Δ2-20)-R	gaacatgacatgtttttttggatgcttgtttatg
oEB0039	ubc4(Δ139-148)-F	ctacagccggtggttctggtggttctttaattaac
oEB0040	ubc4(Δ139-148)-R	gaaccaccggctgtagcttcgtacttggg
oEB0043	VC_F	tggtggttctttaattaacggtggttctggtggtggttctggtatggacaaacaaaagaatggtatc
oEB0044	VC_R	gcgccctacttgtacatacaattcatccataccatgggtaatacc
oEB0045	Cdc34-F	cgctgcaggtcgacggatccagaaggacaataaagagcatac
oEB0046	Cdc34-R	ccagaaccaccgttaattaaaccagaaccacctattttctttgaaactctttctacatcc
oEB0047	Ubc10-F	cgctgcaggtcgacggatccccctgaaatttattgatgc
oEB0048	Ubc10-R	ccagaaccaccgttaattaaaccagaaccaccatggttgttgatccgctctctttctgctagg
oEB0049	Ubc7-F	cgctgcaggtcgacggatccgagcttgaagaacttaccagac
oEB0050	Ubc7-R	ccagaaccaccgttaattaaaccagaaccaccgaatcctaatgatttcaaaatggataactttacc
oEB0051	Rad6-F	cgctgcaggtcgacggatcccatattcggaatattagtatgg
oEB0052	Rad6-R	ccagaaccaccgttaattaaaccagaaccaccgtctgcttcgtcgtcgtcgtcg
oEB0053	Ubc1-F	cgctgcaggtcgacggatcctcacataatacgaacattaatatcc
oEB0054	Ubc1-R	ccagaaccaccgttaattaaaccagaaccaccccttcaacaattcctcgatgatacgg
oEB0055	Ubc5-F	cgctgcaggtcgacggatccattagatatctagatgtattgc
oEB0056	Ubc5-R	ccagaaccaccgttaattaaaccagaaccaccaacagcatatttttttagtccactcc
oEB0057	Ubc6-F	cgctgcaggtcgacggatccaatattgcactttacaattagg
oEB0058	Ubc6-R	ccagaaccaccgttaattaaaccagaaccacctttcataaaaaggccaaccaaaaac
oEB0059	Ubc8-F	cgctgcaggtcgacggatcctgcgtaaatatacattcttacg
oEB0060	Ubc8-R	ccagaaccaccgttaattaaaccagaaccaccttgatttgcgacttcgtcgtag
oEB0061	Ubc9-F	cgctgcaggtcgacggatccgatcttcatctaaaaggtcatc
oEB0062	Ubc9-R	ccagaaccaccgttaattaaaccagaaccacctttagagtactgtttagcttgaagc
oEB0063	Ubc11-F	cgctgcaggtcgacggatcctcaatagtcctgcatacgtagc
oEB0064	Ubc11-R	ccagaaccaccgttaattaaaccagaaccaccgtaatcgtcgatttcttcataacaggcc
oEB0065	Ubc12-F	cgctgcaggtcgacggatccaatctcatctgccttaaacgag
oEB0066	Ubc12-R	ccagaaccaccgttaattaaaccagaaccaccaggagaaactatgttatcatatttgac
oEB0067	Ubc13-F	cgctgcaggtcgacggatccaatataatgggcatctaacagg
oEB0068	Ubc13-R	ccagaaccaccgttaattaaaccagaaccaccctcgggtttcttctttgcatacaatttc

oEB0069	LYP1(5'UTR)-F	cgtagtgcgctttcattgac
oEB0070	LYP1(3'UTR)-R	gaacatatcgtgaataatgacc
oEB0073	Cdc34-F	gcagcatcgtcttgtgtttg
oEB0074	Ubc10-F	atacctcaaccgttgcatcc
oEB0075	Ubc7-F	tctgatgcacgatgcacacg
oEB0076	Ubc9-F	acacagaacccttcgcttgc
oEB0077	Ubc11-F	tggtgaatcgagtgatagtg
oEB0078	Ubc12-F	agaggctttcaatcctctgg
oEB0079	Ubc13-F	ctttgccttctctacatgtg
oEB0080	Ubc1-F	aacaatttggataactatcc
oEB0081	Ubc5-F	ggtactcattcattaggctc
oEB0082	Ubc6-F	catcctattccactggtcgc
oEB0083	Ubc8-F	atgctcgtgtgcacatctgc
oEB0084	Rad6-F	gcaacttgatgaagcatacg
oEB0085	Cdc34 (3'UTR)-F	gatgaattgtatgtacaataaaaaagaacagtaagaaagaagac
oEB0086	Cdc34(3'UTR)-R	gcaagctaaacagatctaaaggtaatgaggaattagatgc
oEB0087	Ubc1(3'UTR)-F	gatgaattgtatgtacaatgaatagataaaaaaaaaacgcaccaag
oEB0088	Ubc1(3'UTR)-R	gcaagctaaacagatctcagaatgggaaattagatacgac
oEB0090	ymEVC155-Cdc34(5'UTR)	tgtcgttaattaacatatttacgttgtattgttctttttcc
oEB0091	ymEVC155-Ubc1(5'UTR)	tgtcgttaattaacatcgcttacttcttactactactac
oEB0092	Pac1-ymEVC155	atgttaattaacgacaaacaaaagaatggtatcaaagctaacttc
oEB0093	ymEVC155-Cdc34	cggaggtggaggttctgcggccgctatgagtagtcgcaaaagcaccgc
oEB0094	ymEVC155-Ubc1	cggaggtggaggttctgcggccgctatgtctagggctaagagaattatg
oEB0095	SE_Cdc34(5'UTR)-F	taggacttatagcgactg
oEB0096	SE_Ubc1(5'UTR)-F	gtatcgtaatttagtggttgg
oEB0097	SE_Ubc1(5'UTR)-F	aattacatgactcgagcgaggcaagctaaacagatct
oEB0098	Gibson_Cdc34(5'UTR)-F	acaaaagctggagctctaagatatcccagctttgtgg
oEB0099	Gibson_Ubc1(5'UTR)-F	acaaaagctggagctccgcatataactaacaatttgg
oEB0100	SE_Cdc34(5'UTR)-R	cagtcgctataagtccta
oEB0101	SE_Ubc1(5'UTR)-R	ccaaccactaaattacgatac
oEB0119	To amplify Ubc6	cctgttattactattgtacgtactttgttt
oEB0120	To delete RING of Asi3-F	ttagagttcaagtttgattttgcctttgatagttgcgacgaagtggaggaaatggtgagcaagggcgaggag
oEB0121	To delete RING of Asi3-R	aaaattcctatgatgtcttaaatacgtatacctaataaaataattctacagtatagcgaccagcattca
oEB0122	Delete Asi1 gene and amp KAN	ggtttttttcttctttttacaaagaaactatgctaagaatcggatccccgggttaattaa
oEB0123	Delete Asi1 gene and amp KAN	aaaaacctcttttagataccatgcaaaagttcttaaactagaattcgagctcgtttaaac
oEB0124	Integration - for Asi1 deletion	ctttgaagtcagttgagtaagc
oEB0125	To clone 5'UTR of Ubc7-F	gcaggtcgacggatccagcttgaagaacttaccagactg
oEB0126	To clone 5'UTR of Ubc7-R	tttgtttgtcgttaattaacatgctatgcccttccaaattac
oEB0127	To clone 5'UTR of Rad6-F	tttgtttgtcgttaattaacatgacgctttatcttttagtct
oEB0128	ORF and 5'UTR of Ubc7-F	atgctagcatgtcgaaaaccgctcagaaacgt
oEB0129	ORF and 5'UTR of Ubc7-R	atagatctgctaagataacaggacaagctattgg
oEB0130	ORF and 5'UTR of Rad6-F	atgctagcatgtccacaccagctagaagaagg
oEB0131	ORF and 5'UTR of Rad6- R	atagatctcgaaggagctgcccgcacagaaga
oEB0133	To clone 5'UTR of Stp1- F	gctggagctcaccggtttccgaaaatgatagcgtgagcg
oEB0134	To clone 5'UTR of Stp1-R	agggaacattaattaattttgaacgaatgtggtatagcc
oEB0135	To clone 5'UTR of Stp2-F	gctggagctcaccggttgttacccttcttagagtcatcc
oEB0136	To clone 5'UTR of Stp2-R	agggaacattaattaagataatggatttccttacttccc
oEB0137	ORF and 3'UTR of Stp1-F	aggttctgcggccgctatgccctctaccacgctactgtttcc
oEB0138	ORF and 3'UTR of Stp1-R	caaagaaaccgctcgagcctcttacactctactagtgtc
oEB0139	ORF and 3'UTR of Stp2-F	atgcggccgcaatgcctatcttatcactatcttc
oEB0140	ORF and 3'UTR of Stp2-R	atctcgagacacacagctcacaggccaagc
oEB0141	To clone Asi1-F	gcaggtcgacggatccactttgaagtcagttgagtaagc
oEB0142	To clone Asi1- R	cagaaccaccgttaattaatttactatctgaaacaggatg
oEB0143	To clone Asi2-F	gcaggtcgacggatccacctatgttggcttagtgtgtgc
oEB0144	To clone Asi2-R	cagaaccaccgttaattaagaatacgcctggccctgtaatc

* Primers were named according to the name of the modified gene or other amplified element. The forward (sense) primer is indicated by the letter F. The reverse (antisense) primer is indicated by the letter R.

Plasmids

Table 8. Plasmids used in this study

Plasmid name	Features	Bacterial marker	Eukaryotic marker	Source
pEB0001	pFA6a-VC-HIS3MX6	AmpR	HIS3	Benoit Palancade
pEB0002	pFA6a-VN-HIS3MX6	AmpR	HIS3	Benoit Palancade
pEB0003	pFA6a_VN173-KanMX6	AmpR	KAN	Taddei lab
pEB0004	pFA6a_VC155-KanMX6	AmpR	KAN	Taddei lab
pEB0005	p41HPHtef_nNOS-L-RlucF[1]	AmpR	HPH	Michnick lab
pEB0006	p41NATtef_aSYN-L-RlucF[2]	AmpR	NAT	Michnick lab
pEB0007	pAG25_ZL-RlucF[1]	AmpR	NAT	Michnick lab
pEB0008	pAG32_L-RlucF[2]	AmpR	HPH	Michnick lab
pEB0013	pFA6a_UBC4-VN173-KanMX6	AmpR	KAN	This study
pEB0014	pFA6a_UBC4-VC155-KanMX6	AmpR	KAN	This study
pEB0015	pFA6a_ubc4(F63A)-VN173-KanMX6	AmpR	KAN	This study
pEB0016	pFA6a_ubc4(F63A,A97D)-VN173-KanMX6	AmpR	KAN	This study
pEB0017	pFA6a_ubc4(F63A)-VC155-KanMX6	AmpR	KAN	This study
pEB0018	pFA6a_ubc4(F63A,A97D)-VC155-KanMX6	AmpR	KAN	This study
pEB0022	pFA6a_UBC4-VN173-natMX4	AmpR	NAT	This study
pEB0023	pFA6a_UBC4-VC155-natMX4	AmpR	NAT	This study
pEB0024	pFA6a_ubc4(F63A,A97D)-VN173-natMX4	AmpR	NAT	This study
pEB0025	pFA6a_ubc4(F63A,A97D)-VC155-natMX4	AmpR	NAT	This study
pEB0026	p41NATtef_Rluc	AmpR	NAT	This study
pEB0028	pFA6a_ubc4(delta2-8)-VN173-natMX4	AmpR	NAT	This study
pEB0029	pFA6a_ubc4(delta139-148)-VN173-natMX4	AmpR	NAT	This study
pEB0030	pFA6a_ubc4(delta2-20)-VN173-natMX4	AmpR	NAT	This study
pEB0031	pFA6a_ubc4(delta)-VN173-natMX4	AmpR	NAT	This study
pEB0032	pFA6a_ubc4(delta139-148+delta2-8)-VN173-natMX4	AmpR	NAT	This study
pEB0033	pFA6a_ubc4(delta139-148+delta2-20)-VN173-natMX4	AmpR	NAT	This study
pEB0034	pFA6a_ubc4(P62A,A63N)-VN173-natMX4	AmpR	NAT	This study
pEB0035	pFA6a_ubc4(A63N)-VN173-natMX4	AmpR	NAT	This study
pEB0036	p41NATtef_HA-Rluc	AmpR	NAT	This study
pEB0037	p41NATtef_HA-Rluc8	AmpR	NAT	This study
pEB0038	p41NATtef_HA-GLuc	AmpR	NAT	This study
pEB0039	pFA6-link-yEVenus-Sp.His5	AmpR	NAT	Euroscarf
pEB0040	pFA6a_UBC4-yEVC155-natMX4	AmpR	NAT	This study
pEB0041	pFA6a_UBC7-yEVC155-natMX4	AmpR	NAT	This study
pEB0042	pFA6a_UBC11-yEVC155-natMX4	AmpR	NAT	This study
pEB0043	pFA6a_UBC12-yEVC155-natMX4	AmpR	NAT	This study
pEB0044	pFA6a_UBC10-yEVC155-natMX4	AmpR	NAT	This study
pEB0045	pFA6a_RAD6-yEVC155-natMX4	AmpR	NAT	This study
pEB0046	pFA6a_UBC5-yEVC155-natMX4	AmpR	NAT	This study
pEB0047	pFA6a_UBC6-yEVC155-natMX4	AmpR	NAT	This study
pEB0048	pFA6a_UBC8-yEVC155-natMX4	AmpR	NAT	This study
pEB0049	pFA6a_CDC34-yEVC155-natMX4	AmpR	NAT	This study
pEB0050	pFA6a_UBC1-yEVC155-natMX4	AmpR	NAT	This study
pEB0051	pFA6a_UBC13-yEVC155-natMX4	AmpR	NAT	This study
pEB0052	pFA6a_UBC9-yEVC155-natMX4	AmpR	NAT	This study
pEB0054	pFA6a_3'UBC6-yEVC155-natMX4	AmpR	NAT	This study
pEB0055	pFA6a_CDC34-3'UTR-yEVC155-natMX4	AmpR	NAT	This study
pEB0056	pFA6a_UBC1-3'UTR-yEVC155-natMX4	AmpR	NAT	This study
pEB0057	pFA6a_ymEVC155-CDC34-natMX4	AmpR	NAT	This study
pEB0058	pFA6a_ymEVC155-UBC1-natMX4	AmpR	NAT	This study
pEB0059	p41NAT_CDC34-yEVC155	AmpR	NAT	This study
pEB0060	p41NAT_UBC1-yEVC155	AmpR	NAT	This study
pEB0073	pFA6a_UBC4-yEVC155-3'UTR-natMX4	AmpR	NAT	This study
pEB0074	pFA6a_ubc4(2-8)-yEVC155-3'UTR-natMX4	AmpR	NAT	This study
pEB0075	pFA6a_ubc4(139-148)-yEVC155-3'UTR-natMX4	AmpR	NAT	This study
pEB0076	pFA6a_ubc4(2-8+139-148)-yEVC155-3'UTR-natMX4	AmpR	NAT	This study
pEB0080	pFA6a_pUBC6-natMX4-tUBC6	AmpR	NAT	This study
pEB0085	pFA6a_Asi1-yEVC155-natMX4	AmpR	NAT	This study
pEB0086	pFA6a_Asi2-yEVC155-natMX4	AmpR	NAT	This study

Yeast strains

Table 9. Yeast strains used in this study*

Strain	Back-ground	Genotype	Source
scEB0001	S288C	BY4741	Euroscarf
scEB0002	S288C	BY4741 erg6::KAN	Gwenael Rabut
scEB0003	S288C	BY4743 pdr5::KAN	hKO collection
scEB0004	S288C	BY4745 lyp1Δ can1::STE2pr-Sphis5	Gwenael Rabut
scEB0005		MAT Tester alpha	Gwenael Rabut
scEB0006		MAT Tester A	Gwenael Rabut
scEB0007	S288C	BY4745 pdr5::KAN	This study
scEB0008	S288C	BY4741 ubr1::UBR1-VenusF[C]-KAN	This study
scEB0009	S288C	BY4741 erg6::KAN pEB5 pEB6	This study
scEB0010	S288C	BY4741 ufd4::UFD4-VenusF[C]-KAN	This study
scEB0011	S288C	BY4741 ubr1::UBR1-VenusF[C]-NAT	This study
scEB0012	S288C	BY4741 ufd4::UFD4-VenusF[C]-NAT	This study
scEB0013	S288C	BY4745	Gwenael Rabut
scEB0014	S288C	Y7092 rad6::RAD6-VenusF[N]-KAN	This study
scEB0015	S288C	Y7092 ubc4::UBC4-VenusF[N]-KAN	This study
scEB0016	S288C	BY4741 lyp1Δ can1::STE2pr-Sphis5 rad6::RAD6-VN-KAN ubr1::UBR1-VC-NAT	This study
scEB0017	S288C	BY4741 lyp1Δ can1::STE2pr-Sphis5 rad6::RAD6-VN-KAN ufd4::UFD4-VC-NAT	This study
scEB0018	S288C	BY4741 lyp1Δ can1::STE2pr-Sphis5 ubc4::UBC4-VN KAN ufd4::UFD4-VC- NAT	This study
scEB0019	S288C	BY4741 lyp1Δ can1::STE2pr-Sphis5 ubc4::UBC4-VN-KAN ubr1::UBR1-VC-NAT	This study
scEB0020	S288C	Y7092 rad6::RAD6-RlucF[1]-NATMX4	This study
scEB0021	S288C	Y7092 ubc4::UBC4-RlucF[1]-NATMX4	This study
scEB0022	S288C	BY4745 ubr1::UBR1-RlucF[2]-URA	This study
scEB0023	S288C	BY4745 ufd4::UFD4-RlucF[2]-URA	This study
scEB0024	S288C	MATa erg6::KAN lyp1Δ can1::STE2pr-Sphis5 ubc4::UBC4-RlucF1NAT ufd4::UFD4-RlucF2-URA	This study
scEB0025	S288C	MATa erg6::KAN lyp1Δ can1::STE2pr-Sphis5 ubc4::UBC4-RlucF1-NAT ubr1::UBR1-RlucF2-URA	This sudy
scEB0026	S288C	MATa erg6::KAN lyp1Δ can1::STE2pr-Sphis5 rad6::RAD6-RlucF1 ubr1::UBR1-RlucF2-URA	This study
scEB0027	S288C	MATa erg6::KAN lyp1Δ can1::STE2pr-Sphis5 rad6::RAD6-RlucF1-NATufd4::UFD4-RlucF2-URA	This study
scEB0028	S288C	Y7092 rpn7::RPN7-tdimer2(12)-LEU	This study
scEB0033	S288C	Y7092 ubc4::KAN rpn7::RPN7-tdimer2(12)	This study
scEB0034	S288C	Y7092 ubc4::UBC4-VN173-natMX4 rpn7::RPN7-tdimer2(12)	This study
scEB0035	S288C	Y7092 ubc4::UBC4-VC155-natMX4 rpn7::RPN7-tdimer2(12)	This study
scEB0036	S288C	Y7092 ubc4::ubc4(F63A, A97D)-VN173-natMX4 rpn7::RPN7-tdimer2(12)	This study
scEB0037	S288C	Y7092 ubc4::ubc4(F63A, A97D)-VC155-natMX4 rpn7::RPN7-tdimer2(12)	This study
scEB0038	S288C	MATa lyp1Δ can1::STE2pr-Sphis5 ubc4::UBC4-VN173-NAT ufd4::UFD4-VC-KAN rpn7::RPN7	This study
scEB0040	S288C	scEB0038 ufd4::UFD4-VC-KAN ubc4::ubc4(F63A, A97D)-VN173-NAT	This study
scEB0046	S288C	BY4741 erg6::KAN rtt101::NAT pdr1::pdr1(DBD)-cyc8-LEU	This study
scEB0047	S288C	BY4745 erg6::KAN rtt101::NAT pdr1::pdr1(DBD)-cyc8-LEU	This study
scEB0062	S288C	Y7092 ubc4(Δ2-8)-VN173-natMX4 rpn7::RPN7-tdimer2(12) pEB28	This study
scEB0063	S288C	Y7092 ubc4(Δ139-148)-VN173-natMX4 rpn7::RPN7-tdimer2(12) pEB29	This study
scEB0064	S288C	Y7092 ubc4(Δ2-20)-VN173-natMX4 rpn7::RPN7-tdimer2(12) pEB30	This study
scEB0065	S288C	Y7092 ubc4(Δ)-VN173-natMX4 rpn7::RPN7-tdimer2(12) pEB31	This study
scEB0066	S288C	Y7092 ubc4(Δ139-148+delta2-8)-VN173-natMX4 rpn7::RPN7-tdimer2(12) pEB32	This study
scEB0067	S288C	Y7092 ubc4(Δ139-148+delta2-20)-VN173-natMX4 rpn7::RPN7-tdimer2(12) pEB33	This study
scEB0068	S288C	Y7092 ubc4::ubc4(P62A, F63N, A97D)-VN173-natMX4 rpn7::RPN7-tdimer2(12)	This study
scEB0069	S288C	Y7092 ubc4::ubc4(F63N, A97D)-VN173-natMX4 rpn7::RPN7-tdimer2(12)	This study
scEB0070	S288C	MATa lyp1Δ can1::STE2pr-Sphis5 ubc4(Δ2-8)-VN173-NAT ufd4::UFD4-VC-KAN rpn7::RPN7	This study
scEB0071	S288C	MAT a lyp1Δ can1::STE2pr-Sphis5 ubc4(Δ139-148)-VN173-NAT ufd4::UFD4-VC-KAN rpn7	This study
scEB0072	S288C	MATa lyp1Δ can1::STE2pr-Sphis5 ubc4(Δ2-20)-VN173-NAT ufd4::UFD4-VC-KAN rpn7::RPN7	This study
scEB0073	S288C	MATa lyp1Δ can1::STE2pr-Sphis5 ubc4::VN173-NAT ufd4::UFD4-VC-KAN rpn7::RPN7	This study
scEB0074	S288C	MATa lyp1Δ can1::STE2pr-Sphis5 ubc4(Δ139-148+delta2-8)-VN173-NAT ufd4::UFD4-VC-KAN rpn7::RPN7	This study
scEB0075	S288C	MATa lyp1Δ can1::STE2pr-Sphis5 ubc4(Δ139-148+Δ2-20)-VN173-NAT ufd4::UFD4-VC-KAN rpn7::RPN7	This study
scEB0078	S288C	MATa lyp1Δ can1::STE2pr-Sphis5 ubc4::ubc4(P62A, F63N, A97D)-VN173-NAT ufd4::UFD4-VC-KAN rpn7::RPN7	This study
scEB0079	S288C	MATa lyp1Δ can1::STE2pr-Sphis5 ubc4::ubc4(F63N, A97D)-VN173-NAT ufd4::UFD4-VC-KAN rpn7::RPN7	This study
scEB0085	S288C	BY4743 cdc34::KAN	This study
scEB0086	S288C	BY4743 ubc1::KAN	hKO collection
scEB0087	S288C	BY4743 ubc9::KAN	hKO collection
scEB0088	S288C	BY4741 rad6::KAN	hKO collection
scEB0089	S288C	BY4741 ubc4::KAN	Gwenael Rabut
scEB0090	S288C	BY4741 ubc5::KAN	Gwenael Rabut
scEB0091	S288C	BY4741 ubc12::KAN	Gwenael Rabut
scEB0092	S288C	BY4741 ubc13::KAN	Gwenael Rabut
scEB0093	S288C	BY4743 ubc7::KAN	hKO collection
scEB0094	S288C	BY4743 ubc8::KAN	hKO collection
scEB0095	S288C	BY4743 ubc10::KAN	hKO collection
scEB0096	S288C	BY4743 ubc11::KAN	hKO collection
scEB0097	S288C	BY4741 ubc7::KAN	This study
scEB0098	S288C	BY4741 ubc8::KAN	This study
scEB0099	S288C	BY4741 ubc10::KAN	This study

scEB0100	S288C	BY4741 ubc11::KAN	This study
scEB0101	S288C	BY4741 ubc9::UBC9-VenusF[C]-NAT	This study
scEB0102	S288C	BY4741 ubc4::UBC4-VenusF[C]-NAT	This study
scEB0103	S288C	BY4741 ubc5::UBC5-VenusF[C]-NAT	This study
scEB0104	S288C	BY4741 ubc12::UBC12-VenusF[C]-NAT	This study
scEB0105	S288C	BY4741 ubc13::UBC13-VenusF[C]-NAT	This study
scEB0106	S288C	BY4741 ubc7::UBC7-VenusF[C]-NAT	This study
scEB0107	S288C	BY4741 ubc8::UBC8-VenusF[C]-NAT	This study
scEB0108	S288C	BY4741 ubc10::UBC10-VenusF[C]-NAT	This study
scEB0109	S288C	BY4741 ubc11::UBC11-VenusF[C]-NAT	This study
scEB0110	S288C	BY4741 ubc6::UBC6(3'UTR)-VenusF[C]-NAT	This study
scEB0111	S288C	BY473 rad6::RAD6-VenusF[C]-NAT	This study
scEB0112	S288C	BY4743 rad6::KAN	This study
scEB0113	S288C	BY4741 rad6::RAD6-VenusF[C]-NAT	This study
scEB0114	S288C	BY4741 cdc34::CDC34-VenusF[C]-NAT	This study
scEB0115	S288C	BY4745 can1::STE2pr-Sphis5 lyp1::STE3pr-HPH rpn7::RPN7-tdimer2(12)-LEU	This study
scEB0116	S288C	BY4745 can1::STE2pr-Sphis5 lyp1::STE3pr-HPH	This study
scEB0117	S288C	BY4741 pEB59 (CDC34)	This study
scEB0118	S288C	BY4741 pEB60 (UBC1)	This study
scEB0119	S288C	scEB0115 ubc9::UBC9-VC-natMX4	This study
scEB0120	S288C	scEB0115 ubc4::UBC4-VC-natMX4	This study
scEB0121	S288C	scEB0115 ubc5::UBC5-VC-natMX4	This study
scEB0122	S288C	scEB0115 ubc12::UBC12-VC-natMX4	This study
scEB0123	S288C	scEB0115 ubc13::UBC13-VC-natMX4	This study
scEB0124	S288C	scEB0115 ubc7::UBC7-VC-natMX4	This study
scEB0125	S288C	scEB0115 ubc8::UBC8-VC-natMX4	This study
scEB0126	S288C	scEB0115 ubc10::UBC10-VC-natMX4	This study
scEB0127	S288C	scEB0115 ubc11::UBC11-VC-natMX4	This study
scEB0128	S288C	scEB0115 ubc6::UBC6-3'UTR-VC-natMX4	This study
scEB0129	S288C	scEB0115 rad6::RAD6-VC-natMX4	This study
scEB0130	S288C	scEB0115 cdc34::CDC34-VC-natMX4	This study
scEB0131	S288C	scEB0115 pEB0059 (CDC34-VC)	This study
scEB0132	S288C	scEB0115 pEB0060 (UBC1-VC)	This study
scEB0133	S288C	scEB0115 ubc1::VC-UBC1-natMX4	This study
scEB0146	S288C	BY4741 ubc1::VC-UBC1-natMX4	This study
scEB0147	S288C	BY4741 ubc6::VC-UBC6-natMX4	This study
scEB0148	S288C	BY4741 ubc4::UBC4-VC-3'UTR-natMX4	This study
scEB0149	S288C	BY4741 ubc4::ubc4(Δ2-8)-VC-3'UTR-natMX4	This study
scEB0150	S288C	BY4741 ubc4::ubc4(Δ139-148)-VC-3'UTR-natMX4	This study
scEB0151	S288C	BY4741 ubc4::ubc4(Δ2-8+139-148)-VC-3'UTR-natMX4	This study
scEB0152	S288C	scEB0115 ubc6::VC-UBC6-natMX4	This study
scEB0153	S288C	scEB0115 ubc4::UBC4-VC-3'UTR-natMX4	This study
scEB0154	S288C	scEB0115 ubc4::ubc4(Δ2-8)-VC-3'UTR-natMX4	This study
scEB0155	S288C	scEB0115 ubc4::ubc4(Δ139-148)-VC-3'UTR-natMX4	This study
scEB0156	S288C	scEB0115 ubc4::ubc4(Δ2-8+139-148)-VC-3'UTR-natMX4	This study
scEB0157	S288C	scEB0115 pEB0066 (ubc1(Δ2-8)-VC)	This study
scEB0158	S288C	scEB0115 pEB0067 (ubc1(Δ141-215)-VC)	This study
scEB0159	S288C	scEB0115 pEB0072 (ubc1(Δ2-8+Δ141-215)-VC)	This study
scEB0160	S288C	scEB0115 rad6(Δ2-10)-yEVC155-natMX4	This study
scEB0161	S288C	scEB0115 rad6(Δ141-173)-yEVC155-natMX4	This study
scEB0162	S288C	scEB0115 rad6(Δ2-10+141-173)-yEVC155-natMX4	This study
scEB0163	S288C	scEB0115 pEB0070 (cdc34(Δ2-15)-VC)	This study
scEB0164	S288C	scEB0115 pEB0065 (cdc34(Δ160-296)-VC)	This study
scEB0165	S288C	scEB0115 pEB0071 (cdc34(Δ2-15+Δ160-296)-VC)	This study
scEB0166	S288C	BY4741 cue1::CUE1-VN-URA3	This study
scEB0167	S288C	BY4741 pex22::PEX22-VN-URA3	This study
scEB0168	S288C	BY4741 mms21::MMS21-VN-URA3	This study
scEB0169	S288C	BY4741 siz1::SIZ1-VN-URA3	This study
scEB0170	S288C	BY4741 siz2::SIZ2-VN-URA3	This study
scEB0171	S288C	BY4741 air1::AIR1-VN-URA3	This study
scEB0172	S288C	BY4741 air2::AIR2-VN-URA3	This study
scEB0173	S288C	BY4741 yvh1::YVH1-VN-URA3	This study
scEB0174	S288C	BY4741 dma2::DMA2-VN-URA3	This study
scEB0175	S288C	BY4741 doa10::DOA10-VN-URA3	This study
scEB0176	S288C	BY4741 mtc5::MTC5-VN-URA3	This study
scEB0177	S288C	BY4741 pex2::PEX2-VN-URA3	This study
scEB0178	S288C	BY4741 pex10::PEX10-VN-URA3	This study
scEB0179	S288C	BY4741 pex12::PEX12-VN-URA3	This study
scEB0185	S288C	scEB0116 ubc10::UBC10-VC-NAT	This study
scEB0186	S288C	scEB0115 pEB0060 (UBC1-VC) dma2::Dma2-VN-URA3	This study
scEB0187	S288C	scEB0115 pEB0066 (ubc1(Δ2-8)-VC) dma2::Dma2-VN-URA3	This study
scEB0188	S288C	scEB0115 pEB0067 (ubc1(Δ141-215)-VC) dma2::Dma2-VN-URA3	This study
scEB0189	S288C	scEB0115 pEB0072 (ubc1(Δ2-8+Δ141-215)-VC) dma2::Dma2-VN-URA3	This study
scEB0190	S288C	scEB0115 pEB0060 (UBC1-VC) doa10::Doa10-VN-URA3	This study
scEB0191	S288C	scEB0115 pEB0066 (ubc1(Δ2-8)-VC) doa10::Doa10-VN-URA3	This study
scEB0192	S288C	scEB0115 pEB0067 (ubc1(Δ141-215)-VC) doa10::Doa10-VN-URA3	This study

scEB0193	S288C	scEB0115 pEB0072 (ubc1(Δ2-8+Δ141-215)-VC) doa10::Doa10-VN-URA3	This study
scEB0194	S288C	scEB0115 pEB0060 (UBC1-VC) mtc5::Mtc5-VN-URA3	This study
scEB0195	S288C	scEB0115 pEB0066 (ubc1(Δ2-8)-VC) mtc5::Mtc5-VN-URA30	This study
scEB0196	S288C	scEB0115 pEB0067 (ubc1(Δ141-215)-VC) mtc5::Mtc5-VN-URA3	This study
scEB0197	S288C	scEB0115 pEB0072 (ubc1(Δ2-8+Δ141-215)-VC) mtc5::Mtc5-VN-URA3	This study
scEB0198	S288C	scEB0116 ubc10::UBC10-VC-NAT pex2::PEX2-VN-URA3	This study
scEB0199	S288C	scEB0116 ubc10::UBC10-VC-NAT pex10::PEX10-VN-URA3	This study
scEB0200	S288C	scEB0116 ubc10::UBC10-VC-NAT pex12::PEX12-VN-URA3	This study
scEB0201	S288C	scEB0116 ubc10::UBC10-VC-NAT nam7::VN-NAM7-URA3	This study
scEB0202	S288C	scEB0116 ubc10::UBC10-VC-NAT pGR0703 (RSP5-VN)	This study
scEB0232	S288C	BY4745 asi3::KAN	This study
scEB0233	S288C	MATα ura3-52	Ljungdahl lab
scEB0234	S288C	MATa ura3-52	Ljungdahl lab
scEB0235	S288C	MATα ssy5-delta	Ljungdahl lab
scEB0236	S288C	Matα asi1-delta	Ljungdahl lab
scEB0237	S288C	MATa asi2-delta	Ljungdahl lab
scEB0238	S288C	MATα asi3-delta	Ljungdahl lab
scEB0239	S288C	MATα ssy5-delta asi1-delta	Ljungdahl lab
scEB0240	S288C	MATα ssy5-delta asi2-delta	Ljungdahl lab
scEB0241	S288C	MATα ssy5-delta asi3-delta	Ljungdahl lab
scEB0242	S288C	MATa stp1-delta stp2-delta	Ljungdahl lab
scEB0243	S288C	MATa stp1-delta stp2-delta ssy5-delta	This study
scEB0244	S288C	MATα stp1-delta stp2-delta ssy5-delta asi1-delta	This study
scEB0245	S288C	scEB0215 x scGR402	Gwenael Rabut
scEB0246	S288C	scEB0216 x scGR402	Gwenael Rabut
scEB0247	S288C	scEB0218 x scGR402	Gwenael Rabut
scEB0248	S288C	BY4745 asi3::NAT	This study
scEB0249	S288C	BY4745 asi3::HPH	This study
scEB0250	S288C	BY4741 asi3::asi3(ΔRING)-VN-KAN	This study
scEB0251	S288C	BY4741 ubc6::NAT	This study
scEB0252	S288C	BY4745 ubc6::NAT	This study
scEB0253	S288C	BY4741 ubc6::KAN	This study
scEB0254	S288C	BY4745 ubc6::KAN	This study
scEB0255	S288C	BY4741 ssy5::KAN	This study
scEB0256	S288C	BY4741 ssy5::HIS	This study
scEB0257	S288C	scEB0115 asi3::asi3(Î”RING)-VN-KAN ubc6::VC-UBC6-natMX4	This study
scEB0258	S288C	scEB0115 asi3::ASI3-VN-ura3 ubc6::VC-UBC6-natMX4	This study
scEB0259	S288C	BY4743 asi2::KAN	hKO collection
scEB0260	S288C	BY4741 asi1::KAN	This study
scEB0261	S288C	BY4741 asi3::KAN ssy5::HIS	This study
scEB0262	S288C	BY4745 asi3::KAN ssy5::HIS	This study
scEB0263	S288C	BY4741 asi2::KAN	This study
scEB0264	S288C	BY4745 asi2::KAN	This study
scEB0265	S288C	asi1::KAN x scEB0115 asi3::ASI3-VN-ura3 ubc6::VC-UBC6-natMX4	This study
scEB0266	S288C	asi2::KAN x scEB0115 asi3::ASI3-VN-ura3 ubc6::VC-UBC6-natMX4	This study
scEB0267	S288C	scEB0115 asi3::ASI3-VN-ura3 rad6::RAD6-VC-natMX4	This study
scEB0268	S288C	scEB0115 asi3::ASI3-VN-ura3 cdc34::CDC34-VC-natMX4	This study
scEB0269	S288C	scEB0115 asi3::ASI3-VN-ura3 ubc1::VC-UBC1-natMX4	This study
scEB0270	S288C	scEB0115 asi3::ASI3-VN-ura3 ubc5::UBC5-VC-natMX4	This study
scEB0271	S288C	scEB0115 asi3::ASI3-VN-ura3 ubc8::UBC8-VC-natMX4	This study
scEB0272	S288C	scEB0115 asi3::ASI3-VN-ura3 ubc13::UBC13-VC-natMX4	This study
scEB0273	S288C	scEB0115 asi3::ASI3-VN-ura3 ubc10::UBC10-VC-natMX4	This study
scEB0274	S288C	scEB0115 asi3::ASI3-VN-ura3 ubc7::UBC7-VC-natMX4	This study
scEB0275	S288C	scEB0115 asi3::ASI3-VN-ura3 ubc11::UBC11-VC-natMX4	This study
scEB0276	S288C	scEB0115 asi3::ASI3-VN-ura3 ubc9::UBC9-VC-natMX4	This study
scEB0277	S288C	scEB0115 asi3::ASI3-VN-ura3 ubc4::UBC4-VC-natMX4	This study
scEB0278	S288C	scEB0115 asi3::ASI3-VN-ura3 ubc12::UBC12-VC-natMX4	This study
scEB0279	S288C	scEB0115 asi1::ASI1-VN-ura3 rad6::RAD6-VC-natMX4	This study
scEB0280	S288C	scEB0115 asi1::ASI1-VN-ura3 cdc34::CDC34-VC-natMX4	This study
scEB0281	S288C	scEB0115 asi1::ASI1-VN-ura3 ubc1::VC-UBC1-natMX4	This study
scEB0282	S288C	scEB0115 asi1::ASI1-VN-ura3 ubc5::UBC5-VC-natMX4	This study
scEB0283	S288C	scEB0115 asi1::ASI1-VN-ura3 ubc8::UBC8-VC-natMX4	This study
scEB0284	S288C	scEB0115 asi1::ASI1-VN-ura3 ubc13::UBC13-VC-natMX4	This study
scEB0285	S288C	scEB0115 asi1::ASI1-VN-ura3 ubc10::UBC10-VC-natMX4	This study
scEB0286	S288C	scEB0115 asi1::ASI1-VN-ura3 ubc7::UBC7-VC-natMX4	This study
scEB0287	S288C	scEB0115 asi1::ASI1-VN-ura3 ubc11::UBC11-VC-natMX4	This study
scEB0288	S288C	scEB0115 asi1::ASI1-VN-ura3 ubc9::UBC9-VC-natMX4	This study
scEB0289	S288C	scEB0115 asi1::ASI1-VN-ura3 ubc4::UBC4-VC-natMX4	This study
scEB0290	S288C	scEB0115 asi1::ASI1-VN-ura3 ubc12::UBC12-VC-natMX4	This study
scEB0291	S288C	BY4745 ssy5::HIS ubc6::NAT	This study
scEB0292	S288C	BY4741 ssy5::HIS ubc6::NAT	This study
scEB0293	S288C	BY4745 ssy5::HIS ubc6::NAT ubc7::KAN	This study
scEB0294	S288C	BY4741 ssy5::HIS ubc6::NAT ubc7::KAN	This study
scEB0295	S288C	BY4745 ssy5::HIS ubc7::KAN	This study
scEB0296	S288C	BY4745 ubc6::NAT ubc7::KAN	This study
scEB0297	S288C	BY4745 ubc7::KAN	This study

scEB0298	S288C	BY4741 ssy5::HIS asi3(ΔRING)-VN::KAN	This study
scEB0299	S288C	BY4741 ssy5::HIS ubc6::NAT asi3(ΔRING)-VN::KAN	This study
scEB0300	S288C	scEB0115 asi1::ASI1-VN-ura3 ubc6::VC-UBC6-natMX4	This study
scEB0301	S288C	ubc6::KAN scEB0115 asi3::ASI3-VN-ura3 rad6::RAD6-VC-natMX4	This study
scEB0302	S288C	ubc6::KAN scEB0115 asi3::ASI3-VN-ura3 cdc34::CDC34-VC-natMX4	This study
scEB0303	S288C	ubc6::KAN scEB0115 asi3::ASI3-VN-ura3 ubc1::VC-UBC1-natMX4	This study
scEB0304	S288C	ubc6::KAN scEB0115 asi3::ASI3-VN-ura3 ubc5::UBC5-VC-natMX4	This study
scEB0305	S288C	ubc6::KAN scEB0115 asi3::ASI3-VN-ura3 ubc8::UBC8-VC-natMX4	This study
scEB0306	S288C	ubc6::KAN scEB0115 asi3::ASI3-VN-ura3 ubc13::UBC13-VC-natMX4	This study
scEB0307	S288C	ubc6::KAN scEB0115 asi3::ASI3-VN-ura3 ubc10::UBC10-VC-natMX4	This study
scEB0308	S288C	ubc6::KAN scEB0115 asi3::ASI3-VN-ura3 ubc7::UBC7-VC-natMX4	This study
scEB0309	S288C	ubc6::KAN scEB0115 asi3::ASI3-VN-ura3 ubc11::UBC11-VC-natMX4	This study
scEB0310	S288C	ubc6::KAN scEB0115 asi3::ASI3-VN-ura3 ubc9::UBC9-VC-natMX4	This study
scEB0311	S288C	ubc6::KAN scEB0115 asi3::ASI3-VN-ura3 ubc4::UBC4-VC-natMX4	This study
scEB0312	S288C	ubc6::KAN scEB0115 asi3::ASI3-VN-ura3 ubc12::UBC12-VC-natMX4	This study
scEB0313	S288C	ubc6::KAN scEB0115 asi1::ASI1-VN-ura3 rad6::RAD6-VC-natMX4	This study
scEB0314	S288C	ubc6::KAN scEB0115 asi1::ASI1-VN-ura3 cdc34::CDC34-VC-natMX4	This study
scEB0315	S288C	ubc6::KAN scEB0115 asi1::ASI1-VN-ura3 ubc1::VC-UBC1-natMX4	This study
scEB0316	S288C	ubc6::KAN scEB0115 asi1::ASI1-VN-ura3 ubc5::UBC5-VC-natMX4	This study
scEB0317	S288C	ubc6::KAN scEB0115 asi1::ASI1-VN-ura3 ubc8::UBC8-VC-natMX4	This study
scEB0318	S288C	ubc6::KAN scEB0115 asi1::ASI1-VN-ura3 ubc13::UBC13-VC-natMX4	This study
scEB0319	S288C	ubc6::KAN scEB0115 asi1::ASI1-VN-ura3 ubc10::UBC10-VC-natMX4	This study
scEB0320	S288C	ubc6::KAN scEB0115 asi1::ASI1-VN-ura3 ubc7::UBC7-VC-natMX4	This study
scEB0321	S288C	ubc6::KAN scEB0115 asi1::ASI1-VN-ura3 ubc11::UBC11-VC-natMX4	This study
scEB0322	S288C	ubc6::KAN scEB0115 asi1::ASI1-VN-ura3 ubc9::UBC9-VC-natMX4	This study
scEB0323	S288C	ubc6::KAN scEB0115 asi1::ASI1-VN-ura3 ubc4::UBC4-VC-natMX4	This study
scEB0324	S288C	ubc6::KAN scEB0115 asi1::ASI1-VN-ura3 ubc12::UBC12-VC-natMX4	This study
scEB0325	S288C	BY4741 asi3::asi3(ΔRING)-VN-NAT	This study

*dKO indicates the yeast diploid knockout collection, hKO indicates the yeast haloid knockout collection, Δ (delta) indicates a deletion of respective gene or particular amino acids

3.2 Methods

3.2.1 Molecular biology

Plasmid construction

Plasmid constructions were produced using standard molecular biology techniques as described by Sambrook and Russell (2001). Plasmid DNA was amplified in *E. coli* and isolated using Macherey-Nagel kits according to the manufacturer's instructions. Plasmid digestions were performed using restriction enzymes from New England Biolabs (NEB), according to the instruction. DNA fragments were assembled using either the T4 DNA (Takara) or the more recent Gibson assembly technique (NEB). Mutagenesis was carried out using a standard site-directed mutagenesis kit (QuickChange Multi Site-Directed Mutagenesis, Stratagene) or using the Gibson assembly kit (NEB). To make point mutants in the Ubc4 test constructs, phenylalanine was mutated to alanine (F63A for a single and double mutant) and alanine was mutated to aspartic acid (A97D for a double mutant). To generate double site mutation, the single site mutated plasmid was used as a PCR template. Deletion mutants were generated as shown by Longtine et al. (1998). For the construction of E2 array to systematically assay E2/E3 interactions using BiFC, all E2s were tagged with the C-terminal fragment of Venus (VC). The C-terminal fragment of Venus was codon-optimized using plasmid pEB0039 with primers oEB0043 and oEB0044 and pEB0023 as a vector linearized with PacI and BsrGI restriction enzymes. Each E2 (promoter and ORF) was cloned into a plasmid construct with a codon-optimized *Venus* variant between the BamHI and PacI restriction sites. All plasmids constructed in this study were sequenced using a dye terminator sequencing kit (BigDye Terminator v.3.1 Cycle Sequencing Kit, Life Technologies) and analyzed in house using the Applied Biosystems 3130 XL sequencer.

Polymerase chain reaction

Polymerase chain reaction (PCR) was used for several applications, including: cloning, plasmid screening, and verification of genetically modified yeast strains. In general, 1 µL of DNA was subject to PCR amplification in the final reaction volume of 50 µL (final concentration <0.5 µg/50 µL). PCR was performed using Phusion High Fidelity PCR Master Mix with GC Buffer (New England Biolabs) for cloning, and long and difficult amplification s whereas GoTaq Polymerase with 5x Green GoTaq Reaction Buffer (Promega) was used for plasmid screening or verification of yeast strains. The annealing temperature for the primers was calculated using OligoAnalyzer 3.1 software (Integrated DNA Technologies). The primers used for this study are presented in the chapter *Materials*, Table 7. The amplification of DNA templates was performed using a T100™ Thermal Cycler from Bio-Rad.

Agarose gel electrophoresis

Agarose gel electrophoresis was performed in order to separate the DNA fragments and determine their length (bp). 5 µL of each PCR product was run on 0.8% (for DNA fragments expected >700 bp) or 2% (for DNA fragments expected 50-2,000 bp) agarose gel, with TAE (40 mM Tris, 20 mM acetic acid, 1 mM EDTA, pH~8.3) as a running buffer. 5 µL of GeneRuler DNA ladder mix (Thermo Scientific) was used as a standard. The gel was stained with GelRed (Biotium) and visualized using a UV transilluminator imaging system.

Transformation of heat-competent E. coli cells

100 µL of DH5α chemically competent *E. coli* cells was thawed on ice for each transformation. 1-2.5 µL of DNA was added and incubated on ice for 10 min. The mixture was plated on pre-warmed LB-Amp plates and incubated O/N at 37°C.

3.2.2 Yeast genetics

Isolation of yeast genomic DNA

A 10 ml yeast culture grown overnight in YPD was harvested by centrifugation (3000 rpm for 5 min). The cell pellet was washed with ddH_2O and transferred to a 1.5 mL microcentrifuge tube. After centrifugation (1 min at max speed in a tabletop centrifuge) the cells were resuspended in 200 µL of yeast DNA extraction buffer (breaking buffer). 200 µL of phenol-chloroform-isoamyl alcohol (PCI 50:49:1) and an equal volume of glass beads (0.5 mm diameter) were then added to the tube (under the hood). The mixture was vortexed for 1 min and placed on ice for 1 min (repeated three times) to break the cells. 200 µL of Tris-EDTA (TE) buffer (pH 8.0) was added and mixed by rapid vortexing, followed by 10 min centrifugation at 4°C. The aqueous top layer containing the chromosomal DNA was transferred to a clean 1.5 mL Eppendorf tube. 1 mL of absolute ethanol (stored at -20°C) was added to precipitate DNA, mixed by inverting the tube and centrifuged for 10 min at RT. After removal of the supernatant the pellet was resuspended in 400 µL of TE buffer (pH 8.0). To digest RNA 3 µL of RNase (10 mg/mL) was added and incubated for 5 min at 37°C. Next, 10 µL of 4M NH_4OAc and 1 mL of absolute ethanol (stored at -20°C) were added and the sample was incubated on ice for 15 min. After a further centrifugation step at 1000 rpm for 10 min at RT, the DNA was washed with 750 µL of 70% ethanol (stored at -20°C). DNA pellet without supernatant was then dried for 5 min at 50°C and the DNA was resuspended in 100 µL of TE buffer (pH 8.0).

Endogenous tagging

Many of the yeast strains used in this study were genetically modified to express E2 and E3 genes fused to reporter proteins. To generate such strains, linear DNA fragments (PCR products or linearized plasmids) were introduced into the yeast genome and targeted at the desired locus by homologous recombination. The primers used for PCR amplification of the tagging module were designed as previously described by Longtine et al. (1998). The sequences of all ORFs used for the design of the primers (ORF plus the untranslated region 1000 bases upstream of the start codon ATG and 1000 bases downstream of the stop codon) were downloaded from the *Saccharomyces* Genome Database (SGD). The primers were purchased from Sigma. Most E2s were tagged at the C-terminal. Ubc6 was tagged N-terminally due to the presence of its C-

terminal transmembrane domain. Ubc1 was tagged at its N-terminal because the C-terminal seems to be important for Ubc1 function, as the C-terminally tagged Ubc1 strain was nonviable (personal observation). Strains with E3s were obtained from the commercial collection (Bioneer), where most genes were fused C-terminally to the N-terminal fragment of Venus fluorescent protein. Additionally, several strains with E3s that harbor E2 interacting domains at their N-terminal were generated using N-terminal tagging. Among these are E3s such as Tfb3, Prp19, Mot2, Psh1, Nam7 and Ste5.

Yeast transformation

Transformation of yeast cells using plasmids and PCR products was achieved using a slightly modified method of Gietz and Woods (2006). In brief, yeast cells were cultured overnight in 10 mL of YPD at 30°C. The next day, cells were diluted 1:20 into fresh YPD and grown for an additional 2-3 h until the culture reached an OD_{600} of 0.4-0.8. Cells were harvested by centrifugation (3200 rpm for 5 min at RT). The cell pellet was resuspended in 5 mL of LiAc mix and again harvested by centrifugation (3200 rpm for 5 min at RT). Cells were resuspended in 100 µL of 1M LiAc mix (one transformation) and transferred to a microcentrifuge tube. For each transformation reaction, the following reagents were added to the cell pellet:

- 700 µL of PEG mix (autoclaved)
- 30 µL of salmon sperm DNA (10 mg/mL), incubated at 95°C for 5 min, placed on ice prior to being added to the mixture. Salmon sperm DNA is used as a carrier in yeast transformations.
- 2 µL of a plasmid DNA preparation (for replicative plasmids), 25 µL of previously digested plasmid in case of integrative plasmids, or 20 µL of PCR product.

The components were mixed gently by inverting the tube several times. The mix was heat shocked in a thermomixer at 42°C for 40 min under agitation. After a centrifugation step (3200 rpm, 3 min), the pellet was resuspended in 100 µL of sterile ddH_2O and the cell suspension was plated with sterile glass beads (Ø 3 mm) on selective media. For drug selection on the plates containing antibiotics, cells were allowed to recover prior plating and were therefore incubated in the thermomixer, in liquid YPD at 30°C for 2-3 h. Transformants were restreaked on the new plates and screened for the proper integration by PCR. PCR was performed using a Taq polymerase and 20 base pairs primers. The forward primer binds to the region 300-400 bp from the stop codon of a targeted gene, whereas the reverse primer binds to the resistance cassette.

Generation of yeast strains

The deletion and tagging of particular genes of interest were performed according to the methods described by Güldener et al. (1996) and Knop et al. (1999), respectively. For the initial tests of BiFC optimization, the strain BY4741 (*MAT*a *ura3Δ0 leu2Δ0 his3Δ1 met15Δ0*) was transformed using PCR products generated after the amplification of pFA6a_VC155-*kanMX6*, carrying *Escherichia coli* kanamycin-resistance gene (Longtine et al., 1998) plasmid DNA. The primers designed for this PCR were to amplify the genes of interest *Ubr1* and *Ufd4*, coding for the ubiquitin ligases. The strains obtained had the following genotypes BY4741 *ura3Δ0 leu2Δ0 his3Δ1 met15Δ0 ubr1*::*UBR1*-VenusF[C]-KAN and BY4741 *ura3Δ0 leu2Δ0 his3Δ1 met15Δ0 ufd4*::*UFD4*-VenusF[C]-KAN, respectively. Since strains derived from BY4741 and Y7092 carry the kanamycin-resistance (*kanMX6*), the resistance of strains derived from BY4741 was switched to nourseothricin resistance (*natMX4*). The strain Y7092 (*MATα ura3Δ0 leu2Δ0 his3Δ1 met15Δ0 can1::STE2pr-Sphis5 lyp1Δ*) was transformed using PCR products generated after amplification of pFA6a_VN173-*kanMX6* plasmid DNA. The primers designed for this PCR were to amplify the genes of interest *Rad6* and *Ubc4*, coding for ubiquitin conjugating enzymes. The strains obtained had the genotype BY4745 Y7092 *ura3Δ0 leu2Δ0 his3Δ1 met15Δ0 can1::STE2pr-Sphis5 lyp1Δ rad6*::*RAD6*-VenusF[C]-*KAN* and BY4745 Y7092 *ura3Δ0 leu2Δ0 his3Δ met15Δ0 can1::STE2pr-Sphis5 lyp1Δ ubc4*::*UBC4*-VenusF[C]-*KAN*, respectively. The strains obtained carry a query mutation linked to a dominant selectable marker, such as the kanamycin-resistance (*kanMX6*) module, and *can1::STE2pr-Sphis5 lyp1Δ* of the *CAN1* gene that normally confers sensitivity to canavanine. The strain also has *lyp1* gene deletion that confers resistance to thialysine. These genetic elements are necessary for the selection of haploid double mutant progeny. For BiFC optimization we generated four endogenously tagged haploid yeast strains, which were then manually mated to one another by mixing them together on YPD media and leaving overnight at 30°C, to produce diploid yeast that expressed the desired C-terminally tagged proteins of interest. We confirmed the successful tagging by PCR and sequencing. Upon mating, the yeast were restricted on double selection plates with kanamycine (G418) and nourseothricin (clonNAT), grown for 2 days at 30°C and then sporulated in ZnSPO media for 3-4 days. Double mutant *MATa* was selected directly after sporulation on SED medium lacking histidine, arginine and lysine (–His/Agr/Lys), with addition of G418 (350 µg/ml), clonNAT (100 µg/ml), canavanine (50 mg/ml) and thialysine (50 mg/ml). The strains

for luciferase experiments were generated in a similar manner. ORFs of interest, *Rad6, Ubc4* (E2s) and *Ubr1, Ufd4* (E3s), were tagged with *Renilla* luciferase fragments, RlucF[1] and RlucF[2] respectively.

The construction of an array of yeast strains, in which each endogenous E2 gene was fused to the C-terminal fragment of Venus and the library construction of haploid yeast cells with E2/E3 pair combinations and C- and N-terminal fragments of Venus, was carried out as follows. The respective yeast strains, where the ORF of each E2 had been replaced with a kanamycin resistance module, were transformed using plasmids containing E2s that were tagged with a C-terminal fragment of Venus and a nourseothricin resistance cassette. The correct integration of these plasmids into the yeast was verified by PCR. All the tagged E2 strains were then crossed with a modified scEB0028 strain (Y7092 rpn7::RPN7-tdimer2(12)-LEU). This strain expresses Rpn7 proteasome subunit fused to the red fluorescent protein tdimer2, which enables to quantify the fluorescent signal not only in the cytoplasm but also in the nucleus. The genetic elements of the background strain Y7092 (*MATα ura3Δ0 leu2Δ0 his3Δ1 met15Δ0 can1*::STE2pr-Sphis5 *lyp1Δ*) enable the selection of haploid double mutant progeny. The strain scEB0028 was additionally modified to enable selection of *MATα* progeny using a plasmid pEB0053 (pUC57, ProteoGenix). This is the plasmid used for the integration of the yeast a-factor receptor (Ste3p), which is expressed only in *MATα* cells and is resistant to hygromycin (HPH), into the *lyp1* locus. All the E2 strains obtained were then ready for random spore selection after crossing with E3 strains. The strain crossing procedure, based on synthetic genetic array (SGA) technology (Tong and Boone, 2006), was performed in 96-well plates containing liquid media. Unique well coordinates were assigned to each tagged E2 and E3. Strains were mated in YPD with the addition of tetracycline (10 mg/mL) to avoid possible contamination. After diploid selection, followed by sporulation, the haploid double mutant *MATα* was directly selected. All crossing and selection steps were carried out in a horizontal shaker at 20°C, as during our initial tests we observed stronger fluorescence signal than at 30°C.

3.2.3 Immunoblot

To determine the expression levels of the proteins of interest and to determine whether the fusion of PCA fragments to the respective N- or C-terminal of the proteins of interest do interfere with their normal expression levels, strains expressing fusion proteins were analyzed by immunoblot using specific antibodies (see Table 6, *Materials*). Total yeast protein extracts were prepared from the whole cells according to standard protocols. In brief, cells were grown overnight in 10 mL of YPD medium at 30°C in a horizontal shaker. The following day, the cultures were used to inoculate fresh 10 mL cultures at cell density of 0.5 OD_{600} and grown for additional 3 h. OD at 600 nm was measured again for each sample and was adjusted if necessary prior to the extraction procedure. The cells were pelleted for 3 min at 4000 rpm and resuspended in 300 µL of 20% trichloroacetic acid (TCA). Samples were then transferred to 1.5 mL Eppendorf tubes containing approximately 1 ml of glass beads (1.25 mm diameter). Cells were homogenized for 2 min in a cell disruptor (Disruptor Genie). The tubes were then pierced with an 18 G needle and the broken cells collected in fresh tubes by centrifugation (5 s at 5000 rpm in a tabletop centrifuge). The cells were then spun at maximum speed to precipitate proteins, TCA was removed and each pellet was resuspended in 90 µL of TCA-sample buffer. 10 µL of dithiotretiol (DTT) was added to each sample as a reducing agent, and samples were denatured for 5 min at 95°C. The samples were pelleted to remove debris for 5 min at maximum speed in a tabletop centrifuge. Supernatant was collected in fresh tubes and 5 µL of each sample was loaded on sodium dodecyl sulphate (SDS)-PAGE mini gels. The samples were run on 4-15% polyacrylamide gels (Mini-PROTEAN® TGX™ Precast Gels, BioRad) in a Tris-Glycine-SDS 1x buffer at 200 V for approximately 30 min. The proteins were then transferred from the gel to the PVDF membranes using a semi-dry transfer method. After the transfer, the membrane was blocked with 5% milk solution in PBS-T (PBS with 0.1% Tween 20) for 1 h at RT. The blots were probed with respective primary antibodies in 5% milk solution in PBS-T at 4°C O/N with gentle shaking. The blots were then washed five times with PBS-T, each wash lasting 10 min at RT on a rocker. After the washes they were incubated with respective secondary antibody in 5% milk solution in PBS-T for 1 h at RT. They were washed again five times prior to the distribution of chemiluminescent reagent (non-commercial ECL solution or Super Signal West Femto from Thermo Scientific), and then exposed to the radiography films.

3.2.4 Luciferase assay

Yeast transformed using the plasmids p41HPHtef_nNOS-L-*R*lucF (neuronal nitric oxide synthase domain, nNOS) and p41NATtef_aSYN-L-*R*lucF (aSyntrophin domain, aSYN) as well as untransformed yeast (as a control to determine the background ratio) were picked from the selection plates and grown O/N at 30°C in 10 ml of YPD medium in a horizontal shaker. The cultures of transformed strains were supplemented with both nourseothricin (100 µg/L) and hygromycin b (50 mg/mL). The following morning, the cultures were diluted in a fresh YPD medium. The above-mentioned antibiotics were again added to the transformed strains. Yeast was grown at 30°C in a horizontal shaker until they reached an OD_{600} of 1 (exponential phase of growth). 100 µl of each culture was then distributed to white 96-well plates. Luciferase activity was measured using a Centro LB 960 Microplate Luminometer (Berthold Technologies). The luciferase substrate used for this study was the coelenterazine analog – coelenterazine h (CTZ h), as it has previously been shown by Zhao et al. (2004) to increase the luminescence intensity more than the native coelenterazine. CTZ h aliquots were freshly prepared at the desired concentration prior to each experiment. The plate was briefly shaken and the measurements were performed immediately after the addition of CTZ h. *R*luc PCA signal was integrated for 15 s. In a single experiment, the signal was measured in triplicates for each sample and experiments were repeated independently three times. In order to determine *R*luc PCA signal from the background autoluminescence of CTZ h, the luminescence signal of medium and substrate alone was subtracted from all measured signals combined to obtain the net luminescence. Opaque white plates were used for measurements since they gave the best performance; they maximized the signal in luciferase assays, whereas black plates reduced the signal (personal observation, data not shown). However, white plates absorb energy from the ambient light in the room and emit the energy as light during luciferase measurement. Therefore, they should preferably be stored in a dark and also exposed to reduced light while pipetting the samples. Alternatively, they can be left in the dark for approximately 10 min prior to measurements. All BiLC tests were performed at least in two independent experiments in duplicates.

3.2.5 Confocal microscopy

For microscopic analysis of BiFC yeast cells were grown to mid-logarithmic phase in a YPD medium. The cells were transferred to 96-well optical quality clear bottom plates containing 100 µL of visualization medium in each well. The cells were left to sit at the bottom of the wells for 30 min. Images were acquired on the Leica TCS SP8 MP confocal microscope using water-immersed objective at x 63 magnification and an argon laser. To image and process the 96-well plates the matrix screener mode was applied. Excitation and emission spectra for Venus fluorescent protein were 515 nm and 528 nm, respectively. Image acquisition was carried out using the Leica Application Suite X (LAS X) software. Data management and analysis was performed using ImagJ software.

3.2.6 Quantification of the efficiency of BiFC complex formation and statistical analysis

BiFC screen measurements were analyzed statistically using the GraphPad software with standard statistical test available. BiFC signals in cells co-expressing VC-tagged E2s and VN-tagged E3s were quantified in both the cytoplasm and the nucleus of individual cells. Kurtosis measurements were incorporated as a measure of the distribution of the fluorescent pixels that enables to detect localized BiFC signals.

4 RESULTS

4.1 Bioluminescent versus fluorescent protein complementation assays to study E2/E3 interactions in living cells

As outlined in the introduction, our initial objective was to establish a suitable method to systematically assay interactions between ubiquitin conjugating (E2) and ligating (E3) enzymes in living cells. This was carried out in budding yeast, a model organism, in which it is easy to express tagged proteins from their endogenous chromosomal locus. It was challenging however, since E2/E3 interactions are weak and transient (typical Kds of E2/E3 interactions are in the low µM range) (Deshaies and Joazeiro, 2009; Ye and Rape, 2009) and therefore require very sensitive detection methods. Protein-fragment complementation assays (PCAs) have been proven suitable to study weak and transient protein-protein interactions without the need to disrupt cell integrity (Remy and Michnick, 2006; Ozbabacan et al, 2011). Here, we aimed to test, optimize and compare bioluminescent versus fluorescent PCAs in order to study E2/E3 interactions. These PCAs are known as Bimolecular Luminescence Complementation (BiLC) and Bimolecular Fluorescence Complementation (BiFC), respectively. We evaluated the ability to detect E2/E3 interactions using these methods, exemplified by the interaction of well described E2/E3 pairs in yeast, namely Ubc4/Ufd4 and Rad6/Ubr1.

4.1.1 Bimolecular Luminescence Complementation (BiLC)

One of the method belonging to protein fragment complementation assays (PCAs) that we decided to test was Bimolecular Luminescence Complementation (BiLC) (Luker et al., 2004). We chose to test BiLC, which is based on the *Renilla* luciferase (*R*luc) due to its reported simplicity and sensitivity. *R*luc PCA relies on the reconstitution of the enzymatic activity of luciferase from two split fragments upon the interaction of two proteins to which they are genetically fused (Stefan et al., 2007). Luciferase utilizes molecular oxygen and catalyzes the oxidation of its cell membrane-permeable substrate coelenterazine, emitting photon of light (Sherf et al., 1996). The

permeability of coelenterazine differs among the cells, which might impact the results. Therefore, we started by testing different yeast cells for their substrate permeability (Figure 21 A). Among these were *pdr1*, *pdr5* and *erg6* mutants. These were previously shown to be more permeable for different chemicals (Jensen-Pergakes et al., 1998; Emter et al., 2002). Wild type cells (BY4741) served as a control. The strains used here were transformed using control plasmids containing two luciferase fragments fused to the neuronal nitric oxide synthase (nNOS) and aSyntrophin (aSYN) PDZ domains that are known to form a heterodimer, p41HPHtef_nNOS-L-RlucF[1] and p41NATtef_aSYN-L-RlucF[2], respectively. *Erg6Δ* cells generated a luminescence signal ~2.5 times higher than that of the wild type cells, whereas the signal of *pdr5Δ* cells was reduced by half (Figure 21 A). No difference in signal was observed for the *pdr1* mutant in comparison with the wild type cells. Since *erg6Δ* cells had the highest luminescence signal-to-background ratio, we used these cells for BiLC assay optimization. We also compared different luminometers (data not shown), the FLUOstar Omega (BMG Labtech) and Centro LB 960 Microplate Luminometer (Berthold Technologies), with the latter performing best and therefore used in further analysis.

In our first tests, using *erg6Δ* cells, we compared different concentrations (10 µM and 50 µM) of the *Renilla* luciferase substrate, coelenterazine h (CTZ h) (Figure 21 B). Untransformed *erg6Δ* cells served as a negative control. The bioluminescence signal was integrated every 15 s for 150 s after the addition of CTZ h. The highest signal was observed 45 s after substrate addition. As expected, an addition of 50 µM of CTZ h increased the luciferase activity ~2.2 times more than an addition of 10 µM (45 s after the addition of CTZ h). Nonetheless, the concentration of 10 µM was sufficient to observe ~10 times more signal than the negative control (45 s after the addition of CTZ h). For assay calibration we used a zero control, which was YPD media alone with no biological samples. Coelenterazine is a substrate known to be oxidized and produce light even when luciferase is absent. This is known as autoluminescence and creates a background signal which in turn reduces the assay sensitivity. We, therefore, additionally tested various autoluminescence reducing agents such as KI, $Na_2S_2O_3$ and vitamin C (Harry, 2009). We noticed that the addition of these compounds results in a slight increase in substrate stability and therefore an increase in luminescent signal (Figure 21 C).

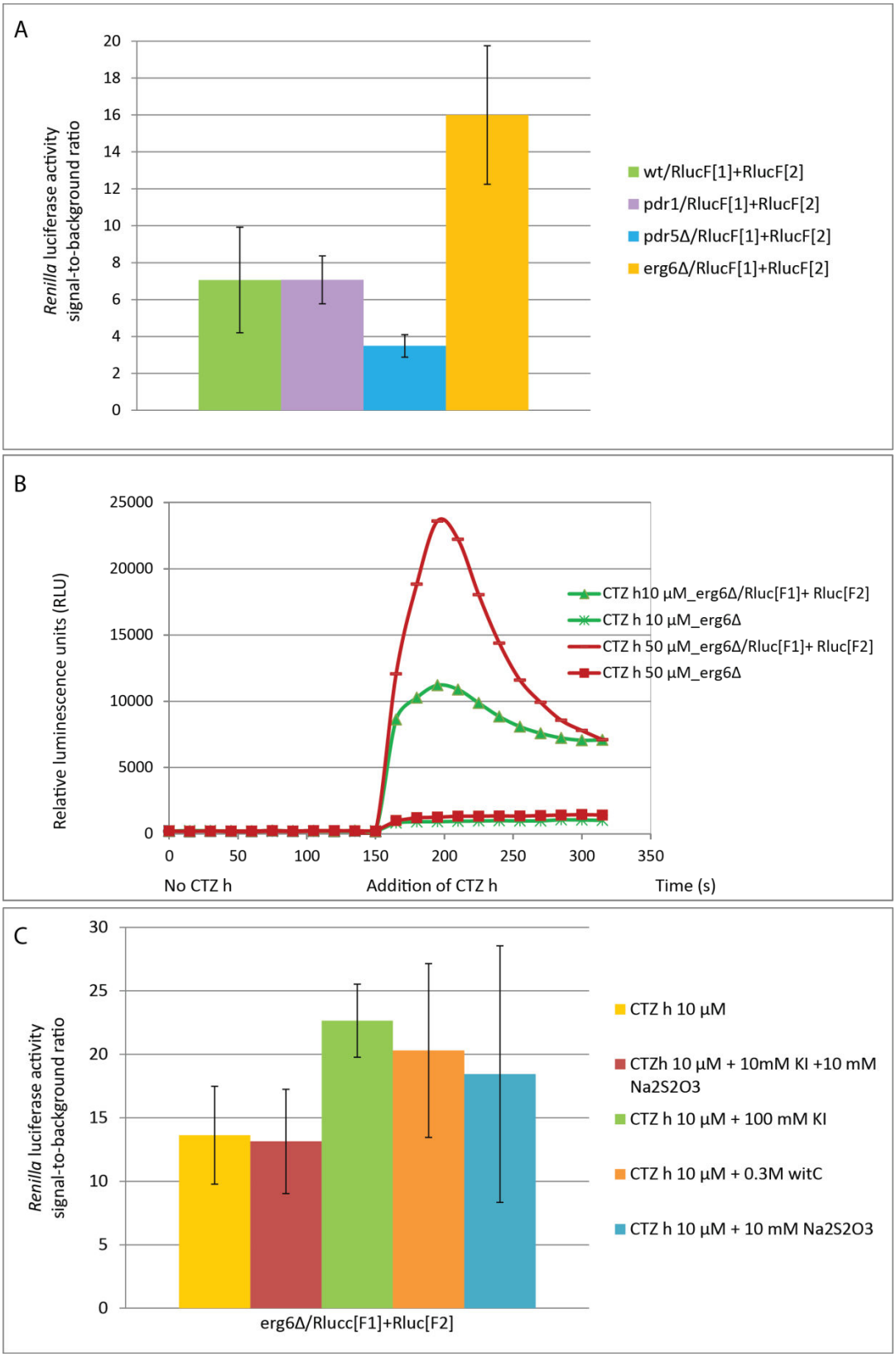

Figure 21. BiLC assay optimization. A) Different strains permeability to the *Renilla* luciferase substrate coelenterazine h, CTZ h (10 µM). B) Different CTZ h concentrations used for assay optimization (10 µM in green and 50µM in red) C) The influence of autoluminescence reducing agents on assay performance.

This can be especially helpful for weak interactions. However, as there was not a significant reduction in the CTZ h autoluminescence, we decided to perform further analysis in the most natural cellular context. Omitting any exogenous reagents would definitely provide more accurate information on the E2/E3 interaction network in the cells.

Finally, we studied the detection of E2/E3 interactions using BiLC with two well described E2/E3 pairs in yeast, Ubc4/Ufd4 and Rad6/Ubr1, which were previously shown to interact and form a complex. Ubc4/Ufd4 are involved in the degradation of abnormal or excess Ub-fusion proteins by the so-called UFD pathway, whereas Rad6/Ubr1 in the polyubiquitylation of proteins containing non-acetylated N-terminal residues as part of the Ac/N-end rule pathway (Varshavsky, 2011). The e*rg6Δ* strain with plasmids containing two luciferase fragments, p41HPHtef_nNOS-L-RlucF[1] and p41NATtef_aSYN-L-RlucF[2], served as a positive control whilst wild type strain BY4741 served as a negative control (Figure 22). The experiment was performed in triplicates using 10 µM of CTZ h. We assessed the interactions between endogenously tagged Ubc4 or Rad6 and Ufd4 or Ubr1 in a e*rg6Δ* strain background. No signal was detected in the four pairs studied in comparison with a positive control. Although Ubc4/Ufd4 and Rad6/Ubr1 were expected to interact, the absence of luminescent signal may also be due to the fact that the BiLC is reversible assay and may not capture these transient interactions. Additionally, the geometry of the fragments may prevent them from coming into close proximity with one another. Low BiLC signal could also be masked by the background autoluminescence.

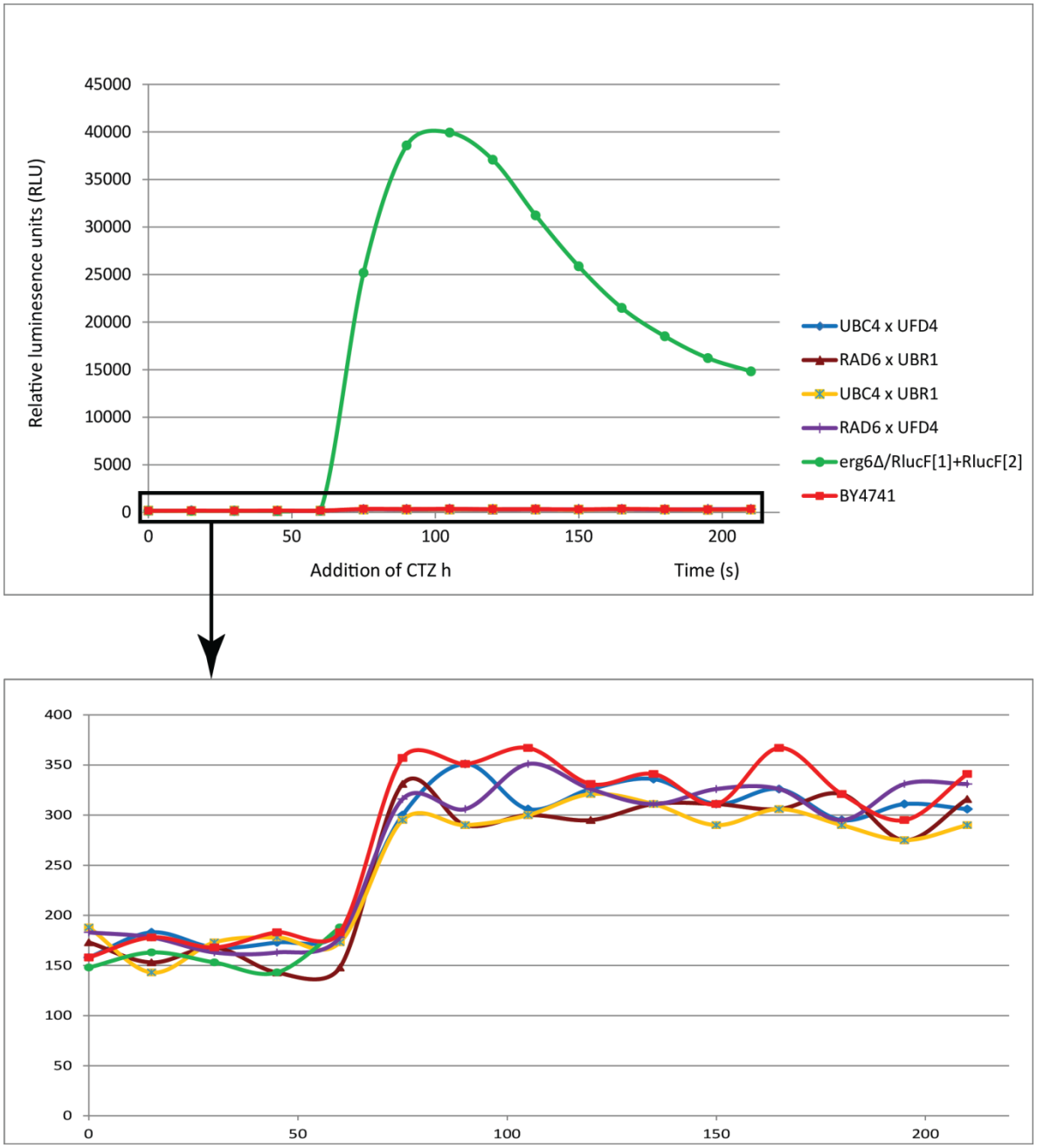

Figure 22. The BiLC assay tested with Ubc4/Ufd4, Rad6/Ubr1 and Ubc4/Ubr1, Rad6/Ufd4. BiLC signal detected with positive control (in green). There was no signal detected for all tested E2/E3 pairs (magnification of the graph at the bottom part of this figure).

4.1.2 Bimolecular Fluorescence Complementation (BiFC)

BiFC relies on the fusion of two proteins of interest, in our case an E2 and an E3 tagged with two complementary N- and C-terminal fragments of the Venus reporter protein (henceforth respectively termed VN and VC), which remains inactive. The interaction between the proteins of interest brings the VN and VC fragments into close proximity. Venus folds into its native structure and the reporter activity is reconstituted, which can be observed as a fluorescence signal. In order to test the BiFC assay, we constructed yeast strains that expressed combinations of chromosomally tagged versions of the E2s Ubc4 or Rad6 and the E3s Ufd4 or Ubr1, fused to VN and VC, respectively. Interestingly, we were this time able to detect a clear fluorescence signals in cells expressing Ubc4-VN and Ufd4-VC, but in no other strains (data not shown). We therefore further investigated the BiFC signal obtained in those cells. First, we verified by Western blot that Ubc4-VN is functional and can be loaded with ubiquitin (Figure 23 A, bottom panel). Next, we addressed the question of the specificity of BiFC signal, since it has been observed in mammalian cells that highly expressed VN and VC can in some cases spontaneously reassemble into a fluorescent Venus protein and lead to false positive results (Kodama and Hu, 2012). We noticed that expressing, for instance, the VC-tag alone (not fused to Ufd4) from the Ufd4 promoter was not a proper strategy, because its level of expression was much weaker than that of the Ufd4-VC. This could probably be due to the fact that VC-tag expressed on its own does not fold properly in the cell (data not shown). To test the specificity of the BiFC signal observed between Ubc4 and Ufd4 proteins, we therefore decided to generate Ubc4 mutants that could not interact with Ufd4. We first generated point Ubc4 point mutants in its canonical E3 interaction surface (ubc4(F63A) and ubc4(A97D)), but those were still able to produce a BiFC signal. We therefore decided to more dramatically mutate Ubc4 and truncate its N-terminal helix (which is involved in the canonical E2/E3 interface) and few amino acids in its C-terminal helix (which could be involved in ‘backside’ interactions (Figure 23 B). We checked by Western blot that those mutants are properly expressed and folded, since they can be charged with ubiquitin (Figure 23 C). Interestingly, the deletion mutants reduced the BiFC signal (Figure 23 D-E). The expression levels of the deletion mutants were higher than those of the wild type (not shown). Furthermore, the BiFC signal was almost completely abolished when Ubc4 was truncated in both its N- and C-terminus (Figure 23 D). Although this form of Ubc4 could not be loaded with

ubiquitin, it was still expressed to a level comparable to the other truncated mutants Ubc4 (Figure 23 C) and was therefore probably not completely unfolded.

While we were optimizing our imaging conditions to monitor the BiFC signal, we noticed that Ubc4/Ufd4 test pair generated a higher BiFC signal when cells were grown at lower temperatures (20°C) in comparison with standard growth conditions at 30°C (data not shown). Therefore, we used 20°C as standard growth conditions for all experiments performed. Furthermore, to minimize the background fluorescence of yeast cells and therefore increase the assay sensitivity, we visualized the cells in a home-made visualization media prepared as described by Sheff and Thorn, (2004).

The results obtained with the truncation mutants of Ubc4 suggested that the BiFC signal produced between Ubc4 and Ufd4 is at least in part due to a bona fide E2/E3 interaction, and therefore convinced us to use this method to more systematically assay E2/E3 interactions in yeast. Since we detected signal by BiFC and not BiLC with the same E2/E3 pair (Ubc4/Ud4), we decided not to do further experiments using BiLC. However, it is still possible that BiLC could be suitable to detect certain E2/E3 interactions, depending on the geometry and the level of expression of the proteins.

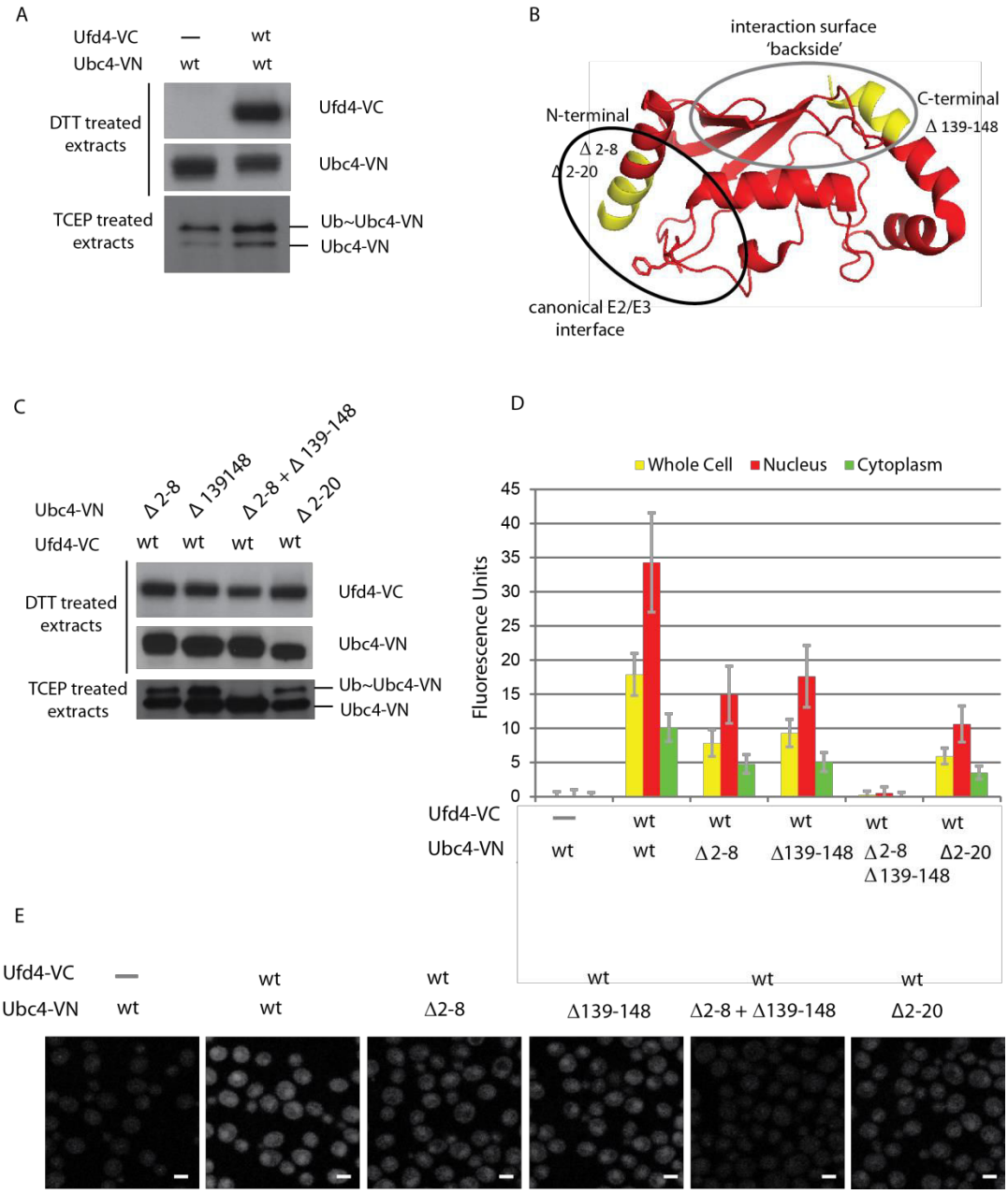

Figure 23. Specific detection of Ubc4/Ufd4 interaction using BiFC. A) Assessment of the expression level of VN and VC tagged Ubc4 and Ufd4 by Western blot (immunoblots of total protein extracts). The top panels refer to the whole cell extracts treated with DTT as a reducing agent. The bottom panel refers to the whole cell extracts treated with TCEP to preserve thioester bonds, therefore see the E2-Ub conjugate. B) Ubc4 deletion mutants used in this study. Regions deleted in the *Ubc4* gene (PDB ID: 1QCQ) are presented in yellow. The canonical E2/E3 interface is highlighted in black, whilst the additional so-called 'backside' E2 interacting surface is highlighted in grey. C) Immunoblots of total protein extracts from Ubc4 deletion mutants. The top panels refer to the whole cell extracts treated with DTT as a reducing agent. The bottom panel refers to the whole cell extracts treated with TCEP to preserve thioester bonds, therefore see the E2-Ub conjugate. D) Quantification of BiFC signal. To quantify the fluorescence signal in different subcellular compartments, all yeast strains express nuclear protein (here Rpn7) fused to the red fluorescent protein tdimer2. This enables to automatically segment the fluorescence images and to specifically quantify the BiFC signal in both the nucleus and the cytoplasm. E) BiFC imaging of the interaction between the Ufd4-VC and the Ubc4-VN constructs. Fluorescence images of yeast strains expressing Ubc4 and Ufd4 tagged with VN and VC at their endogenous chromosomal locus. Various strains expressing Ubc4 mutated in its interaction surface with Ufd4 were used to test the specificity of the BiFC signal.

4.2 Construction and use of an array of yeast strains to assess E2/E3 interactions

To enable the application of the BiFC assay in screening for E2/E3 interactions in yeast under physiological conditions we constructed an array of eleven strains in which each endogenous E2 gene was C-terminally tagged with a C-terminal fragment of Venus (VC), with the exception of the *Ubc1* and *Ubc6* genes, which were tagged N-terminally. This was because the strain with C-terminally tagged *Ubc1* was not viable (personal observation), whereas Ubc6 is an E2 that possesses a transmembrane domain and is a C-terminal membrane-anchored protein (Yang et al., 1997). Simultaneously, we acquired 55 strains with endogenously tagged genes that encode E3s/putative E3s from a genome-wide library of yeast strains, where most yeast ORFs have been C-terminally fused to VN (*S. cerevisiae* VN-Fusion Library, Bioneer Corporation). Additionally, we generated E3 strains of interest that were missing in the library (such as *Far1* and *Rsp5*) or that were fused N-terminally to VN. These E3 genes include *Tfb3*, *Prp19, Mot2*, *Psh1*, *Nam7* and *Ste5* and they encode E3s that harbor their E2 interacting domain in their N-terminus. Indeed, since it is estimated that BiFC can occur when two Venus fragments are fused with a distance no greater than ~10 nm (Hu et al., 2002), it is possible that the position of the VN-tag greatly influence the possibility to reform a properly folded Venus protein. We also used as a control, the E1 enzyme Uba1, which is expected to interact with all eleven ubiquitin E2s. In total we therefore had 63 VN-tagged strains representing 57 different E3s (six E3s were tagged both N- and C-terminally). The E2 strains were then crossed systematically with the E3 strains and the Uba1 strains to produce an array of 704 haploid yeast strains, with 627 strains expressing a unique combination of tagged E2 and E3 ORFs. The strain crossing procedure was performed in 96-well plates and the strains were then subjected to live cell imaging and analyzed for fluorescence upon BiFC complex formation in two independent experiments (Figure 24). We generated all these strains with an Rpn7 proteasome subunit fused to the red fluorescent protein tdimer2 to visualize the signal in the nucleus. This allowed not only to detect the particular E2/E3 interactions but also provided information on the subcellular localization of E2/E3 pairs. When measuring the BiFC signal, we also measured the Kurtosis of the fluorescent signal, which give information on the distribution of the fluorescent pixels that enables to more easily detect localized BiFC signals.

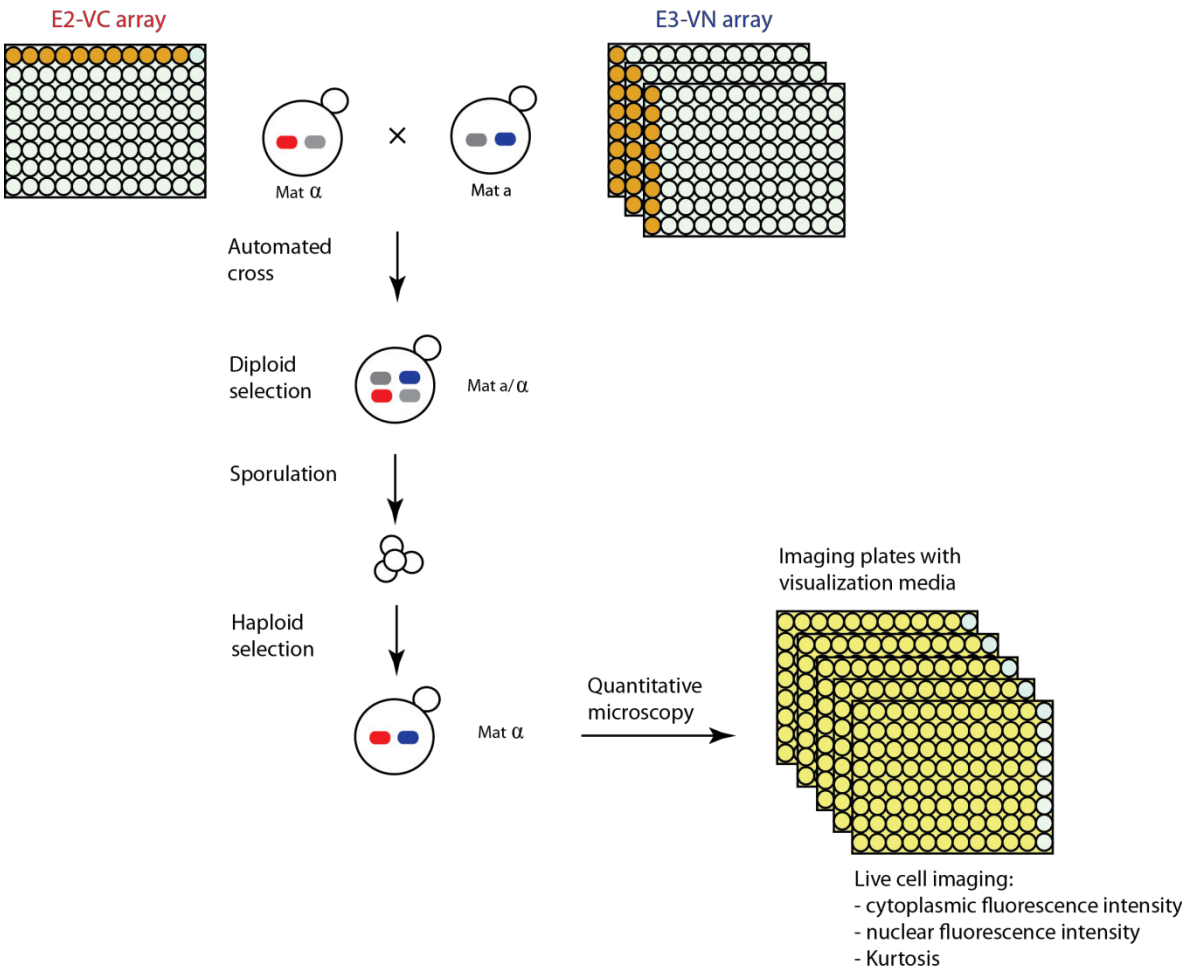

Figure 24. BiFC array construction to assay E2/E3 interactions. Yeast strains with the E2s tagged with VC and the E3s tagged with VN were incubated in liquid cultures. The strains were then mated in rich medium (YPD). Resulting haploid and diploid mixture strains were transferred onto the plates with diploid selective medium. Following diploid selection, strains were sporulated and haploid cells were selected in medium containing desired antibiotics, auxotrophic markers, canavanine and thialysine. E2/E3 interactions were assayed using quantitative microscopy. Fluorescence intensity was visualized both in the cytoplasm and in the nucleus. Rpn7 proteasome subunit, fused to the red fluorescent protein tdimer2, served as a nuclear marker.

Since yeast can easily be manipulated with plasmids that integrate into the genome by homologous recombination, their genes can be tagged endogenously. The endogenous tagging enables each fusion protein to be expressed from its own native promoter (Janke et al., 2004). To assay the expression level of the tagged E2s and verify that they are not overexpressed, we compared the expression level of a few of them (tagged with VC) with the endogenous E2s across the generated strains (Figure 25).

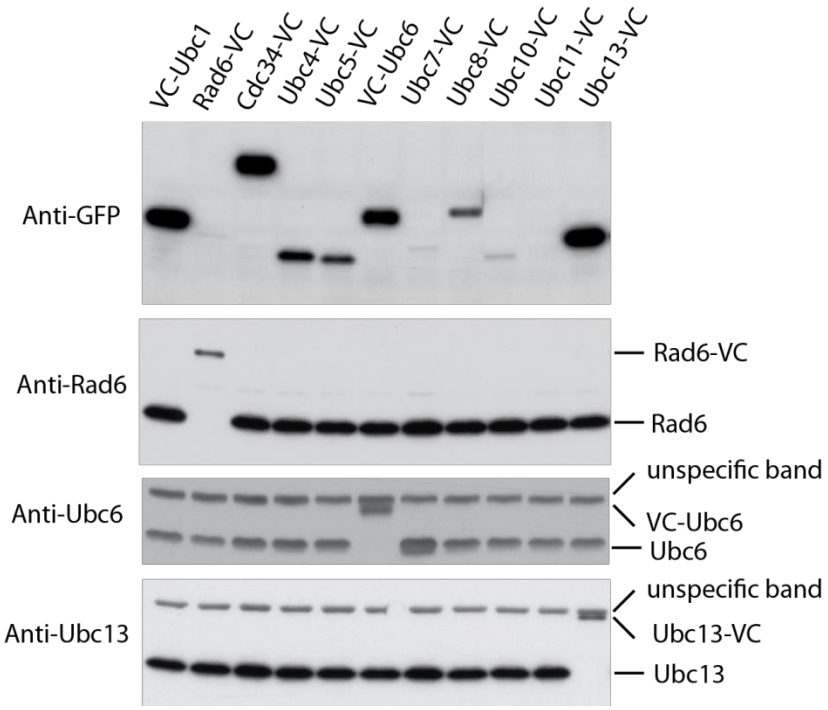

Figure 25. Yeast strains expressing 11 E2s (tagged with VC) from their own endogenous promoters. Expression assessed by Western Blot using Anti-GFP antibody (top). Rad6-VC, VC-Ubc6 and Ubc13-VC as the examples of tagged E2s versus endogenous E2s across the strains. The expression levels were compared using Rad6, Ubc6 and Ubc13-specific antibodies, respectively.

4.3 Detection and localization of E2/E3 pairs with BiFC

Overall, our results enabled us to identify 128 putative E2/E3 interactions, 33 of which were previously reported in the literature (approximately 57% of already known interactions), and 95 constitute new putative E2/E3 pairs. Few E3s interacted only with a single E2, whereas others produced a BiFC signal with multiple E2s. Ubc13, Ubc1 and Ubc4 were found to be the most frequently interacting E2s. The ubiquitin activating enzyme Uba1 served as a positive control in BiFC assay, and there was a BiFC signal detected across all E2s crossed with the strain with VN tagged Uba1. The summary of the screen result are presented in Figure 26, which is then summarized by Table 10.

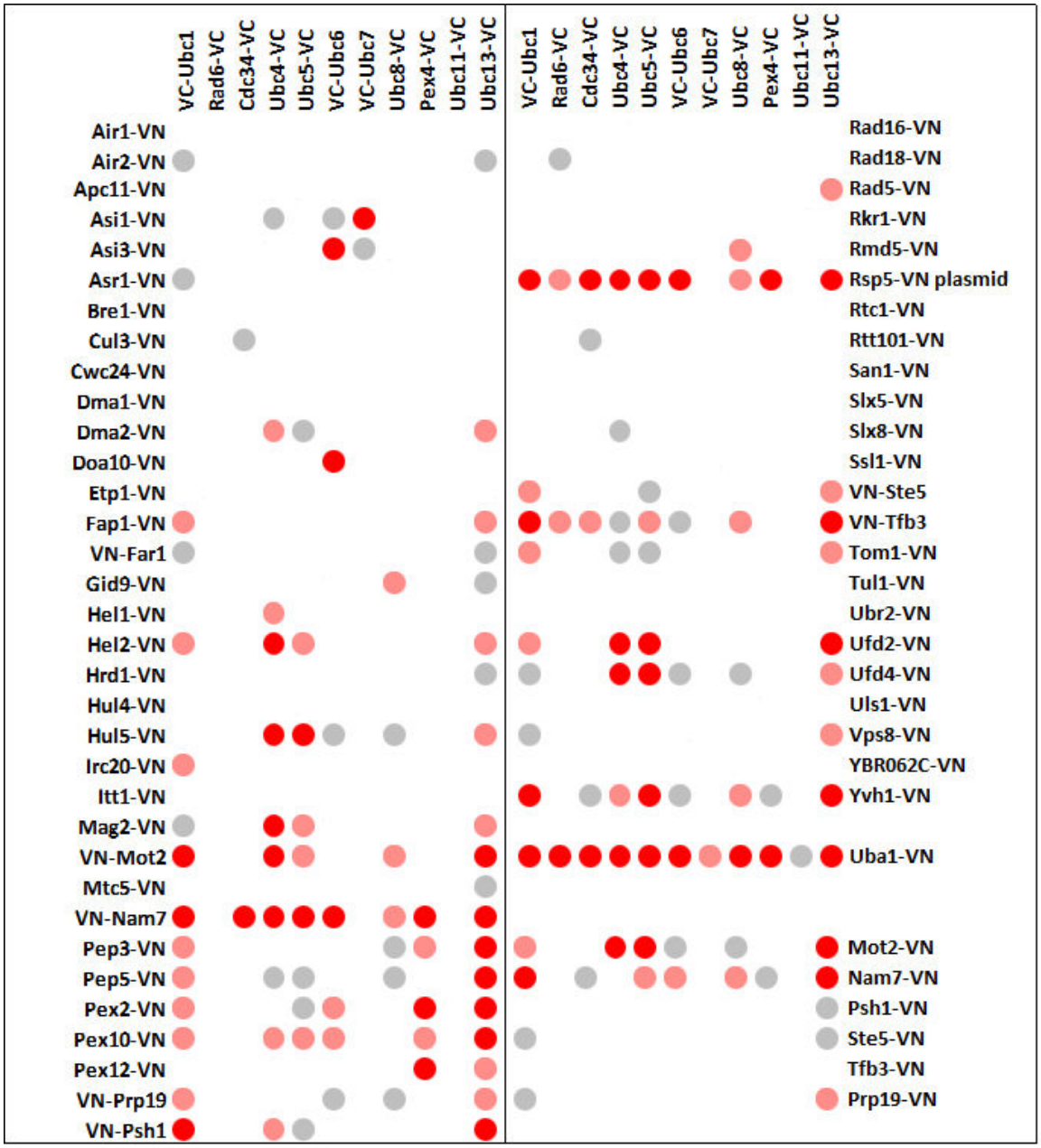

Figure 26. BiFC screen results of the putative detected E2/E3 interactions. Red dot represents a very strong or strong BiFC signal, pink indicates a moderate BiFC signal and grey indicates a weak BiFC signal. Uba1, which is an E1 activating enzyme serves here as a control.

Table 10. Summary table of BiFC screen results

BiFC signal	Number of positive hits
Overall signal detected	128
Very strong/strong signal (red dots)	42
Moderate signal (pink dots)	47
Weak signal (grey dots)	39
Interactions previously reported	33
New putative E2/E3 pairs	95

Comparison of the BiFC signal produced with N-terminally and C-terminally tagged E3s

Since the reconstruction of a functional Venus fluorescent protein is constrained by the topology of the interacting proteins, it is expected that BiFC can give different results when using N- and C-terminally tagged proteins. In our screen we used six E3s that were tagged at their N-terminal, in addition to the C-terminally tagged strains that were available from the commercial collection (Bioneer). These E3s, namely Tfb3, Prp19, Mot2, Psh1, Nam7 and Ste5, have their E2 interaction domain in their N-terminus. Indeed, we did observe different BiFC signals for some of these E3s, suggesting that the reconstitution of Venus is subject to topological constrains. In the figures below (Figures 27-30) those results are illustrated with the three E3s, namely Tfb3, Prp19 and Psh1. In the case of Psh1 and Tfb3, we observed that the N-terminally tagged E3s gave much stronger signal that the C-terminally tagged E3s, suggesting that the interaction signal is specific and strongly dependent on the close proximity of the VN-tag to the E2 interaction domain of the E3. In contrast, in the case of Prp19, the difference in signal produced by N- and C-terminally tagged Prp19 suggests that in this case the signal could be non-specific or that this E3 is subject to different topological constraints. Indeed, yeast Prp19 is known to form head-to-tail tetramers (Ohi et al., 2005), which could explain why tagging this E3 at the N- or its C-terminus does not strongly influence the BiFC signal. Note that due to difficulties in detecting the VN-tag of those proteins by Western blot, we were not able to compare the expression level of the N- and C-terminally tagged proteins.

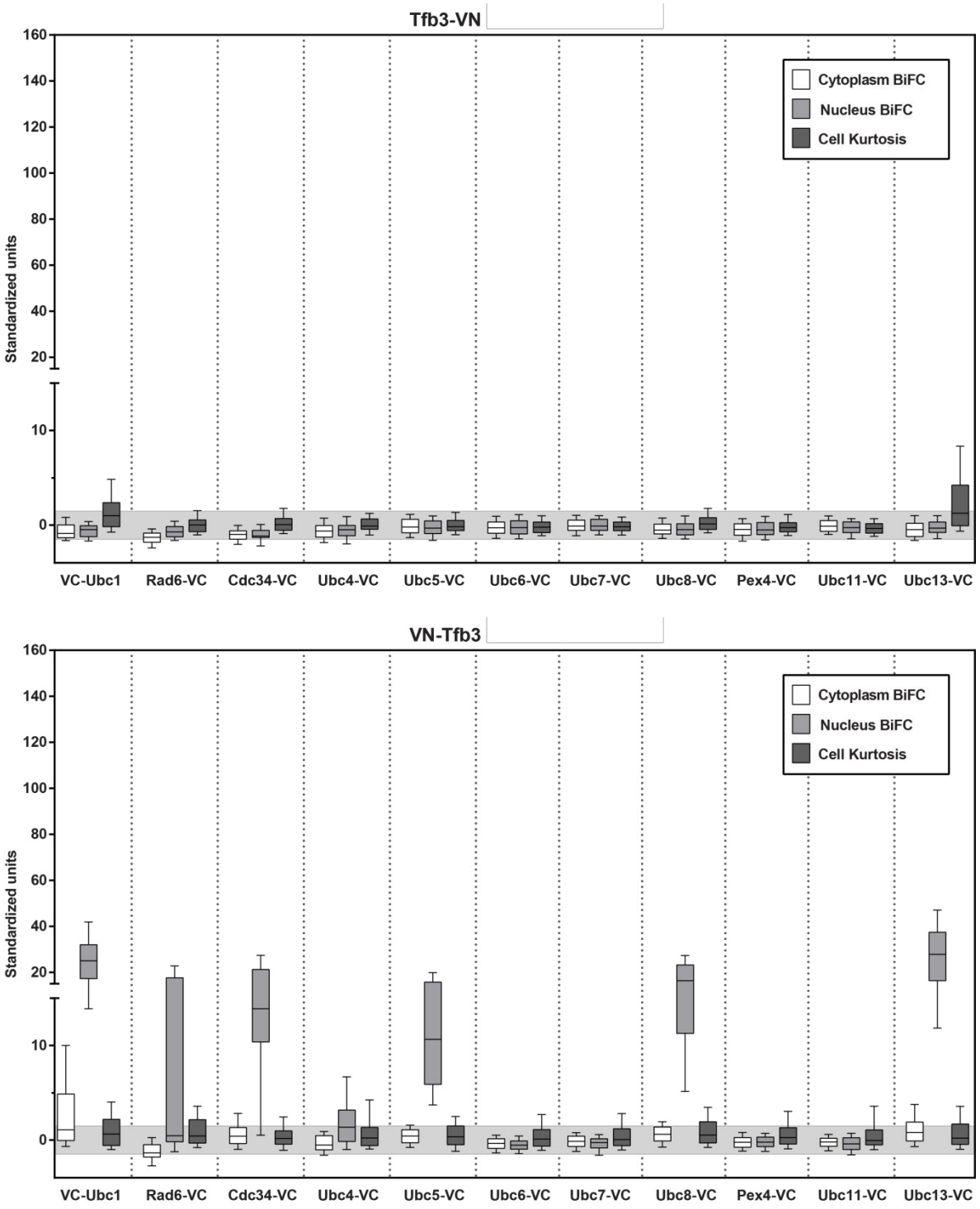

Figure 27. Quantification of the BiFC signal in the cytoplasm and the nucleus of the yeast cells with C-terminally (top) and N-terminally (bottom) tagged Tfb3 ligase. N-terminally tagged Tfb3 showed a strong BiFC signal in the nucleus with several E2s such as Ubc1, Rad6, Cdc34, Ubc4, Ubc5, Ubc8 and Ubc13 contrary to C-terminally tagged Tfb3. Here, a very weak BiFC signal was only detected for Ubc1 and Ubc13.

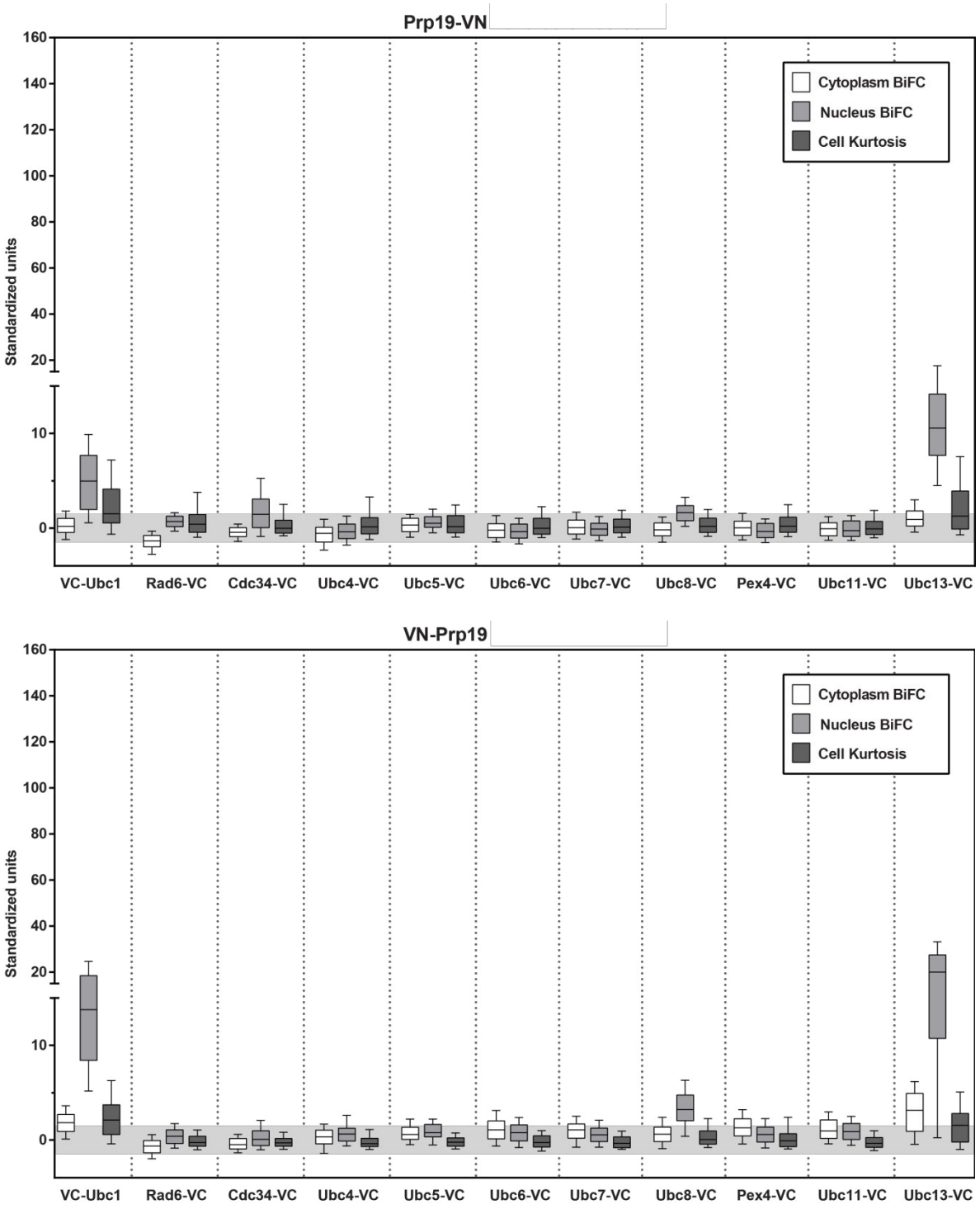

Figure 28. Quantification of the BiFC signal in the cytoplasm and the nucleus of the yeast cells with C-terminally (top) and N-terminally (bottom) tagged Prp19 ligase. N-terminally tagged Prp19 showed slightly stronger BiFC signal in the nucleus for Ubc1, Ubc13 and Ubc8 conjugating enzymes in comparison with C-terminally tagged Prp19.

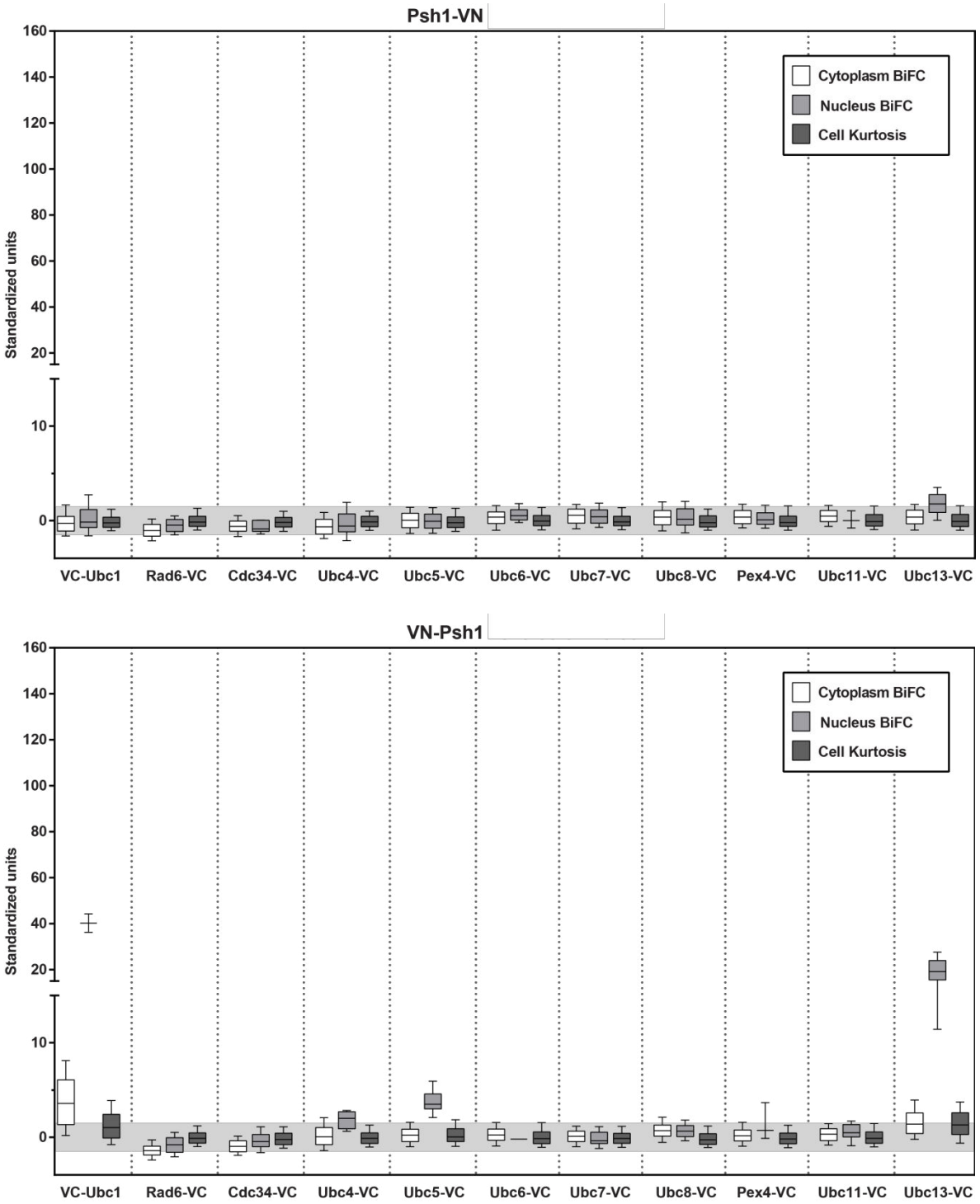

Figure 29. Quantification of the BiFC signal in the cytoplasm and the nucleus of the yeast cells with C-terminally (top) and N-terminally (bottom) tagged Psh1 ligase. N-terminally tagged Psh1 showed BiFC signal in the cytoplasm and nucleus when interacting with Ubc1 and in the nucleus when interacting with Ubc5 and Ubc13. No significant signal was detected for C-terminally tagged Psh1.

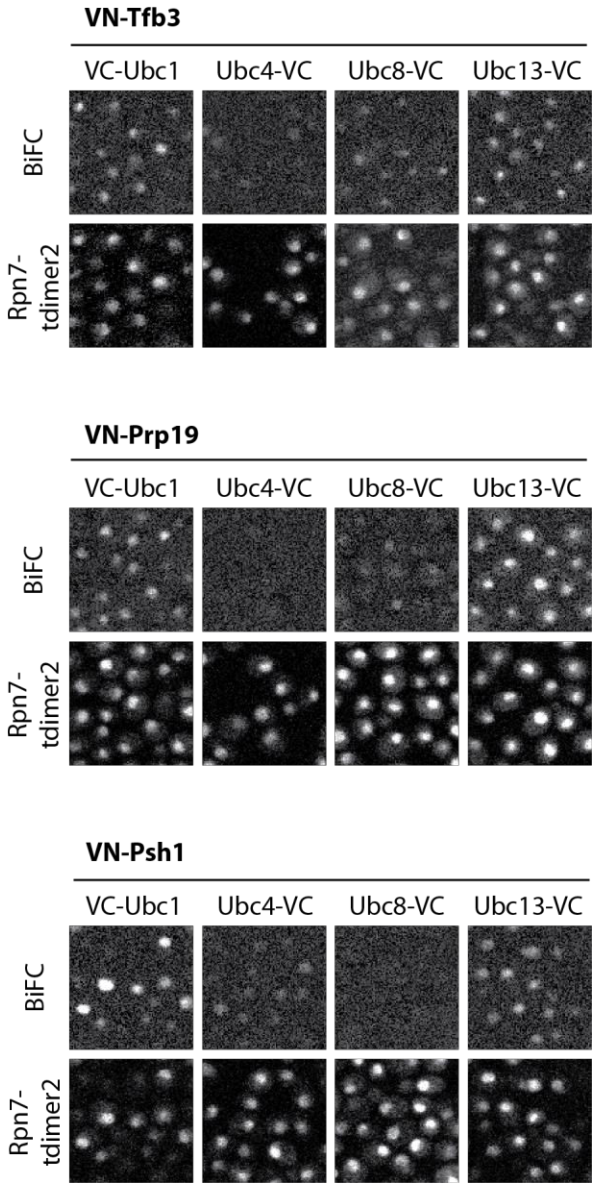

Figure 30. BiFC imaging of the N-terminally tagged Tfb3, Prp19 and Psh1 with Ubc1, Ubc4, Ubc8 and Ubc13 as examples. Top panel for each ligase shows BiFC signal and bottom panel Rpn7 proteasome subunit fused with red fluorescent protein tdimer2 that serves as a nuclear marker. A significant BiFC signal was not detected for Tfb3 in combination with Ubc4, Prp19 with Ubc4 and Psh1 with Ubc8 and Ubc4.

Examples of E3s that interact with a single E2

Few E3s showed specificity only for a single E2. This was for instance the case of the E3s Rad5 and Irc20, which produced a clear BiFC signal in the nucleus with Ubc1 and Ubc13, respectively (Figures 31-32). The fact that no signal was detected with other E2s, such as Cdc34 which is expressed at a similar level as Ubc1 or Ubc13 (Figure 25), further indicate that the BiFC signal produced with these E3s is likely to be specific. Rad5 is indeed known to function with Ubc13 and to mediate polyubiquitylation of PCNA (Parker and Ulrich, 2009). In contrast, Irc20 has not yet been described to function as a ubiquitin ligase. It is an adenosine triphosphatase (ATPase) protein with a RING domain and it is involved in DNA repair (Richardson et al., 2013). Our results thus suggest that it could indeed function as an E3 and it would be really interesting to further investigate its function in response to DNA damage. Note however that at this stage we cannot exclude that its interaction with Ubc1 reflects an E2/substrate interaction rather than a bona fide E2/E3 interaction.

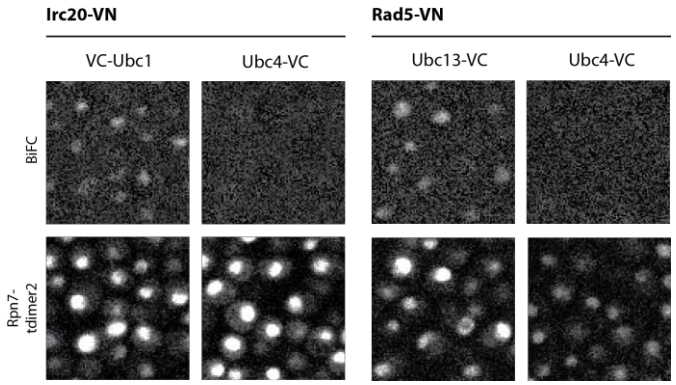

Figure 31. BiFC imaging of the Irc20 with Ubc1 and Rad5 with Ubc13. Top panel shows BiFC signal and bottom panel Rpn7 proteasome subunit fused with red fluorescent protein tdimer2 that serves as a nuclear marker. No BiFC signal was detected with Ubc4 conjugating enzyme (shown here as an example for a better visualization of the positive BiFC signal).

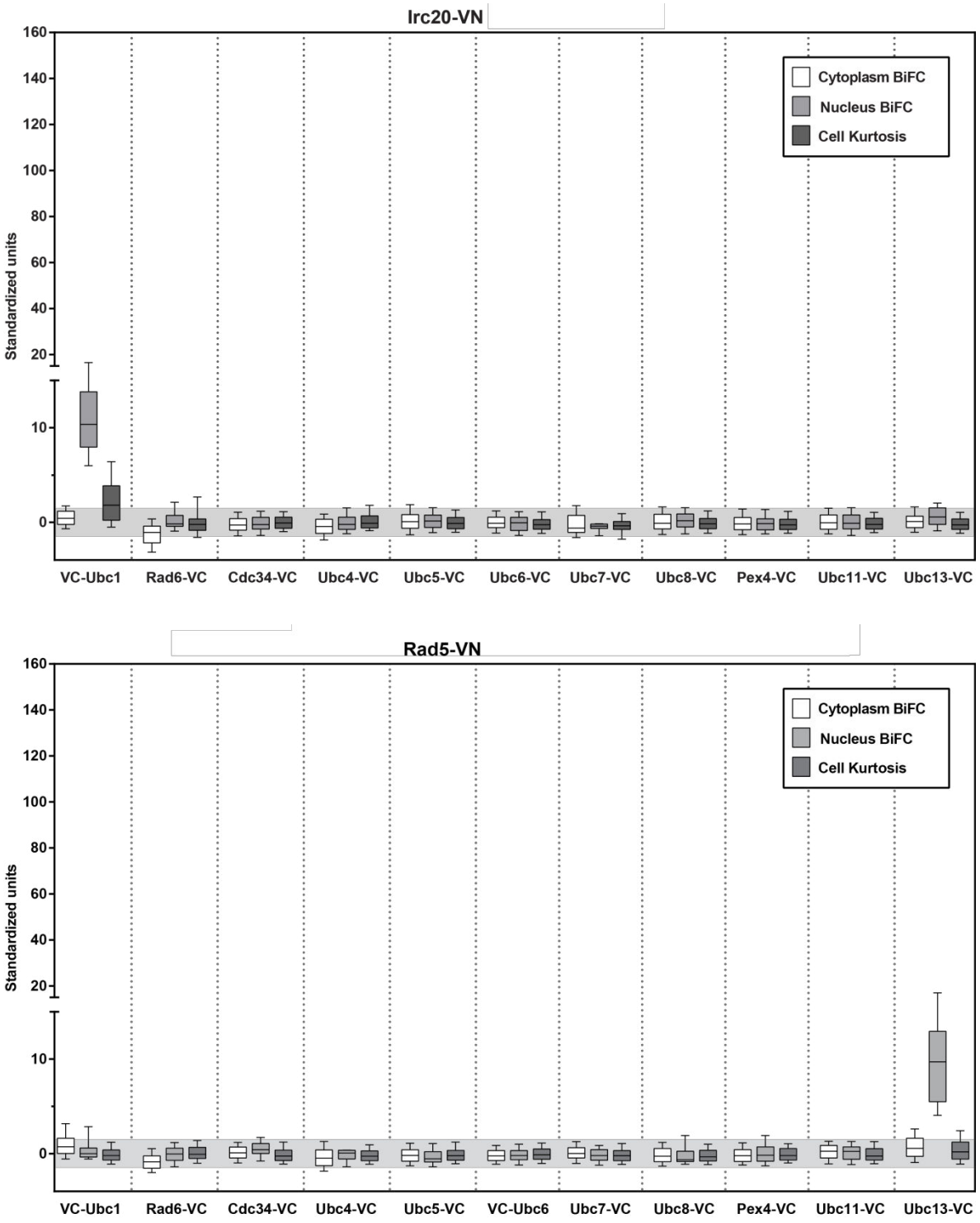

Figure 32. Quantification of the BiFC signal in the cytoplasm and the nucleus of the yeast cells with a C-terminally tagged putative ubiquitin ligase Irc20 (top) and ubiquitin ligase Rad5 (bottom). The fluorescence signal was detected in the nucleus upon the interaction of Irc20 with Ubc1 conjugating enzyme and Rad5 with Ubc13.

Figures 33 and 34 also present a single E3 interacting with a single E2, namely interactions of ubiquitin conjugating enzyme Ubc8, called also Gid3, with ubiquitin ligases Gid9 and Rmd5 (or Gid2). These results are fully consistent with the current literature on these proteins. Indeed, it has previously been shown that Gid9 and Rmd5 form a complex (the so-called 'Gid complex') that functions with Ubc8 to polyubiquitylate gluconegenic proteins, being therefore required for catabolite degradation (Braun et al., 2011). Interestingly, our data show that Ubc8 is rather weakly expressed E2 (Figure 25), suggesting that the BiFC is indeed a sensitive assay to detect E2/E3 interactions. In addition, we note that although Ubc8 was shown to function with the Gid complex by genetic means, it had never been shown to physically interact with this complex. Again, this illustrates the power of BiFC to investigate weak protein-protein interaction in the context of living cells.

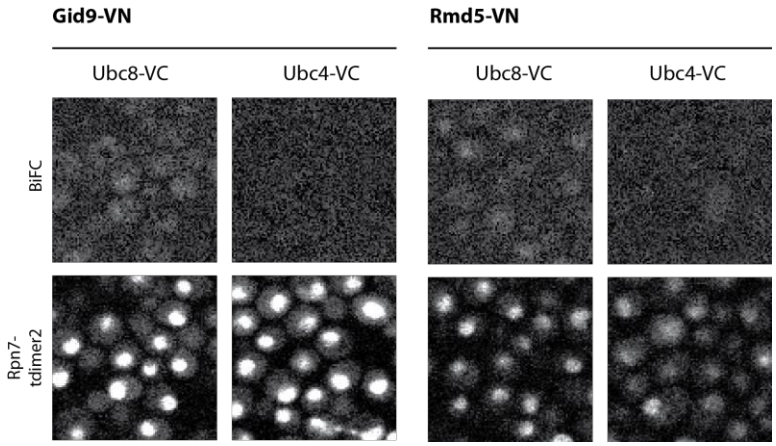

Figure 33. BiFC imaging of the Gid9 and Rmd5 (Gid2) with Ubc8. Top panel shows BiFC signal and bottom panel Rpn7 proteasome subunit fused with red fluorescent protein tdimer2 that serves as a nuclear marker. No BiFC signal was detected with Ubc4 conjugating enzyme (shown here as an example for a better visualization of the positive BiFC signal).

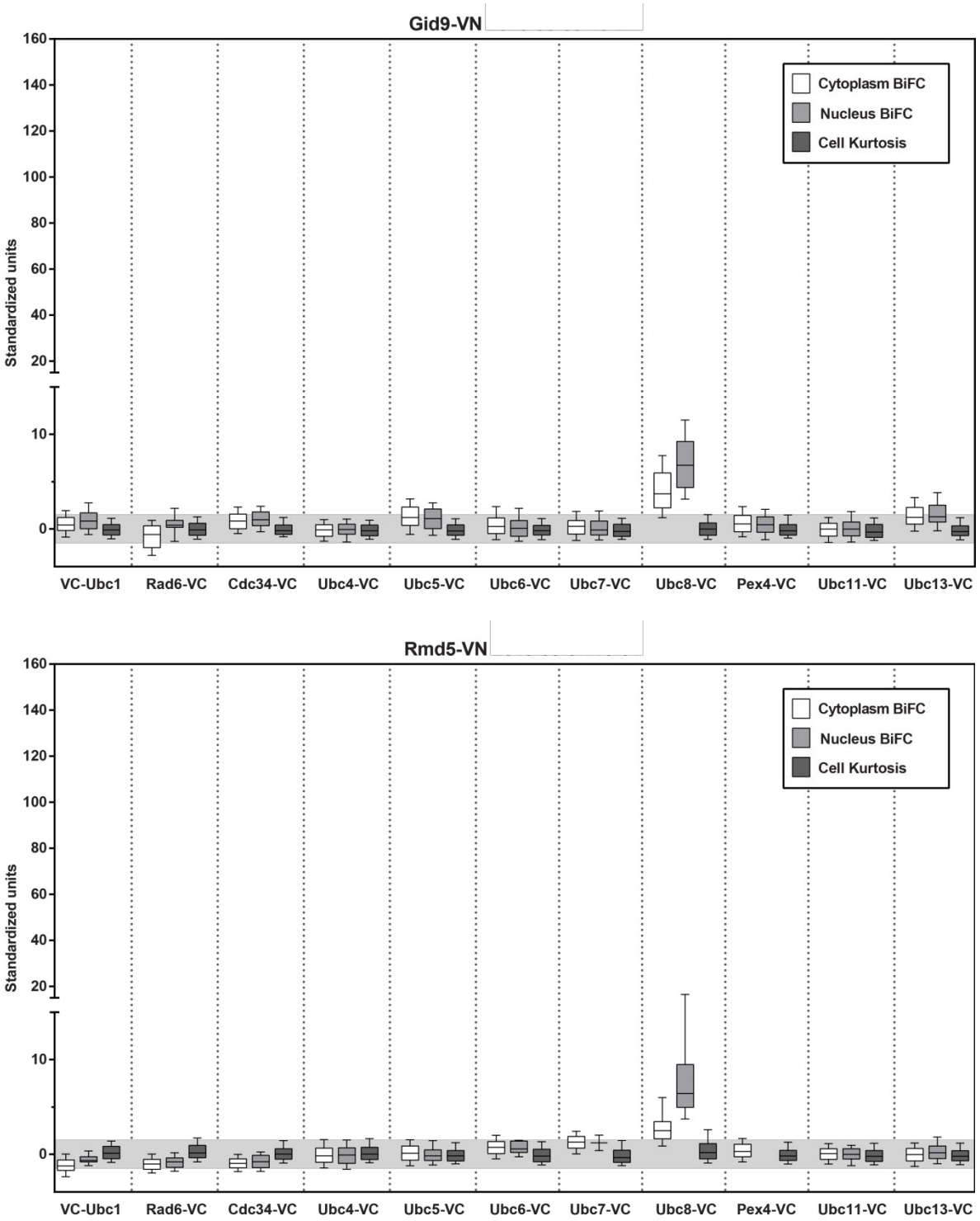

Figure 34. Quantification of the BiFC signal in the cytoplasm and the nucleus of the yeast cells with a C-terminally tagged ubiquitin ligases Gid9 (top) and Rmd5, also called Gid2 (bottom) with Ubc8 conjugating enzyme. The fluorescence signal was detected both in the cytoplasm and in the nucleus.

Examples of E3s that interact with several E2s

Below are included some examples of E3s that produced a BiFC signal with several E2s. The most prominent of such E3 is Rsp5, which we found to interact with all E2s, except the weekly expressed Ubc7 and Ubc11 (Figure 35). Despite the fact that this E3 interact with many E2s, the subcellular localization of the BiFC signal suggest that all E2s might be equivalent for this E3. For instance, the BiFC signal produced with Rad6 and Cdc34 was enriched in the nucleus, while the other E2s produced a stronger fluorescence signal in the cytoplasm rather than in the nucleus. This suggests that different E2s could function with Rsp5 in different subcellular compartments.

Other examples of E3s that interacted with several E2s are Ufd2, Ufd4 and the peroxisomal E3s Pex2, Pex10 and Pex12. Both Ufd2 and Ufd4 produced a clear BiFC signal with Ubc1, Ubc4, Ubc5 and Ubc13 (Figure 36). This result is intriguing since Ubc1 and Ubc13 are E2s dedicated to the assembly of Lys48- and Lys63-linked ubiquitin chains, respectively, while Ubc4 and Ubc5 assemble different kinds of ubiquitin chains (Rodrigo-Brenni et al., 2010; Eddins et al., 2006). It would be interesting to determine whether and how those different E2s contribute to the modification of the substrates of Ufd2 and Ufd4. The Pex2, Pex10 and Pex12 proteins are known to form a complex at the peroxisomes where they have been described to function with Ubc10 (also called Pex4) and Ubc4. Surprisingly, Pex2 and Pex10 also produced a clear BiFC signal with Ubc1 and Ubc13 (Figures 37 and 38). Moreover, Pex10 BiFC signal produced with Ubc1 and Ubc13 (but not Pex4) was not localized at the peroxisomes (which gives a strong kurtosis measurement in the quantification data) but at the vacuole (Figure 38). This result could indicate that Pex10 has a unique function at the vacuole, independent of Pex2 and Pex12.

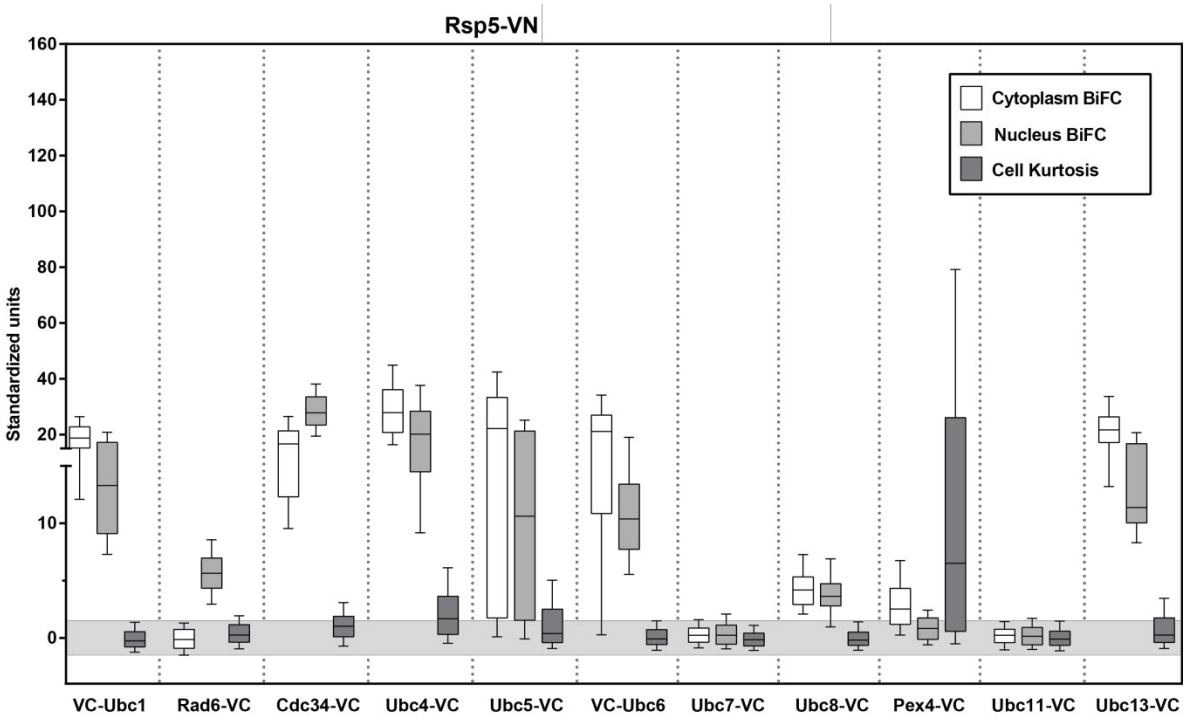

Figure 35. Quantification of the BiFC signal in the cytoplasm and the nucleus of the yeast cells with a C-terminally tagged ubiquitin ligase Rsp5 on a replicative plasmid. The fluorescence signal was detected nearly with all ubiquitin conjugating enzymes, except Ubc7 and Ubc11.

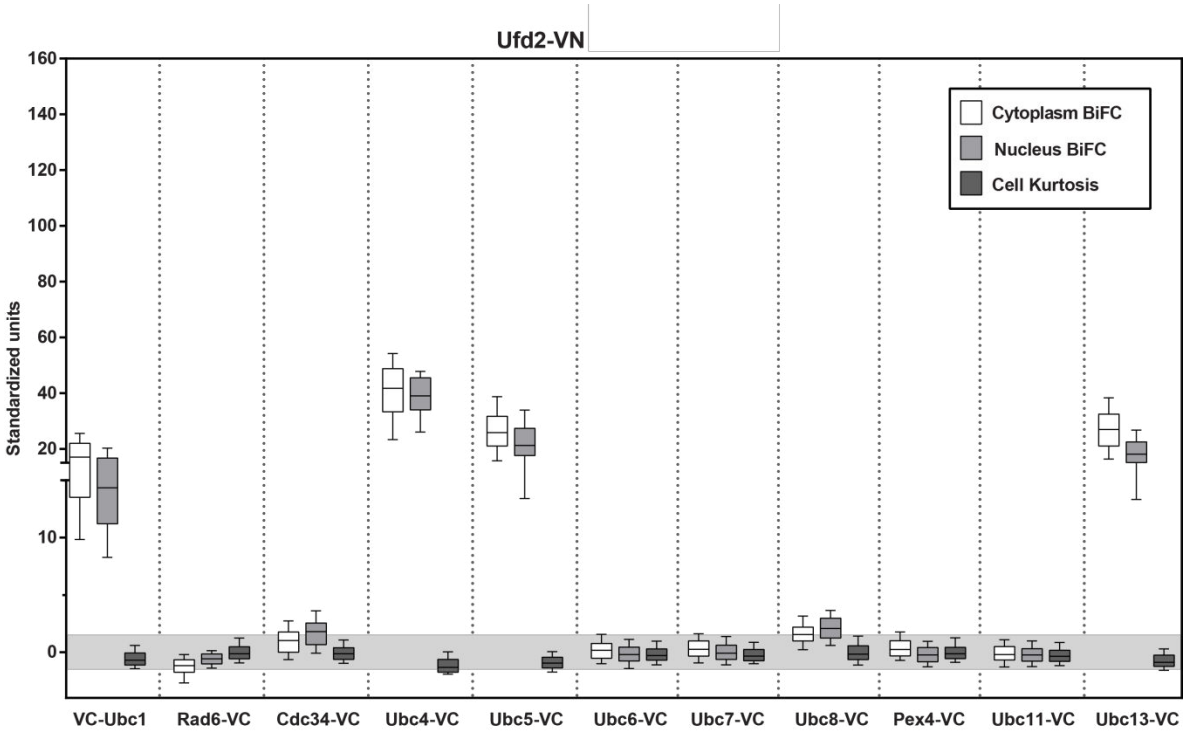

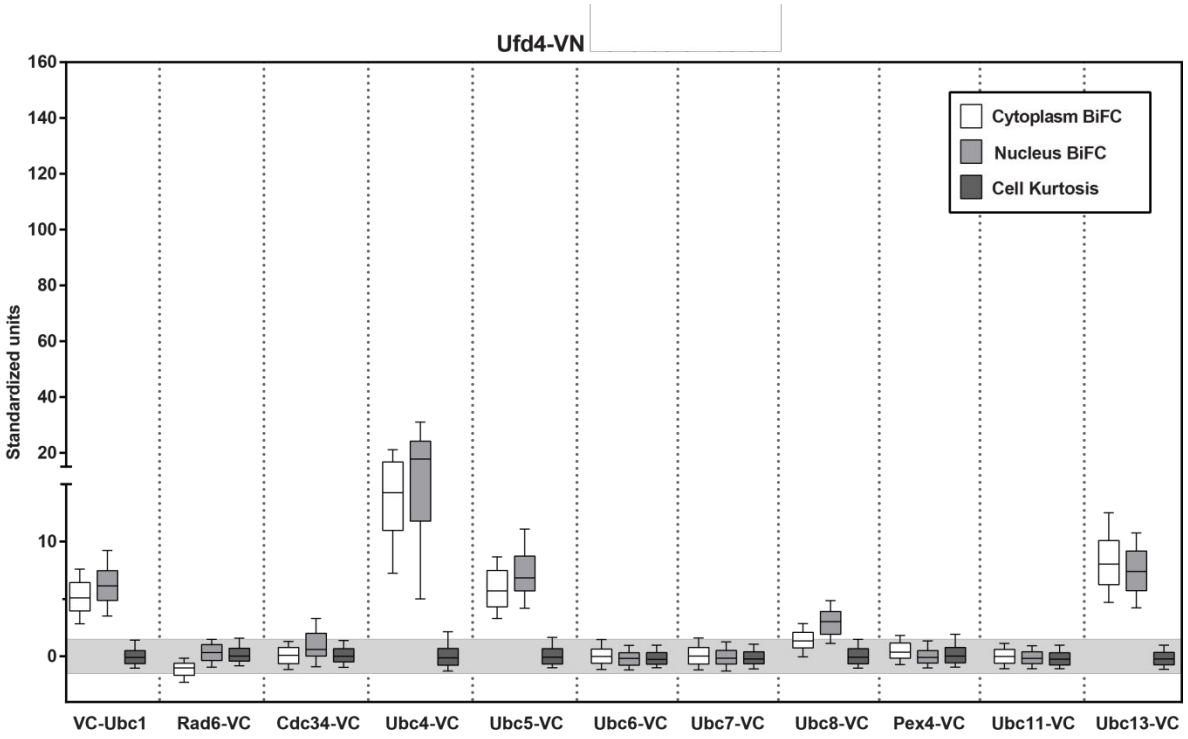

Figure 36. Quantification of the BiFC signal in the cytoplasm and the nucleus of the yeast cells with a C-terminally tagged ubiquitin ligases Ufd2 and Ufd4. The fluorescence signal was detected in the cytoplasm and nucleus upon interaction with Ubc1, Ubc4, Ubc5, Ubc8 and Ubc13.

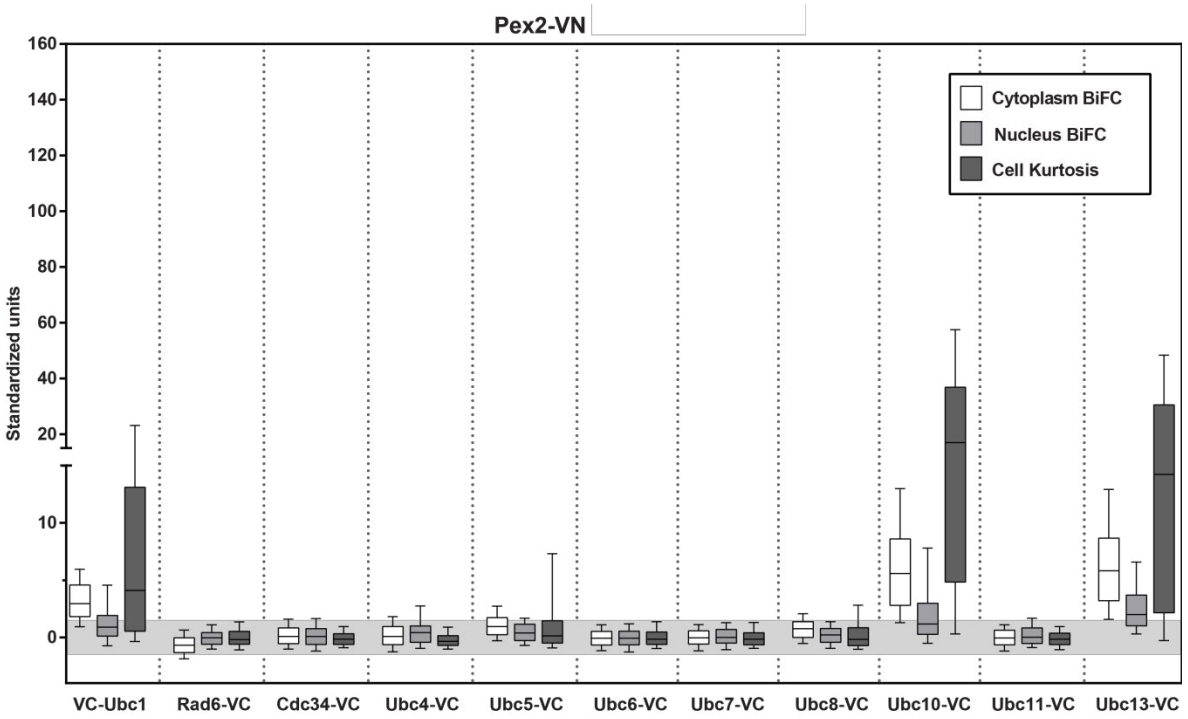

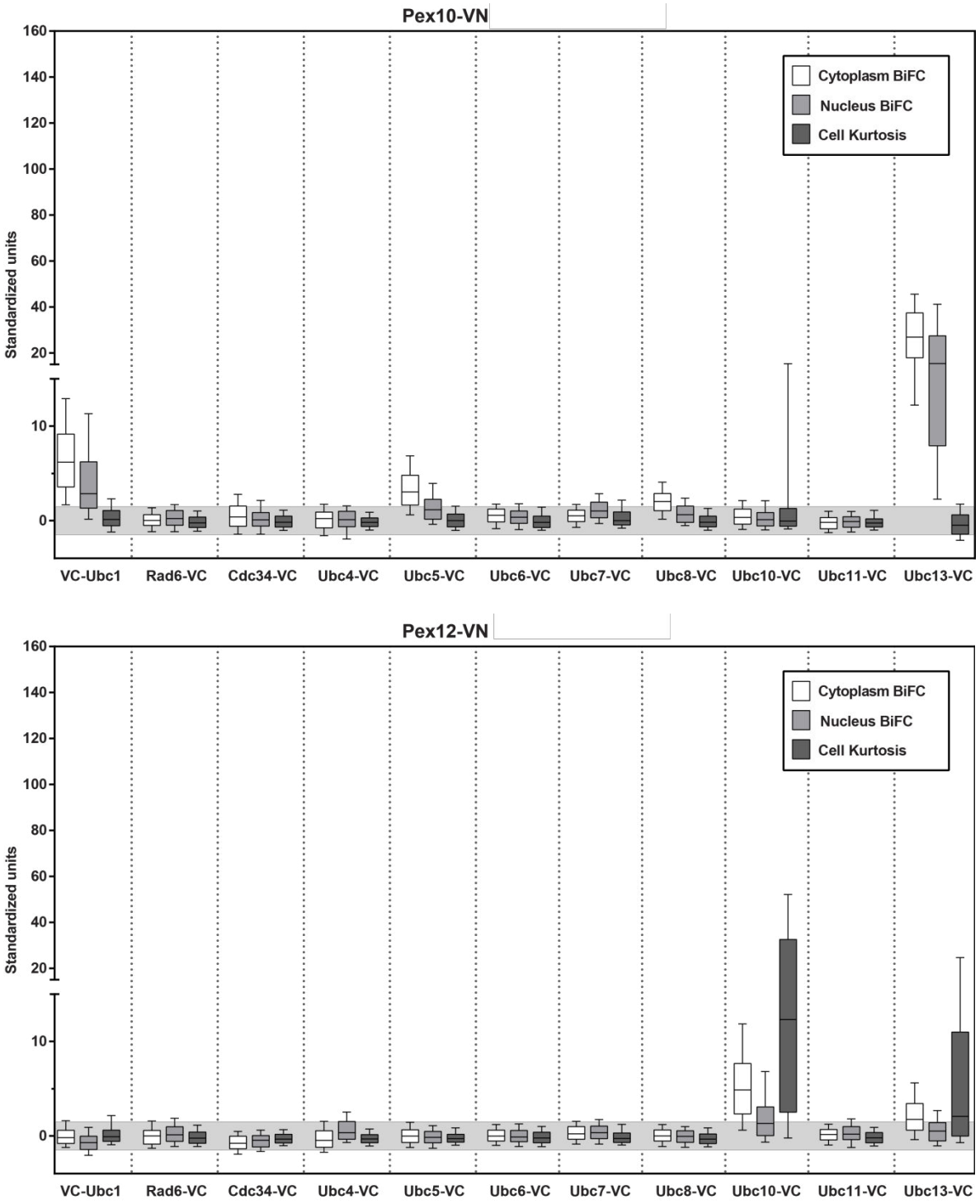

Figure 37. Quantification of the BiFC signal in the cytoplasm and the nucleus of the yeast cells with a C-terminally tagged ubiquitin ligases Pex2 (top), Pex10 (middle) and Pex12 (bottom). The fluorescence signal was detected with ubiquitin conjugating enzymes, Ubc1, Ubc10 and Ubc13 for Pex2 and Pex10 and Ubc1 and Ubc13 for Pex12.

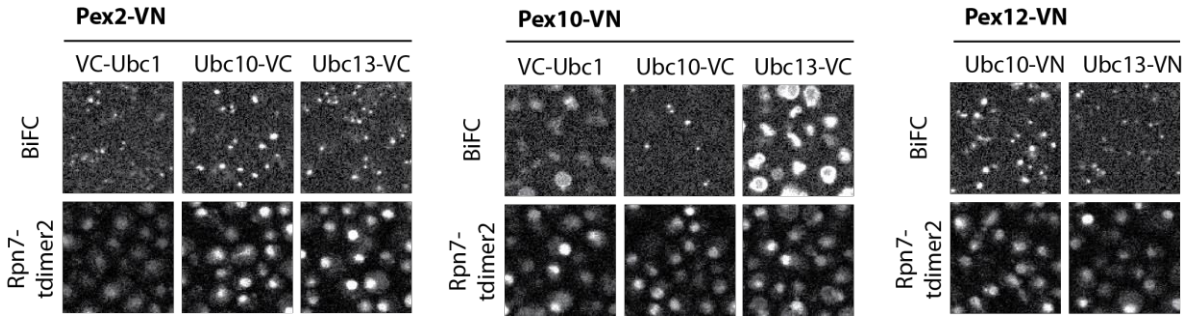

Figure 38. BiFC imaging of the Pex2, Pex10 and Pex12. Top panel shows BiFC signal and bottom panel Rpn7 proteasome subunit fused with red fluorescent protein tdimer2 that serves as a nuclear marker.

4.4 Functional characterization of the candidate E2/E3 pair

Interestingly, while performing the BiFC screen, we identified an interaction between the proteins Asi1 and Asi3 and the ubiquitin conjugating enzymes Ubc6 and Ubc7 (Figure 39). The fluorescence signal was localized at the nuclear rim and was specific to these E2s. Together with another protein, Asi2, Asi1 and Asi3 are known to form a complex (the Amino acid Signaling Independent, known as the 'Asi complex') at the inner nuclear membrane (INM) (Zargari et al., 2007). Both Asi1 and Asi3 contain a RING domain and were therefore postulated to function as E3s (Forsberg et al., 2001) but such an activity had never been demonstrated. Furthermore, the activity of the Asi-complex had been well characterized to function in the Ssy1-Ptr3-Ssy5 (SPS) amino acid-sensing pathway of *S. cerevisiae*. This is a nutrient induced signal transduction pathway via which yeast responds to the extracellular amino acids (reviewed by Ljungdahl, 2009). In this pathway, the function of the Asi complex was described to inhibit the activity of Stp1 and Stp2, two transcription factors required for the expression of amino-acid permeases. These transcription factors were therefore candidate to be ubiquitylation substrates of Asi1 and Asi3.

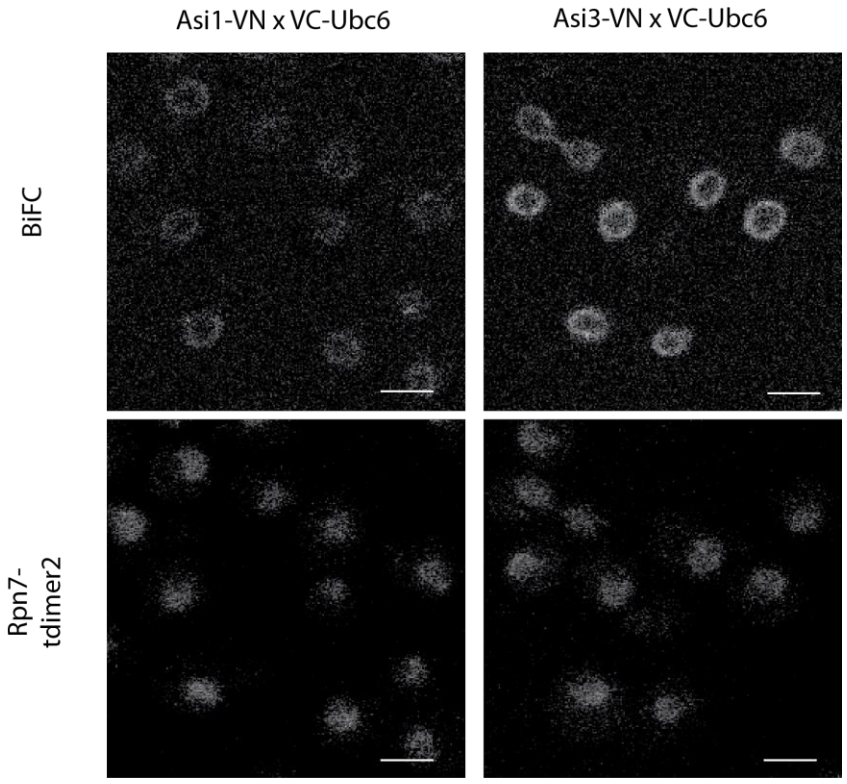

Figure 39. BiFC imaging of the cells with VN-tagged Asi1 and Asi3 together with VC-tagged Ubc6. Top panel shows BiFC signal and bottom panel Rpn7 proteasome subunit fused with red fluorescent protein tdimer2 that serves as a nuclear marker. Scale bar, 5 μm.

Since Asi3 has a RING domain and was considered as a putative ubiquitin ligase, we decided to further test the specificity of the detected interaction with Ubc6 by deleting the RING domain of Asi3. This dramatically decreased the BiFC signal, suggesting that the interaction is indeed specific. However, we could not verify that the two forms of Asi3 have the same expression level (we did not manage to detect endogenously expressed Asi3-VN by Western blot) and this data is therefore not conclusive. We further tested whether the deletion of the Asi complex components in the Asi3-VN/VC-Ubc6 strain would influence the BiFC signal. Our results showed that deletion of Asi1 dramatically reduces BiFC signal, while the deletion of Asi2 causes only a slight decrease in the fluorescence intensity. This result again suggests that the detected Asi3/Ubc6 is specific but the interpretation of this data is difficult because we could not verify that Asi3-VN is properly expressed in *asi1*Δ or *asi2*Δ cells.

To further analyse the interaction of Asi1 and Asi3 with Ubc6 and Ubc7 we turned to *in vitro* experiments, which were mainly performed by an engineer, Gaëlle Le Dez. We purified the RING domains of Asi1 and Asi3, as well as those of Ubc6 and Ubc7 (alone or in complex with a fragment of its partner protein Cue1) produced recombinantly. As control, we also used the RING domain of Hrd1 which is known to function with Ubc7 but not Ubc6. The interaction between those proteins was tested using a method called MicroScale Thermophoresis. Our results demonstrated that both Asi1 and Asi3 can interact with Ubc7 and also with Ubc6, but with a weaker Kd. These results thus confirmed the *in vivo* BiFC data and showed that Ubc6 and Ubc7 can directly interact with the RING domains of Asi1 and Asi3.

To determine whether the interaction between the Asi complex and the E2s Ubc6 and Ubc7 were productive, we analyzed the ubiquitylation of the N-terminal sequence of Stp2, which had previously been shown to contain the minimal signal for Asi-dependent repression of Stp2 activity. Those experiments were performed by Audrey Brossard and showed that the N-terminal fragment of Stp2 fused to the TAP-tag was indeed ubiquitylated in an Asi3 dependent manner. Furthermore, ubiquitylation of Stp2 N-terminus was diminished in *ubc6*Δ cells and almost fully abolished in *ubc7*Δ cells. Those results strongly suggest that the Asi complex ubiquitylates Stp2 in a Ubc6 and Ubc7 dependent manner, with Ubc7 being the primary E2 for Stp2 ubiquitylation. It is possible that other E2s, such as Ubc4 which we found to weakly interact with Asi3 in the absence of Ubc6, also contributes to Stp2 ubiquitylation *in vivo*.

While working on this project, we started to collaborate with the laboratories of Per Ljungdahl from Stockholm University and Michael Knop from the University of Heidelberg. Most importantly, the laboratory of Michael Knop was able to demonstrate that in addition to Stp2, the Asi-complex and Ubc7 target for degradation several transmembrane proteins that normally localize to the endomembrane system. Altogether, our work demonstrates the existence of a novel quality control pathway associated with the inner nuclear membrane (Inner Nuclear Membrane Associated Degradation, INMAD) and suggests that the primary function of the Asi proteins is to act as a shield against proteins that mislocalize to the nucleus. This pathway is distinct from the previously described ER associated degradation pathway and since Asi proteins do not have clear orthologues in higher eukaryotes, it is not yet known whether a similar INMAD pathway exists outside yeasts.

Publication

This part of the results has been included in a publication which is joined at the end of the manuscript.

Khmelinskii A.*, Blaszczak E.*, Pantazopoulou M., Fischer B., Omnus D.J., Le Dez G., Brossard A., Gunnarsson A., Barry J.D., Meurer M., Kirrmaier D., Boone C., Huber W., Rabut G., Ljungdahl P.O., Knop M., (2014). Protein quality control at the inner nuclear membrane. *Nature.* **516** (7531), 410-413.

*equal contribution

5 DISCUSSION

The initial aim of this study was to establish a method to assay E2/E3 interactions in living cells. We have compared two methods based on protein-fragment complementation, as this has been shown to detect weak and transient interactions *in vivo* (reviewed by Morell et al., 2007). Among the PCAs that we tested were BiFC assay, based on the fluorescent protein complementation and BiLC assay, based on the luminescent protein complementation. Fluorescent protein fusions have been particularly useful, as they allow fluorescence microscopy of living cells with a minimal perturbations (Sheff and Thorn, 2004). Similarly BiLC assays, with the luciferase assay as an example, also display minimal cell perturbation in the system under investigation (Zhang et al., 2009).

Here we report that the BiFC assay can detect E2/E3 interactions in living yeast. First, we have shown that BiFC can detect the interaction between Ubc4 and Ufd4, a well characterized E2/E3 pair in yeast. To evaluate whether this method reliably detects this interaction, a BiFC experiment was performed using deletion mutants. We generated a series of deletion mutants with truncated N-terminal or C-terminal domains. The various deletion constructs yielded a significant decrease in the BiFC signal, indicating that the detected BiFC signal is likely due to the E2/E3 interaction and not due to unspecific reconstitution of the Venus protein. Interestingly, these results suggest that Ufd4 utilizes not only the canonical E2/E3 interacting surface but also the 'backside' of Ubc4, since it is necessary to truncate not only the N-terminus but also the C-terminus of Ubc4 to abolish the BiFC signal. However, due to the fact that BiFC can lead to false positive results, the putative interactions have to be assayed using other methods before being able to draw definitive conclusions. BiLC, which has to our knowledge never been reported to lead to the false positive signals, does not have this drawback. However, despite several attempts, we did not detect the Ubc4/Ufd4 interaction using BiLC. This could be for various reasons and we could probably optimize this assay even more. However, it seems likely that the difference with BiFC comes mainly from the fact that BiLC is reversible and does not trap transient interactions contrary to irreversible BiFC (once the Venus is reconstituted, it cannot unfold into the VN and VC fragments), which 'locks' the protein-protein interactions

(Hu et al., 2002). This irreversibility is a limitation of BiFC when dynamic changes in protein complexes need to be examined (Vidi and Watts, 2009). However, in the case of weak and transient interactions it seems to be advantageous over BiLC. In a way, the sensitivity of BiFC is at the cost of specificity and secondary assays are required to further make sure that the detected interactions are biologically relevant. Finally, it is still possible that BiLC could detect certain E2/E3 interactions, depending on the geometry and the level of expression of the proteins. Since we detected an interaction signal using BiFC with the same E2/E3 pair as for the BiLC experiments, we decided not to perform further tests with the later method but rather to screen for E2/E3 interactions using BiFC.

With this limitation of BiFC in mind, we decided to perform a systematic screen for new E2/E3 interactions. As aptly noted by Kerppola (2008) 'the challenge for implementing a screen for interaction partners is that the levels of expression of different fusion proteins in a library is likely to vary over the level of expression of the corresponding endogenous proteins. Thus the differences in BiFC signal are likely to be affected by a variety of factors unrelated to the efficiency of the protein interaction'. In our case, all proteins except Rsp5 were expressed from their endogenous chromosomal loci (Rsp5-VN was cloned in a centromeric plasmid containing its endogenous promoter). For some E2s, for which we had suitable antibodies, we compared the level of expression of the VC-tagged and untagged E2s. Surprisingly, we noted a lower expression level of the tagged versus endogenous E2s. This is probably due to the fact that the VC-tag is mainly unfolded in the cells and targets the fusion protein for degradation. In any case, we did not observe any overexpression of the tagged-E2s, which limits the risk that the fusion proteins are mislocalized to cellular compartments, where they do not reside in normal cells. Despite this lower expression level, we noticed that the different E2s were expressed at different levels, which likely reflects differences in the abundance of the endogenous E2s. We noticed that weaker expressed E2s produced less detectable interactions than stronger expressed E2s. This observation is consistent with recent research by Levy et al. (2014) who reported that PPIs depend greatly on protein abundance. It is also likely that the interactions of proteins with relatively low expression levels are difficult to detect. BiFC can therefore suffer from false negatives, and some interactions can be missed using this method. However, we detected some E2/E3 interactions with the less abundant E2s such as Rad6. The only E2

for which we did not detect any interaction is Ubc11, which is also the sole E2 that we could not detect by Western blot. Still, this protein must be slightly expressed since we could detect a weak BiFC interaction with Uba1. Finally, this that we found more interactions with highly expressed E2s could also be due to the fact that some E2s such as Ubc13 are expressed at a level that tends to produce non-specific interactions. We therefore need to be very careful in the way we interpret our data.

In addition to the sensitive detection of E2/E3 interactions, BiFC enables us to visualize individual cell compartments, therefore providing information on interaction localization. However it does not enable a real-time detection of BiFC complex formation due to the slow fluorophore maturation (Hu et al., 2002). The localization of the BiFC signal may therefore not always reflect the initial subcellular interaction localization, as this may develop later in a different region, especially in the case of dynamic protein complexes (Sung et al., 2013). It cannot be excluded that similarly to all other recombinant protein tagging approaches, BiFC fragments may alter the localization and/or the function of the fused partner proteins. It therefore is important to compare the subcellular localization of tagged versus untagged proteins (Vidi and Watts, 2009). Despite these limitations the fact that BiFC enables to detect subcellular localization of proteins can help to select interesting E2/E3 pairs for further investigation and can give some clues on their function. The prominent nuclear rim localization of the Ubc6/Asi3 BiFC signal caught our attention and is one of the observations that prompted us to further investigate this interaction. Similarly, the fact that Pex10, but not its partners Pex2 and Pex12, produces a strong BiFC signal with Ubc13 at the vacuole is intriguing and suggests that the Ubc13/Pex10 pair could have a specific function in this compartment.

The BiFC screen for E2/E3 interactions enabled us to identify numerous new putative E2/E3 pairs. Among those interactions we could demonstrate, thanks to collaboration with the Knop and Ljungdahl laboratories, that the Asi-complex proteins Asi1 and Asi3 functionally interact with Ubc6 and Ubc7 and this led to the identification of a new quality control pathway at the inner nuclear membrane. Because BiFC can give false positive results, it is however very difficult to say how many of the other newly E2/E3 interaction are really active in the cell. One way to address this question systematically would be to perform subscreens with E2s mutants designed to abolish E3 interactions. However such mutants are difficult to design since there is more

and more data in the literature indicating that many E3s engage multiple interactions with E2s (see for instance Brown et al., 2015). Therefore, designing simple mutations in the canonical E3 interaction surface of E2s might not be sufficient to abolish the observed BiFC signal. Conversely, mutating RING or HECT domains of E3s may not abolish E2 interactions *in vivo* if other domains or partners of the E3s contribute to the interaction in the cell. Therefore, the best way to determine whether an E2/E3 pair is really active in the cell is to assay the ubiquitylation of its substrate(s).

6 CONCLUSIONS AND PERSPECTIVES

Despite all the limitations of BiFC discussed above, we are convinced that our approach can help to uncover the range of E2s that function in the cell with certain E3s. This opens a perspective on analyzing how the different E2s, which function with an E3, collaborate to assemble specific ubiquitin signals on their substrates. Performing such an analysis however would require efficient tools to determine the architecture of ubiquitin chains. Such assays are still being developed and one of the most promising way to analyze the type of ubiquitin signals assembled on the ubiquitylation substrates is the UbiCRest method, which makes use of chain specific deubiquitylating enzymes and has been developed in the laboratory of David Komander (Hospenthal et al., 2015). It would be very interesting to use this method to, for instance determine if Ubc13, which is dedicated to the assembly of Lys63-linked ubiquitin and which we found to produce a BiFC signal with numerous E3s, indeed assembles Lys63 ubiquitin chains on the substrates of these E3s.

Another appealing perspective of our work is the possibility to use our collection of strains expressing 627 unique combinations of VC-tagged E2s and VN-tagged E3s/putative E3s to assay how the ubiquitin machinery responds to specific growth or stress conditions. Indeed we have developed the pipeline for high-throughput imaging and image analysis of BiFC and it would be possible to identify new E2/E3 pairs that only interact under specific conditions, for example, upon DNA damage.

7 REFERENCES

Aguilera, M., Oliveros, M., Martínez-Padrón, M., Barbas, J. A., & Ferrús, A. (2000). Ariadne-1: a vital Drosophila gene is required in development and defines a new conserved family of ring-finger proteins. *Genetics*, *155*(3), 1231–44.

Aichem, A., Pelzer, C., Lukasiak, S., Kalveram, B., Sheppard, P. W., Rani, N., Schmidtke, G., Groettrup, M. (2010). USE1 is a bispecific conjugating enzyme for ubiquitin and FAT10, which FAT10ylates itself in cis. *Nature Communications*, *1*, 1–10.

Alam, S. L., Sun, J., Payne, M., Welch, B. D., Blake, B. K., Davis, D. R., Meyer, H.H., Blake, S.D., Sundquist, W. I. (2004). Ubiquitin interactions of NZF zinc fingers. *The EMBO Journal*, *23*(7), 1411–21.

Amerik, A. Y., Li, S. J., & Hochstrasser, M. (2000). Analysis of the deubiquitinating enzymes of the yeast Saccharomyces cerevisiae. *Biological Chemistry*, *381*(9-10), 981–92.

Anderie, I., Schulz, I., & Schmid, A. (2007). Direct interaction between ER membrane-bound PTP1B and its plasma membrane-anchored targets. *Cellular Signalling*, *19*(3), 582–592.

Atanassov, B. S., Koutelou, E., & Dent, S. Y. (2011). The role of deubiquitinating enzymes in chromatin regulation. *FEBS Letters*, *585*(13), 2016–23.

Aviel, S., Winberg, G., Massucci, M., & Ciechanover, A. (2000). Degradation of the epstein-barr virus latent membrane protein 1 (LMP1) by the ubiquitin-proteasome pathway. Targeting via ubiquitination of the N-terminal residue. *The Journal of Biological Chemistry*, *275*(31), 23491–9.

Bacia, K., Kim, S. A., & Schwille, P. (2006). Fluorescence cross-correlation spectroscopy in living cells. *Nature Methods*, *3*(2), 83–89.

Bacia, K., & Schwille, P. (2007). Practical guidelines for dual-color fluorescence cross-correlation spectroscopy. *Nature Protocols*, *2*(11), 2842–56.

Bagola, K., von Delbrück, M., Dittmar, G., Scheffner, M., Ziv, I., Glickman, M. H., Ciechanover, A., Sommer, T. (2013). Ubiquitin binding by a CUE domain regulates ubiquitin chain formation by ERAD E3 ligases. *Molecular Cell*, *50*(4), 528–39.

Bailly, V., Prakash, S., & Prakash, L. (1997). Domains required for dimerization of yeast Rad6 ubiquitin-conjugating enzyme and Rad18 DNA binding protein. *Molecular and Cellular Biology*, *17*(8), 4536–4543.

Bartel, P., Chien, C. T., Sternglanz, R., & Fields, S. (1993). *Elimination of false positives that arise in using the two-hybrid system. BioTechniques*, *14*, 920–924.

Bartke, T., Pohl, C., Pyrowolakis, G., & Jentsch, S. (2004). Dual role of BRUCE as an antiapoptotic IAP and a chimeric E2/E3 ubiquitin ligase. *Molecular Cell*, *14*(6), 801–811.

Bassermann, F., Eichner, R., & Pagano, M. (2014). The ubiquitin proteasome system - implications for cell cycle control and the targeted treatment of cancer. *Biochimica et Biophysica Acta*, *1843*(1), 150–62.

Beal, R., Deveraux, Q., Xia, G., Rechsteiner, M., & Pickart, C. (1996). Surface hydrophobic residues of multiubiquitin chains essential for proteolytic targeting. *Proceedings of the National Academy of Sciences*, *93*(2), 861–866.

Berggård, T., Linse, S., & James, P. (2007). Methods for the detection and analysis of protein-protein interactions. *Proteomics*, *7*(16), 2833–42.

Biederer, T., Volkwein, C., & Sommer, T. (1997). Role of Cue1p in ubiquitination and degradation at the ER surface. *Science*, *278*(5344), 1806–9.

Bilodeau, P. S., Winistorfer, S. C., Allaman, M. M., Surendhran, K., Kearney, W. R., Robertson, A. D., & Piper, R. C. (2004). The GAT domains of clathrin-associated GGA proteins have two ubiquitin binding motifs. *The Journal of Biological Chemistry*, *279*(52), 54808–16.

Blastyák, A., Pintér, L., Unk, I., Prakash, L., Prakash, S., & Haracska, L. (2007). Yeast Rad5 Protein Required for Postreplication Repair Has a DNA Helicase Activity Specific for Replication Fork Regression. *Molecular Cell*, *28*(1), 167–175.

Blondel, M., Bach, S., Bamps, S., Dobbelaere, J., Wiget, P., Longaretti, C., Barral, Y., Meijer, L., Peter, M. (2005). Degradation of Hof1 by SCF(Grr1) is important for actomyosin contraction during cytokinesis in yeast. *The EMBO Journal*, *24*(7), 1440–1452.

Boute, N., Jockers, R., & Issad, T. (2002). The use of resonance energy transfer in high-throughput screening: BRET versus FRET. *Trends in Pharmacological Sciences*, *23*(8), 351–4.

Boutet, S. C., Biressi, S., Iori, K., Natu, V., & Rando, T. A. (2010). Taf1 regulates Pax3 protein by monoubiquitination in skeletal muscle progenitors. *Molecular Cell*, *40*(5), 749–61.

Bracha-Drori, K., Shichrur, K., Katz, A., Oliva, M., Angelovici, R., Yalovsky, S., & Ohad, N. (2004). Detection of protein-protein interactions in plants using bimolecular fluorescence complementation. *The Plant Journal : For Cell and Molecular Biology*, *40*(3), 419–427.

Braun, B., Pfirrmann, T., Menssen, R., Hofmann, K., Scheel, H., & Wolf, D. H. (2011). Gid9, a second RING finger protein contributes to the ubiquitin ligase activity of the Gid complex required for catabolite degradation. *FEBS Letters*, *585*(24), 3856–61.

Breitschopf, K., Bengal, E., Ziv, T., Admon, A., & Ciechanover, A. (1998). A novel site for ubiquitination: the N-terminal residue, and not internal lysines of MyoD, is essential for conjugation and degradation of the protein. *The EMBO Journal*, *17*(20), 5964–73.

Bremm, A., Freund, S. M. V, & Komander, D. (2010). Lys11-linked ubiquitin chains adopt compact conformations and are preferentially hydrolyzed by the deubiquitinase Cezanne. *Nature Structural & Molecular Biology*, *17*(8), 939–47.

Brown, N. G., VanderLinden, R., Watson, E. R., Qiao, R., Grace, C. R. R., Yamaguchi, M., Weissmann, F., Frye, J.J., Dube, P., Ei Cho, S., Actis, M.L., Rodrigues, P., Fujii, N., Peters, J.M., Stark, H., Schulman, B. A. (2015). RING E3 mechanism for ubiquitin ligation to a disordered substrate visualized for human anaphase-promoting complex. *Proceedings of the National Academy of Sciences of the United States of America*, *112*(17), 5272–9.

Brzovic, P. S., Lissounov, A., Christensen, D. E., Hoyt, D. W., & Klevit, R. E. (2006). A UbcH5/ubiquitin noncovalent complex is required for processive BRCA1-directed ubiquitination. *Molecular Cell*, *21*(6), 873–80.

Brzovic, P. S., Rajagopal, P., Hoyt, D. W., King, M. C., & Klevit, R. E. (2001). Structure of a BRCA1-BARD1 heterodimeric RING-RING complex. *Nature Structural Biology*, *8*(10), 833–7.

Budhidarmo, R., Nakatani, Y., & Day, C. L. (2012). RINGs hold the key to ubiquitin transfer. *Trends in Biochemical Sciences*, *37*(2), 58–65.

Burroughs, A. M., Jaffee, M., Iyer, L. M., & Aravind, L. (2008). Anatomy of the E2 ligase fold: implications for enzymology and evolution of ubiquitin/Ub-like protein conjugation. *Journal of Structural Biology*, *162*(2), 205–218.

Cabantous, S., Terwilliger, T. C., & Waldo, G. S. (2005). Protein tagging and detection with engineered self-assembling fragments of green fluorescent protein. *Nature Biotechnology*, *23*(1), 102–107.

Cadwell, K., & Coscoy, L. (2005). Ubiquitination on nonlysine residues by a viral E3 ubiquitin ligase. *Science*, *309*(5731), 127–30.

Cadwell, K., & Coscoy, L. (2008). The specificities of Kaposi's sarcoma-associated herpesvirus-encoded E3 ubiquitin ligases are determined by the positions of lysine or cysteine residues within the intracytoplasmic domains of their targets. *Journal of Virology*, *82*(8), 4184–9.

Capili, A. D., Edghill, E. L., Wu, K., & Borden, K. L. B. (2004). Structure of the C-terminal RING finger from a RING-IBR-RING/TRIAD motif reveals a novel zinc-binding domain distinct from a RING. *Journal of Molecular Biology*, *340*(5), 1117–29.

Carvallo, L., Muñoz, R., Bustos, F., Escobedo, N., Carrasco, H., Olivares, G., & Larraín, J. (2010). Non-canonical Wnt signaling induces ubiquitination and degradation of Syndecan4. *The Journal of Biological Chemistry*, *285*(38), 29546–55.

Cascales, E., Atmakuri, K., Liu, Z., Binns, A. N., & Christie, P. J. (2005). Agrobacterium tumefaciens oncogenic suppressors inhibit T-DNA and VirE2 protein substrate binding to the VirD4 coupling protein. *Molecular Microbiology*, *58*(2), 565–579.

Cheng, T. H., Chang, C. R., Joy, P., Yablok, S., & Gartenberg, M. R. (2000). Controlling gene expression in yeast by inducible site-specific recombination. *Nucleic Acids Research*, *28*(24), E108.

Choi, K., Batke, S., Szakal, B., Lowther, J., Hao, F., Sarangi, P., Branzei, D., Urlich, H.D., Zhao, X. (2015). Concerted and differential actions of two enzymatic domains underlie Rad5 contributions to DNA damage tolerance. *Nucleic Acids Research*, *43*(5), 2666–2677.

Christensen, D. E., Brzovic, P. S., & Klevit, R. E. (2007). E2-BRCA1 RING interactions dictate synthesis of mono- or specific polyubiquitin chain linkages. *Nature Structural & Molecular Biology*, *14*(10), 941–948.

Christensen, D. E., & Klevit, R. E. (2009). Dynamic interactions of proteins in complex networks: identifying the complete set of interacting E2s for functional investigation of E3-dependent protein ubiquitination. *The FEBS Journal*, *276*(19), 5381–9.

Ciechanover, A. (2005). Proteolysis: from the lysosome to ubiquitin and the proteasome. *Nature Reviews. Molecular Cell Biology*, *6*(1), 79–87.

Ciechanover, A., & Ben-Saadon, R. (2004). N-terminal ubiquitination: More protein substrates join in. *Trends in Cell Biology*, *14*(3), 103-6.

Ciehanover, A., Hod, Y., & Hershko, A. (1978). A heat-stable polypeptide component of an ATP-dependent proteolytic system from reticulocytes. *Biochemical and Biophysical Research Communications*, *81*(4), 1100–1105.

Clague, M. J., Coulson, J. M., & Urbé, S. (2012). Cellular functions of the DUBs. *Journal of Cell Science*, *125*(Pt 2), 277–86.

Cole, K. C., McLaughlin, H. W., & Johnson, D. I. (2007). Use of bimolecular fluorescence complementation to study in vivo interactions between Cdc42p and Rdi1p of Saccharomyces cerevisiae. *Eukaryotic Cell*, *6*(3), 378–387.

Collins, B. M., Watson, P. J., & Owen, D. J. (2003). The Structure of the GGA1-GAT Domain Reveals the Molecular Basis for ARF Binding and Membrane Association of GGAs. *Developmental Cell*, *4*(3), 321–332.

Das, R., Mariano, J., Tsai, Y. C., Kalathur, R. C., Kostova, Z., Li, J., Tarasov, S. G., McFeeters, R.L., Altieri, A.S., Ji, X., Byrd, R.A., Weissman, A. M. (2009). Allosteric activation of E2-RING finger-mediated ubiquitylation by a structurally defined specific E2-binding region of gp78. *Molecular Cell*, *34*(6), 674–85.

Davies, B. A., Topp, J. D., Sfeir, A. J., Katzmann, D. J., Carney, D. S., Tall, G.G., Friedberg, A. S., Deng, L., Chen, Z., Horazdovsky, B. F. (2003). Vps9p CUE domain ubiquitin binding is required for efficient endocytic protein traffic. *The Journal of Biological Chemistry*, *278*(22), 19826–33.

Dawson, T. M., & Dawson, V. L. (2010). The role of parkin in familial and sporadic Parkinson's disease. *Movement Disorders, 25(1)*, S32–9.

Dell'Angelica, E. C. (2000). GGAs: A Family of ADP Ribosylation Factor-binding Proteins Related to Adaptors and Associated with the Golgi Complex. *The Journal of Cell Biology*, *149*(1), 81–94.

Deshaies, R. J., & Joazeiro, C. a P. (2009). RING domain E3 ubiquitin ligases. *Annual Review of Biochemistry*, *78*, 399–434.

Dikic, I., Wakatsuki, S., & Walters, K. J. (2009). Ubiquitin-binding domains - from structures to functions. *Nature Reviews: Molecular Cell Biology*, *10*(10), 659–671.

Donaldson, K. M., Yin, H., Gekakis, N., Supek, F., & Joazeiro, C. A. P. (2003). Ubiquitin Signals Protein Trafficking via Interaction with a Novel Ubiquitin Binding Domain in the Membrane Fusion Regulator, Vps9p. *Current Biology*, *13*(3), 258–262.

Duan, X., Trent, J. O., & Ye, H. (2009). Targeting the SUMO E2 conjugating enzyme Ubc9 interaction for anti-cancer drug design. *Anti-Cancer Agents in Medicinal Chemistry*, *9*(1), 51–4.

Dye, B. T., & Schulman, B. A. (2007). Structural mechanisms underlying posttranslational modification by ubiquitin-like proteins. *Annual Review of Biophysics and Biomolecular Structure*, *36*, 131–150.

Emter, R., Heese-Peck, A., & Kralli, A. (2002). ERG6 and PDR5 regulate small lipophilic drug accumulation in yeast cells via distinct mechanisms. *FEBS Letters*, *521*(1-3), 57–61.

Etlinger, J. D., & Goldberg, A. L. (1977). A soluble ATP-dependent proteolytic system responsible for the degradation of abnormal proteins in reticulocytes. *Proceedings of the National Academy of Sciences of the United States of America*, *74*(1), 54–8.

Fan, J. Y., Cui, Z. Q., Wei, H. P., Zhang, Z. P., Zhou, Y. F., Wang, Y. P., & Zhang, X. E. (2008). Split mCherry as a new red bimolecular fluorescence complementation system for visualizing protein-protein interactions in living cells. *Biochemical and Biophysical Research Communications*, *367*(1), 47–53.

Fang, D., & Kerppola, T. K. (2004). Ubiquitin-mediated fluorescence complementation reveals that Jun ubiquitinated by Itch/AIP4 is localized to lysosomes. *Proceedings of the National Academy of Sciences of the United States of America*, *101*(41), 14782–14787.

Fang, N. N., Ng, A. H. M., Measday, V., & Mayor, T. (2011). Hul5 HECT ubiquitin ligase plays a major role in the ubiquitylation and turnover of cytosolic misfolded proteins. *Nature Cell Biology*, *13*(11), 1344–52.

Fields, S., & Song, O. (1989). A novel genetic system to detect protein-protein interactions. *Nature*, *340*(6230), 245–246.

Finley, D. (2009). Recognition and processing of ubiquitin-protein conjugates by the proteasome. *Annual Review of Biochemistry*, *78*, 477–513.

Finley, D., Bartel, B., & Varshavsky, A. (1989). The tails of ubiquitin precursors are ribosomal proteins whose fusion to ubiquitin facilitates ribosome biogenesis. *Nature*, *338*(6214), 394–401.

Finley, D., Ciechanover, A., & Varshavsky, A. (1984). Thermolability of ubiquitin-activating enzyme from the mammalian cell cycle mutant ts85. *Cell*, *37*(1), 43–55.

Finley, D., Ozkaynak, E., & Varshavsky, A. (1987). The yeast polyubiquitin gene is essential for resistance to high temperatures, starvation, and other stresses. *Cell*, *48*(6), 1035–46.

Foo, Y. H., Naredi-Rainer, N., Lamb, D. C., Ahmed, S., & Wohland, T. (2012). Factors affecting the quantification of biomolecular interactions by fluorescence cross-correlation spectroscopy. *Biophysical Journal*, *102*(5), 1174–83.

Forsberg, H., Hammar, M., Andreasson, C., Moliner, A., & Ljungdahl, P. O. (2001). Suppressors of ssy1 and ptr3 null mutations define novel amino acid sensor-independent genes in *Saccharomyces cerevisiae*. *Genetics*, *158*(3), 973–988.

Förster, T. (1959). Transfer mechanisms of electronic excitation. *Discussions of the Faraday Society*, *27*, 7–17.

Galarneau, A., Primeau, M., Trudeau, L.-E., & Michnick, S. W. (2002). Beta-lactamase protein fragment complementation assays as in vivo and in vitro sensors of protein protein interactions. *Nature Biotechnology*, *20*(6), 619–22.

Gardner, R. G., Nelson, Z. W., & Gottschling, D. E. (2005). Degradation-mediated protein quality control in the nucleus. *Cell*, *120*(6), 803–15.

Geiler-Samerotte, K. A., Dion, M. F., Budnik, B. A., Wang, S. M., Hartl, D. L., & Drummond, D. A. (2011). Misfolded proteins impose a dosage-dependent fitness cost and trigger a cytosolic unfolded protein response in yeast. *Proceedings of the National Academy of Sciences of the United States of America*, *108*(2), 680–5.

Ghosh, I., Hamilton, A. D., & Regan, L. (2000). Antiparallel leucine zipper-directed protein reassembly: application to the green fluorescent protein. *Journal of the American Chemical Society*, *122*, 5658-5659.

Gietz, R. D., & Woods, R. A. (2006). Yeast transformation by the LiAc/SS Carrier DNA/PEG method. *Methods in Molecular Biology*, *313*, 107–20.

Goldstein, G. (1974). Isolation of bovine thymin: a polypeptide hormone of the thymus. *Nature*, *247*(5435), 11–4.

Goldstein, G., Scheid, M., Hammerling, U., Schlesinger, D. H., Niall, H. D., & Boyse, E. A. (1975). Isolation of a polypeptide that has lymphocyte-differentiating properties and is probably represented universally in living cells. *Proceedings of the National Academy of Sciences of the United States of America*, *72*(1), 11–5.

Granneman, J. G., Moore, H.-P. H., Granneman, R. L., Greenberg, A. S., Obin, M. S., & Zhu, Z. (2007). Analysis of lipolytic protein trafficking and interactions in adipocytes. *The Journal of Biological Chemistry*, *282*(8), 5726–5735.

Guerriero, C. J., & Brodsky, J. L. (2012). The delicate balance between secreted protein folding and endoplasmic reticulum-associated degradation in human physiology. *Physiological Reviews*, *92*(2), 537–76.

Güldener, U., Heck, S., Fielder, T., Beinhauer, J., & Hegemann, J. H. (1996). A new efficient gene disruption cassette for repeated use in budding yeast. *Nucleic Acids Research*, *24*(13), 2519–24.

Haas, A. L., & Rose, I. A. (1982). The mechanism of ubiquitin activating enzyme. A kinetic and equilibrium analysis. *The Journal of Biological Chemistry*, *257*(17), 10329–37.

Haglund, K., & Dikic, I. (2005). Ubiquitylation and cell signaling. *The EMBO Journal*, *24*(19), 3353–9.

Haglund, K., Sigismund, S., Polo, S., Szymkiewicz, I., Di Fiore, P. P., & Dikic, I. (2003). Multiple monoubiquitination of RTKs is sufficient for their endocytosis and degradation. *Nature Cell Biology*, *5*(5), 461–466.

Harry, van L. (2009). Methods, reagents and kits for luciferase assay. Published under the Patent Cooperation Treaty (PCT).

Heck, J. W., Cheung, S. K., & Hampton, R. Y. (2010). Cytoplasmic protein quality control degradation mediated by parallel actions of the E3 ubiquitin ligases Ubr1 and San1. *Proceedings of the National Academy of Sciences of the United States of America*, *107*(3), 1106–11.

Herr, R. A., Harris, J., Fang, S., Wang, X., & Hansen, T. H. (2009). Role of the RING-CH domain of viral ligase mK3 in ubiquitination of non-lysine and lysine MHC I residues. *Traffic (Copenhagen, Denmark)*, *10*(9), 1301–17.

Hershko, A., Ciechanover, A., Heller, H., Haas, A. L., & Rose, I. A. (1980). Proposed role of ATP in protein breakdown: conjugation of protein with multiple chains of the polypeptide of ATP-dependent proteolysis. *Proceedings of the National Academy of Sciences of the United States of America*, *77*(4), 1783–1786.

Hesselberth, J. R., Miller, J. P., Golob, A., Stajich, J. E., Michaud, G. A., & Fields, S. (2006). Comparative analysis of Saccharomyces cerevisiae WW domains and their interacting proteins. *Genome Biology*, *7*(4), 2666-77.

Hiatt, S. M., Shyu, Y. J., Duren, H. M., & Hu, C. D. (2008). Bimolecular fluorescence complementation (BiFC) analysis of protein interactions in Caenorhabditis elegans. *Methods*, *45*(3), 185–191.

Hibbert, R. G., Huang, A., Boelens, R., & Sixma, T. K. (2011). E3 ligase Rad18 promotes monoubiquitination rather than ubiquitin chain formation by E2 enzyme Rad6. *Proceedings of the National Academy of Sciences of the United States of America*, *108*(14), 5590–5.

Hicke, L. (2001). Protein regulation by monoubiquitin. *Nature Reviews. Molecular Cell Biology*, *2*(3), 195–201.

Hicke, L., & Riezman, H. (1996). Ubiquitination of a yeast plasma membrane receptor signals its ligand-stimulated endocytosis. *Cell*, *84*(2), 277–87.

Hicke, L., Schubert, H. L., & Hill, C. P. (2005). Ubiquitin-binding domains. *Nature Reviews. Molecular Cell Biology*, *6*(8), 610–21.

Hochstrasser, M. (1996). Protein degradation or regulation: Ub the judge. *Cell*, *84*(6), 813–5.

Hofmann, K., & Bucher, P. (1996). The UBA domain: a sequence motif present in multiple enzyme classes of the ubiquitination pathway. *Trends in Biochemical Sciences*, *21*(5), 172–173.

Hofmann, K., & Falquet, L. (2001). A ubiquitin-interacting motif conserved in components of the proteasomal and lysosomal protein degradation systems. *Trends in Biochemical Sciences*, *26*(6), 347–350.

Hospenthal, M. K., Mevissen, T. E. T., & Komander, D. (2015). Deubiquitinase-based analysis of ubiquitin chain architecture using Ubiquitin Chain Restriction (UbiCRest). *Nature Protocols*, *10*(2), 349–61.

Hough, R., Pratt, G., & Rechsteiner, M. (1986). Ubiquitin-lysozyme conjugates. Identification and characterization of an ATP-dependent protease from rabbit reticulocyte lysates. *The Journal of Biological Chemistry*, *261*(5), 2400–2408.

Hough, R., Pratt, G., & Rechsteiner, M. (1987). Purification of two high molecular weight proteases from rabbit reticulocyte lysate. *The Journal of Biological Chemistry*, *262*(17), 8303–13.

Howell, J. M., Winstone, T. L., Coorssen, J. R., & Turner, R. J. (2006). An evaluation of in vitro protein-protein interaction techniques: assessing contaminating background proteins. *Proteomics*, *6*(7), 2050–69.

Hu, C. D., Chinenov, Y., & Kerppola, T. K. (2002). Visualization of interactions among bZIP and Rel family proteins in living cells using bimolecular fluorescence complementation. *Molecular Cell*, *9*(4), 789–798.

Hu, C.-D., Chinenov, Y., & Kerppola, T. K. (2002). Visualization of interactions among bZIP and Rel family proteins in living cells using bimolecular fluorescence complementation. *Molecular Cell*, *9*(4), 789–798.

Hu, C.-D., & Kerppola, T. K. (2003). Simultaneous visualization of multiple protein interactions in living cells using multicolor fluorescence complementation analysis. *Nature Biotechnology*, *21*(5), 539–545.

Hu, M., Li, P., Song, L., Jeffrey, P. D., Chenova, T. A., Wilkinson, K. D., et al., Shi, Y. (2005). Structure and mechanisms of the proteasome-associated deubiquitinating enzyme USP14. *The EMBO Journal*, *24*(21), 3747–56.

Huang, D. T., Ayrault, O., Hunt, H. W., Taherbhoy, A. M., Duda, D. M., Scott, D. C., Borg, L.A., Neale, G., Murray, P.J., Roussel, M.F., Schulman, B. A. (2009). E2-RING expansion of the NEDD8 cascade confers specificity to cullin modification. *Molecular Cell*, *33*(4), 483–495.

Huang, L., Kinnucan, E., Wang, G., Beaudenon, S., Howley, P. M., Huibregtse, J. M., & Pavletich, N. P. (1999). Structure of an E6AP-UbcH7 complex: insights into ubiquitination by the E2-E3 enzyme cascade. *Science*, *286*(5443), 1321–6.

Hudry, B., Viala, S., Graba, Y., & Merabet, S. (2011). Visualization of protein interactions in living Drosophila embryos by the bimolecular fluorescence complementation assay. *BMC Biology*, *9*, 5.

Huibregtse, J. M., Scheffner, M., Beaudenon, S., & Howley, P. M. (1995). A family of proteins structurally and functionally related to the E6-AP ubiquitin-protein ligase. *Proceedings of the National Academy of Sciences of the United States of America*, *92*(7), 2563–7.

Hurley, J. H., Lee, S., & Prag, G. (2006). Ubiquitin-binding domains. *The Biochemical Journal*, *399*(3), 361–372.

Husnjak, K., & Dikic, I. (2012). Ubiquitin-Binding Proteins: decoders of ubiquitin-mediated cellular functions. *Annual Review of Biochemistry*, *81*, 291-322.

Hutchins, A. P., Liu, S., Diez, D., & Miranda-Saavedra, D. (2013). The repertoires of ubiquitinating and deubiquitinating enzymes in eukaryotic genomes. *Molecular Biology and Evolution*, *30*(5), 1172–87.

Hynes, T. R., Tang, L., Mervine, S. M., Sabo, J. L., Yost, E. A., Devreotes, P. N., & Berlot, C. H. (2004). Visualization of G protein betagamma dimers using bimolecular fluorescence complementation demonstrates roles for both beta and gamma in subcellular targeting. *The Journal of Biological Chemistry*, *279*(29), 30279–30286.

Ikeda, F., Crosetto, N., & Dikic, I. (2010). What determines the specificity and outcomes of ubiquitin signaling? *Cell*, *143*(5), 677–681.

Ikeda, F., & Dikic, I. (2008). Atypical ubiquitin chains: new molecular signals. 'Protein modifications: beyond the usual suspects' review series. *EMBO Reports*, *9*(6), 536–42.

Ikeda, M., Ikeda, A., & Longnecker, R. (2002). Lysine-Independent Ubiquitination of Epstein–Barr Virus LMP2A. *Virology*, *300*(1), 153–159.

Ito, T., Chiba, T., Ozawa, R., Yoshida, M., Hattori, M., & Sakaki, Y. (2001). A comprehensive two-hybrid analysis to explore the yeast protein interactome. *Proceedings of the National Academy of Sciences of the United States of America*, *98*(8), 4569–4574.

Iyer, L. M., Burroughs, A. M., & Aravind, L. (2008). Unraveling the biochemistry and provenance of pupylation: a prokaryotic analog of ubiquitination. *Biology Direct*, *3*, 45.

Jach, G., Pesch, M., Richter, K., Frings, S., & Uhrig, J. F. (2006). An improved mRFP1 adds red to bimolecular fluorescence complementation. *Nature Methods*, *3*(8), 597–600.

Janke, C., Magiera, M. M., Rathfelder, N., Taxis, C., Reber, S., Maekawa, H., Moreno-Borchart, A., Doenges, G., Schwob, E., Schiebel E., Knop, M. (2004). A versatile toolbox for PCR-based tagging of yeast genes: new fluorescent proteins, more markers and promoter substitution cassettes. *Yeast*, *21*(11), 947–62.

Jensen-Pergakes, K. L., Kennedy, M. A., Lees, N. D., Barbuch, R., Koegel, C., & Bard, M. (1998). Sequencing, disruption, and characterization of the Candida albicans sterol methyltransferase (ERG6) gene: drug susceptibility studies in erg6 mutants. *Antimicrobial Agents and Chemotherapy*, *42*(5), 1160–7.

Jentsch, S., McGrath, J. P., & Varshavsky, A. (1987). The yeast DNA repair gene RAD6 encodes a ubiquitin-conjugating enzyme. *Nature*, *329*(6135), 131–134.

Jin, J., Li, X., Gygi, S. P., & Harper, J. W. (2007). Dual E1 activation systems for ubiquitin differentially regulate E2 enzyme charging. *Nature*, *447*(7148), 1135–8.

Jin, L., Williamson, A., Banerjee, S., Philipp, I., & Rape, M. (2008). Mechanism of ubiquitin-chain formation by the human anaphase-promoting complex. *Cell*, *133*(4), 653–665.

Johnson, E. S., & Blobel, G. (1997). Ubc9p is the conjugating enzyme for the ubiquitin-like protein Smt3p. *The Journal of Biological Chemistry*, *272*(43), 26799–26802.

Johnsson, N., & Varshavsky, A. (1994). Split ubiquitin as a sensor of protein interactions in vivo. *Proceedings of the National Academy of Sciences*, *91*(22), 10340–10344.

Kaihara, A., Kawai, Y., Sato, M., Ozawa, T., & Umezawa, Y. (2003). Locating a Protein−Protein Interaction in Living Cells via Split Renilla Luciferase Complementation. *Analytical Chemistry*, *75*(16), 4176–4181.

Kaiser, S. E., Riley, B. E., Shaler, T. A., Trevino, R. S., Becker, C. H., Schulman, H., & Kopito, R. R. (2011). Protein standard absolute quantification (PSAQ) method for the measurement of cellular ubiquitin pools. *Nature Methods*, *8*(8), 691–6.

Kamadurai, H. B., Souphron, J., Scott, D. C., Duda, D. M., Miller, D. J., Stringer, D., Piper, R. C., Schulman, B. A. (2009). Insights into ubiquitin transfer cascades from a structure of a UbcH5B approximately ubiquitin-HECT(NEDD4L) complex. *Molecular Cell*, *36*(6), 1095–102.

Kayagaki, N., Phung, Q., Chan, S., Chaudhari, R., Quan, C., O'Rourke, K. M., Eby, M., Pietras, E., Cheng, G., Bazan, J.F., Zhang, Z., Arnott, D., Dixit, V. M. (2007). DUBA: a deubiquitinase that regulates type I interferon production. *Science*, *318*(5856), 1628–32.

Kee, Y., Lyon, N., & Huibregtse, J. M. (2005). The Rsp5 ubiquitin ligase is coupled to and antagonized by the Ubp2 deubiquitinating enzyme. *The EMBO Journal*, *24*(13), 2414–2424.

Kerppola, T. K. (2006). Design and implementation of bimolecular fluorescence complementation (BiFC) assays for the visualization of protein interactions in living cells. *Nature Protocols*, *1*(3), 1278–86.

Kerppola, T. K. (2008). Bimolecular fluorescence complementation (BiFC) analysis as a probe of protein interactions in living cells. *Annual Review of Biophysics*, *37*, 465–87.

Kerppola, T. K. (2013). Design of Fusion Proteins for Bimolecular Fluorescence Complementation (BiFC). *Cold Spring Harbor Protocols*, *2013*(8).

Khazak, V., Golemis, E. A., & Weber, L. (2005). Development of a yeast two-hybrid screen for selection of human Ras-Raf protein interaction inhibitors. *Methods in Molecular Biology* , *(310*, 253–271.

Kim, H. C., Steffen, A. M., Oldham, M. L., Chen, J., & Huibregtse, J. M. (2011). Structure and function of a HECT domain ubiquitin-binding site. *EMBO Reports*, *12*(4), 334–41.

Kim, H. T., Kim, K. P., Lledias, F., Kisselev, A. F., Scaglione, K. M., Skowyra, D., Gygi, S. P., Goldberg, A. L. (2007). Certain pairs of ubiquitin-conjugating enzymes (E2s) and ubiquitin-protein ligases (E3s) synthesize nondegradable forked ubiquitin chains containing all possible isopeptide linkages. *The Journal of Biological Chemistry*, *282*(24), 17375–17386.

Kim, S. B., Ozawa, T., Watanabe, S., & Umezawa, Y. (2004). High-throughput sensing and noninvasive imaging of protein nuclear transport by using reconstitution of split Renilla luciferase. *Proceedings of the National Academy of Sciences of the United States of America*, *101*(32), 11542–7.

Kinner, A., & Kölling, R. (2003). The yeast deubiquitinating enzyme Ubp16 is anchored to the outer mitochondrial membrane. *FEBS Letters*, *549*(1-3), 135–140.

Kirisako, T., Kamei, K., Murata, S., Kato, M., Fukumoto, H., Kanie, M., Sano, S., Tokunaga, F., Tanaka, K., Iwai, K. (2006). A ubiquitin ligase complex assembles linear polyubiquitin chains. *The EMBO Journal*, *25*(20), 4877–87.

Kirkpatrick, D. S., Hathaway, N. A., Hanna, J., Elsasser, S., Rush, J., Finley, D., King, R. W., Gygi, S. P. (2006). Quantitative analysis of in vitro ubiquitinated cyclin B1 reveals complex chain topology. *Nature Cell Biology*, *8*(7), 700–710.

Kitada, T., Asakawa, S., Hattori, N., Matsumine, H., Yamamura, Y., Minoshima, S., Yokochi, M., Mizuno, Y., Shimizu, N. (1998). Mutations in the parkin gene cause autosomal recessive juvenile parkinsonism. *Nature*. *392*(6676), 605-8.

Knop, M., Siegers, K., Pereira, G., Zachariae, W., Winsor, B., Nasmyth, K., & Schiebel, E. (1999). Epitope tagging of yeast genes using a PCR-based strategy: more tags and improved practical routines. *Yeast, 15*(10B), 963–72.

Kodama, Y., & Hu, C.-D. (2012). Bimolecular fluorescence complementation (BiFC): a 5-year update and future perspectives. *BioTechniques*, *53*(5), 285–98.

Koegl, M., Hoppe, T., Schlenker, S., Ulrich, H. D., Mayer, T. U., & Jentsch, S. (1999). A novel ubiquitination factor, E4, is involved in multiubiquitin chain assembly. *Cell*, *96*(5), 635–644.

Komander, D., Clague, M. J., & Urbé, S. (2009). Breaking the chains: structure and function of the deubiquitinases. *Nature Reviews. Molecular Cell Biology*, *10*(8), 550–63.

Komander, D., Lord, C. J., Scheel, H., Swift, S., Hofmann, K., Ashworth, A., & Barford, D. (2008). The structure of the CYLD USP domain explains its specificity for Lys63-linked polyubiquitin and reveals a B box module. *Molecular Cell*, *29*(4), 451–64.

Komander, D., & Rape, M. (2012). The ubiquitin code. *Annual Review of Biochemistry*, *81*, 203–29.

Kravtsova-Ivantsiv, Y., Cohen, S., & Ciechanover, A. (2009). Modification by Single Ubiquitin Moieties Rather Than Polyubiquitination Is Sufficient for Proteasomal Processing of the p105 NF-κB Precursor. *Molecular Cell*, *33*(4), 496–504.

Krieger, J. W., Singh, A. P., Garbe, C. S., Wohland, T., & Langowski, J. (2014). Dual-color fluorescence cross-correlation spectroscopy on a single plane illumination microscope (SPIM-FCCS). *Optics Express*, *22*(3), 2358–75.

Kulathu, Y., & Komander, D. (2012). Atypical ubiquitylation - the unexplored world of polyubiquitin beyond Lys48 and Lys63 linkages. *Nature Reviews. Molecular Cell Biology*, *13*(8), 508–23.

Lee, P. C. W., Sowa, M. E., Gygi, S. P., & Harper, J. W. (2011). Alternative ubiquitin activation/conjugation cascades interact with N-end rule ubiquitin ligases to control degradation of RGS proteins. *Molecular Cell*, *43*(3), 392–405.

Lee, S., Tsai, Y. C., Mattera, R., Smith, W. J., Kostelansky, M. S., Weissman, A. M., Bonifacio, J. S., Hurley, J. H. (2006). Structural basis for ubiquitin recognition and autoubiquitination by Rabex-5. *Nature Structural & Molecular Biology*, *13*(3), 264–71.

Lee, Y. R., Park, J.-H., Hahm, S.-H., Kang, L.-W., Chung, J. H., Nam, K.-H., Hwang, K.Y., Kwon I.C., Han, Y. S. (2010). Development of bimolecular fluorescence complementation using Dronpa for visualization of protein-protein interactions in cells. *Molecular Imaging and Biology* , *12*(5), 468–478.

Lenk, U., Yu, H., Walter, J., Gelman, M. S., Hartmann, E., Kopito, R. R., & Sommer, T. (2002). A role for mammalian Ubc6 homologues in ER-associated protein degradation. *Journal of Cell Science*, *115*, 3007–14.

Levy, E. D., Kowarzyk, J., & Michnick, S. W. (2014). High-resolution mapping of protein concentration reveals principles of proteome architecture and adaptation. *Cell Reports*, *7*(4), 1333–40.

Li, W., Bengtson, M. H., Ulbrich, A., Matsuda, A., Reddy, V. A., Orth, A., Chanda, S.K., Batalov, S., Joazeiro, C. A. P. (2008). Genome-wide and functional annotation of human E3 ubiquitin ligases identifies MULAN, a mitochondrial E3 that regulates the organelle's dynamics and signaling. *PLoS ONE*, *3*(1).

Li, W., Tu, D., Brunger, A. T., & Ye, Y. (2007). A ubiquitin ligase transfers preformed polyubiquitin chains from a conjugating enzyme to a substrate. *Nature*, *446*(7133), 333–7.

Li, W., Tu, D., Li, L., Wollert, T., Ghirlando, R., Brunger, A. T., & Ye, Y. (2009). Mechanistic insights into active site-associated polyubiquitination by the ubiquitin-conjugating enzyme Ube2g2. *Proceedings of the National Academy of Sciences of the United States of America*, *106*(10), 3722–7.

Liakopoulos, D., Doenges, G., Matuschewski, K., & Jentsch, S. (1998). A novel protein modification pathway related to the ubiquitin system. *The EMBO Journal*, *17*(8), 2208–14.

Lin, S.-C., Chung, J. Y., Lamothe, B., Rajashankar, K., Lu, M., Lo, Y.-C., Lam, A.Y., Darnay, B. G., Wu, H. (2008). Molecular basis for the unique deubiquitinating activity of the NF-kappaB inhibitor A20. *Journal of Molecular Biology*, *376*(2), 526–40.

Ljungdahl, P. O. (2009). Amino-acid-induced signalling via the SPS-sensing pathway in yeast. *Biochemical Society Transactions*, *37*(1), 242–7.

Longtine, M. S., McKenzie, A., Demarini, D. J., Shah, N. G., Wach, A., Brachat, A., Phillippsen, P., Pringle, J. R. (1998). Additional modules for versatile and economical PCR-based gene deletion and modification in Saccharomyces cerevisiae. *Yeast*, *14*(10), 953–61.

Lorick, K. L., Jensen, J. P., Fang, S., Ong, A. M., Hatakeyama, S., & Weissman, A. M. (1999). RING fingers mediate ubiquitin-conjugating enzyme (E2)-dependent ubiquitination. *Proceedings of the National Academy of Sciences of the United States of America*, *96*(20), 11364–9.

Lotz, K., Pyrowolakis, G., & Jentsch, S. (2004). BRUCE, a giant E2/E3 ubiquitin ligase and inhibitor of apoptosis protein of the trans-Golgi network, is required for normal placenta development and mouse survival. *Molecular and Cellular Biology*, *24*(21), 9339–50.

Luker, K. E., & Luker, G. D. (2014). Split Gaussia luciferase for imaging ligand-receptor binding. *Methods in Molecular Biology*, *1098*, 59–69.

Luker, K. E., Smith, M. C. P., Luker, G. D., Gammon, S. T., Piwnica-Worms, H., & Piwnica-Worms, D. (2004a). Kinetics of regulated protein-protein interactions revealed with firefly luciferase complementation imaging in cells and living animals. *Proceedings of the National Academy of Sciences of the United States of America*, *101*(33), 12288–93.

Luker, K. E., Smith, M. C. P., Luker, G. D., Gammon, S. T., Piwnica-Worms, H., & Piwnica-Worms, D. (2004b). Kinetics of regulated protein-protein interactions revealed with firefly luciferase complementation imaging in cells and living animals. *Proceedings of the National Academy of Sciences of the United States of America*, *101*(33), 12288–93.

Lund, P. K., Moats-Staats, B. M., Simmons, J. G., Hoyt, E., D'Ercole, A. J., Martin, F., & Van Wyk, J. J. (1985). Nucleotide sequence analysis of a cDNA encoding human ubiquitin reveals that ubiquitin is synthesized as a precursor. *Journal of Biological Chemistry, 260*(12), 7609–7613.

Ma, X., Foo, Y. H., & Wohland, T. (2014). Fluorescence cross-correlation spectroscopy (FCCS) in living cells. *Methods in Molecular Biology*, *1076*, 557–73.

Magliery, T. J., Wilson, C. G. M., Pan, W., Mishler, D., Ghosh, I., Hamilton, A. D., & Regan, L. (2005). Detecting protein-protein interactions with a green fluorescent protein fragment reassembly trap: scope and mechanism. *Journal of the American Chemical Society*, *127*(1), 146–157.

Markson, G., Kiel, C., Hyde, R., Brown, S., Charalabous, P., Bremm, A., Semple J, Woodsmith, J., Duley, S., Salehi-Ashtiani, K., Vidal, M., Komander, D.,Sanderson, C. M. (2009). Analysis of the human E2 ubiquitin conjugating enzyme protein interaction network. *Genome Research*, *19*(10), 1905–11.

Maspero, E., Mari, S., Valentini, E., Musacchio, A., Fish, A., Pasqualato, S., & Polo, S. (2011). Structure of the HECT:ubiquitin complex and its role in ubiquitin chain elongation. *EMBO Reports*, *12*(4), 342–9.

Mathias, N., Steussy, C. N., & Goebl, M. G. (1998). An essential domain within Cdc34p is required for binding to a complex containing Cdc4p and Cdc53p in Saccharomyces cerevisiae. *The Journal of Biological Chemistry*, *273*(7), 4040–4045.

Matsumoto, M. L., Wickliffe, K. E., Dong, K. C., Yu, C., Bosanac, I., Bustos, D., Bustos, D., Phu, L., Kirkpatrick, D. S., Hymowitz, S. G., Rape, M., Kelley, R. F., Dixit, V. M. (2010). K11-linked polyubiquitination in cell cycle control revealed by a K11 linkage-specific antibody. *Molecular Cell*, *39*(3), 477–84.

Matta-Camacho, E., Kozlov, G., Menade, M., & Gehring, K. (2012). Structure of the HECT C-lobe of the UBR5 E3 ubiquitin ligase. *Acta Crystallographica. Section F, Structural Biology and Crystallization Communications*, *68*(10), 1158–63.

Mattera, R., Tsai, Y. C., Weissman, A. M., & Bonifacino, J. S. (2006). The Rab5 guanine nucleotide exchange factor Rabex-5 binds ubiquitin (Ub) and functions as a Ub ligase through an atypical Ub-interacting motif and a zinc finger domain. *The Journal of Biological Chemistry*, *281*(10), 6874–83.

McKenna, S., Hu, J., Moraes, T., Xiao, W., Ellison, M. J., & Spyracopoulos, L. (2003). Energetics and specificity of interactions within Ub.Uev.Ubc13 human ubiquitin conjugation complexes. *Biochemistry*, *42*(26), 7922–30.

McNabb, D. S., Reed, R., & Marciniak, R. A. (2005). Dual luciferase assay system for rapid assessment of gene expression in Saccharomyces cerevisiae. *Eukaryotic Cell*, *4*(9), 1539–49.

Metzger, M. B., Liang, Y.-H., Das, R., Mariano, J., Li, S., Li, J., Kostova, Z., Byrd, R.A., Ji, X., Weissman, A. M. (2013). A structurally unique E2-binding domain activates ubiquitination by the ERAD E2, Ubc7p, through multiple mechanisms. *Molecular Cell*, *50*(4), 516–27.

Metzger, M. B., Pruneda, J. N., Klevit, R. E., & Weissman, A. M. (2013). RING-type E3 ligases: Master manipulators of E2 ubiquitin-conjugating enzymes and ubiquitination. *Biochimica et Biophysica Acta*, *1843*(1), 47-60.

Meyer, H. H., Wang, Y., & Warren, G. (2002). Direct binding of ubiquitin conjugates by the mammalian p97 adaptor complexes, p47 and Ufd1-Npl4. *The EMBO Journal*, *21*(21), 5645–52.

Meyer, H.-J., & Rape, M. (2014). Enhanced protein degradation by branched ubiquitin chains. *Cell*, *157*(4), 910-21.

Moldovan, G.-L., & D'Andrea, A. D. (2009). How the fanconi anemia pathway guards the genome. *Annual Review of Genetics*, *43*, 223–249.

Morell, M., Espargaró, A., Avilés, F. X., & Ventura, S. (2007). Detection of transient protein-protein interactions by bimolecular fluorescence complementation: the Abl-SH3 case. *Proteomics*, *7*(7), 1023–1036.

Morett, E., & Bork, P. (1999). A novel transactivation domain in parkin. *Trends in Biochemical Sciences*, *24*(6), 229–31.

Mueller, T. D., & Feigon, J. (2002). Solution structures of UBA domains reveal a conserved hydrophobic surface for protein-protein interactions. *Journal of Molecular Biology*, *319*(5), 1243–1255.

Nagai, T., Ibata, K., Park, E. S., Kubota, M., Mikoshiba, K., & Miyawaki, A. (2002). A variant of yellow fluorescent protein with fast and efficient maturation for cell-biological applications. *Nature Biotechnology*, *20*(1), 87–90.

Nakagawa, C., Inahata, K., Nishimura, S., & Sugimoto, K. (2011). Improvement of a Venus-based bimolecular fluorescence complementation assay to visualize bFos-bJun interaction in living cells. *Bioscience, Biotechnology, and Biochemistry*, *75*(7), 1399–401.

Nijman, S. M. B., Luna-Vargas, M. P. A., Velds, A., Brummelkamp, T. R., Dirac, A. M. G., Sixma, T. K., & Bernards, R. (2005). A genomic and functional inventory of deubiquitinating enzymes. *Cell*, *23*(5), 773-86.

Notenboom, V., Hibbert, R. G., van Rossum-Fikkert, S. E., Olsen, J. V, Mann, M., & Sixma, T. K. (2007). Functional characterization of Rad18 domains for Rad6, ubiquitin, DNA binding and PCNA modification. *Nucleic Acids Research*, *35*(17), 5819–30.

Nyfeler, B., Michnick, S. W., & Hauri, H.-P. (2005). Capturing protein interactions in the secretory pathway of living cells. *Proceedings of the National Academy of Sciences of the United States of America*, *102*(18), 6350–5.

Ogunjimi, A. A., Briant, D. J., Pece-Barbara, N., Le Roy, C., Di Guglielmo, G. M., Kavsak, P., Rasmussen, R. K., Seet, B.T., Sicheri, F., Wrana, J. L. (2005). Regulation of Smurf2 ubiquitin ligase activity by anchoring the E2 to the HECT domain. *Molecular Cell*, *19*(3), 297–308.

Ohashi, K., Kiuchi, T., Shoji, K., Sampei, K., & Mizuno, K. (2012). Visualization of cofilin-actin and Ras-Raf interactions by bimolecular fluorescence complementation assays using a new pair of split Venus fragments. *BioTechniques*, *52*(1), 45–50.

Olzmann, J. A., Kopito, R. R., & Christianson, J. C. (2013). The mammalian endoplasmic reticulum-associated degradation system. *Cold Spring Harbor Perspectives in Biology*, *5*(9).

Omnus, D. J., & Ljungdahl, P. O. (2014). Latency of transcription factor Stp1 depends on a modular regulatory motif that functions as cytoplasmic retention determinant and nuclear degron. *Molecular Biology of the Cell*, *25*(23), 3823–33.

Ozbabacan, S. E. A., Engin, H. B., Gursoy, A., & Keskin, O. (2011). Transient protein-protein interactions. *Protein Engineering, Design & Selection : PEDS*, *24*(9), 635–48.

Ozkaynak, E., Finley, D., Solomon, M. J., & Varshavsky, A. (1987). The yeast ubiquitin genes: a family of natural gene fusions. *The EMBO Journal*, *6*(5), 1429–39.

Padilla-Parra, S., Audugé, N., Coppey-Moisan, M., & Tramier, M. (2011). Dual-color fluorescence lifetime correlation spectroscopy to quantify protein-protein interactions in live cell. *Microscopy Research and Technique*, *74*(8), 788–93.

Pandya, R. K., Partridge, J. R., Love, K. R., Schwartz, T. U., & Ploegh, H. L. (2010). A structural element within the HUWE1 HECT domain modulates self-ubiquitination and substrate ubiquitination activities. *The Journal of Biological Chemistry*, *285*(8), 5664–73.

Parker, J. L., & Ulrich, H. D. (2009). Mechanistic analysis of PCNA poly-ubiquitylation by the ubiquitin protein ligases Rad18 and Rad5. *The EMBO Journal*, *28*(23), 3657–3666.

Parrish, J. R., Gulyas, K. D., & Finley, R. L. (2006). Yeast two-hybrid contributions to interactome mapping. *Current Opinion in Biotechnology*, *17*(4), 387–93.

Paulmurugan, R., & Gambhir, S. S. (2003). Monitoring protein-protein interactions using split synthetic renilla luciferase protein-fragment-assisted complementation. *Analytical Chemistry*, *75*(7), 1584–9.

Paulmurugan, R., Umezawa, Y., & Gambhir, S. S. (2002). Noninvasive imaging of protein-protein interactions in living subjects by using reporter protein complementation and reconstitution strategies. *Proceedings of the National Academy of Sciences of the United States of America*, *99*(24), 15608–13.

Pazos, M., Natale, P., Margolin, W., & Vicente, M. (2013). Interactions among the early Escherichia coli divisome proteins revealed by bimolecular fluorescence complementation. *Environmental Microbiology*, *15*(12), 3282-91.

Pearce, M. J., Mintseris, J., Ferreyra, J., Gygi, S. P., & Darwin, K. H. (2008). Ubiquitin-like protein involved in the proteasome pathway of *Mycobacterium tuberculosis*. *Science*, *322*(5904), 1104–1107.

Pelletier, J. N., Campbell-Valois, F.-X., & Michnick, S. W. (1998). Oligomerization domain-directed reassembly of active dihydrofolate reductase from rationally designed fragments. *Proceedings of the National Academy of Sciences*, *95*(21), 12141–12146.

Pelzer, C., & Groettrup, M. (2010). FAT10 : Activated by UBA6 and functioning in protein degradation. *Sub-Cellular Biochemistry*, *54*, 238–46.

Pelzer, C., Kassner, I., Matentzoglu, K., Singh, R. K., Wollscheid, H.-P., Scheffner, M., Schmidtke, G., Groettrup, M. (2007). UBE1L2, a novel E1 enzyme specific for ubiquitin. *The Journal of Biological Chemistry*, *282*(32), 23010–4.

Peng, J., Schwartz, D., Elias, J. E., Thoreen, C. C., Cheng, D., Marsischky, G., Roelofs, J., Finley, D., Gygi, S. P. (2003). A proteomics approach to understanding protein ubiquitination. *Nature Biotechnology*, *21*(8), 921–926.

Petroski, M. D. (2008). The ubiquitin system, disease, and drug discovery. *BMC Biochemistry*, *9*(1), S7.

Petroski, M. D., & Deshaies, R. J. (2005). Mechanism of lysine 48-linked ubiquitin-chain synthesis by the cullin-RING ubiquitin-ligase complex SCF-Cdc34. *Cell*, *123*(6), 1107–1120.

Petroski, M. D., Zhou, X., Dong, G., Daniel-Issakani, S., Payan, D. G., & Huang, J. (2007). Substrate modification with lysine 63-linked ubiquitin chains through the UBC13-UEV1A ubiquitin-conjugating enzyme. *The Journal of Biological Chemistry*, *282*(41), 29936–45.

Pfleger, K. D. G. (2009). Analysis of protein–protein interactions using Bioluminescence Resonance Energy Transfer. *Bioluminescence, Methods in Molecular Biology*, *574*(1), 173–183.

Pfleger, K. D. G., Seeber, R. M., & Eidne, K. A. (2006). Bioluminescence resonance energy transfer (BRET) for the real-time detection of protein-protein interactions. *Nature Protocols*, *1*(1), 337–345.

Phillip, Y., Kiss, V., & Schreiber, G. (2012). Protein-binding dynamics imaged in a living cell. *Proceedings of the National Academy of Sciences of the United States of America*, *109*(5), 1461–6.

Pickart, C. M., & Eddins, M. J. (2004). Ubiquitin: structures, functions, mechanisms. *Biochimica et Biophysica Acta*, *1695*(1-3), 55–72.

Pickart, C. M., & Fushman, D. (2004). Polyubiquitin chains: polymeric protein signals. *Current Opinion in Chemical Biology*, *8*(6), 610–616.

Piehler, J. (2005). New methodologies for measuring protein interactions in vivo and in vitro. *Current Opinion in Structural Biology*, *15*(1), 4–14.

Piehler, J. (2014). Spectroscopic techniques for monitoring protein interactions in living cells. *Current Opinion in Structural Biology*, *24*, 54–62.

Ponting, C. (2000). Proteins of the endoplasmic-reticulum-associated degradation pathway: domain detection and function prediction. *Biochemical Journal*, *351*, 527–535.

Ponting, C. P., Cai, Y. D., & Bork, P. (1997). The breast cancer gene product TSG101: a regulator of ubiquitination? *Journal of Molecular Medicine*, *75*(7), 467–9.

Pornillos, O., Alam, S. L., Rich, R. L., Myszka, D. G., Davis, D. R., & Sundquist, W. I. (2002). Structure and functional interactions of the Tsg101 UEV domain. *The EMBO Journal*, *21*(10), 2397–406.

Prag, G., Misra, S., Jones, E. A., Ghirlando, R., Davies, B. A., Horazdovsky, B. F., & Hurley, J. H. (2003). Mechanism of Ubiquitin Recognition by the CUE Domain of Vps9p. *Cell*, *113*(5), 609–620.

Prasher, D. C., Eckenrode, V. K., Ward, W. W., Prendergast, F. G., & Cormier, M. J. (1992). Primary structure of the Aequorea victoria green-fluorescent protein. *Gene*, *111*(2), 229–233.

Puertollano, R., & Bonifacino, J. S. (2004). Interactions of GGA3 with the ubiquitin sorting machinery. *Nature Cell Biology*, *6*(3), 244–51.

Raasi, S., Varadan, R., Fushman, D., & Pickart, C. M. (2005). Diverse polyubiquitin interaction properties of ubiquitin-associated domains. *Nature Structural & Molecular Biology*, *12*(8), 708–14.

Rao, H., & Sastry, A. (2002). Recognition of specific ubiquitin conjugates is important for the proteolytic functions of the ubiquitin-associated domain proteins Dsk2 and Rad23. *Journal of Biological Chemistry*, *277*(14), 11691–11695.

Ravid, T., & Hochstrasser, M. (2007). Autoregulation of an E2 enzyme by ubiquitin-chain assembly on its catalytic residue. *Nature Cell Biology*, *9*(4), 422–427.

Redman, K. L., & Rechsteiner, M. (1989). Identification of the long ubiquitin extension as ribosomal protein S27a. *Nature*, *338*(6214), 438–40.

Remy, I., & Michnick, S. W. (2004). Regulation of apoptosis by the Ft1 protein, a new modulator of protein kinase B/Akt. *Molecular and Cellular Biology*, *24*(4), 1493–1504.

Remy, I., & Michnick, S. W. (2006). A highly sensitive protein-protein interaction assay based on Gaussia luciferase. *Nature Methods*, *3*(12), 977–9.

Richardson, A., Gardner, R. G., & Prelich, G. (2013). Physical and genetic associations of the Irc20 ubiquitin ligase with Cdc48 and SUMO. *PloS One*, *8*(10), e76424.

Robzyk, K., Recht, J., & Osley, M. A. (2000). Rad6-dependent ubiquitination of histone H2B in yeast. *Science*, *287*(5452), 501–504.

Rodrigo-Brenni, M. C., & Morgan, D. O. (2007). Sequential E2s drive polyubiquitin chain assembly on APC targets. *Cell*, *130*(1), 127–139.

Rotin, D., Staub, O., & Haguenauer-Tsapis, R. (2000). Ubiquitination and endocytosis of plasma membrane proteins: role of Nedd4/Rsp5p family of ubiquitin-protein ligases. *The Journal of Membrane Biology*, *176*(1), 1–17.

Sadaie, W., Harada, Y., Matsuda, M., & Aoki, K. (2014). Quantitative in vivo fluorescence cross-correlation analyses highlight the importance of competitive effects in the regulation of protein-protein interactions. *Molecular and Cellular Biology*, *34*(17), 3272–90.

Sambrook, J., & Russell, D. W. (2001). *Molecular Cloning: A Laboratory Manual*. *Cold Spring Harbor Laboratory* (Vol. 3, p. 2344). Cold Spring Harbour Press.

Sato, Y., Fujita, H., Yoshikawa, A., Yamashita, M., Yamagata, A., Kaiser, S. E., Iwai, K., Fukai, S. (2011). Specific recognition of linear ubiquitin chains by the Npl4 zinc finger (NZF) domain of the

HOIL-1L subunit of the linear ubiquitin chain assembly complex. *Proceedings of the National Academy of Sciences of the United States of America*, *108*(51), 20520–5.

Scaglione, K. M., Basrur, V., Ashraf, N. S., Konen, J. R., Elenitoba-Johnson, K. S. J., Todi, S. V, & Paulson, H. L. (2013). The ubiquitin-conjugating enzyme (E2) Ube2w ubiquitinates the N terminus of substrates. *The Journal of Biological Chemistry*, *288*(26), 18784–8.

Schaefer, J. B., & Morgan, D. O. (2011). Protein-linked ubiquitin chain structure restricts activity of deubiquitinating enzymes. *The Journal of Biological Chemistry*, *286*(52), 45186–96.

Scheffner, M., & Kumar, S. (2014). Mammalian HECT ubiquitin-protein ligases: biological and pathophysiological aspects. *Biochimica et Biophysica Acta*, *1843*(1), 61–74.

Scheffner, M., Nuber, U., & Huibregtse, J. M. (1995). Protein ubiquitination involving an E1-E2-E3 enzyme ubiquitin thioester cascade. *Nature*, *373*(6509), 81–83.

Schlesinger, D. H., Goldstein, G., & Niall, H. D. (1975). The complete amino acid sequence of ubiquitin, an adenylate cyclase stimulating polypeptide probably universal in living cells. *Biochemistry*, *14*(10), 2214–8.

Schnell, J. D., & Hicke, L. (2003). Non-traditional functions of ubiquitin and ubiquitin-binding proteins. *Journal of Biological Chemistry*, *278*(38), 35857-60.

Schwarz, S. E., Matuschewski, K., Liakopoulos, D., Scheffner, M., & Jentsch, S. (1998). The ubiquitin-like proteins SMT3 and SUMO-1 are conjugated by the UBC9 E2 enzyme. *Proceedings of the National Academy of Sciences of the United States of America*, *95*(2), 560–564.

Schwille, P., Meyer-Almes, F. J., & Rigler, R. (1997). Dual-color fluorescence cross-correlation spectroscopy for multicomponent diffusional analysis in solution. *Biophysical Journal*, *72*(4), 1878–86.

Sekar, R. B., & Periasamy, A. (2003). Fluorescence resonance energy transfer (FRET) microscopy imaging of live cell protein localizations. *The Journal of Cell Biology*, *160*(5), 629–633.

Semple, J. I., Sanderson, C. M., & Campbell, R. D. (2002). The jury is out on “guilt by association” trials. *Briefings in Functional Genomics & Proteomics*, *1*(1), 40–52.

Serebriiskii, I., Estojak, J., Berman, M., & Golemis, E. A. (2000). Approaches to detecting false positives in yeast two-hybrid systems. *BioTechniques*, *28*(2), 328–330, 332–336.

Seufert, W., & Jentsch, S. (1990). Ubiquitin conjugating enzymes UBC4 and UBC5 mediate selective degradation of short-lived and abnormal proteins. *EMBO Journal*, *9*(2), 543–550.

Sheff, M. A., & Thorn, K. S. (2004). Optimized cassettes for fluorescent protein tagging in Saccharomyces cerevisiae. *Yeast*, *21*(8), 661–70.

Shekhtman, A., & Cowburn, D. (2002). A ubiquitin-interacting motif from Hrs binds to and occludes the ubiquitin surface necessary for polyubiquitination in monoubiquitinated proteins. *Biochemical and Biophysical Research Communications*, *296*(5), 1222–7.

Sheng, Y., Hong, J. H., Doherty, R., Srikumar, T., Shloush, J., Avvakumov, G. V., Walker, J.R., Xue, S., Neculai, D., Wan, J.W., Kim, S. K., Arrowsmith, C.H., Raught, B., Dhe-Paganon, S. (2012). A human ubiquitin conjugating enzyme (E2)-HECT E3 ligase structure-function screen. *Molecular & Cellular Proteomics , 11*(8), 329–41.

Sherf, B., Navarro, S., Hannah, R., & Wood, K. (1996). Dual-Luciferase® reporter assay: An advanced co-reporter technology integrating firefly and Renilla luciferase assays. *Promega Notes*, *57*, 2–8.

Shih, S. C., Prag, G., Francis, S. A., Sutanto, M. A., Hurley, J. H., & Hicke, L. (2003). A ubiquitin-binding motif required for intramolecular monoubiquitylation, the CUE domain. *EMBO Journal*, *22*(6), 1273–1281.

Shyu, Y. J., Liu, H., Deng, X., & Hu, C.-D. (2006). Identification of new fluorescent protein fragments for bimolecular fluorescence complementation analysis under physiological conditions. *BioTechniques*, *40*(1), 61–66.

Singh, A. P., Krieger, J., Pernus, A., Langowski, J., & Wohland, T. (2013). SPIM-FCCS: A novel technique to quantitate protein-protein interaction in live cells. *Biophysical Journal*, *104*(2), 61.

Sorkin, A., McClure, M., Huang, F., & Carter, R. (2000). Interaction of EGF receptor and Grb2 in living cells visualized by fluorescence resonance energy transfer (FRET) microscopy. *Current Biology*, *10*(21), 1395–1398.

Spratt, D. E., Walden, H., & Shaw, G. S. (2014). RBR E3 ubiquitin ligases: new structures, new insights, new questions. *The Biochemical Journal*, *458*(3), 421–37.

Stefan, E., Aquin, S., Berger, N., Landry, C. R., Nyfeler, B., Bouvier, M., & Michnick, S. W. (2007). Quantification of dynamic protein complexes using Renilla luciferase fragment complementation applied to protein kinase A activities in vivo. *Proceedings of the National Academy of Sciences of the United States of America*, *104*(43), 16916–21.

Suer, S., Misra, S., Saidi, L. F., & Hurley, J. H. (2003). Structure of the GAT domain of human GGA1: a syntaxin amino-terminal domain fold in an endosomal trafficking adaptor. *Proceedings of the National Academy of Sciences of the United States of America*, *100*(8), 4451–6.

Sung, M.-K., & Huh, W.-K. (2007). Bimolecular fluorescence complementation analysis system for in vivo detection of protein-protein interaction in Saccharomyces cerevisiae. *Yeast*, *24*(9), 767–775.

Sung, M.-K., Lim, G., Yi, D.-G., Chang, Y. J., Yang, E. Bin, Lee, K., & Huh, W.-K. (2013). Genome-wide bimolecular fluorescence complementation analysis of SUMO interactome in yeast. *Genome Research*, *23*(4), 736–46.

Thrower, J. S., Hoffman, L., Rechsteiner, M., & Pickart, C. M. (2000). Recognition of the polyubiquitin proteolytic signal. *The EMBO Journal*, *19*(1), 94–102.

Tokunaga, F., Sakata, S., Saeki, Y., Satomi, Y., Kirisako, T., Kamei, K., Nakagawa, T., Kato, M., Murata, S., Yamaoka, S., Yamamoto, M., Akira, S., Takao, T., Tanaka, K., Iwai, K. (2009). Involvement of linear polyubiquitylation of NEMO in NF-kappaB activation. *Nature Cell Biology*, *11*(2), 123–132.

Tong, A. H. Y., & Boone, C. (2006). Synthetic genetic array analysis in Saccharomyces cerevisiae. *Methods in Molecular Biology*, *313*, 171–92.

Tran, H., Hamada, F., Schwarz-Romond, T., & Bienz, M. (2008). Trabid, a new positive regulator of Wnt-induced transcription with preference for binding and cleaving K63-linked ubiquitin chains. *Genes & Development*, *22*(4), 528–42.

Turco, E., Gallego, L. D., Schneider, M., & Koehler, A. (2014). Monoubiquitination of histone H2B is intrinsic to the Bre1 RING - Rad6 interaction and augmented by a second Rad6 binding site on Bre1. *The Journal of Biological Chemistry*, *290*(9), 5298-310.

Uetz, P., Giot, L., Cagney, G., Mansfield, T. A., Judson, R. S., Knight, J. R., Lockshon, D., Narayan, V., Srinivasan, M., Pochart, P., Qureshi-Emili, A., Li, Y., Godwin, B., Conover, D., Kalbfleisch, T., Vijayadamodar, G., Yang, M., Johnston, M., Fields, S., Rothberg, J. M. (2000). A comprehensive analysis of protein-protein interactions in *Saccharomyces cerevisiae*. *Nature*, *403*(6770), 623–627.

Van der Reijden, B. A., Erpelinck-Verschueren, C. A., Löwenberg, B., & Jansen, J. H. (1999). TRIADs: a new class of proteins with a novel cysteine-rich signature. *Protein Science : A Publication of the Protein Society*, *8*(7), 1557–61.

Van Wijk, S. J. L., De Vries, S. J., Kemmeren, P., Huang, A., Boelens, R., Bonvin, A. M. J. J., & Timmers, H. T. M. (2009). A comprehensive framework of E2–RING E3 interactions of the human ubiquitin–proteasome system. *Molecular Systems Biology*, *5*(295), 295.

Van Wijk, S. J. L., Melquiond, A. S. J., de Vries, S. J., Timmers, H. T. M., & Bonvin, A. M. J. J. (2012). Dynamic control of selectivity in the ubiquitination pathway revealed by an ASP to GLU substitution in an intra-molecular salt-bridge network. *PLoS Computational Biology*, *8*(11).

Van Wijk, S. J. L., & Timmers, H. T. M. (2010). The family of ubiquitin-conjugating enzymes (E2s): deciding between life and death of proteins. *FASEB Journal : Official Publication of the Federation of American Societies for Experimental Biology*, *24*(4), 981–93.

VanDemark, A. P., & Hill, C. P. (2002). Structural basis of ubiquitylation. *Current Opinion in Structural Biology*, *12*(6), 822–830.

Varshavsky, A. (2006). The early history of the ubiquitin field. *Protein Science : A Publication of the Protein Society*, *15*(3), 647–654.

Verdecia, M. A., Joazeiro, C. A. P., Wells, N. J., Ferrer, J.-L., Bowman, M. E., Hunter, T., & Noel, J. P. (2003). Conformational flexibility underlies ubiquitin ligation mediated by the WWP1 HECT domain E3 ligase. *Molecular Cell*, *11*(1), 249–59.

Vidi, P.-A., & Watts, V. J. (2009). Fluorescent and bioluminescent protein-fragment complementation assays in the study of G protein-coupled receptor oligomerization and signaling. *Molecular Pharmacology*, *75*(4), 733–9.

Vijay-Kumar, S., Bugg, C. E., & Cook, W. J. (1987). Structure of ubiquitin refined at 1.8 A resolution. *Journal of Molecular Biology*, *194*(3), 531–44.

Walinda, E., Morimoto, D., Sugase, K., Konuma, T., Tochio, H., & Shirakawa, M. (2014). Solution Structure of the Ubiquitin-associated (UBA) Domain of Human Autophagy Receptor NBR1 and Its Interaction with Ubiquitin and Polyubiquitin. *The Journal of Biological Chemistry*, *289*(20), 13890–902.

Walter, M., Chaban, C., Schütze, K., Batistic, O., Weckermann, K., Näke, C., Blazevic, D., Grefen, C., Schumacher, K., Oecking, C., Harter, K., Kudla, J. (2004). Visualization of protein interactions in living plant cells using bimolecular fluorescence complementation. *The Plant Journal: For Cell and Molecular Biology*, *40*(3), 428–438.

Wang, M., & Pickart, C. M. (2005). Different HECT domain ubiquitin ligases employ distinct mechanisms of polyubiquitin chain synthesis. *The EMBO Journal*, *24*(24), 4324–33.

Wang, T., Yin, L., Cooper, E. M., Lai, M.-Y., Dickey, S., Pickart, C. M., Fushman, D., Wilkinson, K. D., Cohen, R. E., Wolberger, C. (2009). Evidence for bidentate substrate binding as the basis for the K48 linkage specificity of otubain 1. *Journal of Molecular Biology*, *386*(4), 1011–23.

Wang, X., Herr, R. A., Chua, W.-J., Lybarger, L., Wiertz, E. J. H. J., & Hansen, T. H. (2007). Ubiquitination of serine, threonine, or lysine residues on the cytoplasmic tail can induce ERAD of MHC-I by viral E3 ligase mK3. *The Journal of Cell Biology*, *177*(4), 613–624.

Wehrman, T., Kleaveland, B., Her, J.-H., Balint, R. F., & Blau, H. M. (2002). Protein-protein interactions monitored in mammalian cells via complementation of beta -lactamase enzyme fragments. *Proceedings of the National Academy of Sciences of the United States of America*, *99*(6), 3469–74.

Weissman, A. M. (2001). Themes and variations on ubiquitylation. *Nature Reviews. Molecular Cell Biology*, *2*(3), 169–78.

Weissman, C. A. P. J. and A. M. (2000). RING Finger Proteins: Mediators of Ubiquitin Ligase Activity. *Cell*, *102*, 549–552.

Welcsh, P. L., & King, M. C. (2001). BRCA1 and BRCA2 and the genetics of breast and ovarian cancer. *Human Molecular Genetics*, *10*(7), 705–713.

Wenzel, D. M., Lissounov, A., Brzovic, P. S., & Klevit, R. E. (2011). UBCH7 reactivity profile reveals parkin and HHARI to be RING/HECT hybrids. *Nature*, *474*(7349), 105–8.

Wenzel, D. M., Stoll, K. E., & Klevit, R. E. (2011). E2s: structurally economical and functionally replete. *The Biochemical Journal*, *433*(1), 31–42.

Wertz, I. E., O'Rourke, K. M., Zhou, H., Eby, M., Aravind, L., Seshagiri, S., Wu, P., Wiesmann, C., Baker, R., Boone, D. L., Ma, A., Koonin, E.V., Dixit, V. M. (2004). De-ubiquitination and ubiquitin ligase domains of A20 downregulate NF-kappaB signalling. *Nature*, *430*(7000), 694–699.

Wickliffe, K. E., Lorenz, S., Wemmer, D. E., Kuriyan, J., & Rape, M. (2011). The mechanism of linkage-specific ubiquitin chain elongation by a single-subunit E2. *Cell*, *144*(5), 769–781.

Wilkinson, K. D., Urban, M. K., & Haas, A. L. (1980). Ubiquitin is the ATP-dependent proteolysis factor I of rabbit reticulocytes. *The Journal of Biological Chemistry*, *255*(16), 7529–7532.

Williams, C., van den Berg, M., Sprenger, R. R., & Distel, B. (2007). A conserved cysteine is essential for Pex4p-dependent ubiquitination of the peroxisomal import receptor Pex5p. *The Journal of Biological Chemistry*, *282*(31), 22534–43.

Winborn, B. J., Travis, S. M., Todi, S. V, Scaglione, K. M., Xu, P., Williams, A. J., Cohen, R. E., Peng, J., Paulson, H. L. (2008). The deubiquitinating enzyme ataxin-3, a polyglutamine disease protein, edits Lys63 linkages in mixed linkage ubiquitin chains. *The Journal of Biological Chemistry*, *283*(39), 26436–43.

Winkler, G. S., Albert, T. K., Dominguez, C., Legtenberg, Y. I. A., Boelens, R., & Timmers, H. T. M. (2004). An altered-specificity ubiquitin-conjugating enzyme/ubiquitin-protein ligase pair. *Journal of Molecular Biology*, *337*(1), 157–165.

Wu, T., Merbl, Y., Huo, Y., Gallop, J. L., Tzur, A., & Kirschner, M. W. (2010). UBE2S drives elongation of K11-linked ubiquitin chains by the anaphase-promoting complex. *Proceedings of the National Academy of Sciences of the United States of America*, *107*(4), 1355–60.

Wu-Baer, F., Lagrazon, K., Yuan, W., & Baer, R. (2003). The BRCA1/BARD1 heterodimer assembles polyubiquitin chains through an unconventional linkage involving lysine residue K6 of ubiquitin. *The Journal of Biological Chemistry*, *278*(37), 34743–34746.

Xie, Y., & Varshavsky, A. (1999). The E2-E3 interaction in the N-end rule pathway: the RING-H2 finger of E3 is required for the synthesis of multiubiquitin chain. *The The European Molecular Biology Organization Journal*, *18*(23), 6832–6844.

Xu, P., Duong, D. M., Seyfried, N. T., Cheng, D., Xie, Y., Robert, J., Rush, J., Hochstrasser, M., Finley, D., Peng, J. (2009). Quantitative proteomics reveals the function of unconventional ubiquitin chains in proteasomal degradation. *Cell*, *137*(1), 133–145.

Xu, Y., Piston, D. W., & Johnson, C. H. (1999). A bioluminescence resonance energy transfer (BRET) system: application to interacting circadian clock proteins. *Proceedings of the National Academy of Sciences of the United States of America*, *96*(1), 151–156.

Yang, M., Ellenberg, J., Bonifacino, J. S., & Weissman, A. M. (1997). The Transmembrane Domain of a Carboxyl-terminal Anchored Protein Determines Localization to the Endoplasmic Reticulum. *Journal of Biological Chemistry*, *272*(3), 1970–1975.

Ye, Y., Blaser, G., Horrocks, M. H., Ruedas-Rama, M. J., Ibrahim, S., Zhukov, A. A., Orte, A., Klenerman, D., Jackson, S.E., Komander, D. (2012). Ubiquitin chain conformation regulates recognition and activity of interacting proteins. *Nature*, *492*(7428), 266–70.

Ye, Y., & Rape, M. (2009). Building ubiquitin chains: E2 enzymes at work. *Nature Reviews. Molecular Cell Biology*, *10*(11), 755–64.

Yewdell, J. W. (2001). Not such a dismal science: the economics of protein synthesis, folding, degradation and antigen processing. *Trends in Cell Biology*, *11*(7), 294–7.

Zargari, A., Boban, M., Heessen, S., Andréasson, C., Thyberg, J., & Ljungdahl, P. O. (2007). Inner nuclear membrane proteins Asi1, Asi2, and Asi3 function in concert to maintain the latent properties of transcription factors Stp1 and Stp2. *The Journal of Biological Chemistry*, *282*(1), 594–605.

Zattas, D., & Hochstrasser, M. (2014). Ubiquitin-dependent protein degradation at the yeast endoplasmic reticulum and nuclear envelope. *Critical Reviews in Biochemistry and Molecular Biology*, 1–17.

Zhang, Y., Pohlmann, E. L., & Roberts, G. P. (2009). Effect of perturbation of ATP level on the activity and regulation of nitrogenase in Rhodospirillum rubrum. *Journal of Bacteriology*, *191*(17), 5526–37.

Zhao, H., Doyle, T. C., Wong, R. J., Cao, Y., Stevenson, D. K., Piwnica-Worms, D., & Contag, C. H. (2004). Characterization of coelenterazine analogs for measurements of Renilla luciferase activity in live cells and living animals. *Molecular Imaging*, *3*(1), 43–54.

Zheng, N., Wang, P., Jeffrey, P. D., & Pavletich, N. P. (2000). Structure of a c-Cbl-UbcH7 complex: RING domain function in ubiquitin-protein ligases. *Cell*, *102*(4), 533–9.

Zhou, W., Zhu, P., Wang, J., Pascual, G., Ohgi, K. A., Lozach, J., Glass, C.K., Rosenfeld, M. G. (2008). Histone H2A monoubiquitination represses transcription by inhibiting RNA polymerase II transcriptional elongation. *Molecular Cell*, *29*(1), 69–80.

8 PUBLICATION

LETTER

doi:10.1038/nature14096

Protein quality control at the inner nuclear membrane

Anton Khmelinskii[1]*, Ewa Blaszczak[2,3]*, Marina Pantazopoulou[4], Bernd Fischer[5,6], Deike J. Omnus[4], Gaëlle Le Dez[2,3], Audrey Brossard[2,3], Alexander Gunnarsson[4], Joseph D. Barry[5], Matthias Meurer[1], Daniel Kirrmaier[1], Charles Boone[7], Wolfgang Huber[5], Gwenaël Rabut[2,3], Per O. Ljungdahl[4] & Michael Knop[1,8]

The nuclear envelope is a double membrane that separates the nucleus from the cytoplasm. The inner nuclear membrane (INM) functions in essential nuclear processes including chromatin organization and regulation of gene expression[1]. The outer nuclear membrane is continuous with the endoplasmic reticulum and is the site of membrane protein synthesis. Protein homeostasis in this compartment is ensured by endoplasmic-reticulum-associated protein degradation (ERAD) pathways that in yeast involve the integral membrane E3 ubiquitin ligases Hrd1 and Doa10 operating with the E2 ubiquitin-conjugating enzymes Ubc6 and Ubc7 (refs 2, 3). However, little is known about protein quality control at the INM. Here we describe a protein degradation pathway at the INM in yeast (*Saccharomyces cerevisiae*) mediated by the Asi complex consisting of the RING domain proteins Asi1 and Asi3 (ref. 4). We report that the Asi complex functions together with the ubiquitin-conjugating enzymes Ubc6 and Ubc7 to degrade soluble and integral membrane proteins. Genetic evidence suggests that the Asi ubiquitin ligase defines a pathway distinct from, but complementary to, ERAD. Using unbiased screening with a novel genome-wide yeast library based on a tandem fluorescent protein timer[5], we identify more than 50 substrates of the Asi, Hrd1 and Doa10 E3 ubiquitin ligases. We show that the Asi ubiquitin ligase is involved in degradation of mislocalized integral membrane proteins, thus acting to maintain and safeguard the identity of the INM.

To identify components of INM quality control, we focused on the ubiquitin-conjugating enzyme Ubc6. Ubc6 is an integral membrane protein that localizes to the endoplasmic reticulum and the INM where it targets for degradation soluble and integral membrane proteins together with Ubc7 and Doa10 (refs 6, 7). We established a microscopy-based bimolecular fluorescence complementation (BiFC) assay[8] to screen for new E3 ubiquitin ligases interacting with Ubc6 (Fig. 1a). In total, 10 out of 54 known or putative E3s, including Doa10, interacted with Ubc6 at distinct subcellular locations (Fig. 1b and Extended Data Fig. 1a). Among these, Asi1 and Asi3 displayed a BiFC signal restricted to the nuclear rim (Fig. 1b). Despite their colocalization at the endoplasmic reticulum, no interaction was detected between Ubc6 and Hrd1 (Extended Data Fig. 1a), suggesting a low rate of false-positive interactions in our BiFC assay.

Asi1 and Asi3 are integral membrane RING domain proteins of the INM and form the Asi complex[4,9,10]. Together with the INM protein Asi2, the Asi complex functions in the Ssy1-Ptr3-Ssy5 (SPS) amino-acid-sensing pathway, where it is involved in the degradation of Stp1 and Stp2 transcription factors[11]. We tested the interactions of Asi1 and Asi3 with all E2 ubiquitin-conjugating enzymes using the BiFC assay. In addition to Ubc6, Asi1 and Asi3 interacted with Ubc7 and weakly with Ubc4 (Extended Data Fig. 1b–d). We validated these interactions in microscale thermophoresis experiments[12] with recombinant proteins (Fig. 1c and Extended Data Fig. 1e). The Ubc7-binding region of Cue1 ($Cue1^{U7BR}$)[13], a protein that tethers Ubc7 to the endoplasmic reticulum membrane[14], was included in the assays. A carboxy-terminal fragment of Hrd1 ($Hrd1^{CT}$) expected to interact with Ubc7 but not Ubc6 served as control[2,3]. The RING domains of Asi1 and Asi3 ($Asi1^{RING}$ and $Asi3^{RING}$) interacted with Ubc7, provided it was bound to $Cue1^{U7BR}$, with affinities similar to $Hrd1^{CT}$. $Asi1^{RING}$ and $Asi3^{RING}$, but not $Hrd1^{CT}$, also interacted weakly with Ubc6 lacking its transmembrane domain ($Ubc6^{\Delta TM}$) (Fig. 1c).

The Asi proteins maintain the SPS pathway in the 'off state' in the absence of inducing amino acids, and do so by targeting for proteasomal degradation the low levels of Stp1 and Stp2 that inadvertently mislocalize into the nucleus[11]. Consequently, *asi* mutants exhibit aberrant constitutive Stp1/Stp2-dependent transcription[9]. We observed that *ubc7*Δ and, to a lesser extent, *ubc6*Δ mutants exhibited increased expression of Stp1/Stp2-regulated genes similar to the *asi1*Δ and *asi3*Δ mutants (Fig. 1d and Extended Data Fig. 1f). These effects were not due to inactivation of Hrd1 or Doa10 ubiquitin ligases (Extended Data Fig. 1f), thus implicating Ubc6 and Ubc7 in the SPS pathway.

Next, we assayed the ubiquitylation of an artificial Asi substrate based on the first 45 amino acids of Stp2 ($Stp2^{N}$). This fragment of Stp2 contains a degron that is recognized by the Asi complex[11]. Ubiquitylation of $Stp2^{N}$ fused to the tandem affinity purification (TAP) tag was reduced in *ubc6*Δ and severely impaired in *asi3*Δ and *ubc7*Δ mutants (Fig. 1e). In addition, ubiquitylation of Stp1 and Stp2 mutants with constitutive SPS-independent nuclear localization was impaired in *asi1*Δ and *asi3*Δ strains (Extended Data Fig. 1g). Together, these results establish the Asi complex as an E3 ubiquitin ligase of the INM that functions with Ubc6 and Ubc7.

Functionally related genes can be identified by similarity of genetic interaction profiles[15]. We searched for novel functions of the Asi ubiquitin ligase by mining a genome-scale genetic interaction map[16]. In this data set, the fitness of 5.4 million double-mutant combinations was measured by colony size, generating genetic interaction profiles for ~75% of all *S. cerevisiae* genes. We calculated correlation coefficients between genetic interaction profiles of *ASI* genes and the other 4,458 genes in the genetic interaction map. In this analysis, the genetic interaction profiles of *ASI* genes correlated with each other and, to a similar extent, with *HRD1*, *DOA10*, *UBC6*, *UBC7* and *CUE1* among others (Fig. 2a and Supplementary Table 1), suggesting that Asi and ERAD E3 ubiquitin ligases are functionally related. We sought to determine whether they work in the same or parallel pathways. Strains lacking *HRD1* and

[1]Zentrum für Molekulare Biologie der Universität Heidelberg (ZMBH), DKFZ-ZMBH Alliance, Im Neuenheimer Feld 282, 69120 Heidelberg, Germany. [2]Centre National de la Recherche Scientifique, UMR 6290, 35000 Rennes, France. [3]Institut de Génétique et Développement de Rennes, Université de Rennes 1, 35000 Rennes, France. [4]Department of Molecular Biosciences, The Wenner-Gren Institute, Stockholm University, Svante Arrhenius väg 20B, SE-106 91 Stockholm, Sweden. [5]Genome Biology Unit, European Molecular Biology Laboratory (EMBL), Meyerhofstraße 1, 69117 Heidelberg, Germany. [6]Computational Genome Biology, German Cancer Research Center (DKFZ), Im Neuenheimer Feld 580, 69120 Heidelberg, Germany. [7]Department of Molecular Genetics, Donnelly Centre for Cellular and Biomolecular Research, University of Toronto, 160 College St, Toronto, Ontario M5S 3E1, Canada. [8]Cell Morphogenesis and Signal Transduction, German Cancer Research Center (DKFZ), Im Neuenheimer Feld 280, 69120 Heidelberg, Germany.
*These authors contributed equally to this work.

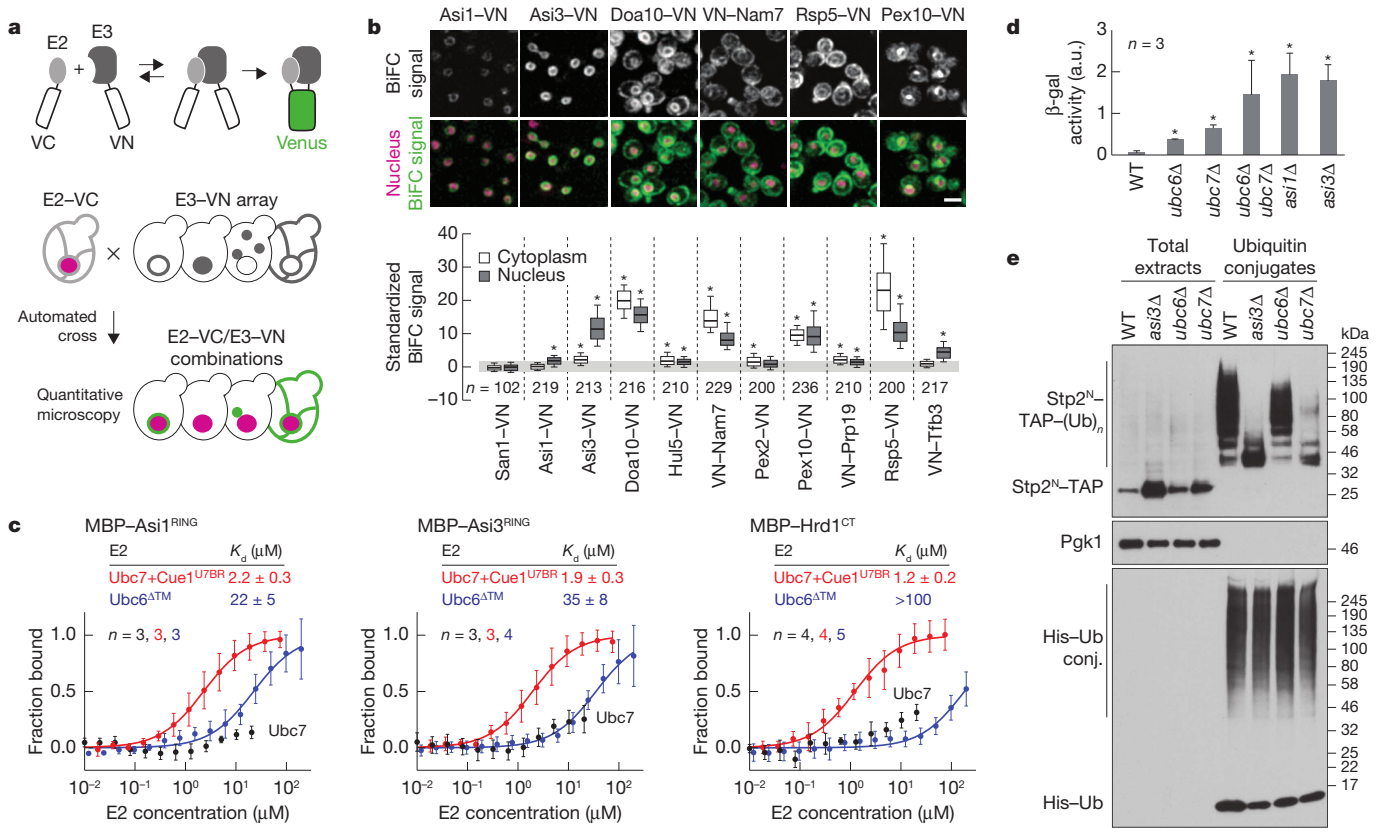

Figure 1 | The Asi complex is a Ubc6/Ubc7-dependent E3 ubiquitin ligase of the INM. **a**, BiFC strategy used to assay E2–E3 interactions. E2 and E3 proteins were endogenously tagged with carboxy- and amino-terminal fragments of the Venus fluorescent protein (VC and VN, respectively). Interactions between E2 and E3 proteins enable reconstitution of functional Venus that is detected with fluorescence microscopy. Rpn7 fused to the red fluorescent protein tDimer2 served as a nuclear marker. **b**, Quantification of BiFC signals in cells co-expressing VC–Ubc6 and VN-tagged E3s. Fluorescence microscopy examples representative of six fields of view (top). Scale bar, 5 μm. BiFC signals were measured in the cytoplasm and nucleus of individual cells (bottom, *n* as shown). Whiskers extend from the tenth to ninetieth percentiles. **c**, Microscale thermophoresis analysis of interactions between recombinant maltose binding protein (MBP)–E3 fragments and the indicated E2s. Plots show the fraction of MBP–E3 bound to the E2 at each tested E2 concentration (mean ± s.d., *n* as shown). Dissociation constants (K_d, mean ± s.d.) were derived from nonlinear fits with the law of mass action (solid lines). **d**, Activity of β-galactosidase (β-gal) expressed from the *AGP1* promoter in the indicated strains (mean ± s.d., $n = 3$ clones). a.u., arbitrary units; WT, wild type. **e**, Ubiquitylation of Stp2^N–TAP in strains expressing 10×histidine (His)-tagged ubiquitin. Total cell extracts and ubiquitin conjugates eluted after immobilized-metal affinity chromatography were separated by SDS–PAGE followed by immunoblotting with antibodies against the TAP tag, Pgk1 and ubiquitin. Representative immunoblots from three technical replicates. $^*P < 10^{-4}$ (**b**; one-way analysis of variance (ANOVA) with Bonferroni correction for multiple testing) and $^*P < 0.05$ (**d**; two-tailed *t*-test).

the unfolded protein response genes *IRE1* or *HAC1* show impaired growth at increased temperature[17]. Additional deletion of *ASI1* resulted in a synthetic lethal phenotype under these conditions[18] (Fig. 2b and Extended Data Fig. 2), suggesting that Asi1 and Hrd1 function in parallel pathways.

We used a tandem fluorescent protein timer (tFT) approach[5] to perform unbiased proteome-wide screens for substrates of the Asi, Hrd1 and Doa10 ubiquitin ligases. A tFT is a tag composed of two fluorescent proteins (mCherry and superfolder green fluorescent protein (sfGFP)) with distinct fluorophore maturation rates. The mCherry/sfGFP intensity ratio is a measure of protein degradation kinetics in steady state (Fig. 3a), with a dynamic range and sensitivity that exceed conventional cycloheximide chase experiments[5] (Supplementary Note 1). We constructed a genome-wide library of yeast strains each expressing a different tFT-tagged protein (Supplementary Methods). Library construction relied on a seamless tagging strategy that minimizes the influence of the tag on gene expression[19] (Extended Data Fig. 3a). In total, 4,044 proteins were successfully tagged to create a tFT library covering ~73% of verified or uncharacterized open reading frames in the *S. cerevisiae* genome (Supplementary Table 2). We introduced *asi1*Δ, *asi3*Δ, *hrd1*Δ, *doa10*Δ, *ubc6*Δ and *ubc7*Δ deletion alleles into the tFT library using high-throughput genetic crosses[20]. The effect of each gene deletion on the stability of each protein in the library was examined with high-throughput fluorescence measurements of colonies[5] (Extended Data Fig. 3b) and quantified as a *z*-score. More proteins were stabilized (positive *z*-score) than destabilized in the six mutants (Extended Data Fig. 3c and Supplementary Table 3), in agreement with the role of Asi, Hrd1 and Doa10 ubiquitin ligases in protein degradation. Hierarchical clustering of top hits recapitulated known E2–E3 interactions and revealed three clusters of 20, 30 and 9 potential substrates for the Asi, Hrd1 and Doa10 ubiquitin ligases, respectively (Fig. 3b). Hrd1 substrates, including the known substrate Der1 (ref. 21), were stabilized only in the *ubc7*Δ mutant, whereas Doa10 substrates were stabilized in both *ubc6*Δ and *ubc7*Δ mutants. Most Asi substrates, including the recently identified Erg11 (ref. 18), were stabilized in the *ubc7*Δ mutant with only weak effects of the *ubc6*Δ mutant (Fig. 3b). Stp1 and Stp2 were not identified as Asi substrates in the screen, probably the consequence of their efficient targeting for degradation by the E3 ubiquitin ligase SCF^{Grr1} in the cytoplasm[11]. The vast majority of potential substrates in each set were integral membrane or secretory proteins distributed along the endomembrane system and the Hrd1 and Asi substrates were enriched in endoplasmic reticulum and vacuolar proteins (Fig. 3c, d and Extended Data Fig. 3d, e). These findings are consistent with the organization and functions of endoplasmic-reticulum-associated ubiquitin ligases, thus establishing the tFT library as a valuable resource for studies of protein degradation (Supplementary Note 2), and indicate that the Asi complex is involved in degradation of a distinct set of integral membrane proteins.

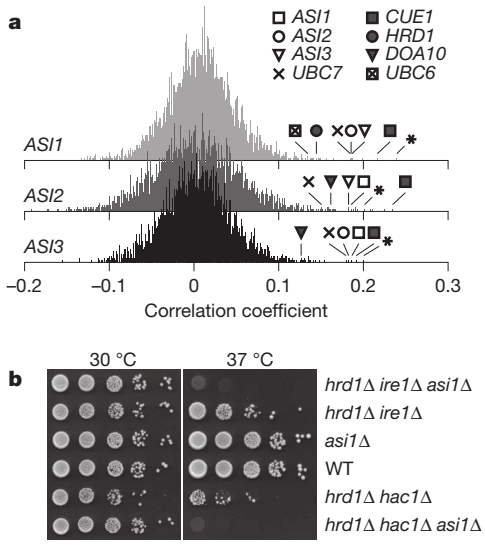

Figure 2 | Functional overlap between Asi and ERAD E3 ubiquitin ligases. **a**, Histograms of Pearson correlation coefficients calculated between the genetic interaction profiles of each *ASI* gene and ~75% of all yeast genes, obtained from a previously published genome-scale genetic interaction map[16]. Asterisks mark the dubious open reading frame *YMR119W-A*, which overlaps with the *ASI1* gene. **b**, Tenfold serial dilutions of strains grown on synthetic complete medium for 2 days at 30 or 37 °C.

We analysed this novel function of the Asi ubiquitin ligase with ten tFT-tagged substrates. Genetic crosses with additional deletion mutants revealed the involvement of Cue1 in Asi-dependent degradation (Extended Data Fig. 4a), in agreement with our biochemical analysis (Fig. 1c). Several Asi substrates that were reproducibly stabilized in *asi1*Δ and *asi3*Δ mutants were not stabilized in strains lacking *ASI2* (Extended Data Fig. 4a), suggesting that Asi2 might function as a substrate-specific recognition factor. The Asi2-independent nature of the interaction between Asi3 and Ubc6 further supports this notion (Extended Data Fig. 4b). With the exception of Aqy2, which was not expressed during exponential growth in liquid medium, all tFT-tagged substrates localized to the endoplasmic reticulum in wild-type cells and eight of them accumulated at the nuclear rim specifically in the *asi1*Δ mutant (Fig. 3e and Extended Data Fig. 4c). This result is consistent with protein stabilization at the INM where the Asi proteins reside. Cycloheximide chase experiments with haemagglutinin epitope (HA)-tagged variants revealed substantial turnover of Vtc1, Erg11, Vcx1 and Vtc4 in wild-type cells. All four proteins were stabilized specifically in the absence of *ASI1* (Fig. 3f and Extended Data Fig. 5), further validating our screening approach (Supplementary Note 1). Interestingly, Vtc1 and Vtc4 were previously shown to localize to the vacuolar membrane[22]. Both

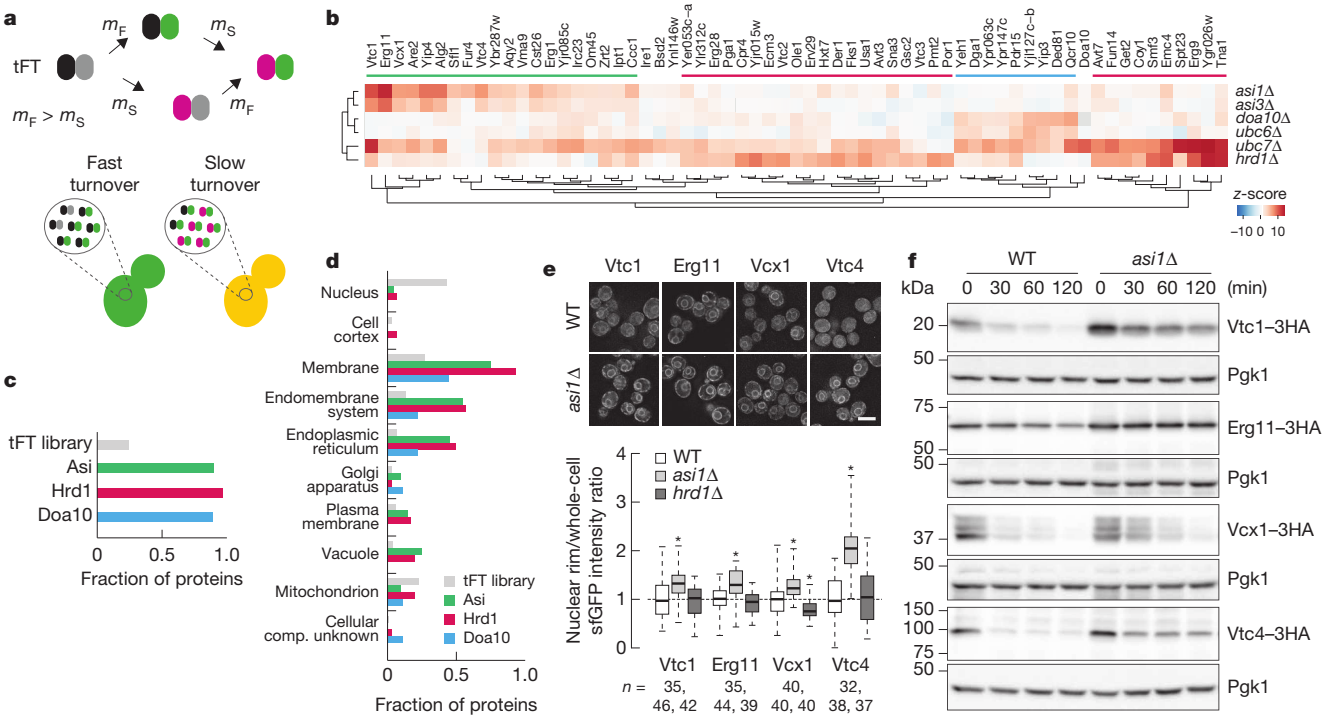

Figure 3 | Systematic identification of substrates for Asi and ERAD E3 ubiquitin ligases. **a**, A tandem fluorescent protein timer (tFT) is composed of two fluorescent proteins: one more slowly maturing (for example, the red fluorescent protein mCherry, maturation rate constant m_S) and the other faster maturing (for example, the green fluorescent protein sfGFP, maturation rate constant m_F). When fused to a protein of interest, a tFT reports on the degradation kinetics of the fusion protein: whereas fusions undergoing fast turnover are degraded before mCherry maturation, resulting in a low mCherry/sfGFP intensity ratio, the relative fraction of mature mCherry increases for proteins with slower turnover. **b**, Summary heat map of the screens for tFT-tagged proteins with altered stability in the indicated mutants. Changes in protein stability (*z*-score) are colour-coded from blue (decrease) to red (increase). Only proteins with a significant change in stability in at least one mutant (1% false discovery rate and *z*-score > 4) are shown. Clusters of potential substrates of Asi (green), Hrd1 (red) and Doa10 (blue) E3 ubiquitin ligases are indicated. **c**, **d**, Fraction of proteins in the tFT library and in the three clusters in **b** with a predicted transmembrane domain or signal peptide (**c**) or mapped to component Gene Ontology (GO) terms (**d**). Each cluster is significantly enriched in proteins with a predicted transmembrane domain or signal peptide compared to the tFT library ($P < 2.2 \times 10^{-16}$, Fisher's exact test). **e**, Quantification of sfGFP signals in strains expressing tFT-tagged proteins from the Asi cluster in **b**. Fluorescence microscopy examples representative of five fields of view (top). Scale bar, 5 μm. sfGFP intensities were measured in individual cells and at the nuclear rim (bottom, *n* as shown). For each protein, measurements were normalized to the mean of the respective wild type. Whiskers extend from minimum to maximum values. $^*P < 0.05$ (two-tailed *t*-test). **f**, Degradation of 3×HA-tagged proteins after blocking translation with cycloheximide. Whole-cell extracts were separated by SDS–PAGE followed by immunoblotting with antibodies against the HA tag and Pgk1 as loading control. Representative immunoblots from three technical replicates.

proteins mislocalize to the endoplasmic reticulum and nuclear rim only on overexpression or C-terminal tagging (Extended Data Fig. 6). Whether the Asi ubiquitin ligase recognizes such mislocalized proteins through specific degrons, as is the case with Stp1 and Stp2 transcription factors[11], or other features such as compartment-specific properties of transmembrane domains[23] is an open question.

The nuclear pore complex establishes a barrier between the cytoplasm and the nucleoplasm. However, increasing evidence suggests that not only small soluble proteins but also integral membrane proteins with cytoplasmic domains of up to 60 kilodaltons (kDa) can passively diffuse past the nuclear pore, the latter through a ~10 nm side channel[6,24–28]. We propose that the Asi ubiquitin ligase targets such mislocalized and potentially harmful proteins for degradation. Although the Asi proteins are not obviously conserved outside of yeast, the general importance of membrane-associated protein degradation mechanisms and the large diversity of integral membrane RING domain proteins in mammalian cells[29] suggest that dedicated E3 ubiquitin ligases functioning in INM-associated protein degradation exist also in metazoans.

Online Content Methods, along with any additional Extended Data display items and Source Data, are available in the online version of the paper; references unique to these sections appear only in the online paper.

Received 21 September; accepted 20 November 2014.

1. Mekhail, K. & Moazed, D. The nuclear envelope in genome organization, expression and stability. *Nature Rev. Mol. Cell Biol.* **11,** 317–328 (2010).
2. Zattas, D. & Hochstrasser, M. Ubiquitin-dependent protein degradation at the yeast endoplasmic reticulum and nuclear envelope. *Crit. Rev. Biochem. Mol. Biol.* http://dx.doi.org/10.3109/10409238.2014.959889 (2014).
3. Ruggiano, A., Foresti, O. & Carvalho, P. Quality control: ER-associated degradation: protein quality control and beyond. *J. Cell Biol.* **204,** 869–879 (2014).
4. Zargari, A. *et al.* Inner nuclear membrane proteins Asi1, Asi2, and Asi3 function in concert to maintain the latent properties of transcription factors Stp1 and Stp2. *J. Biol. Chem.* **282,** 594–605 (2007).
5. Khmelinskii, A. *et al.* Tandem fluorescent protein timers for *in vivo* analysis of protein dynamics. *Nature Biotechnol.* **30,** 708–714 (2012).
6. Deng, M. & Hochstrasser, M. Spatially regulated ubiquitin ligation by an ER/nuclear membrane ligase. *Nature* **443,** 827–831 (2006).
7. Boban, M., Pantazopoulou, M., Schick, A., Ljungdahl, P. O. & Foisner, R. A nuclear ubiquitin-proteasome pathway targets the inner nuclear membrane protein Asi2 for degradation. *J. Cell Sci.* **127,** 3603–3613 (2014).
8. Hu, C.-D., Chinenov, Y. & Kerppola, T. K. Visualization of interactions among bZIP and Rel family proteins in living cells using bimolecular fluorescence complementation. *Mol. Cell* **9,** 789–798 (2002).
9. Forsberg, H., Hammar, M., Andréasson, C., Molinér, A. & Ljungdahl, P. O. Suppressors of *ssy1* and *ptr3* null mutations define novel amino acid sensor-independent genes in *Saccharomyces cerevisiae*. *Genetics* **158,** 973–988 (2001).
10. Boban, M. *et al.* Asi1 is an inner nuclear membrane protein that restricts promoter access of two latent transcription factors. *J. Cell Biol.* **173,** 695–707 (2006).
11. Omnus, D. J. & Ljungdahl, P. O. Latency of transcription factor Stp1 depends on a modular regulatory motif that functions as cytoplasmic retention determinant and nuclear degron. *Mol. Biol. Cell* **25,** 3823–3833 (2014).
12. Wienken, C. J., Baaske, P., Rothbauer, U., Braun, D. & Duhr, S. Protein-binding assays in biological liquids using microscale thermophoresis. *Nature Commun.* **1,** 100 (2010).
13. Kostova, Z., Mariano, J., Scholz, S., Koenig, C. & Weissman, A. M. A. Ubc7p-binding domain in Cue1p activates ER-associated protein degradation. *J. Cell Sci.* **122,** 1374–1381 (2009).
14. Biederer, T., Volkwein, C. & Sommer, T. Role of Cue1p in ubiquitination and degradation at the ER surface. *Science* **278,** 1806–1809 (1997).
15. Costanzo, M., Baryshnikova, A., Myers, C. L., Andrews, B. & Boone, C. Charting the genetic interaction map of a cell. *Curr. Opin. Biotechnol.* **22,** 66–74 (2011).
16. Costanzo, M. *et al.* The genetic landscape of a cell. *Science* **327,** 425–431 (2010).
17. Friedlander, R., Jarosch, E., Urban, J., Volkwein, C. & Sommer, T. A regulatory link between ER-associated protein degradation and the unfolded-protein response. *Nature Cell Biol.* **2,** 379–384 (2000).
18. Foresti, O., Rodriguez-Vaello, V., Funaya, C. & Carvalho, P. Quality control of inner nuclear membrane proteins by the Asi complex. *Science* **346,** 751–755 (2014).
19. Khmelinskii, A., Meurer, M., Duishoev, N., Delhomme, N. & Knop, M. Seamless gene tagging by endonuclease-driven homologous recombination. *PLoS ONE* **6,** e23794 (2011).
20. Baryshnikova, A. *et al.* Synthetic genetic array (SGA) analysis in *Saccharomyces cerevisiae* and *Schizosaccharomyces pombe*. *Methods Enzymol.* **470,** 145–179 (2010).
21. Zattas, D., Adle, D. J., Rubenstein, E. M. & Hochstrasser, M. N-terminal acetylation of the yeast Derlin Der1 is essential for Hrd1 ubiquitin-ligase activity toward luminal ER substrates. *Mol. Biol. Cell* **24,** 890–900 (2013).
22. Uttenweiler, A., Schwarz, H., Neumann, H. & Mayer, A. The vacuolar transporter chaperone (VTC) complex is required for microautophagy. *Mol. Biol. Cell* **18,** 166–175 (2007).
23. Sharpe, H. J., Stevens, T. J. & Munro, S. A comprehensive comparison of transmembrane domains reveals organelle-specific properties. *Cell* **142,** 158–169 (2010).
24. Meinema, A. C., Poolman, B. & Veenhoff, L. M. The transport of integral membrane proteins across the nuclear pore complex. *Nucleus* **3,** 322–329 (2012).
25. Ellenberg, J. *et al.* Nuclear membrane dynamics and reassembly in living cells: targeting of an inner nuclear membrane protein in interphase and mitosis. *J. Cell Biol.* **138,** 1193–1206 (1997).
26. Soullam, B. & Worman, H. J. The amino-terminal domain of the lamin B receptor is a nuclear envelope targeting signal. *J. Cell Biol.* **120,** 1093–1100 (1993).
27. Hinshaw, J. E., Carragher, B. O. & Milligan, R. A. Architecture and design of the nuclear pore complex. *Cell* **69,** 1133–1141 (1992).
28. Beck, M., Lucić, V., Förster, F., Baumeister, W. & Medalia, O. Snapshots of nuclear pore complexes in action captured by cryo-electron tomography. *Nature* **449,** 611–615 (2007).
29. Nakamura, N. The Role of the transmembrane RING finger proteins in cellular and organelle function. *Membranes* **1,** 354–393 (2011).

Supplementary Information is available in the online version of the paper.

Acknowledgements We thank M. Lemberg, E. Schiebel and B. Bukau for support and discussions, A. Kaufmann, C.-T. Ho, A. Bartosik and B. Besenbeck for help with tFT library construction, K. Ryman for the qRT–PCR analysis of gene expression, M. Hochstrasser for strains, the GeneCore and the media kitchen facilities of the European Molecular Biology Laboratory (EMBL) and Donnelly Centre for support with infrastructure and media. This work was supported by the Sonderforschungsbereich 1036 (SFB1036, TP10) from the Deutsche Forschungsgemeinschaft (DFG) (M.K.), the Swedish Research Council grant VR2011-5925 (P.O.L.), INSERM and grants from ANR (ANR-12-JSV8-0003-001) and Biosit (G.R.), fellowships from the European Molecular Biology Organization (EMBO ALTF 1124-2010 and EMBO ASTF 546-2012) (A.K.) and fellowships from the Ministère de la Recherche et de l'Enseignement Supérieur and La Ligue Contre le Cancer (E.B.). M.K. received funds from the CellNetworks Cluster of Excellence (DFG) for support with tFT library construction. W.H. acknowledges funding from the EC Network of Excellence Systems Microscopy. C.B. was supported by funds from the Canadian Institute for Advanced Research (GNE-BOON-141871), National Institutes of Health (R01HG005853-01), Canadian Institute for Health Research (MOP-102629) and the National Science and Engineering Research Council (RGPIN 204899-6).

Author Contributions G.R. designed the BiFC, microscale thermophoresis and ubiquitin pulldown experiments that were performed by E.B., G.L.D. and A.B. M.P., D.J.O. and A.G. contributed the biochemical analysis of Asi-dependent ubiquitylation. M.K. and A.K. designed and coordinated the tFT project. A.K. and M.M. designed and constructed the tFT library and performed the screens with help from D.K. and C.B. B.F. and J.D.B. developed the screen analysis methods, with input from A.K., M.K., W.H. and C.B. M.K., A.K., G.R. and P.O.L. prepared the figures and wrote the paper with input from all authors.

Author Information Reprints and permissions information is available at www.nature.com/reprints. The authors declare no competing financial interests. Readers are welcome to comment on the online version of the paper. Correspondence and requests for materials should be addressed to M.K. (m.knop@zmbh.uni-heidelberg.de), P.O.L. (per.ljungdahl@su.se) or G.R. (gwenael.rabut@inserm.fr).

METHODS

Yeast methods and plasmids. Yeast genome manipulations (gene deletions and tagging) were performed using PCR targeting, as described[30]. Yeast strains and plasmids used in this study are listed in Supplementary Tables 4 and 5, respectively.

β-galactosidase activity assay. Cells were grown in synthetic minimal medium and β-galactosidase activity was measured in *N*-lauroyl-sarcosine-permeabilized cells as described[31].

RNA isolation and qRT–PCR. Strains with auxotrophies complemented by plasmids pRS316 (*URA3*), pRS317 (*LYS2*) and pAB1 (*HIS3*, *MET15* and *LEU2*) were grown in synthetic minimal medium to 10^7 cells ml^{-1} and collected by centrifugation. RNA was isolated using the RiboPure Yeast Kit and treated with Turbo-DNase (Ambion). The quality of RNA preparations was assessed by electrophoresis on a 1% agarose gel with 10 mM guanidine thiocyanate, and the lack of DNA contamination was confirmed by PCR. One microgram of RNA was used for complementary DNA synthesis with oligo (dT)12-19 (Invitrogen) using SuperScript III Reverse Transcriptase (Life Technologies). Quantitative reverse transcriptase PCR (qRT–PCR) reactions were prepared using Kapa SybrFast qPCR Master Mix (Kapa-Biosystems). cDNA mixtures were diluted 1:40 and 5 µl were used in a reaction volume of 20 µl with the following primer pairs: AGP1fwd 5′-CTGCCGTGCG TAGGTTTT-3′ and AGP1rev 5′-AGAAGAAGGTGAGATAGCCGA-3′; GNP1fwd 5′-CACCACAAGAACAAGAACAGAAAC-3′ and GNP1rev 5′-ACCGACCAG CAAACCAGTA-3′; TAF10fwd 5′-ATATTCCAGGATCAGGTCTTCCGTAGC-3′ and TAF10rev 5′-CAACAACAACATCAACAGAATGAGAAGACTAC-3′.

The levels of gene expression in three biological replicates were determined in two separate amplifications with triplicate technical replicates of each of the three genes analysed using the comparative ΔC_T method (RotorGene 6000, Corbett Life Science). Relative levels of *AGP1* and *GNP1* messenger RNA were normalized with respect to the levels of the invariant reference gene *TAF10*; the levels of *AGP1* and *GNP1* in strains carrying the indicated mutations were subsequently averaged and normalized to the levels of expression in the corresponding isogenic wild-type strains.

Purification of decahistidine–ubiquitin protein conjugates. Ubiquitylated proteins were purified from 1×10^9 exponentially growing yeast cells expressing 10×His-tagged ubiquitin using a protocol adapted from ref. 32. Cell pellets were resuspended in 2 ml 20% trichloroacetic acid and lysed for 2 min using glass beads in a Disrupter Genie homogenizer (Scientific Industries). After precipitation, proteins were resuspended in 3 ml guanidium buffer (6 M guanidinium chloride, 100 mM Tris-HCl, pH 9, 300 mM NaCl, 10 mM imidazole, 0.2% Triton X-100 and 5 mM chloroacetamide), clarified at 30,000*g* and incubated for 1.5 h at room temperature with TALON Metal Affinity Resin (Clontech). The beads were then washed with wash buffer (8 M urea, 100 mM sodium phosphate, pH 7.0, 300 mM NaCl, 5 mM imidazole, 0.2% Triton X-100 and 5 mM chloroacetamide) containing 0.2% SDS (twice) and lacking SDS (twice). 10×His–ubiquitin conjugates were finally eluted with 200 µl elution buffer (8 M urea, 100 mM sodium phosphate, pH 7.0, 300 mM NaCl, 250 mM imidazole, 0.2% Triton X-100 and 5 mM chloroacetamide). Total extracts (1% of the amount used for purification) and ubiquitin conjugate eluates were analysed by SDS–PAGE and immunoblotting with antibodies against the TAP tag (PAP, 1:1,000, Sigma). As controls, levels of ubiquitin conjugates and Pgk1 were assessed with anti-ubiquitin (P4D1 horseradish peroxidase (HRP) conjugate, 1:1,000, Santa Cruz) and anti-Pgk1 antibodies (clone 22C5D8, 1:10,000, Invitrogen), respectively. Immunogenic proteins were detected by chemiluminescence using SuperSignal West Femto Substrate (Thermo Scientific) and recorded using autoradiographic films (CP-BU, Agfa) processed with a Curix 60 developing machine (Agfa).

Purification of hexahistidine–ubiquitin protein conjugates. Ubiquitylated proteins were purified from 5×10^8 exponentially growing yeast cells expressing 6×His-tagged ubiquitin as previously described[33]. 6×His–ubiquitin conjugates were retained on nickel-nitrilotriacetic acid Sepharose beads (Qiagen) and eluted in the presence of 300 mM (Stp1–HA, Stp1-RI_{17-33}–HA) or 500 mM (Stp2–HA, Stp2Δ_{2-13}–HA) imidazole. Total extracts, flow-through and eluate fractions were precipitated with 10% trichloroacetic acid, analysed by SDS–PAGE and immunoblotting with antibodies against the haemagglutinin tag (1:5,000, Roche) and the signals were recorded using autoradiographic film (CL-Xposure, Thermo Scientific). As controls, levels of ubiquitin conjugates and Pgk1 were assessed with anti-His_5 (1:5,000, Qiagen) and anti-Pgk1 antibodies (1:10,000, InVitrogen), respectively, and detected by chemiluminescence using SuperSignal West Dura Extended Duration Substrate (Thermo Scientific) and a Molecular Imager ChemiDoc XRS+ with Image Lab v3 build 11 software (BioRad). Loaded total and flow-through fractions correspond to 2% (Stp1–HA or Stp1-RI_{17-33}–HA) and 0.7% (Stp2–HA or Stp2Δ_{2-13}–HA) of the amount used for purification of ubiquitin conjugates.

Bimolecular fluorescence complementation. BiFC interaction assays were performed using E2 and E3 proteins tagged with the VC173 and VN155 fragments (VC and VN) of the Venus fluorescent protein, respectively[34]. All E2 and E3 proteins were tagged C-terminally, with the following exceptions that were N-terminally tagged: Ubc6, because the C terminus of Ubc6 faces the endoplasmic reticulum lumen[35]; Ubc7, to preserve its interaction with Cue1 (ref. 36); Ubc1, because the growth of strains expressing Ubc1 endogenously tagged at the C terminus with VC appears compromised; the E3 proteins Far1, Mot2, Nam7, Prp19, Ste5 and Tfb3, as they all have their E2 binding domain at the N terminus. All fusions were expressed from their endogenous chromosomal loci, with the exception of Rsp5–VN, which was expressed from its endogenous promoter on the centromeric plasmid pGR703 (Supplementary Table 5).

Strains expressing VC-tagged E2 proteins were constructed in the scEB115 background. scEB115 carries markers for selection of haploid progeny in automated crosses (*can1::STE2pr-spHIS5* and *lyp1::STE3pr-HPH*) and expresses the proteasomal subunit Rpn7 fused to the red fluorescent protein tDimer2 as nuclear marker (Supplementary Table 4). Strains expressing VN-tagged E3 proteins were either obtained from a commercially available collection (Bioneer Corporation) or constructed by homologous recombination in the BY4741 background. Expression of VC- and TAP-tagged fusions was validated by immunoblotting with mouse anti-GFP (clones 7.1 and 13.1, Roche) and peroxidase anti-peroxidase (Sigma) antibodies to detect the VC and TAP tag, respectively, and mouse anti-actin (clone c4, Merck Millipore) for loading controls.

Strains expressing individual E2 and E3 protein fusions were crossed to produce an array of yeast strains each expressing Rpn7–tDimer2 and a unique combination of tagged E2 and E3 proteins, as described[20]. The resulting strains were cultivated overnight at 20 °C in YPD medium and diluted in low fluorescence medium[37] 3–4 h before imaging. Imaging was performed in 8-well LabTek chambers or 96-well plates (Imaging plates CG, Zell-Kontakt) using an inverted Leica SP8 confocal microscope. Images of the BiFC signal were collected using a 514 nm laser and a narrow band-pass filter (525–538 nm) around the emission peak of the Venus fluorescent protein to reduce the contribution of cellular autofluorescence. Rpn7–tDimer2 was imaged simultaneously using a 580–630 nm filter. Cellular autofluorescence was imaged separately using the same band-pass filter as for BiFC images, but with a 458 nm excitation. Rpn7 localizes to the nucleus throughout the cell cycle in growing cells and relocalizes to cytoplasmic structures when cells enter quiescence[38]. Rpn7–tDimer2 images were visually inspected before image processing to verify that cells are not quiescent. Rpn7–tDimer2 and autofluorescence images were used to segment the BiFC images into nuclear and cytoplasmic (whole cell minus nucleus) regions and to unmix the BiFC signal. Image segmentation and single-cell fluorescence measurements were performed using custom plugins in ImageJ[39] (available on request). To enable comparison of data from different experiments, the quantification results were rescaled so that BiFC signals of control cells had a mean of zero and a standard deviation of one. Statistical analysis and graphical representation were performed with GraphPad Prism software. Statistically significant differences from control cells were identified by one-way ANOVA followed by Bonferroni post-hoc tests to correct for multiple comparisons. No statistical method was used to predetermine sample size.

Recombinant protein expression and purification. *Escherichia coli* BL21(DE3) were transformed with plasmids encoding MBP–$Hrd1^{CT}$ (Hrd1 residues 321–551), MBP–$Asi1^{RING}$ (Asi1 residues 559–624), MBP–$Asi3^{RING}$ (Asi3 residues 613–676), glutathione *S*-transferase (GST)–$Ubc6^{\Delta TM}$ (Ubc6 residues 1–230), GST–Ubc7 or $Cue1^{U7BR}$ (Cue1 residues 151–203) and were cultivated in LB medium. $Cue1^{U7BR}$ was coexpressed with GST–Ubc7. Protein expression was induced by addition of 1 mM isopropyl-β-D-thiogalactoside (IPTG) during 4 h at 25 °C. Cells were pelleted, resuspended in PBS, and lysed by sonication. Lysates were rotated with glutathione (GE Healthcare) or amylose beads (New England Biolab) for 1 h at 4 °C. Beads were washed with PBS containing 1 mM dithiothreitol (DTT). E2s were cleaved from GST using thrombin (Stago). MBP–E3s were eluted using 10 mM amylose and dialysed against PBS plus 1 mM DTT. All recombinant proteins were concentrated using spin filters (3 kDa, Amicon). Protein purity was tested by Coomassie staining after SDS–PAGE. Protein concentration was estimated by absorbance at 280 nm.

Microscale thermophoresis. Microscale thermophoresis analysis was performed essentially as described[12] using MBP–$Asi1^{RING}$, MBP–$Asi3^{RING}$ or MBP–$Hrd1^{CT}$ fluorescently labelled with the fluorescent dye NT-647 (labelling was performed with the Monolith Protein Labelling Kit RED-NHS according to the instructions of the supplier) and high precision standard treated capillaries. MBP–E3s were diluted to 100 nM in PBS, 5% glycerol, 0.1% Tween 20, 1 mM DTT, 10 µM ZnAc and titrated with varying concentrations of unlabelled E2s before loading into capillaries. The difference of the thermophoretic properties of MBP–E3s were measured using a Monolith NT.115 instrument (NanoTemper Technologies GmbH) and a laser power of 60%. A nonlinear fit with the law of mass action was used to derive the dissociation constant (K_d) of the interaction as well as the theoretical thermophoretic properties of the MBP–E3 in its fully bound and unbound states. Those values were then used to normalize the measurements and calculate the

fraction of E3 bound at each E2 concentration. Data were plotted and fitted with the GraphPad Prism software.

tFT library construction. A total of 4,081 verified or uncharacterized *S. cerevisiae* open reading frames were selected for tagging based on structural and functional criteria (detailed in Supplementary Methods) to increase the probability that the C-terminal tFT tag would not affect protein functionality, and to avoid exposing the tag to an environment that could affect folding and maturation of the fluorescent proteins. Protocols for strain construction and validation are described in the Supplementary Methods. In brief, strain manipulations were automated and performed in 96-well format whenever possible. Using PCR targeting[30] and lithium acetate transformation of yeast[40], the module for seamless protein tagging with the mCherry-sfGFP timer (pMaM168 in Supplementary Table 5) was integrated into each selected genomic locus in the strain yMaM330 (Supplementary Table 4), a strain compatible with automated yeast genetics that carried a construct for conditional expression of the I-SceI meganuclease from the *GAL1* promoter integrated into the *leu2* locus. Correct integration of the tagging module into each locus and expression of tFT protein fusions was verified by PCR and whole colony fluorescence measurements for 4,044 open reading frames, with two independent clones validated for 3,952 open reading frames (Supplementary Table 2).

tFT library screening. Haploid array strains carrying deletions of individual components of the ubiquitin–proteasome system were obtained from the genome-wide heterozygous diploid yeast deletion library[41] by sporulation and tetrad dissection. Screens were conducted in 1536-colony format. Using pinning robots (BioMatrix, S&P Robotics), tFT query strains (before marker excision) were mated with array mutants. Selection of diploids, sporulation and selection of haploids carrying simultaneously a tFT protein fusion and a gene deletion were performed by sequential pinning on appropriate selective media, as described[20], followed by seamless marker excision[19]. In each screen, a single tFT strain was crossed to a set of mutants in the ubiquitin–proteasome pathway (including the *asi1*Δ, *asi3*Δ, *hrd1*Δ, *doa10*Δ, *ubc6*Δ and *ubc7*Δ mutants) (A.K. *et al.*, manuscript in preparation) with four technical replicates of each cross. Technical replicates were arranged next to each other. Fluorescence intensities of the final colonies were measured after 24 h of growth on synthetic complete medium lacking histidine at 30 °C using Infinite M1000 or Infinite M1000 Pro plate readers equipped with stackers for automated plate loading (Tecan) and custom temperature control chambers. Measurements in mCherry (587/10 nm excitation, 610/10 nm emission, optimal detector gain) and sfGFP (488/10 nm excitation, 510/10 nm emission, optimal detector gain) channels were performed at 400 Hz frequency of the flash lamp, with ten flashes averaged for each measurement.

Measurements were filtered for potentially failed crosses based on colony size after haploid selection. Fluorescence intensity measurements were log-transformed and the data were normalized for spatial effects on plates by local regression. To estimate the changes from normal protein stability, median effects for tFT and deletion strains were subtracted from log-ratios of mCherry and sfGFP intensities. To avoid variance-mean dependences, standard deviations were regressed against the absolute fluorescence intensities. Changes in protein stability were divided by the regressed standard deviations, yielding a measurement comparable to a *z*-score, and tested against the hypothesis of zero change. A moderated *t*-test implemented in the R/Bioconductor package limma[42] was used to compute *P* values. *P* values were adjusted for multiple testing by controlling the false discovery rate using the method of Benjamini–Hochberg.

Crosses with additional mutants were performed with independently constructed deletion strains using identical procedures on a RoToR pinning robot (Singer). Whole colony fluorescence intensities were corrected for autofluorescence using measurements of corresponding mutant colonies crossed to strain yMaM344-2 (Supplementary Table 4) expressing a truncated non-fluorescent $mCherry^{AN}$ protein. For each tFT fusion, mCherry/sfGFP intensity ratios in each mutant were compared to a control cross with a wild-type strain carrying the *kanMX* selection marker in the *his3*Δ locus.

Fluorescence microscopy. Strains were grown at 30 °C in low fluorescence medium (synthetic complete medium prepared with yeast nitrogen base lacking folic acid and riboflavin; CYN6501, ForMedium) to 0.4–1.2 × 10^7 cells ml^{-1} and attached to glass-bottom 96-well plates (MGB096-1-2-LG-L, Matrical) using Concanavalin A (C7275, Sigma) as described[43]. Single plane images were acquired on a DeltaVision Elite system (Applied Precision) consisting of an inverted epifluorescence microscope (IX71; Olympus) equipped with an LED light engine (SpectraX, Lumencor), 475/28 and 575/25 nm excitation, and 525/50 and 624/40 nm emission filters (Semrock), a dual-band beam splitter 89021 (Chroma Technology), using either a 100× numerical aperture (NA) 1.4 UPlanSApo or a 60× NA 1.42 PlanApoN oil immersion objective (Olympus), an sCMOS camera (pco.edge 4.2, PCO) and a motorized stage contained in a temperature-controlled chamber. Image correction and quantification were performed in ImageJ[39]. Dark signal and flat field corrections were applied to all images as described[43]. Image deconvolution was performed with Softworx software (Applied Precision) using the conservative ratio algorithm with default parameter settings. Individual cell, perinuclear region and cytoplasm segmentation masks were manually defined in deconvolved images and applied to non-deconvolved images. Mean single-cell fluorescence measurements were corrected for cellular autofluorescence. Mean perinuclear fluorescence measurements were corrected for cytoplasmic fluorescence of each individual cell.

Strains expressing N- and C-terminally tagged Vtc1 and Vtc4 were imaged with exposure setting adjusted to the expression levels: 3.3-fold longer exposure time for C-terminally tagged fusions. Representative deconvolved images were scaled identically.

Cycloheximide chases. Strains were grown at 30 °C in synthetic complete medium to ~0.8 × 10^7 cells ml^{-1} density before addition of cycloheximide to 100 μg ml^{-1} final concentration. One-millilitre samples taken at each time point were immediately mixed with 150 μl of 1.85 M NaOH and 10 μl β-mercaptoethanol, and flash frozen in liquid nitrogen. Whole-cell extracts were prepared as previously described[40], separated by SDS–PAGE followed by semi-dry blotting and probed sequentially with mouse anti-HA (12CA5) and mouse anti-Pgk1 (22C5D8, Molecular Probes) antibodies. A secondary goat anti-mouse antibody (IgG (H+L)-HRP, Dianova) was used for detection on a LAS-4000 system (Fuji).

30. Janke, C. *et al.* A versatile toolbox for PCR-based tagging of yeast genes: new fluorescent proteins, more markers and promoter substitution cassettes. *Yeast* **21,** 947–962 (2004).
31. Andréasson, C. & Ljungdahl, P. O. The N-terminal regulatory domain of Stp1p is modular and, fused to an artificial transcription factor, confers full Ssy1p-Ptr3p-Ssy5p sensor control. *Mol. Cell. Biol.* **24,** 7503–7513 (2004).
32. Becuwe, M. *et al.* A molecular switch on an arrestin-like protein relays glucose signaling to transporter endocytosis. *J. Cell Biol.* **196,** 247–259 (2012).
33. Léon, S., Erpapazoglou, Z. & Haguenauer-Tsapis, R. Ear1p and Ssh4p are new adaptors of the ubiquitin ligase Rsp5p for cargo ubiquitylation and sorting at multivesicular bodies. *Mol. Biol. Cell* **19,** 2379–2388 (2008).
34. Shyu, Y. J., Liu, H., Deng, X. & Hu, C. Identification of new fluorescent protein fragments for biomolecular fluorescence complementation analysis under physiological conditions. *Biotechniques* **40,** 61 (2006).
35. Sommer, T. & Jentsch, S. A protein translocation defect linked to ubiquitin conjugation at the endoplasmic reticulum. *Nature* **365,** 176–179 (1993).
36. Metzger, M. B. *et al.* A structurally unique E2-binding domain activates ubiquitination by the ERAD E2, Ubc7p, through multiple mechanisms. *Mol. Cell* **50,** 516–527 (2013).
37. Sheff, M. A. & Thorn, K. S. Optimized cassettes for fluorescent protein tagging in *Saccharomyces cerevisiae*. *Yeast* **21,** 661–670 (2004).
38. Laporte, D., Salin, B., Daignan-Fornier, B. & Sagot, I. Reversible cytoplasmic localization of the proteasome in quiescent yeast cells. *J. Cell Biol.* **181,** 737–745 (2008).
39. Schneider, C. A., Rasband, W. S. & Eliceiri, K. W. NIH Image to ImageJ: 25 years of image analysis. *Nature Methods* **9,** 671–675 (2012).
40. Knop, M. *et al.* Epitope tagging of yeast genes using a PCR-based strategy: more tags and improved practical routines. *Yeast* **15,** 963–972 (1999).
41. Winzeler, E. A. *et al.* Functional characterization of the *S. cerevisiae* genome by gene deletion and parallel analysis. *Science* **285,** 901–906 (1999).
42. Smyth, G. K. in *Bioinformatics and Computational Biology Solutions Using R and Bioconductor* (eds Gentleman, R., Carey, V., Dudoit, S., Irizarry, R. & Huber, W.) 397–420 (Springer, 2005).
43. Khmelinskii, A. & Knop, M. Analysis of protein dynamics with tandem fluorescent protein timers. *Methods Mol. Biol.* **1174,** 195–210 (2014).

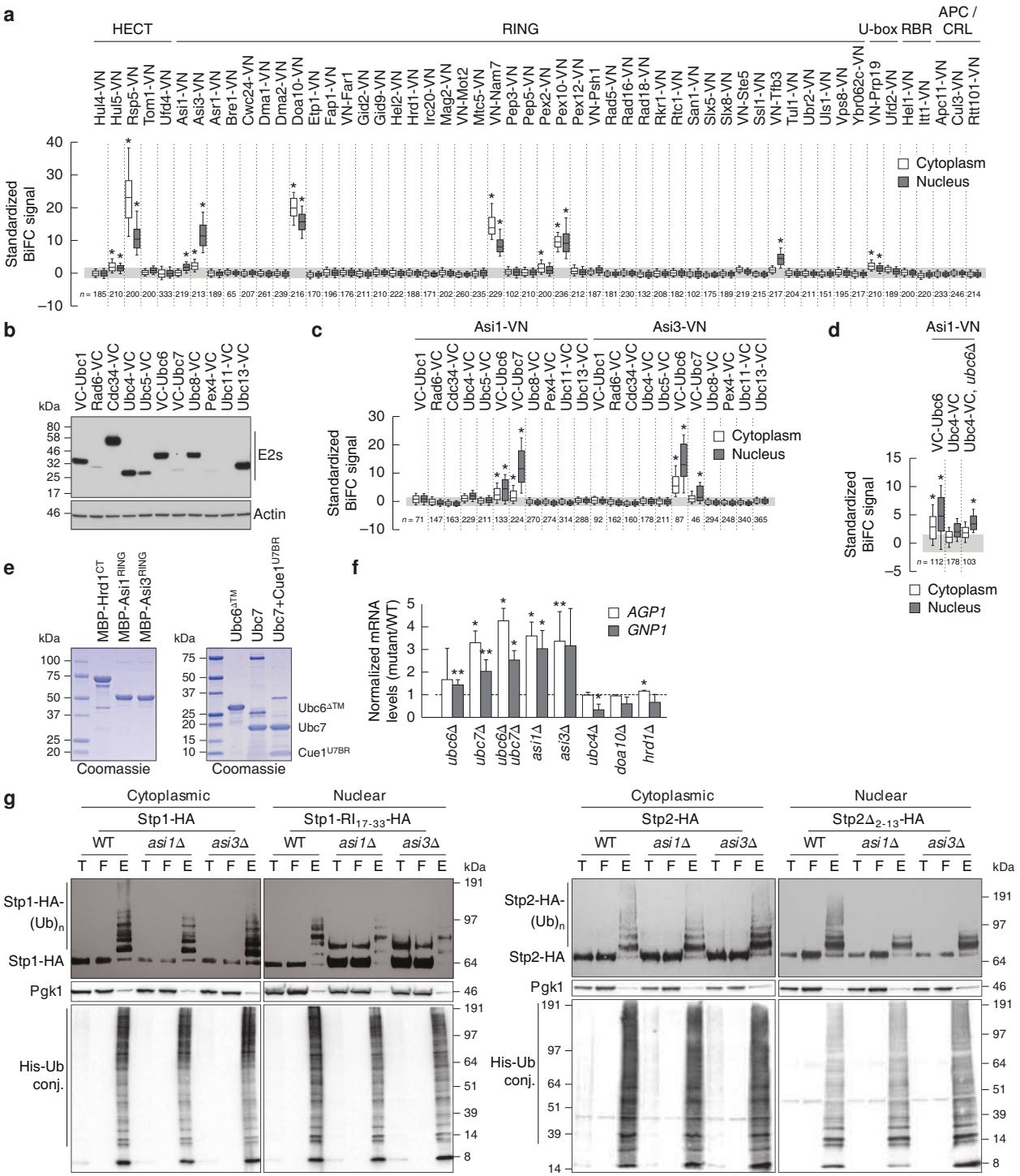

Extended Data Figure 1 | Identification of Ubc6 and Ubc7 ubiquitin-conjugating enzymes as functional interacting partners of Asi1 and Asi3. **a**, Quantification of BiFC signals in cells expressing VC–Ubc6 and all tested E3 ubiquitin ligases. BiFC signals were measured in the cytoplasm and nucleus of individual cells (*n* as shown). Whiskers extend from the tenth to the ninetieth percentiles. The same representation is used in **c** and **d**. **b**, Immunoblot showing expression levels of VC-tagged E2 ubiquitin-conjugating enzymes. Ubc11–VC could not be detected in the growth condition of the BiFC assay. **c**, Quantification of BiFC signals in cells co-expressing VC-tagged E2 ubiquitin-conjugating enzymes and Asi1–VN or Asi3–VN (*n* as shown). **d**, Detection of a significant BiFC signal between Asi1–VN and Ubc4–VC in cells lacking *UBC6* (*n* as shown). **e**, Coomassie-stained gels of recombinant proteins used in microscale thermophoresis experiments. **f**, mRNA levels of *AGP1* and *GNP1* measured with qRT–PCR in the indicated strains (mean ± s.d., $n = 3$ clones). The signal was normalized to wild type (dashed line). **g**, Ubiquitylation of Stp1–HA or Stp1-$RI_{17–33}$–HA (Stp1 variant in which amino acid residues 2–64 were replaced with Stp1 residues 17–33 flanked by minimal linker sequences) (left) and Stp2–HA or $Stp2\Delta_{2–13}$–HA (Stp2 variant lacking amino acid residues 2–13) (right) in strains expressing 6×His–ubiquitin. Stp1-$RI_{17–33}$ and $Stp2\Delta_{2–13}$ variants exhibit compromised cytoplasmic retention and enhanced Asi-dependent degradation, whereas full-length Stp1 is degraded primarily in the cytoplasm in a SCF^{Grr1}-dependent manner[11]. Total cell extracts (T), flow-through (F) and ubiquitin conjugates (E) eluted after immobilized-metal affinity chromatography were separated by SDS–PAGE followed by immunoblotting with antibodies against the HA-tag, Pgk1 and the His-tag. Representative immunoblots from three technical replicates. $*P < 10^{-4}$ (**a**, **c** and **d**; one-way ANOVA with Bonferroni correction for multiple testing), and $*P < 0.05$, $**P < 0.1$ (**f**; two-tailed *t*-test).

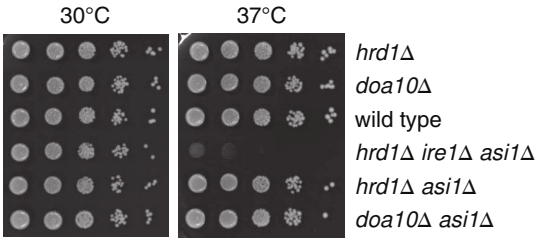

Extended Data Figure 2 | Lack of genetic interaction between *ASI1* and *HRD1* or *DOA10* at 37 °C. Tenfold serial dilutions of strains grown on synthetic complete medium for 2 days at 30 or 37 °C.

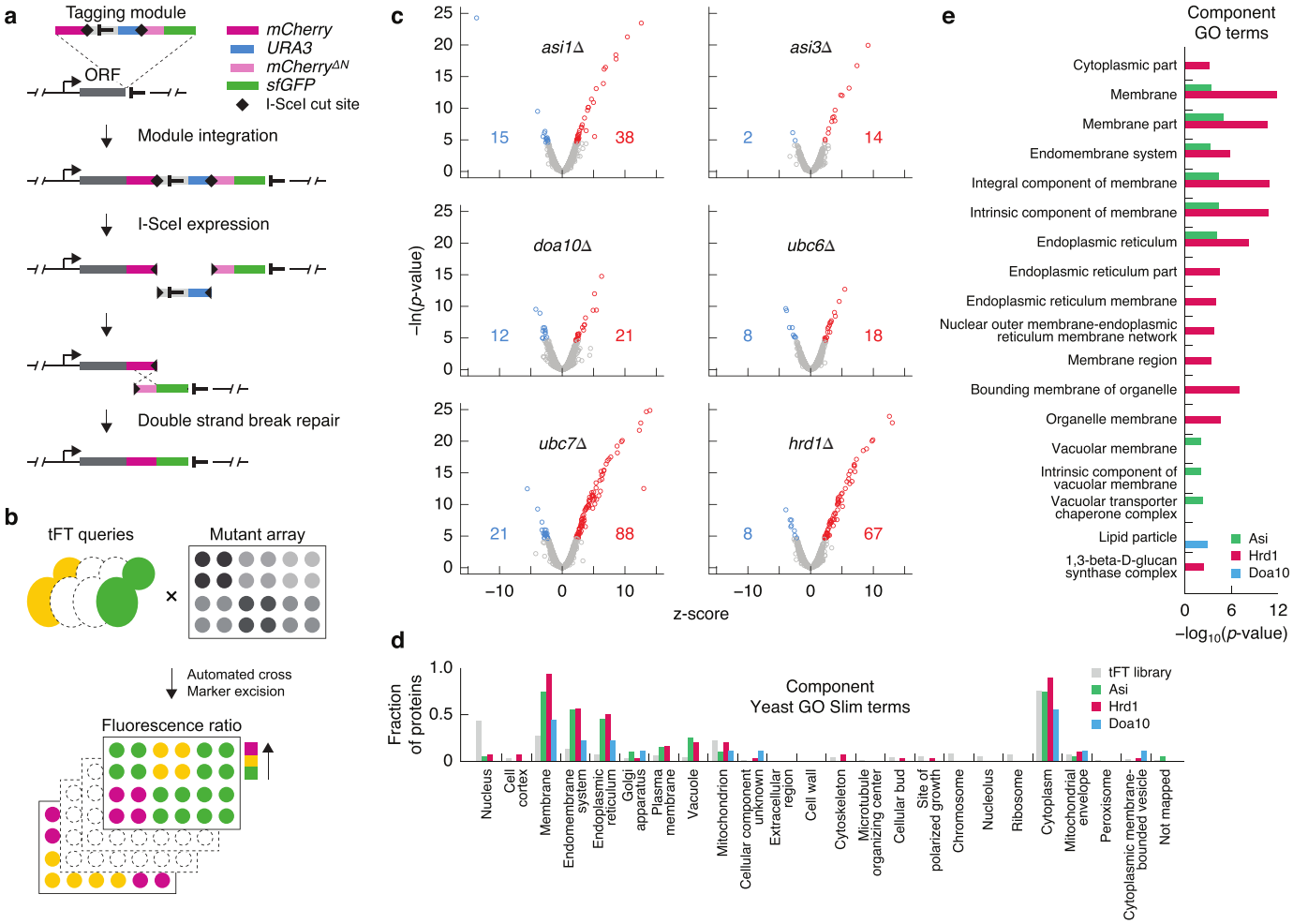

Extended Data Figure 3 | tFT screens for substrates of Asi and ERAD E3 ubiquitin ligases. **a**, Tagging approach used to construct the tFT library in a strain carrying the I-SceI meganuclease under an inducible promoter. First, a module for seamless C-terminal protein tagging with the mCherry-sfGFP timer is integrated into a genomic locus of interest using conventional PCR targeting. Subsequent I-SceI expression leads to excision of the heterologous terminator and the *URA3* selection marker, followed by repair of the double-strand break by homologous recombination between the mCherry and mCherry$^{\Delta N}$ sequences. A tFT fusion protein is expressed under control of endogenous promoter and terminator in the final strain. **b**, Workflow of screens for substrates of E3 ubiquitin ligases involved in protein degradation. Each tFT query strain is crossed to an array of mutants carrying different gene deletion alleles. The resulting strains are imaged with a fluorescence plate reader to identify proteins with altered stability in each mutant. **c**, Volcano plots of the screens for proteins with altered stability in the indicated mutants. Plots show *z*-scores for changes in protein stability on the *x* axis and the negative logarithm of *P* values adjusted for multiple testing on the *y* axis. The number of proteins with increased (red) or decreased (blue) stability at 1% false discovery rate is indicated. **d**, Fraction of proteins in the tFT library and in the three clusters in Fig. 3b mapped to the full yeast slim set of component GO terms. Note that the GO term cytoplasm contains all cellular contents except the nucleus and the plasma membrane. **e**, The three clusters in Fig. 3b are enriched for proteins in the indicated component GO terms. Bar plot shows $-\log_{10}$-transformed *P* values of significant enrichments.

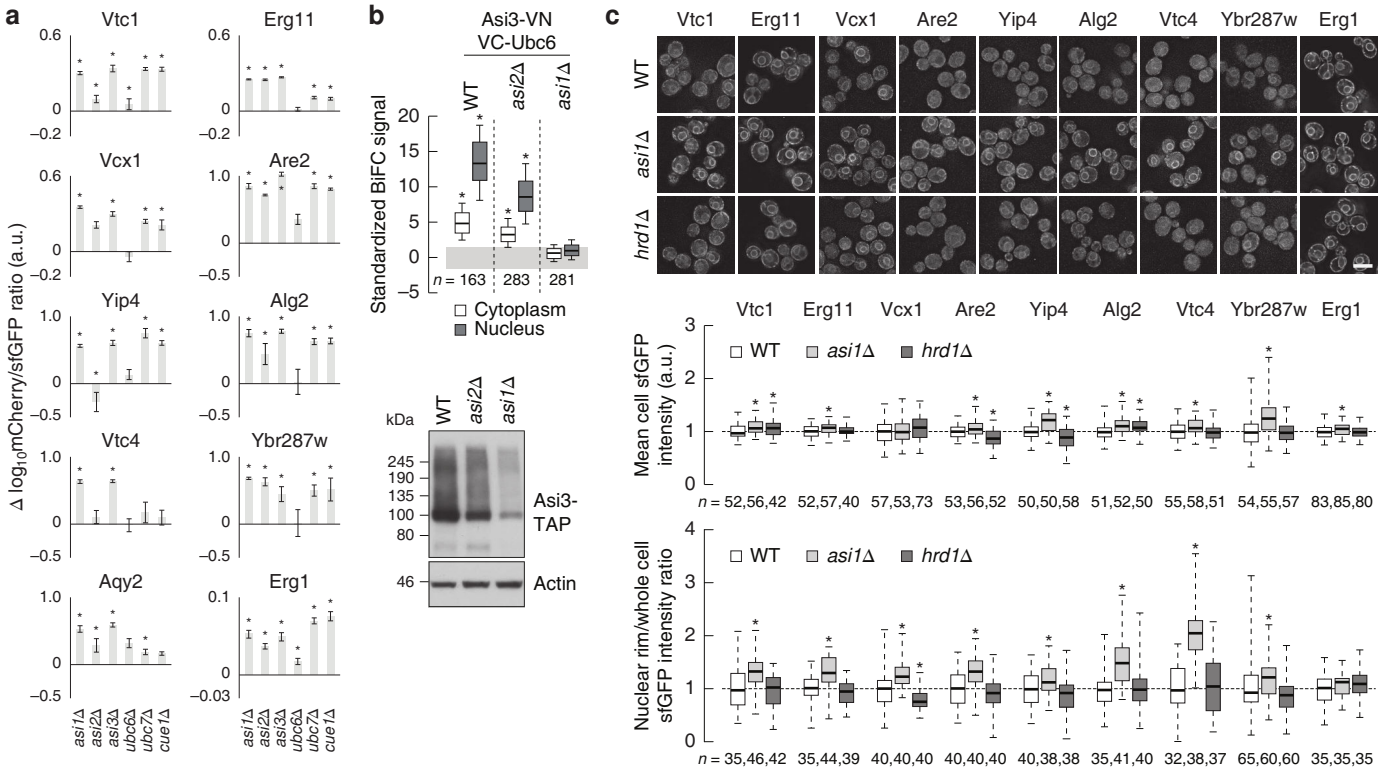

Extended Data Figure 4 | Analysis of integral membrane protein substrates of the Asi E3 ubiquitin ligase. **a**, Differences in the $\log_{10}$ mCherry/sfGFP intensity ratio between the indicated mutants and the wild type (mean ± s.d., $n = 4$) for tFT-tagged proteins from the Asi cluster in Fig. 3b. **b**, Quantification of BiFC signals in strains co-expressing VC–Ubc6 and Asi3–VN (top). BiFC signals were measured in the cytoplasm and nucleus of individual cells (n as shown). Whiskers extend from tenth to ninetieth percentiles. A substantial BiFC signal is retained in the *asi2*Δ mutant, despite reduced expression of Asi3 (immunoblot, bottom). **c**, Quantification of sfGFP signals in strains expressing tFT-tagged proteins from the Asi cluster in Fig. 3b. Fluorescence microscopy examples representative of five fields of view (top). Scale bar, 5 µm. sfGFP intensities were measured in individual cells (middle) and at the nuclear rim (bottom). For each protein, measurements were normalized to the mean of the respective wild type. Whiskers extend from minimum to maximum values. $*P < 0.05$ (**a** and **c**; two-tailed t-test) and $*P < 10^{-4}$ (**b**; one-way ANOVA with Bonferroni correction for multiple testing).

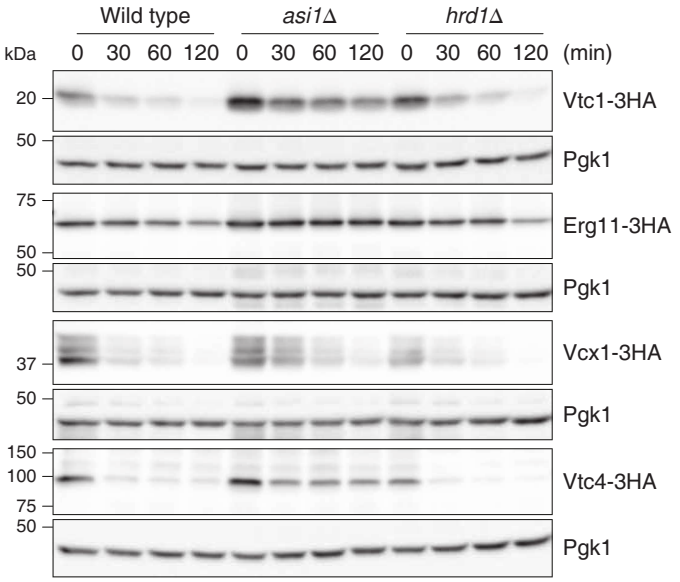

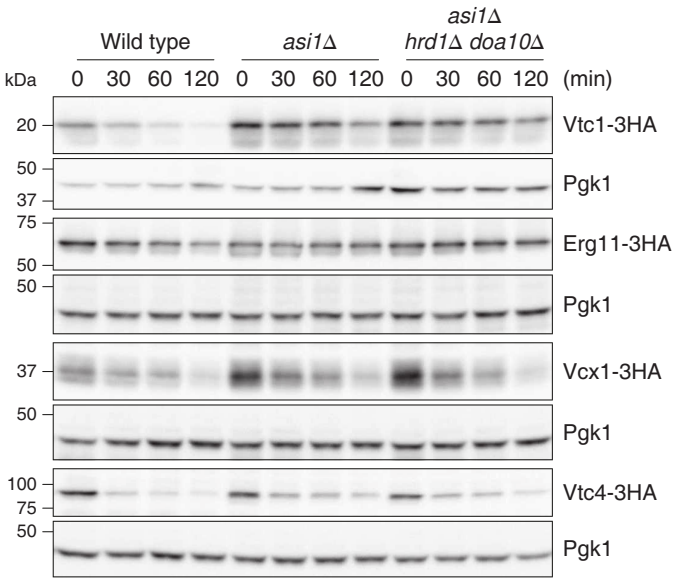

Extended Data Figure 5 | Cycloheximide chase experiments with substrates of the Asi E3 ubiquitin ligase. Degradation of 3×HA-tagged proteins after blocking translation with cycloheximide. Whole-cell extracts were separated by SDS–PAGE followed by immunoblotting with antibodies against the HA tag and Pgk1 as loading control. Representative immunoblots from two technical replicates. Left, wild-type and *asi1*Δ immunoblots are reproduced in Fig. 3f.

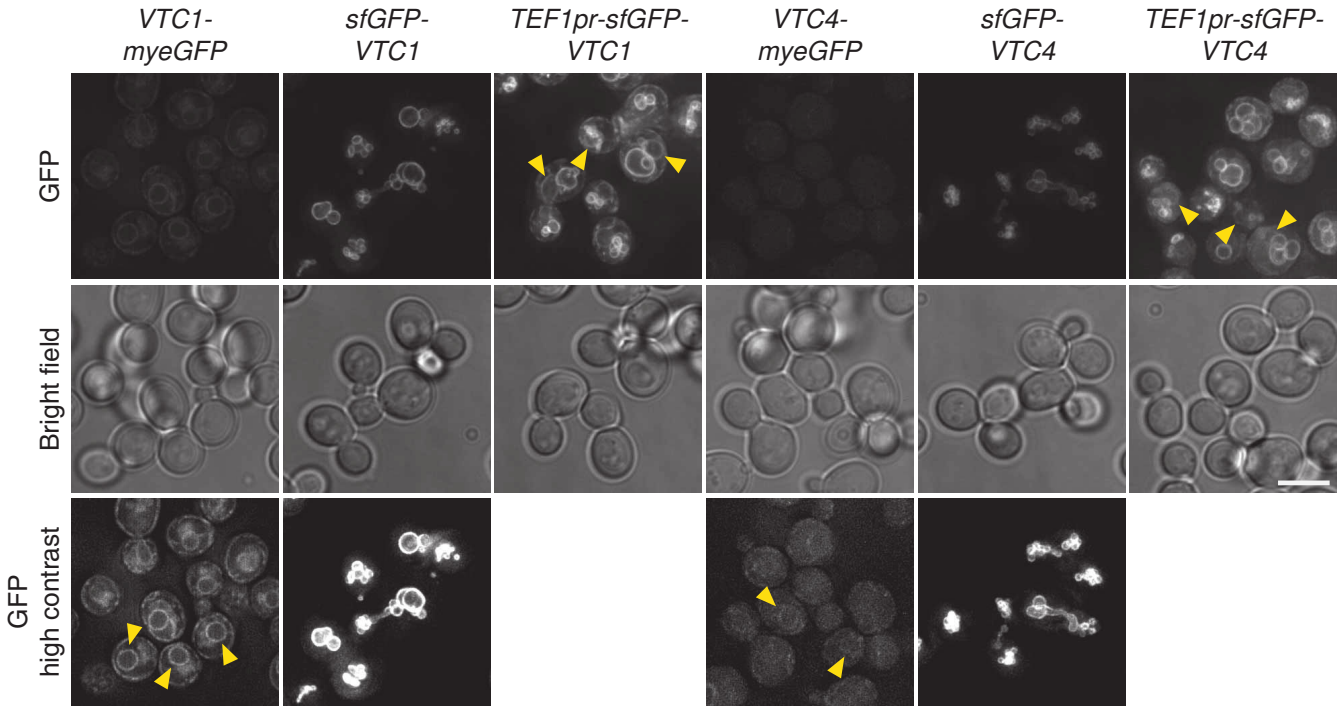

Extended Data Figure 6 | Influence of tagging and expression levels on localization of Vtc1 and Vtc4. Fluorescence microscopy of strains expressing Vtc1 or Vtc4 tagged endogenously with monomeric yeast codon-optimized enhanced GFP (myeGFP) at the C terminus or tagged with sfGFP at the N terminus and expressed under control of endogenous or *TEF1* promoters. Representative deconvolved images of five fields of view with ~100 cells each. Arrowheads indicate nuclear rim localization. Scale bar, 5 µm.

doi:10.1038/nature14096

Table of Contents

1. Supplementary Methods

Here we describe the construction of a genome-wide library of *S. cerevisiae* strains each expressing a different protein tagged with a tFT, hereafter referred to as tFT library.

tFT library construction: overview and workflow

First, we selected a tFT suitable for studies of protein dynamics in this organism. The mean and median half-life of the *S. cerevisiae* proteome is ~43 min, as determined with cycloheximide chase experiments using strains expressing proteins fused to the TAP tag[1]. A tFT composed of the slower maturing red fluorescent protein mCherry[2] and the faster maturing green fluorescent protein sfGFP[3] can be used to study the degradation of proteins with half-lives between ~10 min and ~8 h[4] (see also Supplementary Note 1). The dynamics of most yeast proteins could thus be analyzed with this tFT. Therefore, we constructed a module for seamless protein tagging with the mCherry-sfGFP timer (described in section 1.1).

Second, we selected a strain background for library construction. Various genome-wide libraries of yeast strains carrying genome manipulations such as gene deletions or tagged loci have been constructed over the last fifteen years[5,6]. With synthetic genetic array (SGA) technology, different genome manipulations present in such libraries can be combined using automated procedures[7], greatly expanding the potential applications of each individual library. Therefore, we decided to construct the tFT library in a strain background compatible with SGA. We introduced the genetic elements required for seamless protein tagging into the SGA entry strain Y8205[8], generating the library background strain yMaM330 (described in section 1.2).

Third, we selected the open reading frames (ORFs) to be tagged with the tFT. We sought to reduce potential artifacts (e.g. protein mislocalization) caused by tagging and avoid tagging proteins localized to subcellular compartments that affect the properties of the timer. Moreover, we decided to exclude proteins unlikely to be expressed under standard yeast growth conditions. Using information from previous systematic protein tagging enterprises[9-11] and annotations collected in the *Saccharomyces* Genome Database (http://www.yeastgenome.org), we selected a total of 4081 ORFs (described in section 1.3).

Next, we proceeded to tag each ORF at the respective endogenous chromosomal locus with the mCherry-sfGFP timer. Strain manipulations were automated and performed in 96-well format whenever possible. Each ORF was assigned unique plate and well coordinates to facilitate the construction process. Following this coordinate system, ORF-specific primers required for tagging by PCR targeting (described in section 1.4) were obtained from IDT (Integrated DNA Technologies) in 96-well format. The module for seamless protein tagging with the mCherry-sfGFP timer was integrated into each selected genomic locus using conventional PCR targeting[12] and lithium acetate transformation of yeast[13]. The protocols were optimized for 96-well format such that up to 480 different strains could be constructed in parallel. Briefly, the tagging module was PCR amplified with ORF-specific primers containing short overhangs homologous to each genomic locus (described in section 1.5). Competent yMaM330 cells, prepared from a single colony, were transformed with each PCR product (described in section 1.6). Each transformation mixture (specific for a different ORF) was then manually plated onto a separate 9 cm plate with selective agar medium and incubated at 30°C until distinct colonies were visible. From each plate, six clones were manually purified for single colonies and four purified clones were subsequently inoculated into four separate 96-well plates according to the coordinates assigned to each ORF. Therefore, starting with 45 96-well plates of ORF-specific primers for PCR targeting, we obtained 45x4 plates of purified clones grown in liquid medium that were stored at -80°C at the end of the first round of transformations. Verification primers were obtained from IDT (Integrated DNA Technologies) in 96-well format using the same coordinate system (described in section 1.7) and used to test for correct integration of the tagging module into each locus by diagnostic PCR (described in section 1.8). For a subset of ORFs, the PCR gave unclear or ambiguous results and was therefore repeated using new validation primers (described in section 1.7). ORFs for which correct integration of the tagging module could not be confirmed for at least 2 clones were taken through a

second round of transformations using ORF-specific primers with longer overhangs homologous to each genomic locus (described in section 1.4). ORFs for which correct integration of the tagging module could not be confirmed for at least 2 clones after two rounds of transformation were taken through a third and final round of manual transformations. Finally, fluorescence intensities of all strains were measured with a fluorescence plate reader to identify clones validated by diagnostic PCR that nevertheless failed to express a tFT fusion due to mutations in the ORF-specific primers used for PCR targeting (described in section 1.9). In total, we obtained at least 2 validated clones for 3952 ORFs, 1 validated clone for 92 ORFs and no validated clones for 37 ORFs (Supplementary Table 2).

1.1. Tagging strategy

Studies in *S. cerevisiae* suggest that N-terminal residues of most proteins are likely to encode signals regulating protein turnover[14,15]. Although a variety of signals can also occur at the C-terminus of many proteins, in the absence of a systematic comparison between the effects of N- and C-terminal tagging, the tFT library was constructed using C-terminal tagging. We applied a seamless tagging approach that reduces the impact of introducing foreign sequences into the yeast genome and allows expression of protein fusions for their endogenous chromosomal loci under the control of both upstream and downstream gene regulatory elements[16]. We designed a module for seamless protein tagging with the mCherry-sfGFP timer that contains the following elements: S3 primer annealing site, *mCherry* sequence, I-SceI cut site, terminator sequence of the *CYC1* gene from *Saccharomyces paradoxus*, *URA3* gene with endogenous promoter and terminator from *S. cerevisiae*, second I-SceI cut site, *mCherry$^{\Delta N}$-sfGFP* sequence coding for a C-terminal fragment of mCherry followed by sfGFP, S2 primer annealing site (plasmid pMaM168 in Supplementary Table 5, Extended Data Fig. 3a). After integration of this module into a locus of interest using conventional PCR targeting, an mCherry-tagged protein is expressed. All auxiliary sequences required for clonal selection can then be excised from the genome through conditional expression of the I-SceI endonuclease, leading to the expression of an mCherry-sfGFP-tagged protein (Extended Data Fig. 3a). The seamless excision process is practically error free for the majority of yeast genes and thus does not require validation[16].

1.2. Library background strain

The library background strain is based on the SGA entry strain Y8205[8]. The Y8205 strain (MATα *can1*Δ::*STE2pr-SpHIS5 lyp1*Δ::*STE3pr-LEU2 his3*Δ*1 leu2*Δ*0 ura3*Δ*0*) can be crossed with strains of the opposite mating type carrying genome manipulations such as deletions of non-essential genes[17], temperature-sensitive (*ts*) alleles[18,19] or decreased abundance by mRNA perturbation (DAmP) alleles[20] of essential genes. Importantly, this strain contains the genetic elements (*can1*Δ::*STE2pr-SpHIS5 lyp1*Δ::*STE3pr-LEU2*) necessary for selection of haploid double mutant progeny during the SGA procedure.

The seamless tagging strategy used to construct the tFT library relies on conditional expression of the I-SceI endonuclease[16] (Extended Data Fig. 3a). We constructed the plasmid pND32-8 carrying the *I-SCEI* sequence, placed under the control of the galactose-inducible promoter from the *GAL1* gene, and the nourseothricin resistance gene *natNT2*[12] (Supplementary Table 5). The *GAL1pr-I-SCEI-natNT2* sequence was then integrated into the *leu2*Δ*0* locus in the Y8205 strain by PCR targeting with primers ISce1-Nat-A (tcaaaaagatccatgtataatcttcattattacagccctcttgacttatttcaggaaagtttcggaggag) and ISce1-Nat-B (gtttcgtctaccctatgaacatattccattttgtaatttcgtgtcgcaagaattttcgttttaaaacctaag) and pND32-8 as template. Correct integration was verified by PCR. Tagging of all selected ORFs with the mCherry-sfGFP timer was performed in the resulting strain yMaM330 (Supplementary Table 4).

1.3. Selection of ORFs

We sought to reduce potential artifacts in the tFT library and to rationalize the labor required for library construction. Previously, most *S. cerevisiae* ORFs were successfully fused to a common tag at respective endogenous loci in a haploid reference strain[9-11]. The C-terminally tagged proteins

could be detected by fluorescence microscopy, flow cytometry or immunoblotting at levels close to endogenous[9,10,21,22]. However, some protein fusions could not be detected or analyzed because the C-terminus is important for protein function[9,10]. We sought to avoid tagging ORFs encoding such proteins. Moreover, the properties of the mCherry-sfGFP timer depend on the intracellular environment[23]. We sought to avoid tagging ORFs encoding proteins that localize to compartments with extreme environments such as the lumen of the vacuole or the cell wall/extracellular space.

Therefore, we selected all verified or uncharacterized ORFs from the *Saccharomyces* Genome Database assigned to the following gene ontology (GO) terms: GO:0005829 [cytosol], GO:0005634 [nucleus], GO:0005886 [plasma membrane], GO:0005737 [cytoplasm], GO:0016021 [integral to membrane] (as of 09/08/2010) and GO:0005739 [mitochondrion] (as of 07/09/2010). ORFs from the mitochondrial genome and the 2μ plasmid were not included. For each protein localization pattern defined in a systematic localization study of GFP protein fusions in yeast[9], ORFs absent from our list were manually inspected for possible inclusion. ORFs encoding the following proteins were subsequently removed from the selection:

- cell wall proteins (manually curated list of ORFs assigned to the GO terms GO:0005618 [cell wall] or GO:0009277 [fungal-type cell wall] as of December 2009);
- glycosylphosphatidylinositol (GPI)-anchored proteins[24];
- tail-anchored proteins[20,25];
- proteins with one of the following motifs at the C-terminus: HDEL, KKXX, CaaX ('X' stands for any amino acid, 'a' stands for an aliphatic amino acid) or the PTS1 peroxisomal targeting signal (selected using the Yeast Genome Pattern Matching tool at http://www.yeastgenome.org/cgi-bin/PATMATCH/nph-patmatch as of 30/08/2010);
- proteins fatty acylated at the C-terminus (manually curated list of proteins obtained from the UniProt Knowledgebase, http://www.uniprot.org as of 14/09/2010).

The resulting list was further curated using information from previous genome-wide tagging efforts[9-11] and a proteome-wide mass spectrometry study[22]. We decided to exclude ORFs encoding proteins that were tagged but could not be detected in any previous genome-wide tagging study[9-11]. ORFs encoding proteins that were not detected by mass spectrometry[22] and either were not detected by fluorescence microscopy after tagging with GFP[9] or no information on the expression of tagged proteins was available in any genome-wide library of protein fusions[9-11] were also excluded. This resulted in a list of 4081 ORFs (Supplementary Table 2).

1.4. Primers for PCR targeting of the tagging module

S2/S3 primers for PCR amplification of the tagging module were designed as previously described[13]. Sequences of all ORFs with untranslated regions 1000 bases upstream of the initial ATG and 1000 bases downstream of the stop codon were downloaded from the *Saccharomyces* Genome Database (orf_genomic_1000.fasta.gz as of December 2009) and used for primer design. For each ORF, an S3 primer was composed of 55 nucleotides before the stop codon (excluding stop) followed by cgtacgctgcaggtcgac and an S2 primer was composed of the reverse complement of 55 nucleotides downstream of the stop codon (including stop) followed by atcgatgaattcgagctcg. All primers were obtained from IDT (Integrated DNA Technologies) in 96-well format. Unique plate and well coordinates were assigned to each ORF such that each well contained a mixture of S2/S3 primers for a different ORF at 5 μM concentration. A distinct well was left empty on each plate for identification purposes (plate 1 – well A1 empty, plate 2 – well A2 empty, etc.). Four wells on each plate were served as controls in PCR amplification of the tagging module: well H9 was left empty; well H10 contained a mixture of S2/S3 primers for *HSP104*, which performed robustly in PCR amplification of tagging modules (data not shown); well H11 contained a mixture of S2/S3 primers for *SPC110*, which yielded a PCR product only under optimal conditions (data not shown); well H12 was left empty.

New tagging primers were obtained for the ORFs for which no positive clones were identified by diagnostic PCR in the first round of transformations. For each ORF, the new S3 primer was composed of 62 nucleotides before the stop codon (excluding stop) followed by

cgtacgctgcaggtcgac and the new S2 primer was composed of the reverse complement of 61 nucleotides downstream of the stop codon (including stop) followed by atcgatgaattcgagctcg.

1.5. Amplification of the tagging module

The module for seamless protein tagging with mCherry-sfGFP was PCR amplified in 96-well format using the plasmid pMaM168 (Supplementary Table 5) as template and ORF-specific S2/S3 primers in each well, as follows. Cooled 96-well PCR plates (4titude, 4ti-0960) were filled with 45 µl per well of a PCR mix (each well received 10 µl of 5x Herculase II buffer (Agilent Technologies), 0.5 µl of 100mM stock of dNTPs (Fermentas, R0141/0151/0161/0171), 0.075 µl of 1M stock $MgCl_2$, 5 µl of 5M stock of betaine (Sigma-Aldrich, 61962), 0.5 µl of template DNA (200 ng/µl stock), 28.675 µl of H_2O and 0.25 µl of Herculase II Fusion DNA polymerase (Agilent Technologies, 600679)) using a Multiprobe II liquid handling 8-channel robot (Perkin Elmer). A mixture of ORF-specific S2/S3 primers (5 µl of 5µM stock) was added to each well from 96-well primer source plates (see section 1.4) using the liquid handling 8-channel robot. The plates were sealed with peelable aluminum seals (Agilent, 24210-001) using a Velocity11 PlateLoc sealer. PCR was then carried out in PTC-225 PCR cyclers (MJ Research) using the following program: 2 min at 95°C, 30 cycles of 20 s at 95°C/20 s at 64°C/2 min 20 s at 72°C, 3 min at 72°C and incubation at 4°C. Control reactions in wells H8-H11 of each 96-well plate were examined by agarose gel electrophoresis to ensure successful amplification of the tagging module.

1.6. Transformation

Preparation of yeast competent cells and transformations were carried out essentially as previously described[13]. Briefly, a pre-culture of the strain yMaM330 was grown to saturation in rich YPD medium (1% yeast extract, 2% peptone, 2% glucose) and used to inoculate a 5 L YPD culture to optical density of 0.2 (OD_{600nm}). After growth at 30°C to OD_{600nm} of 2.0, the cells were collected by centrifugation (500 g for 5 min at room temperature), washed first with 5 L of sterile water and finally with 1 L of LiSorb (100mM lithium acetate (L4158, Sigma), 1M sorbitol (1.07758.1000, Merck), 10mM Tris/HCl pH 8, 1mM EDTA/NaOH pH 8, adjusted to pH 8 with acetic acid). The cell pellet was resuspended in 45 ml of LiSorb, aliquoted and stored at -80°C. For transformations, a thawed aliquot of cells was mixed 18:2 with pre-boiled carrier DNA (salmon sperm DNA, #15632-011, Invitrogen).

Transformations were performed in 96-deepwell plates (Eppendorf, 0030 502.132). 50 µl of competent yMaM330 cells were pipetted into each well. Using a Platetrak 96-channel liquid handling robot (Perkin Elmer), 5 µl of amplified tagging module were transferred from each PCR plate (see section 1.5) into the corresponding transformation plate. 300 µl of LiPEG (100mM lithium acetate (L4158, Sigma), 10mM Tris/HCl pH 8, 1mM EDTA/NaOH pH 8, 40% (w/v) polyethylene glycol (P4338, Sigma)) were subsequently added to each well and thoroughly mixed. The plates were sealed with gas permeable adhesive seals (AB-0718, Thermo Scientific) and incubated for 40 min in a 42°C water bath. After a centrifugation step (5 min at 500 g), the supernatant was removed and the cell pellet was resuspended in 100 µl per well of synthetic medium devoid of uracil (SC-Ura) using the 96-channel liquid handling robot. The cell suspension from each well was manually plated onto a separate 9 cm plate with SC-Ura agar medium. The plates were incubated at 30°C for 3 days until clear colonies were visible in the control transformations (wells H10 and H11 in each 96-deepwell transformation plate).

Six clones from each 9 cm plate were manually streaked for single colonies on SC-Ura agar medium and incubated at 30°C for 2 days. For each ORF, four purified clones were inoculated in 96-well format (each well contained 150 µl of SC-Ura medium with 15% (v/v) of glycerol), with each clone at the same well position in a separate 96-well plate. The plates were sealed with gas permeable adhesive seals, incubated at 30°C for 2 days and stored at -80°C.

1.7. Verification primers

ORF-specific verification primers that anneal within each ORF were designed using BatchPrimer3 v1.0[26] (http://batchprimer3.bioinformatics.ucdavis.edu/index.html as of 22/10/2010),

a high-throughput web implementation of Primer3[27]. For each ORF, a sequence composed of 1000 nucleotides before the STOP codon followed by the tag was entered into BatchPrimer3. Using the 1st set of constraints indicated below (min/optimal/max values are specified for each parameter), a unique primer with two consecutive G and/or C nucleotides at the 3' end that would yield a PCR product around 450 nucleotides long, when used together with a generic reverse primer (atggccatgttatcctcctcg) that anneals 71 nucleotides downstream of the start of the tag, was selected for each ORF. When no satisfactory primer could be found, the 2nd set of relaxed constraints or finally the 3rd set were used.

Selection of verification primers (first round)

	1st set	2nd set	3rd set
PCR product length (nucleotides)	300/450/600	300/450/600	300/450/670
primer length (nucleotides)	19/20/21	18/20/22	18/20/24
melting temperature (°C)	60/63/65	59/63/66	59/63/66
GC content (%)	25/50/75	25/50/75	25/50/75
satisfactory primers	3911	158	12

These primers were used in the first round of diagnostic PCR. For 360 ORFs with ambiguous results, the diagnostic PCR was repeated with new ORF-specific primers, designed using the constraints indicated below (no optimal PCR product length in the 1st set, optimal PCR product length of 250 or 600 nucleotides in the 2nd and 3rd sets of constraints).

Selection of verification primers (second round)

	1st set	2nd set	3rd set
PCR product length (nucleotides)	300/0/600	250/<>/600	250/<>/600
primer length (nucleotides)	19/20/21	18/20/22	18/20/24
melting temperature (°C)	60/63/65	59/63/66	59/63/66
GC content (%)	25/50/75	25/50/75	25/50/75
satisfactory primers	253	104	3

1.8. Diagnostic PCR

Integration of the tagging module into each genomic locus was tested by PCR. The junction between each ORF and the tag was verified using a forward ORF-specific primer annealing within the ORF and a generic reverse primer annealing within the tag (see section 1.7). Cooled 96-well PCR plates (4titude, 4ti-0960) were filled with 35 µl per well of a PCR mix (each well received 4 µl of 10x long incubation buffer (200mM Tris pH8.8, 100mM $(NH_4)_2SO_4$, 100mM KCl), 0.16 µl of 100mM stock of dNTPs (Fermentas, R0141/0151/0161/0171), 0.1 µl of 1M stock $MgCl_2$, 4 µl of 5M stock of betaine (Sigma-Aldrich, 61962), 0.2 µl of 100µM stock of the generic reverse primer (see section 1.7), 25.94 µl of H_20 and 0.6 µl of Taq DNA polymerase (self-made, ~5 U/µl) using a Perkin Elmer Multiprobe II liquid handling 8-channel robot. A distinct forward ORF-specific validation primer (4 µl of 5µM stock) was added to each well from 96-well validation primer source plates (see section 1.7). A dense culture of each strain (stored at -80°C as glycerol stock, see section 1.6) added to each well (1 µl) provided the genomic DNA template. For each ORF-specific

primer, a control PCR was set up with the library background strain yMaM330 as a source of template DNA. The plates were sealed with peelable aluminum seal using a Velocity11 PlateLoc sealer. PCR was then carried out in MJ Research PTC-225 PCR cyclers using the following program: 7 min at 97°C, 38 cycles of 30 s at 95°C/30 s at 58°C/30 s at 72°C, 5 min at 72°C and incubation at 4°C.

All PCR products were examined by agarose gel electrophoresis using 96-well precast gels (2% E-Gel® 96 gels (G7008-02), Invitrogen) and a reference DNA ladder (FastRuler low range DNA ladder (SM1103), Fermentas). Clones with correct chromosomal integration of the tagging module were identified by the presence of a PCR product of expected size in the sample but not in the control PCR.

1.9. Whole colony imaging

Using a RoToR pinning robot (Singer Instruments), all clones from a single 96-well transformation plate were combined in 1536-colony format with 4 technical replicates of each clone. All strains underwent seamless marker excision by sequential growth on galactose (synthetic complete medium containing 2% galactose and 2% raffinose instead of glucose) and 5-FOA plates (synthetic medium containing 5-fluoroorotic acid)[16]. Fluorescence intensities of all colonies were measured after ~21 h of growth on glucose medium (synthetic complete medium containing 2% glucose) using an Infinite M1000 Pro microplate reader (Tecan).

2. Supplementary Notes

2.1. Supplementary Note 1

We have previously shown that measurements of protein turnover with the mCherry-sfGFP timer exceed cycloheximide or pulse-chase experiments in both dynamic range and sensitivity. For instance, the turnover of 20 N-degrons differing in the N-terminal residue, which were previously classified into five stability groups based on pulse-chase experiments[28,29], could be reliably resolved with the tFT, showing that each of the 20 N-degrons possesses a specific turnover (Supplementary Figure 7 in Ref.[4]).

Cycloheximide chase experiments are limited by the availability of free ubiquitin in the cell. Upon inhibition of translation, ubiquitin is depleted from yeast cell with a half-life of ~2 h[30]. This prevents reliable turnover measurements for relatively stable proteins. In contrast, the tFT approach is not limited by ubiquitin availability but by the maturation kinetics of the used fluorescent proteins. Degradation of proteins with half-lives between ~10 min and ~8 h can be analyzed with the mCherry-sfGFP timer[4]. Thus, although 3HA-tagged Are2, Yip4, Alg2 and Ybr287w appear rather stable in cycloheximide chase experiments (data not shown), tFT-tagged Are2, Yip4, Alg2 and Ybr287w were identified as Asi substrates in our screens (Fig. 3b) and, accordingly, accumulated at the nuclear rim in the *asi1*Δ mutant (Extended Data Fig. 4c).

Besides the aforementioned differences, we note that protein stability measurements with the tFT based on whole colony fluorescence measurements are not directly comparable with cycloheximide experiments also due to differences in growth conditions. Cycloheximide chase experiments are typically performed with exponentially growing cultures. However, measurements of colony fluorescence detect the signal mostly from the colony surface, where nutrient supply is limited and cells grow slower[31], with a potential influence on protein expression and turnover. For instance, Aqy2 was identified as an Asi substrate in our screens (Fig. 3b) but was not expressed during exponential growth in synthetic complete medium (data not shown).

2.2. Supplementary Note 2

SILAC mass spectrometry[32] or quantitative microscopy can be used to identify potential substrates of degradation pathways based on changes in protein abundance[33-35]. However, these methods cannot distinguish between changes in abundance that result from altered protein stability and those caused by changes in protein expression. The tFT strategy directly identifies proteins with altered stability. However, in contrast to approached based on mass spectrometry, it has the disadvantage that fusion to the tFT might compromise protein function[36]. Nevertheless, our screens identified Erg11 among the substrates of the Asi ubiquitin ligase, in agreement with the recent work of Foresti et al.[37] Nsg1, another Asi substrate identified by Foresti et al., is a false-negative in our screens, as retesting showed stabilization of Nsg1-tFT upon deletion of *ASI1* (data not shown).

3. Supplementary Tables

3.1. Supplementary Table 1: Correlation coefficients between genetic interaction profiles

Pearson correlation coefficients between genetic interaction profiles of *ASI1, ASI2, ASI3, UBC6, UBC7, CUE1, HRD1, DOA10* genes and of all the other genes in the genome-wide genetic interaction map[38]. The data (Excel file) is available online.

3.2. Supplementary Table 2: Strains in the tFT library

Number of validated clones for each ORF in the tFT library, including ORFs with zero validated clones. The data (Excel file) is available online.

3.3. Supplementary Table 3: Protein stability changes in screens with the tFT library

Stability changes of each protein in the tFT library in *asi1*Δ, *asi3*Δ, *hrd1*Δ, *doa10*Δ, *ubc6*Δ and *ubc7*Δ mutants. z-scores and p-values adjusted for multiple testing are provided. The data (Excel file) is available online.

3.4. Supplementary Table 4: Yeast strains used in this study

Strain	Background	Genotype	Source
PLY127	S288c	*MATa ura3-52 lys2Δ201*	Ljungdahl lab
PLY966	S288c	*MATa ura3-52 lys2Δ201 leu2-3,112 ubc6Δ::LEU2*	Ref.[39]
PLY967	S288c	*MATa ura3-52 lys2Δ201 leu2-3,112 ubc7Δ::LEU2*	Ref.[39]
PLY1558	S288c	*MATa ura3-52 lys2Δ201 leu2-3,112 ubc6Δ::LEU2 ubc7Δ::natMX4*	Ref.[39]
PLY1327	S288c	*MATa ura3-52 lys2Δ201 asi1Δ80::hphMX*	Ljungdahl lab
PLY1329	S288c	*MATa ura3-52 lys2Δ201 asi3Δ::kanMX*	Ljungdahl lab
BY4741	S288c	*MATa his3Δ1 leu2Δ0 met15Δ0 ura3Δ0*	Ref.[40]
MHY2241	BY4741	*ubc4Δ::kanMX*	Hochstrasser lab
MHY3032	BY4741	*hrd1Δ::kanMX*	Ref.[41]
MHY3033	BY4741	*doa10Δ::kanMX*	Ref.[41]
Y7092	S288c	*MATalpha his3Δ1 leu2Δ0 met15Δ0 ura3Δ0 can1Δ::STE2pr-spHIS5 lyp1Δ*	Ref.[40]
Y8205	S288c	*MATalpha his3Δ1 leu2Δ0 met15Δ0 ura3Δ0 can1Δ:: STE2pr-spHIS5 lyp1Δ::STE3pr-LEU2*	Ref.[40]
scEB115	Y7092	*MATalpha can1Δ::STE2pr-spHIS5 lyp1Δ::STE3pr-HPH rpn7Δ::RPN7-tDimer2(12)-LEU2*	Rabut lab
scEB133	scEB115	*ubc1Δ::VC-UBC1-natMX*	Rabut lab
scEB129	scEB115	*RAD6::VC-natMX*	Rabut lab
scEB130	scEB115	*CDC34::VC-natMX*	Rabut lab
scEB153	scEB115	*UBC4::VC-natMX*	Rabut lab
scEB121	scEB115	*UBC5::VC-natMX*	Rabut lab
scEB152	scEB115	*ubc6Δ::VC-UBC6-natMX*	Rabut lab
scGR1267	scEB115	*ubc7Δ::VC-UBC7-natMX*	Rabut lab
scEB125	scEB115	*UBC8::VC-natMX*	Rabut lab
scEB126	scEB115	*PEX4::VC-natMX*	Rabut lab
scEB127	scEB115	*UBC11::VC-natMX*	Rabut lab
scEB123	scEB115	*UBC13::VC-natMX*	Rabut lab
VN_0484	BY4741	*HUL4::VN-KlURA3*	Bioneer
VN_0394	BY4741	*HUL5::VN-KlURA3*	Bioneer
scGR1173	BY4741	*pRS316-RSP5-VN (pGR703)*	Rabut lab
VN_0034	BY4741	*TOM1::VN-KlURA3*	Bioneer
VN_0045	BY4741	*UFD4::VN-KlURA3*	Bioneer
VN_1027	BY4741	*ASI1::VN-KlURA3*	Bioneer
VN_0927	BY4741	*ASI3::VN-KlURA3*	Bioneer
VN_2780	BY4741	*ASR1::VN-KlURA3*	Bioneer
VN_0860	BY4741	*BRE1::VN-KlURA3*	Bioneer
VN_3152	BY4741	*CWC24::VN-KlURA3*	Bioneer
VN_2108	BY4741	*DMA1::VN-KlURA3*	Bioneer
VN_1460	BY4741	*DMA2::VN-KlURA3*	Bioneer
VN_4936	BY4741	*DOA10::VN-KlURA3*	Bioneer
VN_1175	BY4741	*ETP1::VN-KlURA3*	Bioneer
VN_0376	BY4741	*FAP1::VN-KlURA3*	Bioneer
scGR1165	BY4741	*far1Δ::VN-FAR1-URA3*	Rabut lab
VN_1990	BY4741	*GID2::VN-KlURA3*	Bioneer
VN_1419	BY4741	*GID9::VN-KlURA3*	Bioneer
VN_1031	BY4741	*HEL2::VN-KlURA3*	Bioneer
VN_5317	BY4741	*HRD1::VN-KlURA3*	Bioneer
VN_0043	BY4741	*IRC20::VN-KlURA3*	Bioneer
VN_0884	BY4741	*MAG2::VN-KlURA3*	Bioneer
scGR1166	BY4741	*mot2Δ::VN-MOT2-URA3*	Rabut lab
VN_0246	BY4741	*MTC5::VN-KlURA3*	Bioneer
scGR1172	BY4741	*nam7Δ::VN-NAM7-URA3*	Rabut lab
VN_5066	BY4741	*PEP3::VN-KlURA3*	Bioneer
VN_5052	BY4741	*PEP5::VN-KlURA3*	Bioneer
VN_5657	BY4741	*PEX2::VN-KlURA3*	Bioneer
VN_5559	BY4741	*PEX10::VN-KlURA3*	Bioneer
VN_5469	BY4741	*PEX12::VN-KlURA3*	Bioneer
scGR1160	BY4741	*psh1Δ::VN-PSH1-KlURA3*	Bioneer
VN_0234	BY4741	*RAD5::VN-KlURA3*	Bioneer
VN_0644	BY4741	*RAD16::VN-KlURA3*	Bioneer
VN_1639	BY4741	*RAD18::VN-KlURA3*	Bioneer
VN_0021	BY4741	*RKR1::VN-KlURA3*	Bioneer
VN_0153	BY4741	*RTC1::VN-KlURA3*	Bioneer
VN_1107	BY4741	*SAN1::VN-KlURA3*	Bioneer
VN_1072	BY4741	*SLX5::VN-KlURA3*	Bioneer
VN_3137	BY4741	*SLX8::VN-KlURA3*	Bioneer
scGR1171	BY4741	*ste5Δ::VN-STE5-URA3*	Rabut lab
VN_1785	BY4741	*SSL1::VN-KlURA3*	Bioneer
scGR1167	BY4741	*tfb3Δ::VN-TFB3-URA3*	Rabut lab
VN_0629	BY4741	*TUL1::VN-KlURA3*	Bioneer
VN_0060	BY4741	*UBR2::VN-KlURA3*	Bioneer
VN_0020	BY4741	*ULS1::VN-KlURA3*	Bioneer
VN_4927	BY4741	*VPS8::VN-KlURA3*	Bioneer
VN_4447	BY4741	*YBR062C::VN-KlURA3*	Bioneer

Strain	Background	Genotype	Source
scGR1168	BY4741	*prp19Δ::VN-PRP19-URA3*	Rabut lab
VN_0419	BY4741	*UFD2::VN-KlURA3*	Bioneer
VN_1367	BY4741	*HEL1::VN-KlURA3*	Bioneer
VN_1749	BY4741	*ITT1::VN-KlURA3*	Bioneer
VN_3891	BY4741	*APC11::VN-KlURA3*	Bioneer
VN_0690	BY4741	*CUL3::VN-KlURA3*	Bioneer
VN_0556	BY4741	*RTT101::VN-KlURA3*	Bioneer
scEB300	scEB115	*ASI1::VN-KlURA3 ubc6Δ::VC-UBC6-natMX*	Rabut lab
scEB289	scEB115	*ASI1::VN-KlURA3 UBC4::VC-natMX*	Rabut lab
scEB323	scEB115	*ASI1::VN-KlURA3 UBC4::VC-natMX ubc6Δ::kanMX*	Rabut lab
scEB258	scEB115	*ASI3::VN-KlURA3 ubc6Δ::VC-UBC6-natMX*	Rabut lab
scEB265	scEB115	*ASI1::VN-KlURA3 ubc6Δ::VC-UBC6-natMX asi1Δ::kanMX*	Rabut lab
scEB266	scEB115	*ASI1::VN-KlURA3 ubc6Δ::VC-UBC6-natMX asi2Δ::kanMX*	Rabut lab
scGR1245	BY4741	*ASI3::TAP-HIS3MX*	Open Biosystems
scGR1258	BY4741	*ASI3::TAP-HIS3MX asi1Δ::kanMX*	Rabut lab
scGR1260	BY4741	*ASI3::TAP-HIS3MX asi2Δ::kanMX*	Rabut lab
scAB17	W303	*tor1-1 fpr1::NAT RPL13A::2xFKBP12-TRP1 PRE8::FRBGFP-kanMX6 stp2(1-45)::TAP-URA3*	Rabut lab
scAB22	scAB17	*asi3Δ::HPH*	Rabut lab
scAB23	scAB17	*ubc6Δ::HPH*	Rabut lab
scAB24	scAB17	*ubc7Δ::HPH*	Rabut lab
AK1234	BY4741	*asi1Δ::kanMX6*	Knop lab
YMaM767	BY4741	*ire1Δ::natNT2 hrd1Δ::hphNT1*	Knop lab
YMaM768	BY4741	*hac1Δ::natNT2 hrd1Δ::hphNT1*	Knop lab
YMaM814	BY4741	*ire1Δ::natNT2 hrd1Δ::hphNT1 asi1Δ::kanMX6*	Knop lab
YMaM815	BY4741	*hac1Δ::natNT2 hrd1Δ::hphNT1 asi1Δ::kanMX6*	Knop lab
AK1222	BY4741	*hrd1Δ::hphNT1*	Knop lab
AK1225	BY4741	*doa10Δ::hphNT1*	Knop lab
YMaM891	BY4741	*hrd1Δ::hphNT1 asi1Δ::kanMX6*	Knop lab
YMaM892	BY4741	*doa10Δ::hphNT1 asi1Δ::kanMX6*	Knop lab
YMaM330	Y8205	*leu2Δ::GAL1pr-I-SCEI-natNT2*	Knop lab
YMaM344	YMaM330	*ura3Δ0::mCherryΔN-I-SceIsite-CYC1term-ScURA3-I-SceIsite-mCherryΔN*	Knop lab
AK1235	BY4741	*asi2Δ::kanMX6*	Knop lab
AK1236	BY4741	*asi3Δ::kanMX6*	Knop lab
AK1237	BY4741	*ubc6Δ::kanMX6*	Knop lab
AK1238	BY4741	*ubc7Δ::kanMX6*	Knop lab
AK1239	BY4741	*cue1Δ::kanMX6*	Knop lab
YMaM758	YMaM330	*VTC1::mCherry-sfGFP*	Knop lab
YMaM757	YMaM330	*ERG11::mCherry-sfGFP*	Knop lab
YMaM759	YMaM330	*VCX1::mCherry-sfGFP*	Knop lab
YMaM762	YMaM330	*ARE2::mCherry-sfGFP*	Knop lab
YMaM765	YMaM330	*YIP4::mCherry-sfGFP*	Knop lab
YMaM756	YMaM330	*ALG2::mCherry-sfGFP*	Knop lab
YMaM764	YMaM330	*VTC4::mCherry-sfGFP*	Knop lab
YMaM761	YMaM330	*YBR287W::mCherry-sfGFP*	Knop lab
YMaM763	YMaM330	*AQY2::mCherry-sfGFP*	Knop lab
YMaM760	YMaM330	*ERG1::mCherry-sfGFP*	Knop lab
YMaM828	YMaM330	*VTC1::mCherry-sfGFP asi1Δ::hphNT1*	Knop lab
YMaM827	YMaM330	*ERG11::mCherry-sfGFP asi1Δ::hphNT1*	Knop lab
YMaM830	YMaM330	*VCX1::mCherry-sfGFP asi1Δ::hphNT1*	Knop lab
YMaM831	YMaM330	*ARE2::mCherry-sfGFP asi1Δ::hphNT1*	Knop lab
YMaM833	YMaM330	*YIP4::mCherry-sfGFP asi1Δ::hphNT1*	Knop lab
YMaM829	YMaM330	*ALG2::mCherry-sfGFP asi1Δ::hphNT1*	Knop lab
YMaM832	YMaM330	*VTC4::mCherry-sfGFP asi1Δ::hphNT1*	Knop lab
YMaM835	YMaM330	*YBR287W::mCherry-sfGFP asi1Δ::hphNT1*	Knop lab
YMaM834	YMaM330	*AQY2::mCherry-sfGFP asi1Δ::hphNT1*	Knop lab
YMaM836	YMaM330	*ERG1::mCherry-sfGFP asi1Δ::hphNT1*	Knop lab
YMaM818	YMaM330	*VTC1::mCherry-sfGFP hrd1Δ::hphNT1*	Knop lab
YMaM817	YMaM330	*ERG11::mCherry-sfGFP hrd1Δ::hphNT1*	Knop lab
YMaM820	YMaM330	*VCX1::mCherry-sfGFP hrd1Δ::hphNT1*	Knop lab
YMaM821	YMaM330	*ARE2::mCherry-sfGFP hrd1Δ::hphNT1*	Knop lab
YMaM823	YMaM330	*YIP4::mCherry-sfGFP hrd1Δ::hphNT1*	Knop lab
YMaM819	YMaM330	*ALG2::mCherry-sfGFP hrd1Δ::hphNT1*	Knop lab
YMaM822	YMaM330	*VTC4::mCherry-sfGFP hrd1Δ::hphNT1*	Knop lab
YMaM825	YMaM330	*YBR287W::mCherry-sfGFP hrd1Δ::hphNT1*	Knop lab
YMaM824	YMaM330	*AQY2::mCherry-sfGFP hrd1Δ::hphNT1*	Knop lab
YMaM826	YMaM330	*ERG1::mCherry-sfGFP hrd1Δ::hphNT1*	Knop lab
YMaM791	BY4741	*VTC1::3HA-hphNT1*	Knop lab
YMaM790	BY4741	*ERG11::3HA-hphNT1*	Knop lab
YMaM793	BY4741	*VCX1::3HA-hphNT1*	Knop lab
YMaM795	BY4741	*VTC4::3HA-hphNT1*	Knop lab
YMaM801	BY4741	*VTC1::3HA-hphNT1 asi1Δ::kanMX6*	Knop lab
YMaM800	BY4741	*ERG11::3HA-hphNT1 asi1Δ::kanMX6*	Knop lab
YMaM803	BY4741	*VCX1::3HA-hphNT1 asi1Δ::kanMX6*	Knop lab
YMaM805	BY4741	*VTC4::3HA-hphNT1 asi1Δ::kanMX6*	Knop lab

Strain	Background	Genotype	Source
YMaM864	BY4741	*VTC1::3HA-hphNT1 hrd1Δ::natNT2*	Knop lab
YMaM863	BY4741	*ERG11::3HA-hphNT1 hrd1Δ::natNT2*	Knop lab
YMaM866	BY4741	*VCX1::3HA-hphNT1 hrd1Δ::natNT2*	Knop lab
YMaM868	BY4741	*VTC4::3HA-hphNT1 hrd1Δ::natNT2*	Knop lab
YDK179	BY4741	*VTC1::3HA-hphNT1 asi1Δ::kanMX6 hrd1Δ::natNT2 doa10Δ::KlURA3*	Knop lab
YDK178	BY4741	*ERG11::3HA-hphNT1 asi1Δ::kanMX6 hrd1Δ::natNT2 doa10Δ::KlURA3*	Knop lab
YDK180	BY4741	*VCX1::3HA-hphNT1 asi1Δ::kanMX6 hrd1Δ::natNT2 doa10Δ::KlURA3*	Knop lab
YDK181	BY4741	*VTC4::3HA-hphNT1 asi1Δ::kanMX6 hrd1Δ::natNT2 doa10Δ::KlURA3*	Knop lab
YDK182	BY4741	*VTC1::myeGFP-kanMX*	Knop lab
YDK188	BY4741	*VTC4::myeGFP-kanMX*	Knop lab
YDK223	YMaM330	*sfGFPΔC-I-SceIsite-SpCYC1term-ScURA3-SpTEF1pr-I-SceIsite-sfGFP::VTC1*	Knop lab
YDK224	YMaM330	*sfGFPΔC-I-SceIsite-SpCYC1term-ScURA3-SpTEF1pr-I-SceIsite-sfGFP::VTC4*	Knop lab
YDK266	YMaM330	*sfGFP::VTC1*	Knop lab
YDK267	YMaM330	*sfGFP::VTC4*	Knop lab

3.5. Supplementary Table 5: Plasmids used in this study

Plasmid	Description	Source
pRS316	*CEN ARS URA3* low copy yeast/*E. coli* shuttle plasmid	Ref.[42]
pRS317	*CEN ARS LYS2* low copy yeast/*E. coli* shuttle plasmid	Ref.[42]
pCA047	pRS316 (*URA3*) containing *STP1-3HA*	Ref.[43]
pCA111	pRS316 (*URA3*) containing *STP2-3HA*	Ref.[43]
pDO74	pRS316 (*URA3*) containing *STP1-RI*$_{17-33}$*-3HA*	Ref.[44]
pAG04	pRS316 (*URA3*) containing *STP2Δ*$_{2-13}$*-3HA*	Ljungdahl lab
YCpAGP1-LacZ	*AGP1pr-lacZ* in *CEN URA3*	Ref.[45]
pFA6a	E. coli plasmid containing the ampicillin resistance gene *ampR*	Ref.[46]
pFA6a-kanMX6	pFA6a-kanMX6	Ref.[46]
pKS133	pFA6a-hphNT1	Ref.[12]
pKS134	pFA6a-natNT2	Ref.[12]
pYM24	pFA6a-3HA-hphNT1	Ref.[12]
pMaM168	pFA6a-mCherry-I-SceIsite-SpCYC1term-ScURA3-I-SceIsite-mCherryΔN-sfGFP	Knop lab
pND32-8	pRS305N-GAL1pr-I-SCEI	Ref.[16]
pMaM173	pFA6a-sfGFPΔC-I-SceIsite-SpCYC1term-ScURA3-SpTEF1pr-I-SceIsite-sfGFP	Knop lab
pYM12monomeric	pFA6a-yeGFP-kanMX6 with A206R mutation	Knop lab
pGR731	pGEX4TG containing *GST-UBC6*$^{\Delta TM}$	Rabut lab
pGR732	pGEX4TG containing *GST-UBC7*	Rabut lab
pGR738	pETDuet-1 containing *GST-UBC7* + *CUE1*^{U7BR}	Rabut lab
pGR773	pMALXTG containing *MBP-HRD1*^{CT}	Rabut lab
pGR759	pMALXTG containing *MBP-ASI1*^{RING}	Rabut lab
pGR766	pMALXTG containing *MBP-ASI3*^{RING}	Rabut lab
pGR703	pRS316 (*URA3*) containing *RSP5-VN*	Rabut lab
pGR295	p415TEF1 *(LEU2)* containing 10xHis-Ubiquitin	Rabut lab

4. References

1. Belle, A., Tanay, A., Bitincka, L., Shamir, R. & O'Shea, E. K. Quantification of protein half-lives in the budding yeast proteome. *Proc. Natl. Acad. Sci. U.S.A.* **103,** 13004–13009 (2006).
2. Shaner, N. C. *et al.* Improved monomeric red, orange and yellow fluorescent proteins derived from Discosoma sp. red fluorescent protein. *Nat. Biotechnol.* **22,** 1567–1572 (2004).
3. Pédelacq, J.-D., Cabantous, S., Tran, T., Terwilliger, T. C. & Waldo, G. S. Engineering and characterization of a superfolder green fluorescent protein. *Nat. Biotechnol.* **24,** 79–88 (2006).
4. Khmelinskii, A. *et al.* Tandem fluorescent protein timers for in vivo analysis of protein dynamics. *Nat. Biotechnol.* **30,** 708–714 (2012).
5. Giaever, G. & Nislow, C. The yeast deletion collection: a decade of functional genomics. *Genetics* **197,** 451–465 (2014).
6. Botstein, D. & Fink, G. R. Yeast: an experimental organism for 21st Century biology. *Genetics* **189,** 695–704 (2011).
7. Tong, A. H. *et al.* Systematic genetic analysis with ordered arrays of yeast deletion mutants. *Science* **294,** 2364–2368 (2001).
8. Tong, A. H. Y. & Boone, C. Synthetic genetic array analysis in Saccharomyces cerevisiae. *Methods Mol. Biol.* **313,** 171–192 (2006).
9. Huh, W.-K. *et al.* Global analysis of protein localization in budding yeast. *Nature* **425,** 686–691 (2003).
10. Ghaemmaghami, S. *et al.* Global analysis of protein expression in yeast. *Nature* **425,** 737–741 (2003).
11. Gavin, A.-C. *et al.* Proteome survey reveals modularity of the yeast cell machinery. *Nature* **440,** 631–636 (2006).
12. Janke, C. *et al.* A versatile toolbox for PCR-based tagging of yeast genes: new fluorescent proteins, more markers and promoter substitution cassettes. *Yeast* **21,** 947–962 (2004).
13. Knop, M. *et al.* Epitope tagging of yeast genes using a PCR-based strategy: more tags and improved practical routines. *Yeast* **15,** 963–972 (1999).
14. Hwang, C.-S., Shemorry, A. & Varshavsky, A. N-terminal acetylation of cellular proteins creates specific degradation signals. *Science* **327,** 973–977 (2010).
15. Kim, H.-K. *et al.* The N-terminal methionine of cellular proteins as a degradation signal. *Cell* **156,** 158–169 (2014).
16. Khmelinskii, A., Meurer, M., Duishoev, N., Delhomme, N. & Knop, M. Seamless gene tagging by endonuclease-driven homologous recombination. *PLoS ONE* **6,** e23794 (2011).
17. Winzeler, E. A. *et al.* Functional characterization of the S. cerevisiae genome by gene deletion and parallel analysis. *Science* **285,** 901–906 (1999).
18. Ben-Aroya, S. *et al.* Toward a comprehensive temperature-sensitive mutant repository of the essential genes of Saccharomyces cerevisiae. *Mol. Cell* **30,** 248–258 (2008).
19. Li, Z. *et al.* Systematic exploration of essential yeast gene function with temperature-sensitive mutants. *Nat. Biotechnol.* **29,** 361–367 (2011).
20. Schuldiner, M. *et al.* Exploration of the function and organization of the yeast early secretory pathway through an epistatic miniarray profile. *Cell* **123,** 507–519 (2005).
21. Newman, J. R. S. *et al.* Single-cell proteomic analysis of S. cerevisiae reveals the architecture of biological noise. *Nature* **441,** 840–846 (2006).
22. de Godoy, L. M. F. *et al.* Comprehensive mass-spectrometry-based proteome quantification of haploid versus diploid yeast. *Nature* **455,** 1251–1254 (2008).
23. Khmelinskii, A. & Knop, M. Analysis of protein dynamics with tandem fluorescent protein timers. *Methods Mol. Biol.* **1174,** 195–210 (2014).
24. De Groot, P. W. J., Hellingwerf, K. J. & Klis, F. M. Genome-wide identification of fungal GPI proteins. *Yeast* **20,** 781–796 (2003).
25. Beilharz, T., Egan, B., Silver, P. A., Hofmann, K. & Lithgow, T. Bipartite signals mediate subcellular targeting of tail-anchored membrane proteins in Saccharomyces cerevisiae. *J.*

Biol. Chem. **278,** 8219–8223 (2003).
26. You, F. M. *et al.* BatchPrimer3: a high throughput web application for PCR and sequencing primer design. *BMC Bioinformatics* **9,** 253 (2008).
27. Rozen, S. & Skaletsky, H. Primer3 on the WWW for general users and for biologist programmers. *Methods Mol. Biol.* **132,** 365–386 (2000).
28. Bachmair, A., Finley, D. & Varshavsky, A. In vivo half-life of a protein is a function of its amino-terminal residue. *Science* **234,** 179–186 (1986).
29. Bachmair, A. & Varshavsky, A. The degradation signal in a short-lived protein. *Cell* **56,** 1019–1032 (1989).
30. Hanna, J., Leggett, D. S. & Finley, D. Ubiquitin depletion as a key mediator of toxicity by translational inhibitors. *Mol. Cell. Biol.* **23,** 9251–9261 (2003).
31. Vulin, C. *et al.* Growing yeast into cylindrical colonies. *Biophys. J.* **106,** 2214–2221 (2014).
32. Ong, S.-E. *et al.* Stable isotope labeling by amino acids in cell culture, SILAC, as a simple and accurate approach to expression proteomics. *Mol. Cell Proteomics* **1,** 376–386 (2002).
33. Hemming, M. L., Elias, J. E., Gygi, S. P. & Selkoe, D. J. Proteomic profiling of gamma-secretase substrates and mapping of substrate requirements. *PLoS Biol.* **6,** e257 (2008).
34. Benanti, J. A., Cheung, S. K., Brady, M. C. & Toczyski, D. P. A proteomic screen reveals SCFGrr1 targets that regulate the glycolytic-gluconeogenic switch. *Nat. Cell Biol.* **9,** 1184–1191 (2007).
35. Foresti, O., Ruggiano, A., Hannibal-Bach, H. K., Ejsing, C. S. & Carvalho, P. Sterol homeostasis requires regulated degradation of squalene monooxygenase by the ubiquitin ligase Doa10/Teb4. *Elife* **2,** e00953 (2013).
36. Yewdell, J. W., Lacsina, J. R., Rechsteiner, M. C. & Nicchitta, C. V. Out with the old, in with the new? Comparing methods for measuring protein degradation. *Cell Biol. Int.* **35,** 457–462 (2011).
37. Foresti, O., Rodriguez-Vaello, V., Funaya, C. & Carvalho, P. Quality control of inner nuclear membrane proteins by the Asi complex. *Science* **346,** 751–755 (2014).
38. Costanzo, M. *et al.* The Genetic Landscape of a Cell. *Science* **327,** 425–431 (2010).
39. Kota, J., Gilstring, C. F. & Ljungdahl, P. O. Membrane chaperone Shr3 assists in folding amino acid permeases preventing precocious ERAD. *J. Cell Biol.* **176,** 617–628 (2007).
40. Tong, A. H. Y. & Boone, C. High-Throughput Strain Construction and Systematic Synthetic Lethal Screening in Saccharomyces cerevisiae. *Meth. Microbiol.* **36,** 369–386 (2007).
41. Zattas, D., Adle, D. J., Rubenstein, E. M. & Hochstrasser, M. N-terminal acetylation of the yeast Derlin Der1 is essential for Hrd1 ubiquitin-ligase activity toward luminal ER substrates. *Mol. Biol. Cell* **24,** 890–900 (2013).
42. Sikorski, R. S. & Hieter, P. A system of shuttle vectors and yeast host strains designed for efficient manipulation of DNA in Saccharomyces cerevisiae. *Genetics* **122,** 19–27 (1989).
43. Andreasson, C. Receptor-mediated endoproteolytic activation of two transcription factors in yeast. *Genes Dev.* **16,** 3158–3172 (2002).
44. Omnus, D. J. & Ljungdahl, P. O. Latency of transcription factor Stp1 depends on a modular regulatory motif that functions as cytoplasmic retention determinant and nuclear degron. *Mol. Biol. Cell* **25,** 3823–3833 (2014).
45. Iraqui, I., Vissers, S., Cartiaux, M. & Urrestarazu, A. Characterisation of Saccharomyces cerevisiae ARO8 and ARO9 genes encoding aromatic aminotransferases I and II reveals a new aminotransferase subfamily. *Mol. Gen. Genet.* **257,** 238–248 (1998).
46. Brachmann, C. B. *et al.* Designer deletion strains derived from Saccharomyces cerevisiae S288C: a useful set of strains and plasmids for PCR-mediated gene disruption and other applications. *Yeast* **14,** 115–132 (1998).

ANNEXE 2

VU : VU :

Le Directeur de Thèse Doctorale

(Nom et Prénom)

Le Responsable de l'École

VU pour autorisation de soutenance

Rennes, le

Le Président de l'Université de Rennes 1

Guy CATHELINEAU

VU après soutenance pour autorisation de publication :

Le Président de Jury,

(Nom et Prénom)